8-2002

Mechanisms of Print Gloss Development with Controlled Coating Structure

Sung Jai Jeon

MECHANISMS OF PRINT GLOSS DEVELOPMENT WITH CONTROLLED COATING STRUCTURE

By

Sung Jai Jeon

B.S. Dongguk University, 1994

A THESIS

Submitted in Partial Fulfillment of the

Requirements for the Degree of

Master of Science

(in Chemical Engineering)

The Graduate School

The University of Maine

August, 2002

Advisory Committee:

Douglas W. Bousfield, Professor of Chemical Engineering, Advisor

Adriaan Van Heiningen, Ober Chair and Professor of Chemical Engineering

Joseph S. Aspler, Senior Scientist, Pulp and Paper Research Institute of Canada

MECHANISMS OF PRINT GLOSS DEVELOPMENT WITH CONTROLLED COATING STRUCTURE

By Sung Jai Jeon

Thesis Advisor: Dr. Douglas W. Bousfield

An Abstract of the Thesis Presented
in Partial Fulfillment of the Requirements for the
Degree of Master of Science
(in Chemical Engineering)
August, 2002

Paper gloss and print gloss have long been the subject of research because of their strong influence on end-use performance such as image clarity, contrast, and resolution. This work focuses on the significance of the structural factors of porous coatings on print gloss development in a systematic way to elucidate the governing mechanisms.

The coating roughness, porosity, and pore size were the three experimental variables. Generation of well defined model coating structures was a challenge and required the appropriate combinations of pigment, binder, and calendering conditions. Calendering techniques with rough substrates (polyester films) were found to produce various rough surfaces without compromising pore structure. Pore structures were controlled during the calendering process by adjusting general calendering parameters. Mercury porosimetry with compressibility corrections was used to evaluate the pore structure of model coatings.

Roughness and porosity affect the print gloss from the start moment of evolution indicating their influence on ink transfer and/or ink-film splitting. Once ink film start to level, roughness and pore size determine the level of print gloss in short time (around 10 sec) after the printing nip, while that of porosity controls the evolution of print gloss in time. The major structural factors exert significant effects on print gloss development independently based on the exclusive relations. The effects of the structural factors are consistent overall though there is mild leveling off in extreme conditions, in which other phenomenon such as splitting pattern may also involve in the print gloss development. Inking amount did increase the print gloss generally but did not alter the trends within a given range. Finally, this work highlights the result of a quantitative systematic response of print gloss for the structural factors. Roughness is found to be the most important factor overall followed by pore size and porosity, respectively. The order of main effects is consistent in the low paper gloss region. However, in the high paper gloss region, pore size becomes more important than others. The results suggest that the similar effects may involve in print gloss mottle and other related properties.

ACKNOWLEDGEMENTS

I would like to express my sincere gratitude to my thesis supervisor Prof. Dr. Bousfield for his generous support, constant guidance and valuable advice throughout this research.

I wish to express my special thanks to Prof. Dr. van Heiningen and Dr. Aspler for the time devoted to reviewing and commenting my thesis.

My special thanks to my company, Hansol Paper Co. and ex-CTO Dr. Woo for facilitating and supporting this study. I would like to thank the sponsors of the Paper Surface Science Program for their support. I wish to extend my appreciation to all the staff and the graduate students of the Chemical Engineering Department for being so helpful and nice. I should specially mention Dr. Xiang, Emily, Charles, and Shirke for their practical helps during my experiments.

I am obliged to Dr. Youn and Dr. Lee for being my admirable seniors. I wish to thank Pastor Kim for caring and praying for my family. I am much obliged to my neighbors and the Korean community for unhesitating help and support. I would like to thank Lee family for numerous helps from the start of my settlement.

I am deeply obliged to my wife Geum Ju Choi for her sacrifice, patience, and belief in me all under the name of her everlasting love. God blessed me with my son Hyun min Jeon, who is all the source of my energy.

I would like finally to dedicate this thesis to my family to whom I owe everything. It would not have been possible to complete this thesis without their love, respect and trust.

TABLE OF CONTENTS

LIST OF TABLES

LIST OF FIGURES

LIST OF SYMBOLS

α	Filtercake resistance [L/M]
δV_{blank}	Total change in mercury volume during a blank run
ε	Void fraction [1]
ε_f	Void fraction of filtercake [1]
ε_{bulk}	Bulk porosity corrected intrusion porosity
ε_{int}	Corrected intrusion porosity
ϕ^1	Porosity at 1 atm pressure[1]
ϕ_s	Volume fraction of solids in the ink [1]
ϕ_f	Volume fraction of solids in the filtercake [1]
γ	Surface tension [M/t^2]
λ	Wavelength of disturbance [L]
λ_i	Wavelength of incident light [L]
λ_p	Wavelength of surface roughness
λ^*_p	Dimensionless group which indicates the shear thinning significance [1]
μ	Ink viscosity [M/Lt]
μ'	Viscosity of filtrate or mobile phase [M/Lt]
θ	Contact angle [1]
ρ	Ink mobile phase density [M/L^3]
ρ_s	Density of solid
σ_a	The arithmetic average roughness [L]
σ	Root mean square roughness [L]
τ	Tortuosity [1]
υ	Open-tube velocity [L/t]
ξ	d_f/d_o [1]
a	Amplitude of surface roughness
A	Coverage function
A_f	Filter area measured perpendicular to the direction of the flow [L^2]
b	Empirical constants for immobilized ink

B	Immobilization function
c	Phase difference
c_s	Solid weight per volume of mobile phase [M/L^3]
CPVC	Critical pigment volume concentration
D_{AB}	Binary diffusion coefficient [L^2/t]
d_o	Initial distance between two circular plates [L]
d_f	Finale distance between two circular plates [L]
f	Split factor, remaining free ink film that splits and stays with the paper [1]
FCC	First critical concentration
g	A factor estimating the proportion of scattered light included in specular reflectance measurements at a given angle
s(i,n)	Fresnel coefficient of specular reflection
h	Ink film shape [L]
h_0	Initial ink film thickness [L]
h_f	Thickness of the filter-cake [L]
h_p	Surface profile of substrate
h_s	Depth of penetration of the ink mobile phase into the substrate [L]
<h>	Average film thickness [1]
i	Incident angle of light
k	Empirical constants for surface smoothness
K_0	Constant of leveling time
K_c	Filtration constant
K_f	Darcy's constant of the ink [L^2]
K_s	Darcy's constant of the substrate [L^2]
k_1	Constant equal to 4.17 in the Carman-Kozeny equation
L	Thickness of cake [L]
MFFT	Minimum film formation temperature [T]
M_{sample}	Mass of the sample [M]
M_{ss}	Solid-phase bulk modulus
n	Refractive index
P	Applied pressure [M/Lt^2]

P^1	Atmosphere [M/Lt^2]
PVC	Pigment volume concentration
ΔP	Overall pressure drop [M/Lt^2]
Q	Filtration constant
r	Pore radius [L]
R	Reflectance
R_0	Initial roughness of the printed substrate [L]
R_a	Arithmetic average roughness [L]
R_q	Relative mean square roughness [L]
R_p	Radius of a circular plate [L]
r_p	Radius of particle [L]
S	Constant inversely proportional to multiple scattering, correlated with the optical roughness
S_0	Specific surface area of particle per volume of solid particle [1/L]
SCC	Second critical concentration
T	Absolute temperature [T]
T_g	Glass transition temperature [T]
t	Time [t]
t_0	Initial time [t]
t_1	The penetration time under pressure in the nip [t]
t_2	The time after the release of the applied pressure [t]
t_{lev}	Leveling time [t]
V	Constant speed of separation of 2 unitary-surface plates [L/t]
$V1_{bulk}$	Bulk volume of the sample at 1 atmosphere pressure [L^3]
V_{abs}	Volume of fluid absorbed by unit area [L]
V_{base}	Volume of base substrate [L^3]
V_c	Velocity of capillary absorption [L/t]
V_d	Penetration velocity by diffusion into the latex matrix [L/t]
V_{int}	Volume intruded into the sample [L^3]
V_{obs}	Observed volume of mercury intruded [L^3]
V_p	Velocity of penetration [L/t]

V_{solids}	Volume of coating solid [L^3]
w	Weights of solids [M]
x	Direction parallel to the substrate surface [L]
x_i	Amount of ink initially on the printing plate
y	Direction perpendicular to the substrate surface [L]
y_i	Amount of ink transferred to the paper
z	Height of surface roughness based on center line [L]
Z_0	Initial height of irregularities at a surface [L]
Z_t	Height of irregularities at a surface at instant *t* [L]

1. INTRODUCTION

Paper gloss and print gloss are important optical qualities for the paper along with brightness. These attributes are the primary quality indicators for the end-use performance of papers. Gloss for rough surfaces like papers was described as a function of surface roughness, refractive index of constituent materials, and the wavelength of light (Chinmayanadan, 1919). Since most of components in coating have similar refractive indexes, one can readily presume that gloss is a function of roughness (Lee, 1974). As like gloss itself, print gloss could be determined by final surface roughness of the ink film on substrates given that ink or ink components has similar refractive indexes too. "No gloss without smoothness", a simple conclusion from Stephan (1990).

However, for understanding print gloss, there are many of different factors and process that we need to consider including printing conditions, ink properties, setting, leveling, shrinkage of ink film, and layering of ink components. Surface roughness of substrates was found to be a limiting factor on 'print gloss' while suggesting that penetration and characteristics of ink gloss itself might be a primary factor in the microroughness region (Oittinen, 1980, 1983). Recently, porosity effect was reported with well-defined pigments system (Donigian, 1997), where larger pore size and lower porosity resulted in higher print gloss. Those results were best explained by considering setting and leveling process after the print nip such that high absorptivity gives shorter time for ink film to be leveled down to produce lower print gloss. Xiang and Bousfield (1998) presented a modified pore absorption model; in which larger pore has slow setting when there is filtercake formation with relatively large resistance. This explained further a relationship between

setting and print gloss. Glatter and Bousfield (1997) described print gloss development by modeling leveling process on rough substrate like papers but not on porous materials. Their dynamic glossmeter allowed investigating initial behavior of print gloss development. Some effects of substrate roughness were explained yet in a theoretical way. Desjumaux and Bousfield (1998) modified and further developed the model based on porous substrate and compared with experimental result. They showed that leveling process was clearly a limiting factor on print gloss such that smaller pores with fast setting or mobile phase removal from ink layer stop the leveling giving less time to level down, in turn, lower print gloss. In this attempt, however, as the effect of roughness was being excluded, the suggested model opens a possibility to be applied on realistic porous and rough substrates as seen in commercial papers.

Throughout these earlier works, even though the primary factors were explained, their combined-competitive influences have never been addressed in a systematic way. Therefore, this work focuses on finding the roles and significances of the involved factors on print gloss development in a systematic way such that the mechanisms behind the phenomenon may be further elucidated and utilized ultimately for the industrial benefits.

A set of model coatings with wide range of parameters was aimed to be generated so as to cover as broad as possible practical range of commercial situation. However, there is not any available information that tells the method to generate controlled coating structure in a systematic way. Consequently, the results of extensive trials will be discussed. The differentiation of the structural factors in terms of roughness, porosity, and pore size is for the first time described in this work. Use of real-time glossmeter gives an investigation of initial gloss development at short times, which is the first to be

reported with respect to structural factors. As an ultimate goal of this project, a novel result on quantitative systematic response of print gloss related to structures is to be presented.

In the following sections, previous findings are reviewed with regard to gloss and print gloss including their factors and various aspects related to setting and leveling process, finalized by some models on leveling. This may give us better understandings and draw out practical implications and prospects for this project in a further practical point of view. Experimental methodologies are allotted to Chapter 2, in which experimental procedures are also described. This chapter will be used to explain all the detailed steps to generate the model samples and characterizations. Experiments are composed of two parts; one is a preliminary experiment, in which major methodologies and potential results are remarked, the other is full-scale experiments and results, these are positioned in Chapter 3 and Chapter 4, respectively. This work finally reaches its conclusions and some important findings and recommendations, which are summarized in Chapter 5.

1.1. Gloss

Gloss together with color, brightness and opacity are critical optical properties of the papers. Gloss is an important optical parameter in evaluation of print quality. The psycho-physiological sensation of gloss is a measure of the surface reflection of light in the specular direction. In contrast, a surface reflecting light in all directions produces a sensation of a 'non-shiny' or matte surface.

The appearance of a surface depends on the way the incident light is reflected, absorbed or transmitted by the surface. Hunter (1936, 1952) tried to characterize gloss and led to the conclusion that at least six different visual criteria exist for ranking gloss:

- specular gloss: perceived brightness associated with the specular reflection from a surface
- contrast gloss: perceived relative brightness of specularly and diffusely reflecting areas
- distinctiveness-of-images gloss: perceived sharpness of images reflected in a surface
- absence-of-bloom gloss (haze): perceived cloudiness in reflections near the specular direction
- sheen: perceived shininess at grazing angles in otherwise matte surfaces
- absence-of-texture gloss: perceived surface smoothness and uniformity.

Harrison (1945) published a review discussing how to measure some of these. He also mentioned binocular luster as another possible effect taking place on some surfaces. He pointed out the need for more research on the correlation between gloss and visual estimations, and mentioned texture as being important for gloss. However, he did not discuss the spatial distribution of gloss on one surface or its quantification. Hunter (1963) later published an overview of methods for evaluating the gloss of ink films.

The facet of 'gloss' most frequently measured is related to the light reflected from a surface in the specular angle. Technically, gloss is the fraction of incident light reflected from the surface at the specular angle equal to the incident angle but rotated 180° and directed away from rather than toward the reflective surface.

As the gloss is the portion of light reflected in the specular direction at an angle equal to the incident angle, high gloss implies a higher fraction of incident light being reflected in the specular direction. Scattering reduces the amount of specularly reflected light, thus reducing gloss. Figure 1.1 illustrates the concept of diffuse and specular reflection, while Figure 1.2 shows the interaction of light with the paper and ink layers (Oittinen, 1988).

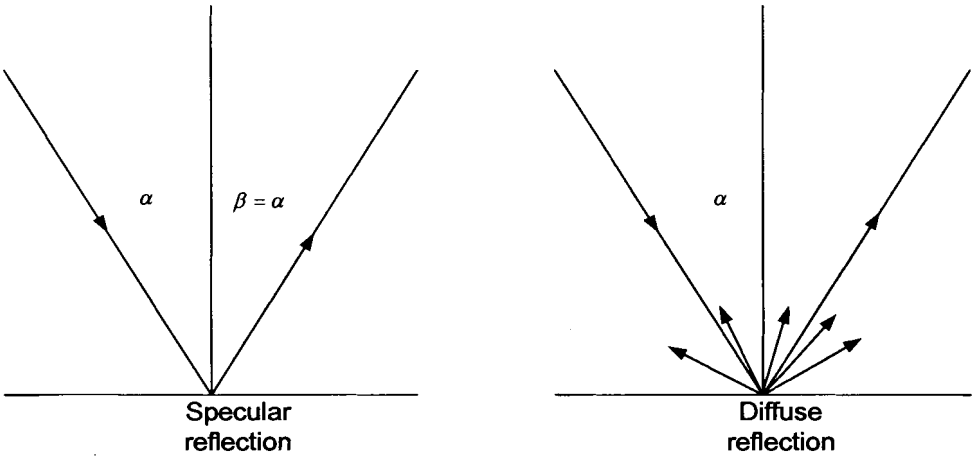

Figure 1.1: Specular (mirror-like) and diffuse reflection (scattering). α: incident angle, β: reflective angle.

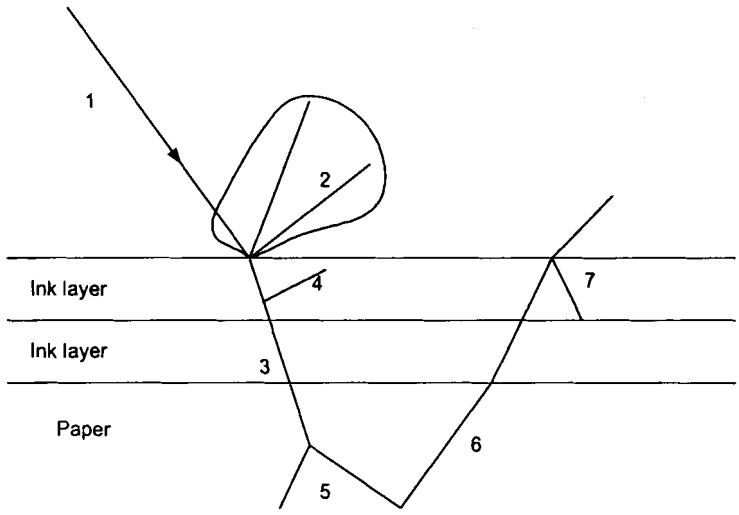

Figure 1.2: The phenomena of light interaction with a print.

where,

① Incident light beam

② Surface reflection distribution

③ Light traveling in the ink layer (absorption)

④ Scattering of light in the ink layer caused by ink opacity

⑤ Scattering of light in the paper causes optical spreading

⑥ Reflection of light from the paper

⑦ Internal surface reflection

The first interaction between the image and the light is the surface reflection from the ink-air interface. Surface reflection from prints has the same spectral composition as the incident light. The unreflected light undergoes refraction in the ink layers. The refractive indices of the various layers determine the amount of surface reflection that can occur. A high refractive index implies a high magnitude of the surface reflected light at any given angle of reflectance. In the ink layer, depending on the color of ink, spectrally selective

light absorption occurs. The refractive indices of inks and paper are approximately the same and hence there is little optical interface between them, which can cause significant surface reflection.

In the paper substrate, light scattering takes place. Scattering is the traveling of light in all directions. A high degree of scattering means that the light penetrates to a smaller depth before backscattering. Scattering also causes random polarization and causes the light to travel sideways into the paper, which causes optical spreading, or an enlarged printed spot. Light scattering and absorption determine the paper opacity. The combined effect of scattering and absorption is that some light reflects from the paper and refracts into the ink layers. At the interface between the topmost ink layer and air, some light undergoes internal surface reflection back into the ink layers. Multiple reflections cause a reduction of light intensity.

There are theories that are designed for one scale of roughness and those that combine large and small-scale variations, treating the contributions from each type of roughness separately. Regardless of the theory used, the properties measured on any surface will depend on the size of the area measured and the resolution at which the measurement was taken (Ogilvy, 1991). Often the correlation length, a measure of the average lateral feature size, and the roughness, a measure of the height variation of a sample will determine which theory can be used. However, neither is an intrinsic surface property. Paper is rough on many scales and it is not always possible to find an applicable theory, especially if the surface statistics vary spatially over the paper sample. The Rayleigh-Rice approximation applies to surfaces with a roughness that is small compared to the wavelength of the incident light, regardless of the correlation length. The Kirchhoff

approximation can be used for surfaces having a large correlation length compared to the wavelength of the incident light, regardless of roughness. However, for surfaces where the correlation length is short and the roughness is large compared with the incident-light wavelength no two-dimensional theory exists to describe properly the surface scattering that occurs (Nieto-Vesperinas, 1991). Therefore, this limits the theoretical gloss approximation for the paper too.

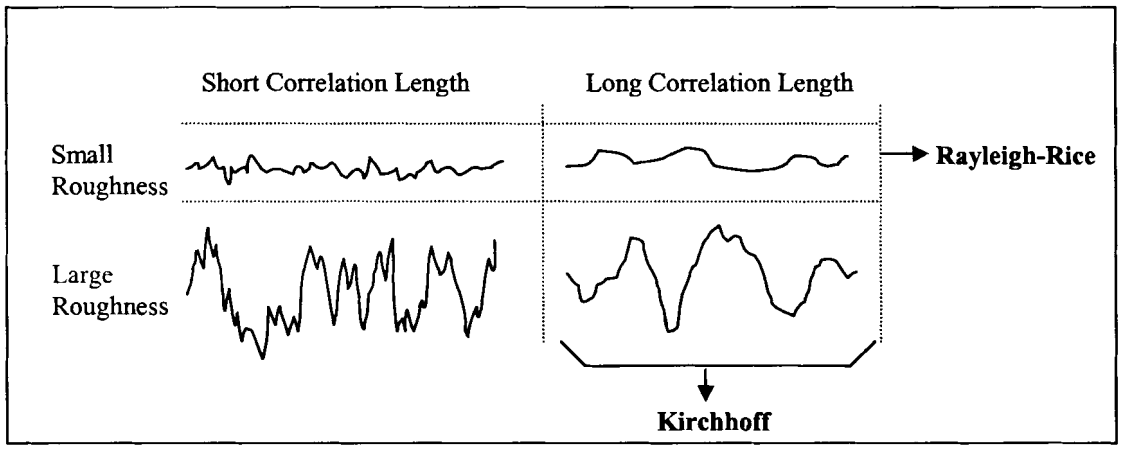

Figure 1.3: Surface having roughness and correlation lengths that are either small or large compared to the incident wavelength. Those are not treated by the same theory.

The index of refraction and the roughness of the substrate are important features. According to Fresnel theory (Moore and Hunter 1941), Eq. (1.1), the specular reflection of an optically smooth surface is supposed to increase with increasing surface refractive index and increasing angle of incident light. Gloss is expected to decrease with increasing diffuse reflectance from the surface and may decrease with increasing radiant energy losses due to transmission through the material, conversion to heat or permanent scattering within the material.

$$s(i,n)=\frac{1}{2}\left[\left(\frac{\cos(i)-\sqrt{n(\lambda_i)^2-\sin^2(i)}}{\cos(i)+\sqrt{n(\lambda_i)^2-\sin^2(i)}}\right)^2+\left(\frac{n(\lambda_i)^2\cos(i)-\sqrt{n(\lambda_i)^2-\sin^2(i)}}{n(\lambda_i)^2\cos(i)+\sqrt{n(\lambda_i)^2-\sin^2(i)}}\right)^2\right] \quad (1.1)$$

where s(i, n) is fresnel coefficient of specular reflection as a function of refractive index n, angle of incident light, i . n(λ) is refractive index and λ_i is effective wavelength of incidnent light.

It is accepted that, if a paper surface is not smooth, some areas locally have orientations that differ from the average plane of the surface. These reflect light at angles differing from the average specular angle, lowering the gloss of the surface. For rough surfaces, Chinmayanandam (1919) has shown that their specular reflection is a function of angle and wave length of incident light as well as surface roughness:

$$I/I_0 = s(i,n)\cdot\exp\left(\left(4\cdot\pi\cdot\sigma\cdot\cos(i)/\lambda_i\right)^2\right) \quad (1.2)$$

where I and I are the specularly reflected and incident light intensities, respectively and σ is the standard deviation of the surface roughness.

Lee (1974) showed that, where coatings were comprised of materials having essentially similar refractive indices, the Tappi gloss of the calendered papers were totally dependent on surface roughness. Lee theoretically related the Tappi gloss units with the incident light angle, the refractive index and the surface roughness as shown in the Eq. (1.3).

$$Tappi\,Gloss = \frac{R_{sample}}{R_{ref}} \cdot 100 = \left[\frac{s(n,i)}{s(1.54,i)}\right].\exp\left[-\left(\frac{4.\pi.\sigma.\cos(i)}{\lambda_i}\right)^2\right] \cdot 100 \qquad (1.3)$$

where σ is the standard deviation of surface roughness about the mean plane of the surface. The Tappi gloss units were based on the scale of 100 units for a polished black glass surface with a refractive index of 1.54 and the effective wavelength, λ_i, equal to 0.55 μm. Figure 1.4 shows the evolution of the Tappi gloss values as a function of the surface roughness parameter, with an angle of incident light of 75°.

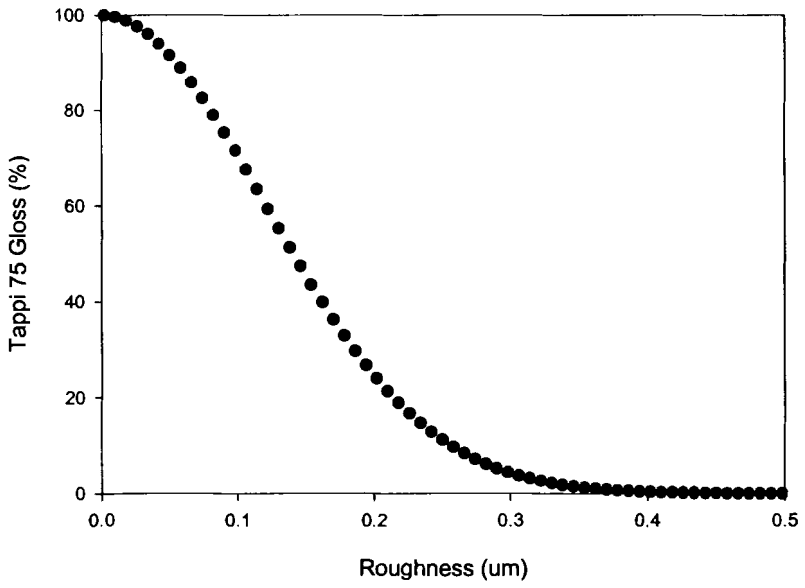

Figure 1.4: Evolution of the Tappi gloss values as a function of the standard deviation of surface roughness about the mean plane of the surface.

1.2. Gloss and Roughness

The contribution of surface roughness to gloss depends on whether the defects are large, features above 10 μm in size, or small, features far below 10 μm, with respect to the

wavelength of incident light. When the root mean square surface roughness is small compared to the wavelength of light, e.g. microscopic roughness, gloss has been found to vary exponentially with the ratio of roughness to the wavelength of light (Bennett and Porteus, 1961; Porteus, 1963).

Gate *et al.* (1973) confirmed experimentally the relationship between the surface micro-texture and Tappi gloss, using both optical and surface profilometry methods to evaluate the roughness of clay coatings prepared on polyester films. They found that the variation in surface roughness was close to a normal distribution with standard deviations on the order of 0.1 μm.

Lee (1974, 1982) elucidated the factors that were responsible for the micro-roughness and reported a quantitative relationship between surface roughness and Tappi gloss. The extent of micro-roughness was found to be related to the pigment particle size distribution, particle shape, binder type, drying temperature and time, pigment wetting, coating hold-out and varying coating weights. More precisely, a greater amount of film shrinkage of binders or "coalescence", e.g. change of volume from the immobilized to the dried film, led to rougher surface. The polymer glass transition temperature T_g controls the degree of shrinkage for latex binders. An improvement in gloss upon calendering has been attributed to smoothing out of the macro-roughness of coated paper and some of the micro-roughness caused by binder shrinkage.

Oittinen (1980) extensively explored the effect of paper roughness on gloss using stylus profilometry. Based on the Davies equation that applied Rayleigh light scattering theory and reflectance measurements to the quantitative characterization of surface roughness and on the Bennett and Porteus equation (1961), Oittinen proposed that two roughness

parameters were required to accurately predict the gloss of paper. The parameters were a Gaussian depth distribution of roughness whose experimental equivalent was the root mean square surface roughness and an auto-correlation function which described the size distribution of roughness. Oittinen did get good correlation between experimental reflectance data and theory by introducing two terms, S and g, to correct for multiple scattering which was affected by the mean square roughness and by the size distribution as shown in Equation (1.4).

$$R = S.e^{-\left(\frac{4.\pi.\sigma_R}{\lambda_i}\right)^2.\cos^2(i)}.(1+g) \qquad (1.4)$$

where R is the reflectance, S, a constant inversely proportional to multiple scattering correlated with the optical roughness, σ_R, the root mean square roughness defined as the root mean square deviation of the surface from the mean surface level, λ_i, the wavelength of incident light, i, the incident angle and g, a factor estimating the proportion of scattered light included in specular reflectance measurements at a given angle.

Specular reflection intensity measurements can partially describe gloss because gloss is a psychophysical phenomenon that depends on the perception of a variety of reflection effects. Settlemeyer (1992) evaluated the topography related to different levels of gloss using a qualitative evaluation of images obtained on a scanning electron microscope (SEM). By changing the magnification, a range of structural features of different sizes could be seen and related to the gloss level of the samples. The images were used to understand differences in surface topography for samples having the same measured

gloss but different assessments of visual gloss. Several examples are discussed but no quantitative data was obtained for the surface topography.

Matsuda *et al* (2000) tried to characterize roughness wavelength features related to gloss and print gloss using a scanning light interferometer. They concluded that surface profile of specific waves with spatial frequencies more than 30 mm^{-1} or 40 mm^{-1} strongly affected sheet gloss of coated paper.

1.3. Origins of the Roughness in Coatings

Each constituent of the coating color, as well as the roughness of the substrates, affects the final roughness of the coating. Researchers have usually preferred to measure gloss rather than roughness. Because it is well accepted that a high roughness results in a low gloss and vice versa, data available about gloss may be used to identify the parameters influencing the coating surface roughness. The fact that gloss data are more important than roughness data is surely due to the difficulties involved in the roughness characterization.

Porosity and surface roughness of base paper are of major importance for the quality of coated paper. There are many of factors which influence roughness and porosity of coated paper: presence of fines, coarseness of fibers, ratio of softwood and hardwood, fiber size and size distribution, filler content effect, formation, precalendering, and so on. The composition of the coating color and the sorption potential of the base paper are crucial. Figure 1.5 shows the relationship between porosity of the base paper and the roughness of coated paper. Figure 1.6 presents the correlation between the roughness of base paper and paper roughness after coating (Lehtinen, 2000).

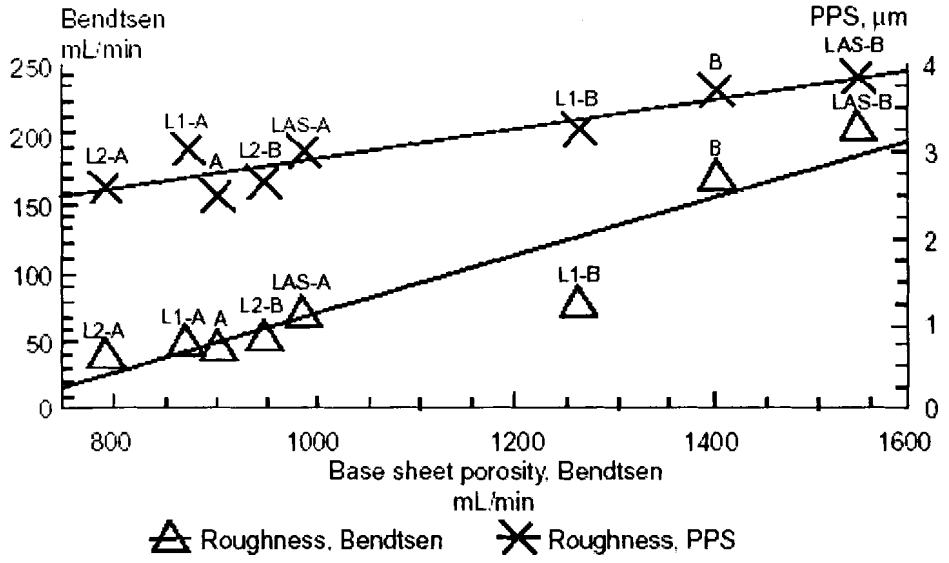

Figure 1.5: Effect of base paper porosity on the bendtsen roughness of the coated sheet. L1 and L2 are precalendering levels, A and B are base papers, and LAS indicates surface treatment of base paper with water. A and B are different industrial base papers. Coat weight: 10 g/m^2 (from Lehtinen, 2000).

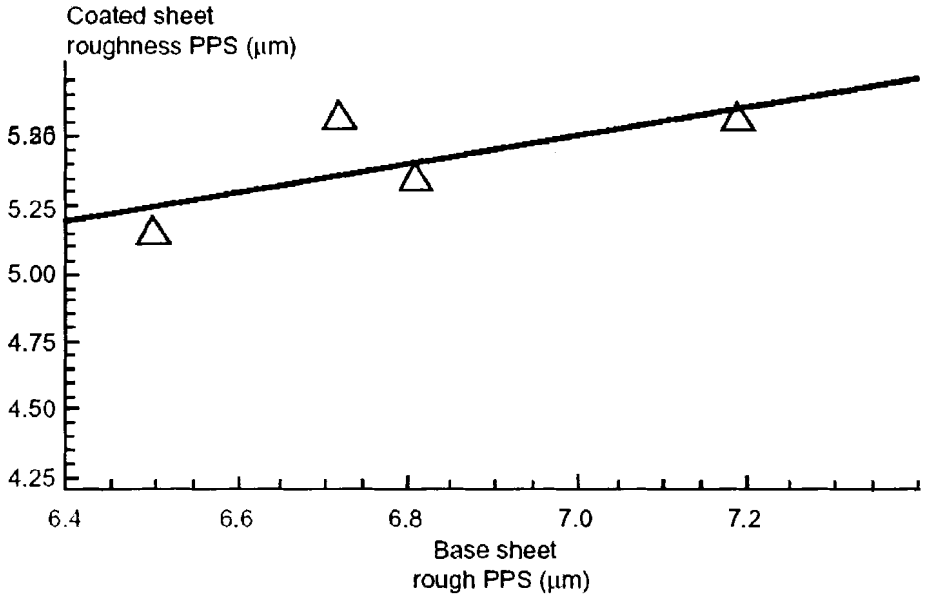

Figure 1.6: The relationship between base paper and coated paper PPS roughness (from Lehtinen, 2000).

Lepoutre *et al* (1982) presented a model to predict the surface roughness of uncalendered coated paper. According to their predictions, the smoothness was optimized when substrate roughness and blade pressure are both minimized and the solids concentration in the coating color is maximized. Huang *et al* (1996) investigated the effect of base-stock absorbency and reported that hydrophobic sizing produced a slight increase in the coat gloss of dense sheets but had no effect on porous sheets even though change in roughness was not observed.

Gloss increases with increasing coating weight and then levels off. The rougher the raw stock, the higher the coat weight to apply to reach the maximum gloss. As the coat weigh increases, surface defects are filled up and the surface becomes smoother. For a certain critical coat weight, all surface defects are leveled and the roughness is then only defined by the coating components and gloss is only a function of the coating formulation (Kent, 1986).

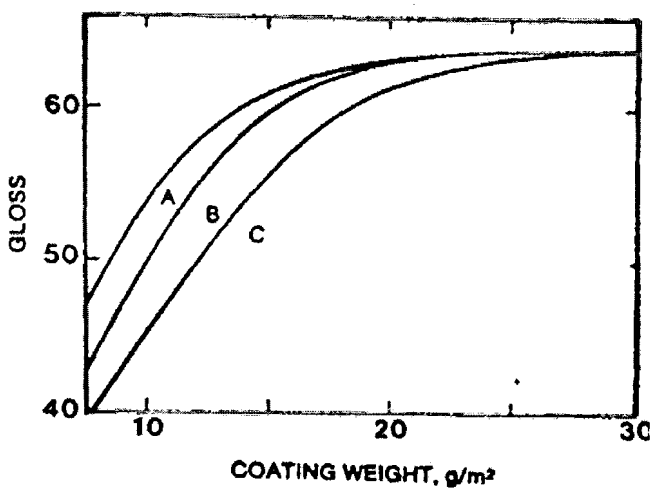

Figure 1.7: Effects of the coat weight on the gloss of coated papers (Kent, 1986).

In order to minimize the effects of the substrate when studying coating gloss, Lee (1974) recommended using a thin smooth polyester film as a substrate because of its wettability, dimensional stability and flexibility. To enhance wetting, he also recommended a thorough cleaning and sometimes the use of a small amount of surfactants.

The fundamental morphological features such as shape, size, and size distribution of pigment particles, are known to affect gloss of coated papers. Sennett *et al* (1967) remarked on the lack of information on the effects of particle shape on surface related properties. One of the major problems in studying effects of particle shapes is that shape can not be changed without affecting other critical properties such as chemical composition, surface nature and charge, and particle size distribution. Eklund (1975) emphasized that pigments differ from one manufacture to another and that production processes are numerous. Even the origins of the raw materials affect the final properties of the pigments. As an example, American clays are more round than English ones. The effects of size and size distribution of pigments on gloss have been well investigated. Alince and Lepoutre (1980) concluded that gloss depends on how the packing of particles affects the smoothness of the surface, and that the shape and the size are fundamental, since the structure is determined by the mutual accommodation of the particles. Based on the fact that higher packing leads to smoother surface, it is easy to understand that high gloss is obtained when using small particles. This has been reported by numerous studies with different kind of pigments. Lee (1974) used spherical polystyrene (PS) spheres and clay and showed that clay gives a higher gloss than PS spheres at a given pigment size. Lee suggested that the platelike shape of the clay may explain this difference but that the size distribution of the clay particles must also be taken into consideration.

Many times, the fact that platelike particles act like mirrors and reflect more light has been quoted as the explanation of the higher gloss development. However, this statement is the subject of controversy. Gate *et al* (1973) showed that clay plate particle orientation was not related to Tappi gloss measurements. To the contrary, Gane *et al* (1995) claimed that there is a distinct correlation between pigment particle orientation and gloss. In both cases, the orientation of the particles was measured using X-ray diffraction techniques. Different researchers stressed the role of the particle size distribution. All of them agree to say that smaller size particles enhance gloss and lower roughness since they increase the packing of particles by filling the void spaces (Lee, 1974, Eklund D., 1975, Alince *et al*, 1980).

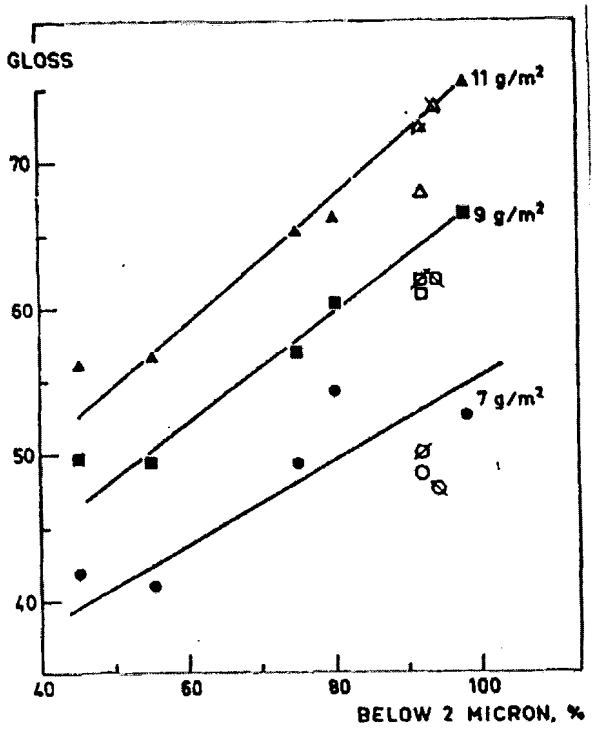

Figure 1.8: Effect of the particle size distribution of pigments on gloss of the coating (Eklund D., 1975).

Crawshaw *et al* (1982) presented a study on the influence of pigment shape on the performance of coated papers. They blended clay with separately scalenohedral PCC (calcite), prismatic PCC (calcite) and Acicular PCC (aragonite) but the size of the particles varied from one pigment to the other. Rosette-like scalenohedral pigments gave the lower gloss, but the large size of the particles must be considered. PCC prisms presented a higher gloss than PCC acicular particles.

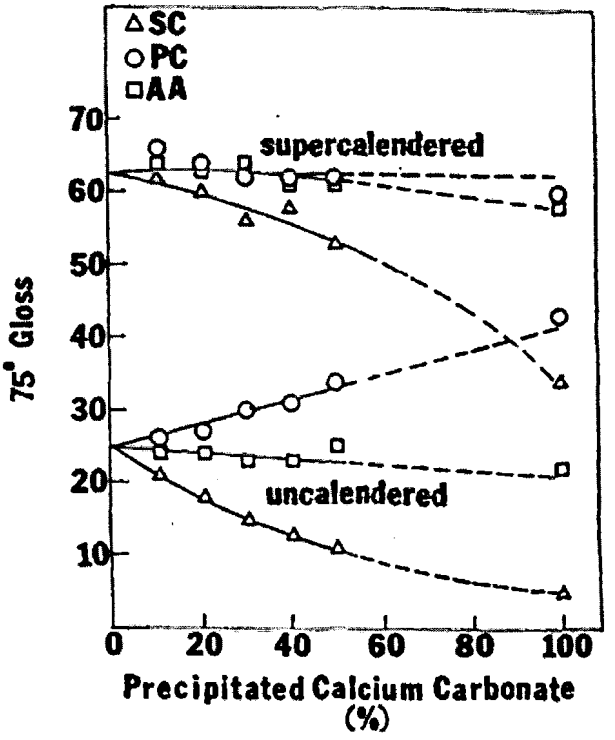

Figure 1.9: Tappi gloss of blend of clay respectively with PCC scalenohedral particles (SC), prisms (PC), and acicular particles (AA) (Crawshaw *et al*, 1982).

Pesenti (1996) investigated the gloss and surface microstructure of coatings made from 12 pigments of various different shapes. He found a good theoretical TAPPI gloss-roughness relationship fitting for every pigment except clay (Figure 1.10). All the

pigments of which shapes were close to the value of unity fit the same TAPPI gloss-ESD (equivalent sphere diameter) curve (Figure 1.11).

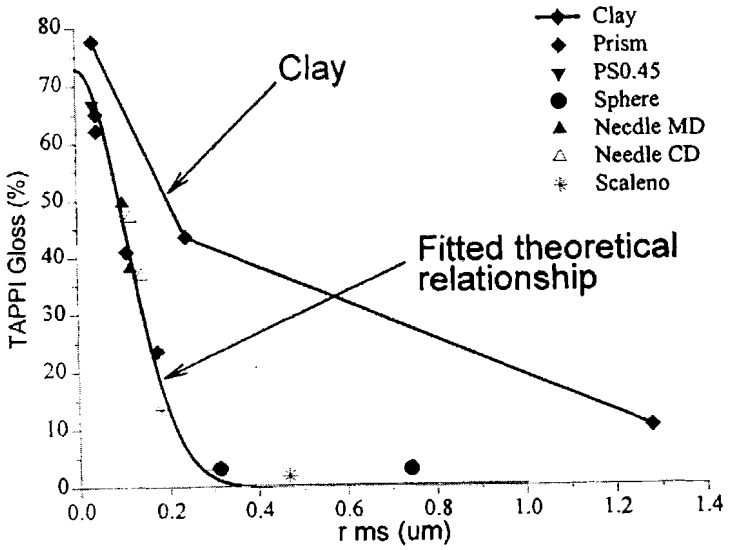

Figure 1.10: Experimental relationship between Tappi gloss and rms roughness (Pesenti, 1966).

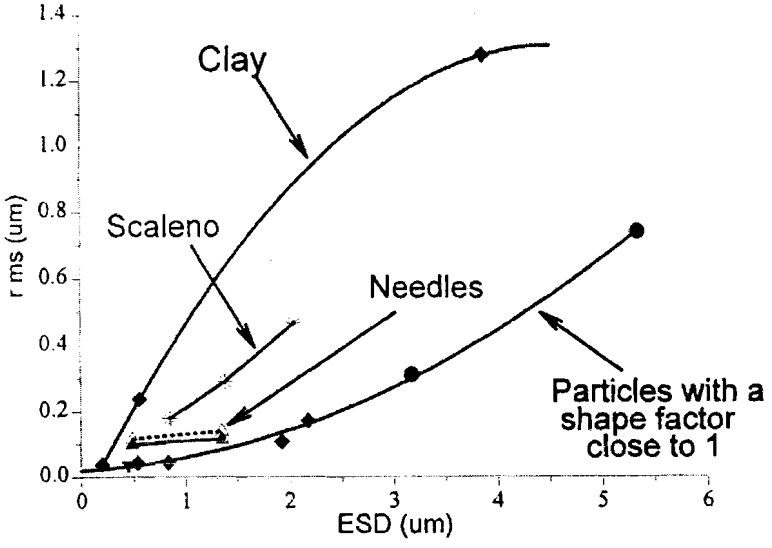

Figure 1.11: Tappi gloss as a function of equivalent spherical diameter (ESD) (Pesenti, 1996).

Lohmander (2000) reported that the influence of pigment particle shape factor on the gloss to be not large compared to particle size. Fundamental data on the relationship between gloss and shape of pigment particles are still lack, however, it is commonly accepted that gloss and roughness are affected by the packing of the particles.

The influence of binders on gloss of coatings was extensively studied by Lee (1974). Lee claimed that gloss is affected by the surface roughness which is ruled by the shrinkage of the coating layer. This shrinkage would be due to the behavior of binders which generates a non-uniform shrinkage in heterogeneous coating systems during drying. Lee found that gloss was decreased by increasing the binder level, and that gloss development was better with styrene-butadiene latex than with natural binders as shown in Figure 1.12. He advanced the idea that for starch the low gloss is due to shrinkage, which may be related to the swelling of the macromolecules when they are in contact with water.

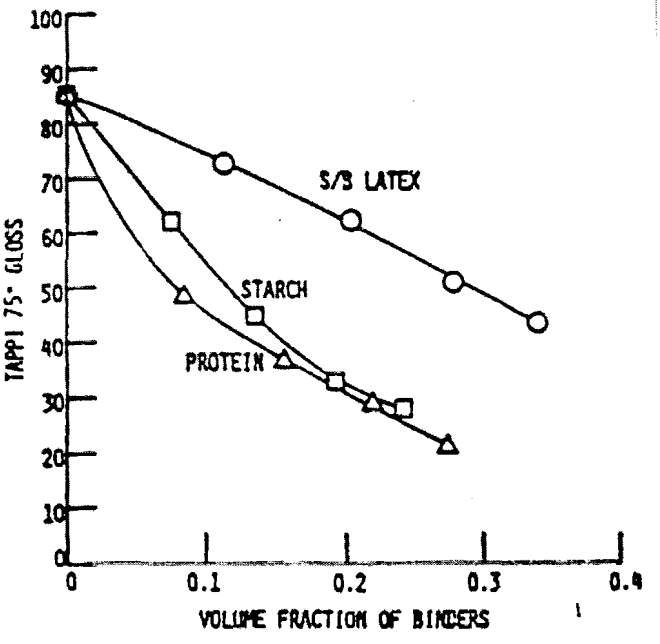

Figure 1.12: Influence of the binder type on gloss. Natural binders develop lower gloss than SB latexes (Lee, 1974).

Watanabe and Lepoutre (1982) measured coating shrinkage and published the first results which related shrinkage and the decrease of the gloss. More details are described later. Coating shrinkage was calculated as defined in Equation 1.5:

$$Shrinkage = \frac{thickness.at.FCC - final.thickness}{final.thickness} \tag{1.5}$$

For latexes, it is the film formation process which occurs during dewatering which is the key to the shrinkage phenomenon. This shrinkage is related to the glass transition temperature (Tg) or the minimum film formation temperature (MFFT). If the drying temperature is higher than the latex Tg, the latex particles are soft and deform under the capillary forces which occur during the dewatering process. Watanabe and Lepoutre (1982) showed that it is possible to limit the extent of the coating shrinkage using hard latex particles (Tg higher than the drying temperature) which do not deform during dewatering. Because coalescence of the latex particles is the key to the binding strengths of the coating, film formation may be obtained with a post treatment exposing the consolidated coating to high temperature. Thus, both gloss and binding strengths may be achieved. However, such a post treatment is very limiting. In a later study, Lee (1982) used these two facts and reached the idea of composite latex. Composite latex, made of a soft polymer phase which ensures adhesion and binding strength, and a hard polymer phase which limits the extent of latex particle deformation, appears to be a good combination. The gloss and surface roughening are then dependent on the temperature.

Coating gloss was found to decrease with increasing destabilization of the coating colors which is a colloidal suspension. Hemstock (1968) reported that the gloss of clay coatings reached a maximum at the point of optimum defloculation and then decreases with further addition of defloculant. This result must come from a poor packing of particles into a coating layer.

1.4. Gloss and Roughness Measurement

In order to characterize surface profile of coated paper, several testing methods have been developed and well documented in the literature (Thomas, 1999, Singh *et al*, 1991, Wygant *et al*, 1995). These instruments can be classified into several categories (Casey, 1981). The first category is air leak methods, which include Bekk (Bekk, 1932), Sheffield (Lashof *et al*, 1960), and Parker Print-Surf type (Parker, 1981). The second category is a method of measuring an optical contact area of a paper surface with a glass plate surface, which is known as the Chapman tester (Chapman, 1955). However, it was understood that the air leak type gave roughness of coated paper surface as a total volume, and the optical contact type showed it as a distribution of depth in roughness. The final category is a method for measuring roughness using profilometry. Stylus profilometry, optical profilometry, laser microscopy, electron microscopy, and so on have been applied for this purpose. Stylus profilometry was originally developed for the evaluation of very smooth surfaces in the metal industry and was later adopted in many other fields including paper surfaces. Apparently, Barber (1953) was the first to apply this method and a number of workers have reported high correlations with the performance of paper in actual printing operation (Roehr, 1955, Gate *et al*, 1973, Ginman *et al*, 1974, Fetsko *et al*, 1974, Kapoor,

1977, Aschan *et al*, 1986, Stout 1981). However, it is cautioned to use stylus profilometry because the size of the stylus tip is not a negligible parameter when micro-roughness is determined. It is also reported that stylus profilometry tends to deform the surface of such a soft specimen as paper from the contact of a stylus tip with paper (Murakami, 1973, Wagberg *et al*, 1993, Enomae, 1994). Enomae (1995) investigated this marking behavior and suggested that one may avoid this marking by careful choice of stylus radius and load conditions for the particular surface, although elastic deformations can still occur. Recently, Atomic Force Microscopy (AFM) has been applied to pulp and paper samples (Bassemir, 1994). It has excellent vertical and lateral resolution, but its measurement area is often too small and it also takes a long time form measurement. Optical profilometry is a method of utilizing variations in reflectance of visible light at each spot on a paper (Lipshitz *et al*, 1990). A shadow image when light is irradiated on a paper surface reflects the surface roughness. Analyses of geometrical surface features from these images were studied (Katsura, 1985). Laser microscopy is one type of optical profilometry with the advantage of permitting application to samples containing water, although it takes a long time for measurement. Lipshitz *et al* (1990) used their own laser profiling system to obtain the topography of different coated samples to identify topographical statistics that related to the gloss level of the samples. Confocal Laser Scanning Microscopy (CLSM) was applied to paper surface topography characterization related to gloss and gloss variation (MacGreger *et al*, 1990) and this technique is well documented by Béland *et al* (1995). In electron microscopy, Scanning Electron Microscopy (SEM) is also usually used for profilometry (Enomae, 1993). For example, stereo SEM method is a representative one applied conventionally (Wakebe, 1986) and provides visual spatial

images that are easy to understand. However, its quantitative analysis is time-consuming, lacking in resolution in height direction. Béland (1997) summarized some attributes of various measuring techniques including SEM, AFM, and CLSM throughout a review. Another type of optical profilometer is a Scanning White-Light Interferometer (SWLI), of which principle is based on the measurement of interference fringe variations to construct surface profiles without contacting the surface. However, Béland (2001) claimed that this technique may have difficulties in imaging large slopes and some rough samples can cause problems in the interferometer.

1.5. Coating Structure

Watanabe and Lepoutre (1982) contributed a great elucidation on structuring that during the drying of the coating, the coating structure undergoes through three phases separated by two critical steps, the First and Second Critical Concentrations (FCC and SCC, respectively). This work constituted a breakthrough in the understanding of the coating structure development. At the FCC, a network is formed and particle motion is greatly restricted. The water air interface recedes into the surface capillaries, creating a capillary pressure that causes shrinkage of the network until the SCC is reached, at which point the network is fixed and air enters the rigid structure. The FCC occurs when the gloss drops sharply and the SCC when the opacity sharply increases. An illustration of the FCC and the SCC is presented in Figure 1.13 which also presents the three phases of the dewatering and the evolution of the thickness of the coating layer. The explanation of the drop in gloss after the FCC is illustrated in Figure 1.14.

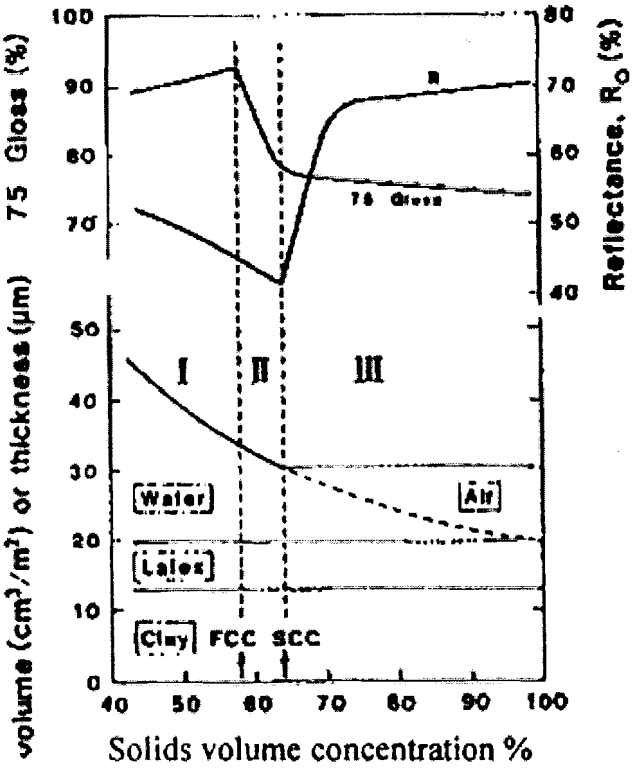

Figure 1.13: Definition of the FCC and the SCC from the gloss and the opacity of the coating during drying (Watanabe and Lepoutre, 1982).

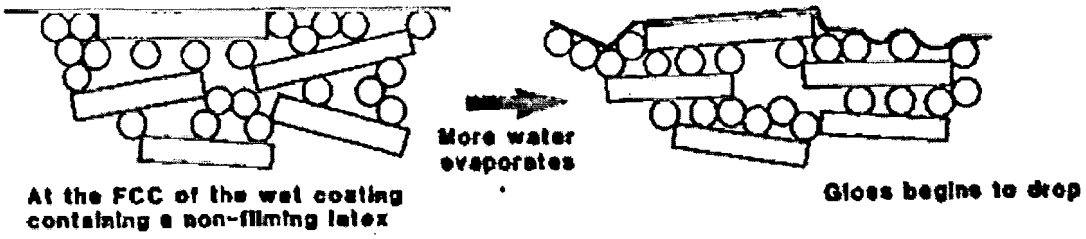

Figure 1.14: Illustrations of the coating structure at the FCC and of the drop of gloss just after it. The drop in gloss after the FCC is due to the breaking of the uniform water line to a rough surface (Watanabe and Lepoutre, 1982).

1.6. Pore Structure Measurements

Air permeability uses literally flow of air through a paper sheet. There are several different devices; Parker Print-Surf, Gurley porometers and Sheffield device. Because of extremely long measurement times, Gurley instruments are generally not suitable for coated papers. Oil porosimetry method can be conveniently used to measure total porosity of paper sheet (Lepoutre 1977, 1978). Stain imbibition is also used to be applied to evaluate porosity related to end-use performance. Arai *et al* (1997) used mercury porosimetry to get an inner structure of coating and SEM for surface pore structure. They reported better correlation between pore characteristics from the surface and print gloss for the case of cast-coated papers. Davis (1989) criticized some artifacts from mercury porosimetry and suggested a novel technique, which use Nuclear Magnetic Resonance (NMR). According to their claims, NMR method was non-destructive, didn't require the sample to be dried state, and didn't need assumption of pore shape. Mercury porosimetry is one of the most widely used methods to access pore size distribution. In fact, the keyword of porosimetry hit the overwhelming number of references. In Wygant's review (1995), it was cautioned to interpret a mean pore radius because the calculated value is typically influenced more by the larger base-stock pores and the system and sample elasticities.

Recently, Abrams *et al* (1996) reported on the correction of high pressure mercury (Hg) porosimetry. They noted that the decrease in volume of the sample and pores as pressure goes up is linear with increasing pressure, which is typical of the behavior of solids in the elastic compressibility region. Then they claimed the slope to be equal to the bulk compressibility modulus and the compressible volume as an artifact of the measurement.

Subsequently, the compressibility volume from the slope was subtracted from the intrusion data. However, this method seems not distinguish or explain the contributions of each component inside to compressibility. Gane *et al* (1996) also presented a paper related to pore structure of compressible coating structure. The difference from Abrams' work was rather clearer procedures to account for each compression contributions though there were still some assumptions. Their final correction equation is presented in Equation 1.6, which was adopted and used for actual correction in this work.

$$V_{\text{int}} = V_{obs} - \delta V_{blank} + \left[0.175\left(V^{1}{}_{bulk}\right)\cdot\log\left(1+\frac{P}{1820}\right)\right] - V^{1}{}_{bulk}\left(1-\phi^{1}\right)\cdot\left(1-\exp\left[\left(\frac{P^{1}-P}{M_{ss}}\right)\right]\right) \quad (1.6)$$

where,

V_{int}; volume intruded into the sample,

V_{obs}; observed volume of mercury intruded,

δV_{blank}; total change in mercury volume during a blank run,

$V1_{bulk}$; bulk volume of the sample at 1 atmosphere pressure,

P; applied pressure,

Φ^{1};porosity at 1 atm pressure,

P^{1}; atmosphere,

M_{ss}; solid-phase bulk modulus.

1.7. Print Gloss and Factors

The final print gloss is routinely measured. Gloss development has been studied for a number of years (Fetsko and Zettlemoyer, 1962; Oittinen, 1983; Micale *et al.*, 1983). However, the mechanisms behind gloss development are not well understood (Aspler and

Lepoutre, 1991) and a fundamental understanding of the factors that influence print gloss dynamics is not reported well in the literature. Figure 1.15 is an exemplary interrelationship on print gloss (Enomae, 2000) to show the complexity though the relationship is probably not complete.

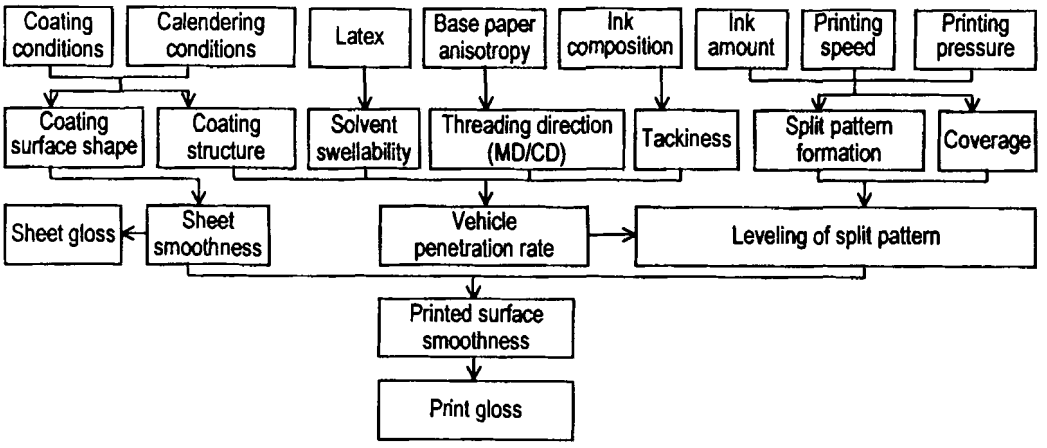

Figure 1.15: Interrelationship between factors affecting print gloss of coated paper (Enomae, 2000).

Fetsko and Zettlemoyer (1962) reported the gloss of printed films as a function of time for coated and uncoated papers. Due to equipment limitations, gloss could not be obtained during the first 10 or 20 seconds after printing. Suzuki *et al.* (1996) showed that the ink setting rate had a significant effect on print gloss in the first minute after printing. Glatter and Bousfield (1996) and Glatter (1996) reported the print gloss changes in time immediately following the printing nip and investigated the influence of the printing speed and the ink film thickness on the rate of gloss development when printing on a plastic film. They found that high printing speeds along with high ink levels produced many defects with a wide range of length scales. The fine scale defects leveled rapidly

while the large scale defects leveled slowly. That caused a rapid increase in ink gloss, at short times, due to the leveling of the fine scale defects and a lower level of ink gloss, at longer times, compared to slower printing speeds or thinner ink films.

Print gloss is a complex function of the ink composition and the ink film roughness. Considering the index of refraction as constant, the print gloss was only a function of the roughness of the ink film that depended by either the roughness of the substrate or the leveling characteristics of the ink film. Fetsko and Zettlemoyer (1962) and Oittinen (1980) proposed an explanation why print gloss increased with increased gloss of the coating depending on the amount of ink transferred. Oittinen (1980, 1983) suggested that the surface of a coated paper had two roughness components, a micro-roughness and a macro-roughness. The micro-roughness was found to be primarily determined by parameters related to the coating such as pigment particle size and distribution, particle shape, colloidal interactions, binder level and thermoplasticity, film shrinkage, drying temperature and time, pigment wetting, coating holdout and varying coating weights. The macro-roughness was found to be determined by parameters related to the base stock such as poor fiber dispersion, ionic destabilization or flocculation, roughness of base paper and insufficient coating or calendering. The disappearance of the macro-roughness and as much of the micro-roughness as possible produced high gloss. According to this view, filling the volumetric roughness of the surface with ink could only lead to increased gloss since ink promoted print gloss by providing a surface with a higher refractive index than paper, enhancing the smoothness of rough paper by filling any depressions, decreasing the diffuse component and increasing the specular component of reflectance. As a result, the print gloss was known to increase with ink film thickness. In fact, print

gloss was found to decrease again at higher inking level since a split pattern was appearing in the ink film.

Zang and Aspler (1994) found that, at low ink levels, the print gloss was mainly influenced by the gloss (or smoothness) of the coatings. At higher ink levels, the print gloss was found to be primarily affected by the micro-roughness (or gloss) of the ink film, which in turn depended on filament patterns produced during ink splitting and on absorbency of the coatings. They found that the lower ink transfer to the less absorbent coatings was not due to reduced ink immobilization but rather to a more pronounced asymmetric splitting of the non-immobilized free inks. They suggested that the transfer of ink to coated papers was primarily influenced by the tack build-up of a thin ink layer near the coating surface due to preferential sorption of the ink solvent. As a result, they suggested that print gloss might increase with coating gloss and decreased with coating absorbency depending on the amount of ink transferred.

In spite of several studies on ink and coating gloss development, the mechanisms controlling the process are not established well (Aspler *et al*, 1991). A study of the dependence of ink gloss development on ink absorption revealed that immediately after the nip printing event, the rate of leveling of the ink layer defects, their magnitudes, the printing speed and ink film thickness affected the gloss development. Print gloss increases over time as the defects leveled out, with the larger defects, which were produced by thick inks, leveling slowly (Glatter *et al*, 1996). Another study found that the coating absorbency, which affects the ink film contribution to gloss, to be strongly dependent on coating pigment size, pigment surface area, and binder content. The sizes of the coating pores were found to be proportional to the pigment pore diameters, while the

number of pores was inversely dependent on the binder content. The smaller pigments produced narrower pores; faster ink setting, and lower print gloss. It was concluded that very small coating pigments may produce high paper gloss but low print gloss (Donigian, 1997).

The gloss of a paint film was found to decrease rapidly around the CPVC. Inks are usually formulated at PVC below the CPVC so that they would have a high intrinsic gloss potential. In the case where ink solvent removal takes place, the PVC might raise to a value near or above the CPVC, reducing the final gloss. The final PVC in the ink film, that controls the final print gloss, depends on the balance between the rate of absorption of the fluid phase into the coating and the rate at which the viscosity increases as a result of the loss of solvent and oxidative polymerization of the binder. Aspler and Lepoutre (1991) quoted that overall ink-paper interactions reflected a subtle combination of pore size effects and binder-ink chemistry. Current researches agree that excessive ink solvent absorption can strongly reduce print gloss. Hecklau and Pavol (1967) discussed the circumstances under which vehicle penetration was more important in gloss control than paper coating smoothness. Weber (1960) found that print gloss together with ink hold out reached a maximum when the ratio of binder to pigment corresponded to the critical pigment volume concentration.

The void fraction of coated papers ranges from 0.2 to 0.4. Ranger (1983) listed values of pore diameters ranging from 0.02 to 0.48 um. A low value of the pore size has been found to give a low value of pore volume (Climpson and Taylor, 1976). Certain coating pores, competing with the ink pigment for the ink vehicle, were found to pull the ink binder into the paper coating to create binder menisci between ink pigment particles,

reducing then the flatness of the ink film surface and its specular reflectance or gloss (Aspler and Lepoutre, 1991; Zang and Aspler, 1994). However, Aspler and Lepoutre (1991) and Lepoutre and De Grâce (1978) still suggested that coating absorbency (and porosity measurements) were poor predictors of print gloss. Lepoutre and De Grâce (1978) could not observe any correlation between the K&N index or the oil absorption rate test and the print gloss on coatings on polyester. Lepoutre *et al.* (1979) observed a drop in print gloss on cast coated paper, e.g. smooth but absorbent substrate, when the K&N absorbency was increased by decreasing the binder content. Ishley and Osterhuber (1990) could not find any correlation between Gurley air permeability (indirect measurement of porosity) and print gloss.

Donigian *et al.* (1997) found that coating absorbency profoundly influenced print gloss in the case of coated papers containing $CaCO_3$ pigments printed with heat-set or sheet-fed inks. Very fine coating particles produced high pigment surface area and very fine coating pores that greatly reduced print gloss. They showed that print gloss was a strong function of the number and the size of the pores in the coating. They concluded that increased total pore volume and decreased average pore diameter caused both faster ink setting and lower 'print snap', e.g. the difference between the print gloss and the initial paper gloss. Higher print gloss correlated with lower ink tack build-up after printing. They concluded that very fine coating pores with high pigment surface area and high capillary force were more effective at pulling solvent from the setting ink film. They suggested that a rapid ink solvent removal was likely to prevent the filaments produced in the nip from leveling or to cause the ink film to shrink forcing the coated surface to buckle in response.

Arai and Nojima (1997) attempted to approach an ideal coating structure for obtaining maximum print gloss by analyzing the coating structure of high gloss sheets such as cast-coated papers. Using mercury porosimetry, oil absorbency and surface analysis with SEM, they found that some cast-coated papers had very different surface pore structures from the middle to the bottom of the coated layer. Surface coating pore structure rather than inner pore structure influenced the print gloss. The authors concluded that coated papers with small pores on the surface and a large internal pore volume produced higher print gloss.

Some solvents used in printing inks are capable of dissolving or swelling polymer films contained in the coatings, affecting ink setting and print gloss. This aspect is not addressed by the capillary sorption approach. Earlier works showed that the amount of ink solvent absorbed and the linear increase or "swelling" of the latex film in the ink solvent depended on the latex polymer and showed correlation to the ink setting behavior of the coating.

Hayes (1994) reported that an increased gel content and acrylonitrile level of a binder increases print gloss. Reducing the particle size of a latex binder generally increases ink gloss due to a decrease in the porosity of the paper. Ink setting is known to be governed by the degree of cross-linking or 'gel content' of latex polymers that can be independently controlled by varying the concentration of chain transfer agents in the case of styrene butadiene polymers. Lee (1982) and Lee and Hendershot (1986) found that styrene butadiene latices promoted high gloss in paper coatings and low glossing variants. They observed that a large latex particle size or a large glass transition temperature of the latex increased ink absorption. Lee and Hendershot (1988) introduced styrene butadiene

latices capable of supplying low sheet gloss with excellent print characteristics. A binder with a high level of polymerized carboxylic acid was found to induce significant shrinkage upon drying with formation of micro-roughness and consequently low gloss. However, calendering retained sufficient roughness while improving printing properties, a high print snap was thus produced. Riley *et al.* (1993) reported that, at a given latex particle size and carboxylation level, an increasing S/B ratio resulted in a decrease in ink hold-out properties in coated paper. However, increasing the styrene levels of the latex was found to increase the coating gloss and the porosity. That is the reason why polystyrene latices are used when high gloss development is required.

Vehicle penetration into the substrate may be minimized by proper ink formulation. Aspler *et al.* (1991) showed that in the case where the vehicle oils contained a dissolved polymer which contributed to the final gloss and the abrasion / rub resistance of the ink film on the substrate, it remained close to the sheet surface. According to Apps (1964), hard resins such as rosin-modified phenolics and rosin-modified maleics were very important in the production of high gloss inks. Fairfield (1960) reported that, to promote gloss, rosin-modified phenolic resins must have had a high molecular weight composed principally of rings joined together and adequate drying oil solubility. Williams (1971) suggested that readily measurable physical characteristics of hard synthetic resins were only of limited value in predicting performance.

In the offset process or in water-based flexography or gravure, interactions between water and paper are known to cause an increase in macro-roughness that lowers print gloss, particularly in the case of on the heat-set offset printing of paper and increase non uniform print gloss and 'linting', e.g. pulling fibers from uncoated stock. Béland *et al.*

(1992) monitored fiber rise by the loss in gloss for a surface. Moisture rather than heat has been suggested to have the greatest effect on the increase of macro-roughness of the printing. Hruzewicz (1990) suggested that multi-color water-based gravure printing would have given similar problems. Film wrinkling or cratering during drying, inappropriate use of waxes (waxes may recrystallize into large particles at the ink surface and ruin film smoothness), use of some paste driers reduced print gloss by increasing surface roughness. Apps (1964) showed that forced dry heat or infra-red radiation could reduce print gloss by promoting ink penetration into the paper. Hachey *et al.* (1994) published scanning electron microscope micro-graphs showing that the oven drying step in offset printing might cause a paper surface roughening and a loss in gloss.

Ink rheology affects strongly print gloss since it influences the ink film splitting in the nip and the ability of the ink to level before drying. Bassemir (1976), by applying the Patton's equation to inks, concluded that rheologically, the most ideal structure would be that of a gel which, upon application of high shear, would flow readily and would retain some flow for a few seconds after transfer to the substrate in order to promote leveling.

1.8. Gloss Variation

The average specular reflection intensity or gloss has been routinely measured for years using conventional gloss meters, however very sparse on gloss variations. Most published results on the measurement of gloss variation are based on some form of electro-mechanical scanning device (Bryntse, 1981, Gunning *et al*, 1976, Parsons *et al*, 1978, Leekley *et al*, 1975, Fujiwara *et al*, 1990). These reflectance measurements were made on discrete spots or lines on the paper surface, with the spot size varying from 10 μm to 900

μm and incidence angles varying mainly between 60°and 75°. Oittinen *et al* (1990) presented work on 45°-incidence micro-scale gloss of printed and unprinted lightweight coated (LWC) papers. They used a linear array camera to measure the reflection intensity from very small areas (15 μm×15 μm), the first time that specular reflection measurements were reported at this resolution. Lindstrand (1996) developed a method to evaluate gloss variation by scanning a sample mounted on a cylindrical holder. The reflection intensity was followed as the sample was rotated on the cylinder.

Image analysis measurements of the gloss variation, a critical factor affecting the appearance of the print, has been shown to relate to the subjective ranking of gloss uniformity. The gloss level and its spatial distribution have been found to affect the subjective ranking of gloss uniformity. A laser scanning microscope has been successfully used to correlate the topographical measurements of a printed paper with its gloss variation (MacGregor and Johansson, 1990). The relationship between the topography of the substrate and the gloss variation merits further investigation (Béland and Mattson, 1996). Béland *et al.* (1998) suggested that the roughness measurements as well as the gloss uniformity investigation were not intrinsic properties of the paper and depended on the equipment configuration like the spatial wavelengths. Beland (2001) summarized the factors affecting gloss variation:

- illumination conditions: light source, light wavelength, light intensity, incident angle;
- sample parameters: surface roughness, paper grade, coating type, ink type, printing method;

- detection conditions: detector type, detector angle, acceptance angle of the detection system, image resolution.

1.9. Phenomena in the Printing Nip and the Ink Tack

The process by which the ink leaves the press is referred to as "ink transfer". In the simple case of a single color process, the ink is transferred from the plate or the rubber blanket to the paper concurrently with a partial drainage of vehicle into the pores of the paper. With respect to ink transfer, an asymmetric pressure is formed as the paper passes through the printing nip and the ink is subjected to hydraulic impression forces into the surface pores of the paper coating. Walker and Fetsko (1955) modeled ink transfer from printing plate or blanket to virgin paper in three steps; contact and adhesion between ink film and paper, immobilization of a portion of the ink into the paper surface, and remaining free-ink film splitting. They considered that there was incomplete contact at low ink levels and that there was insufficient ink to satisfy the ink-immobilizing capacity of paper. In addition they suggested that the non-immobilized free ink between the plate and the paper surface could be divided with any constant fraction, depending on the ink-paper-press interaction. Based on these assumptions, following empirical equation was proposed:

$$y_i = A[bB + f(x_i - bB) \tag{1.7}$$

where, y_i is amount of ink transferred to paper, x_i is amount of ink on plate, A is the coverage function $A= (1-e^{-kx_i})$, B is the immobilization function $B=(1-e^{-x_i/b})$, and k, b and

f are empirical constants that need to be found by printing trials. This equation or its simplified model, Eg. (1.8), at complete contact condition has been widely used to interpret ink transfer phenomena in 'single' color printing.

$$y_i = b + f(x_i - b) \tag{1.8}$$

Later on, many modified models on this equation have been proposed by other researchers (Karttunen *et al*, 1971; Bery, 1978; Yamazaki, 1991; Zang, 1992) to better interpret the ink-paper interaction during printing. Mangin et al (1981) did a critical review on major ink transfer models and found that all were able to fit certain experimental data, but none of them accurately described the physical phenomena involved in ink transfer. Zang (1992, 1993) suggested a model taking into account the dependence of *f* to the ink film thickness and the characteristics of the blanket. The modified Walker-Fetsko model with a new splitting function not only fitted the experimental well but also yielded realistic ink-transfer parameter. Lepoutre *et al.* (1979) measured ink transfer to model clay and $CaCO_3$ coatings on a laboratory press. They found the splitting factor, *f*, to be close to 0.5 indicating that the amount of residual free ink split evenly between the paper and the plate. The immobilization factor *b* was found to be independent on coating void fraction: it was suggested that for coated papers, the ink was solely immobilized in the surface voids of the coating but did not penetrate by pressure penetration or capillary sorption in the nip. De Grâce and Mangin (1988) proved that *f* depended on the ink film thickness on the blanket and showed that the film rarely split evenly between the plate and the paper. They observed that less than half the

available ink transferred to the paper, under normal printing conditions. De Grâce and Mangin (1984) showed that an extremely low surface energy surface material such as polytetrafluoroethylene, called 'teflon', could accept ink: they concluded that the transfer was not affected by the surface energy of the substrate in the case of a monochrome process but more likely by the excessive pressure undergone by the ink in the printing nip. Conversely, in multi-color printing, surface energy appeared to play an important role. In the case of a multi-color printing, ink is transferred both to inked and uninked, dry or dampened, areas. 'Dry trapping', e.g. printing on top of a previously dried ink film, and 'wet trapping', e.g. printing a wet ink film on top of a still-wet previously printed ink, are challenging to the printer. Conventional wisdom holds that the 'tack', described below, of the fresh ink film already on the paper must be greater than that of the next ink in order to allow good wet trapping. In an offset press, as the ink / fountain solution emulsion is printed, the fountain solution is also applied to the non-image area of the paper. In multi-color printing, the dampened non-image area of the paper may become the image area of the second unit. In other words, ink may be locally printed onto a 'water film' rather than onto paper. Water absorbency is relevant for offset printing but for water-based inks in gravure or in flexo will not be discussed here.

A high-speed press has a nip dwell time of approximately 1 ms which makes difficult the investigation of the phenomena taking place in the printing nip (Aspler *et al.*, 1994). In the printing nip, the pressure increases and the shear rate can reach $10^5\ s^{-1}$.

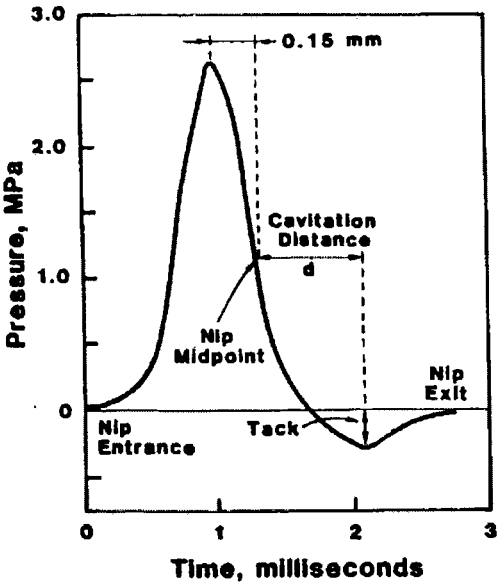

Figure 1.16: Typical pressure profile where printing tack is defined as the maximum negative pressure (Zang and Aspler, 1994).

However, no theory fully described a real printing nip where the mobile phase of a Non-Newtonian and viscoelastic ink penetrated into a porous and deformable substrate (Zang and Aspler, 1991). The notion of 'tack' is widely used to describe the forces or energies involved in the splitting of a thin fluid film between two surfaces. However, the nature of tack remains unclear and there is no universally accepted definition of ink tack. Stefan (1874) calculated the force required to separate two surface parallel plates immersed in a Newtonian fluid;

$$F = \frac{3 \cdot (1+\xi)}{4 \cdot \xi^2} \cdot \frac{\mu \cdot R_p^{\,2} \cdot V}{d_0^3} \qquad \xi = \frac{d_f}{d_0} \tag{1.9}$$

where V is the constant speed of separation of the two plates, μ, the viscosity of the fluid, R_p, the radius of the circular plates, d_f, the finale distance between the two plates, d_0, the initial distance between the two plates, ξ, the ratio of d_f on d_0. It should be noted that the model results in force per unit area or energy per volume rather than the force itself.

This equation was developed for the elongation of a single filament and appeared to be valid for time in excess of one second. However, separation times of this order of magnitude are not realistic in the case of the split of printing inks in a roller system. In addition, the separation of parallel plates in a direction normal to their surfaces does not exactly duplicate the situation existing on a roller system. Xiang and Bousfield (1998) presented a modified model considering filtercake thickness h_f for the splitting force, F, based on the Stefan's law,

$$F = \frac{3\pi \cdot R_p^{\,4} \cdot \mu \cdot V}{4\left(h_0 - h_f\right)^3} \tag{1.10}$$

The model indicates that with the growth of a filtercake, the tack force of ink on the coated paper increases. Aspler *et al.* (1994) defined a new printing property called the 'printing tack', that corresponded to the ink tack, e.g. maximum tensile stress, measured during printing, on a paper surface, as the ink film started to cavitate. They found that the printing tack increased with ink film thickness in the nip and with paper porosity due to a lower ink penetration and a greater effective ink film thickness for less porous papers. They reported that ink immobilization and penetration reduced the free ink thickness and moved the cavitation points closer to the nip center. They showed that there was no

universal correlation between the printing tack and the viscous flow properties of the ink but that tack mainly depended on the amount of dissolved polymer in the ink. They suggested that the initiation of ink splitting appeared to be viscoelastic while the filament elongation and rupture were more affected by flow properties.

1.10. Filamentation

The final step before the ink film splits is the formation of filaments. Voet and Geffken (1951) and Sjodahl (1951) studied the ink film splitting at high speeds and showed that the formation of filaments under high speeds was due to the viscoelastic properties of the ink. Nguyen *et al.* (1992) showed that filament pattern resulting from cavitation appeared at high ink level. Pictures of the filaments formed at the nip exit were taken by Glass (1978), De Grâce *et al.* (1988), Zettlemoyer and Myers (1960) and Hayashi *et al.* (1993). The filamentation has been the subject of a number of other studies including Banks and Mills (1954), Miller (1958), Myers (1959) and Bery *et al.* (1992). Thomson and Young (1975) used high-speed cinematographic and microsecond photographic techniques to investigate ink filamentation between two rotating rollers for a known speed range. They found that the filament volumes and the maximum filament lengths decreased with increasing speed. They suggested that the behavior of the filaments, at low roller speeds, was mainly attributed to elastic flow. De Grâce *et al.* (1988) studied high-speed photographs of ink film splitting in the nip. They found that, with a constant amount of ink in the nip, the point of rupture of filaments moved closer to the nip center with increasing printing speed and that the length of ink filaments at rupture simultaneously decreased. They showed also that, with increasing amounts of ink in the nip, the

filaments were longer at rupture and that with increasing shear viscosity of the ink vehicle, the filaments were longer at rupture. The length of the filaments has been found to reach 40 times the initial thickness of the ink film (Sjodahl, 1951; Hayashi and Amari, 1992). Hayashi and Amari (1992) constructed an ink-monitoring system for lithography in order to observe the transfer and the dynamic behavior of emulsified ink on a printing press. They conducted an acoustic study of the ink splitting using a sound-analyzing system consisting of a microphone with sensitivity at higher frequencies and a FFT Analyzer. They found that the length of ink filaments, the quantity of ink transferred and the ink tack decreased with increasing emulsification. They observed also that the dynamic viscoelasticity and the yield value increased with proceeding emulsification. They concluded that these phenomena were likely to be explained by the alteration in viscoelastic mechanisms in connection with the molecular weight of a disperse medium.

1.11. Ink Leveling

The relaxation properties of the ink together with its ability to flow are responsible for the subsequent leveling of the printed ink film prior to complete immobilization and film formation. The filaments that extend at the exit of the nip from the web to the roll recoil onto the printed surface and create a non-uniform ink film thickness, which must level due to surface tension forces to create a flat and glossy surface. The retraction of a filament into a hill should be a fast event, as reported by some photographic results of the printing nip by De Grâce *et al.* (1988). Figure 1.17 shows some pictures of the surface of an ink film printed on polyester film (Mylar, Dupont) at 8 m/s (Desjumaux, 1999). As time proceeds, the defects of the ink film surface level.

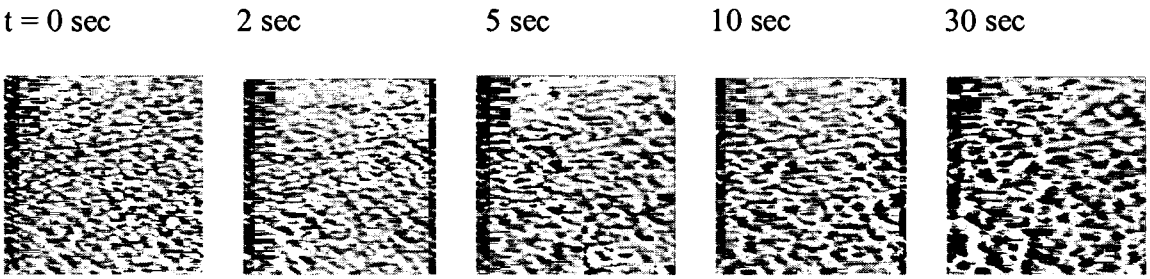

Figure 1.17: Pictures, taken at successive times, of the surface of a yellow heat-set ink film (3.3 μm) printed on Mylar film at 8m/s. Measured area was 1.5 mm^2 (Desjumaux, 1999).

Bery and Loel (1992) concluded that ink filament leveling and spreading determined the printed roughness and gloss. Zang and Aspler (1994) showed that, at high printing speed, the ink gloss passed through a maximum and decreased with increasing ink film thickness. The filaments formed at these speeds caused an increase of the micro-roughness of the deposited ink layer and produced a lower print gloss. Glatter and Bousfield (1996) reported the leveling of ink filaments on plastic Mylar surfaces and showed that the printing speed and the ink film thickness influenced the size of the filaments produced in the nip. The size of the filaments was found to be critical in determining the rate of gloss development and the final gloss since large filaments leveled slowly and produced lower print gloss.

The modeling of leveling of liquid defects has been the subject of a number of studies. Orchard (1962) described the surface-tension-driven leveling of thin films of Newtonian fluids on a planar substrate. Surface tension, viscosity and film body forces were included in the analysis. Bassemir (1976) applied Patton's equation, developed for the leveling of paints, to identify the parameters which contributed to the gloss of UV cured printed ink

films. Patton's equation, Eq. 1.11, expresses the time of leveling, t_{lev}, taking into account the most significant variables with the exception of elasticity.

$$t_{lev} = \frac{K_0 \cdot \mu \cdot \lambda^4 \cdot \log\left(\frac{Z_0}{Z_t}\right)}{\gamma \cdot < h >^3} \tag{1.11}$$

where K_0 is a constant, μ, the viscosity, λ, the wavelength of disturbance (center to center distance between mounds), Z_o, the height of irregularities at $t = 0$, Z_t, the height of irregularities at $t = t$, γ, the surface tension and $<h>$, the average film thickness of ink. Keunings and Bousfield (1987) obtained finite element solutions for leveling problem while including the effects of viscoelasticity: linear analysis for the leveling of Jeffery fluid, a multi-mode Maxwell fluid and the full two-dimensional solution for an Oldroyd–B fluid were given. Kheshgi and Scriven (1988) gave a long wave analysis and a finite element analysis for the leveling of Newtonian fluids. Bousfield (1987, 1991) studied and obtained finite difference solutions for the leveling of coating defects on paper substrates while including absorbing boundary, evaporation effects and viscoelasticity. Bousfield (1991) proposed a one-dimensional model for surface tension leveling of a viscoelastic film using lubrication type arguments. Bousfield (1991) proposed a model to depict the leveling of coating defects. Iyer and Bousfield (1996) reported the analysis for shear-thinning fluids: a one-dimensional model, which took into account the surface tension, the gravity and the viscous forces, was proposed to predict the leveling of coating defects or irregularities on a planar surface. A novel numerical technique was proposed to solve the long-wave equations describing the surface-tension-driven leveling of a non-

Newtonian liquid. A new dimensionless group λ^*_p, which indicated the significance of shear-thinning rheology, was identified. Paulsen *et al.* (1996) gave the dynamics of liquid films under surface forces. Glatter (1996) examined a model to depict the ink film leveling on paper based on the long-wave approximation to the Navier-Stokes equations. The proposed model for the ink film leveling qualitatively predicted the leveling behavior even if the model predictions could not be quantitatively compared to the experimental data because the initial disturbances had a wide range of wavelengths and shapes, which could not be determined. The model indicated that the wavelength of the roughness was the most critical parameter and that long wavelength produced slow leveling rate. Toivakka *et al.* (1997) proposed a mathematical model based on a dynamic simulation technique to clarify the micro-structural mechanisms influencing the leveling of suspension.

1.12. Ink Setting

Increasing printing speeds requires faster setting inks. Ink setting can be considered as a continuous process during which the ink, starting out as a fluid, reaches its final hardness level. The ink setting may be the result of physical transformations, chemical reactions or a combination of the two phenomena. The fundamental processes of ink setting are absorption, polymerization, and solvent evaporation (Leach *et al.*, 1993).

The setting by absorption is also referred to as setting by penetration. The inks basically consist of a pigment dispersed within an oil-based vehicle. Dissolved polymer content is usually small and there is little or no evaporation or polymerization of the vehicle (Durchon, 1991). These inks are called cold-set inks or newsprint inks and dry physically

by infiltration of the mobile phase into the porous structure of the paper. Simple in terms of formulation, low cost cold-set inks are used for cold-set letterpress and offset printing on newsprint and uncoated papers (Aspler, 1991; Leach, 1988). Coupe and Hsu (1960) demonstrated that cold-set inks penetrated under the nip pressure as a homogeneous body on uncoated papers. Past the nip, within 3 seconds after printing, the pigment has been found to stop moving (De Grâce and Dalphond, 1989). On uncoated papers, further setting may involve capillary sorption of the vehicle (Coupe and Hsu, 1960) and long-term spreading of the vehicle oil over the fiber surfaces (Parker, 1976). Newsprint inks often produce rub-off, e.g. dirty fingers problem, set-off, e.g. transfer of ink from the print to the back of the sheet above, and print-through, e.g. transfer of the ink to the reverse side of the sheet.

Quick-set setting is brought about by physical changes within the ink film on the substrate and relies on absorption together with polymerization settings. The principle of quick-set inks, referred to as 'sheet-fed' inks, revolves around the use of a 'two-phase' vehicle system, one 'phase' being a thick oleoresinous varnish system consisting of a medium to high molecular weight binder and the other phase being a low-viscosity mineral oil distillate solvent to adjust the viscosity. After printing, the mineral oil distillate is generally assumed to preferentially and rapidly move into the paper surface by capillary forces, resulting in a rapid increase in tack of the remaining surface film. The top surface sets by oxidative polymerization, a free-radical process where the oxygen attacks the insaturations of drying oils, e.g. esters of glycerine with unsaturated fatty acid chains and alkyd resins, polycondensation of poly-alcohols and isophtalic acid, forming peroxides that break up into free radicals. The catalysts of the oxidative polymerization,

called dryers, such as cobalt naphthenates or other metal soaps, accelerate the polymerization. The polymerization of thin ink films, e.g. 1 to 3 μm, on coated papers has not been reported (Aspler and Lepoutre, 1991). Larsson and Busk (1985) showed that the oxidative polymerization of a quick-set ink went on during several months after printing, causing a dry ink film undesirably soft. Leach *et al.* (1988) and De Jidas and Destree (1988) showed that, in the case of a multi-color printing, a thick ink film thickness slowed down the setting of the successive ink film printed on it. Sheet-fed setting may produce reverse-side transfer.

The most important class of inks used on coated papers set by solvent evaporation in hot air ovens (100 to 140 °C) but also by quick-set setting to some extent. These inks are referred to as heat-set inks. Their formulation is similar to the one of quick-set inks but their vehicle contains low molecular weight hydrocarbon materials with paraffinic and cycloparaffinic solvents with low boiling points (Aspler and Lepoutre, 1991). After printing, part of the solvent is absorbed into the paper. De Jidas and Destree (1988) suggested that the increase in viscosity of the ink is analog to a thixotropic setting where intermolecular bonds were created. The other part of the solvent (80 to 90%) is evaporated when the print goes through the oven. Then, the print is cooled down in order to obtain a hard ink film. Work on deinkability has shown that cross-linking continued for months after printing. Heat-set inks set very rapidly depending on the affinity between the diluent and the resin (Aspler and Lepoutre, 1991; Leach *et al.*, 1988; Plowman, 1992). Liquid inks set by the formation of a film after solvent evaporation and by water / ammonia evaporation, polymer precipitation or latex coalescence. The solvent-based inks are polymer solutions with a very low static and dynamic surface tension and good

filming properties by solvent evaporation. The water-based inks contain alkali-soluble polymers (neutralized by ammonia), latex and surfactant system: in this case, the film formation occurs by polymer precipitation or / and latex coalescence.

The settings by radiation, e.g. ultraviolet radiation or electron beam, are recent. UV or EB inks set almost instantaneously, from a liquid state to a cross-linked solid. The vehicle of the UV inks contains prepolymers (10 to 25 %), multifunctional monomers and oligomers (10 to 25 %) and an initiator (5 %): the latter starts, under the effect of the light, a chain polymerization. The setting proceeds without any solvent evaporation. UV inks have a high gloss but they are expensive and hard to deink. The EB inks have a formulation similar to that of the UV inks. However, they do not contain any initiator (Leach *et al.*, 1988; Oldring *et al.*, 1991; Aspler and Lepoutre, 1991). The two radiation setting processes involve expensive equipment but insure very good adhesion onto difficult substrates.

The capillary absorption has been largely discussed but is not well understood yet. Kinetics of penetration of mineral oil, vegetable oil, drying oil or binders are not well documented yet. Indirect methods were used to investigate the ink setting like measurements of set-off (Bristow and Bergenblad, 1992) and wet ink tack investigation (Gane and Seyler, 1994; Van Gilder and Purfeerst, 1994).

In the case of offset printing, at the moment of the impression, a dispersion of pigment, solvent, polymer and emulsified water is applied to the sheet. Lepoutre *et al.* (1979) showed that, on coated paper, very little ink was impressed into the coated paper surface in the printing nip due to the fine pore structure. Paper coatings have an irregular pore structure that is difficult to characterize. Mercury porosimetry reveals that the pore radius

is more often less than 1 μm (Bristow and Bergenblad, 1992; Abrams *et al.*, 1996). In the case of a monochrome printing, the ink varnish is known to drain into the coating, leaving a pigment filtercake, analogous to the filtercake observed in the drying of a paper coating (Lepoutre, 1989). The tack rapidly builds up. The formation of a filtercake has been observed also on uncoated papers as the first step in ink setting, right after the printing nip. Using K&N model test inks on coated papers, Hattula and Oittinen (1982) showed that there was very little pigment penetration and very considerable solvent penetration. The reflectance of the stain caused by the absorption of K&N inks, e.g. dyed viscous oils, has been measured to investigate the oil absorption rate into papers. The relevance of this test remains elusive (Hattula and Oittinen, 1982).

Bassemir and Krishnan (1991) showed electron micrographs of sectioned coatings in which ink binders could clearly be seen at perhaps 3 layers of coating clay beneath the surface, showing penetration of the fluid phase to that depth before setting. Askew (1969), by mixing a blue dye with a yellow pigment to give a green ink and by printing this ink on coated paper, obtained at equilibrium a yellow print. He assumed the formation of a filtercake by suggesting the selective penetration of the blue dye mixed with the ink mobile phase into the paper coating, leaving the yellow pigments at the surface. Capillary sorption is usually evoked as the driving force of liquid phase removal to form the filtercake. The fluid penetration into the paper is usually explained in terms of capillary sorption given by the Laplace equation. The Lucas-Washburn calculation (Washburn, 1921) was obtained by combining the Laplace equation with the Hagen-Poiseuille equation and depicts the laminar flow in a cylindrical pore under capillary pressure. The

driving force here is the pressure drop that exists across a curved interface in the porous fiber network. The rate of penetration into the cylindrical pore is given by Equation 1.12.

$$\frac{dh_s}{dt} = \frac{R_p \cdot \gamma \cdot \cos(\theta)}{4 \cdot \mu \cdot h_s} \tag{1.12}$$

where h_s is the thickness of penetration of the ink mobile phase into the substrate, t, the time, R_p the pore radius, γ, the surface tension, θ, the contact angle and μ, the viscosity.

The Lucas-Washburn equation assumes that a homogeneous liquid is entering a homogeneous pore structure under laminar flow conditions. However, all the conditions of chromatographic separations, e.g. differences in affinity, solubility and size, may exist in the consolidation of an ink film (Aspler and Lepoutre, 1991). The filtercake formation at the surface is itself an indicator of separation by size exclusion. Aspler and Lepoutre (1991) reported that different ink polymers had different sorption isotherms onto coating pigments. The ink setting is known to depend on the variations in solvent affinity for the coating as well.

In addition, many of the solvents used in inks are capable of interacting with the polymer films of the coating. Kelly *et al.* (1971) measured ink-setting times on coatings containing latex polymers with different structures and degrees of cross-linking. They measured the amount of ink solvent sobbed by each polymer and the degree of swelling of each polymer. Polymers with the greatest swelling and sorption showed the least set-off, e.g. the fastest ink penetration. Polymers with the least solvent interaction had less vehicle sorption and retarded tack-build rate. High binder levels result in reduced ink absorption and the coating is said 'tight'. Garey (1982) showed that polyvinyl acetate and

protein binders had higher ink receptivity presumably due to a more open porous structure.

Van Gilder and Purfeerst (1994) showed that the rate of ink tack-build up was related to the degree of latex polymer solubility in the ink solvents and its influence on the ink / latex film interaction. They showed that the latex solubility parameters depended on both the physical state of the polymer, e.g. amount of cross-linking, and its chemical nature, e.g. surface energy and polarity. They suggested that increasing the solubility parameter of the polymer further away from that of the ink solvents, by modifying the latex polymer to a higher surface energy / polarity level, decreased the interaction of the ink with the polymer film, produced lower ink-tack build up and more printing impressions before coating pick occurred. They found that linear styrene butadiene latex polymers were more interactive with the offset inks than the cross-linked polymers, at comparable surface energy / polarity level.

Aspler and Lepoutre (1991) reported that even a dry ink film contained up to 15% trapped solvent that could lead to softening of the ink film. Solvent retention has been investigated: both the moisture of the paper and the ink viscosity were affecting solvent retention. Finally, some oxidative ink solvent and side-reaction products of the free-radical polymerization process were found to be released from the ink layer as it hardened, reducing ink gloss.

Very few investigations have been conducted to differentiate the ink setting in the case of a multi-color printing process, e.g. thin ink film printed on a dampened coating or on a fresh ink film, from the ink setting in the case of a monochrome printing, e.g. thin ink film printed on a fresh sheet.

1.13. Leveling Theory

The leveling of liquid defects has been the subject of a number of studies. The model proposed in this chapter extends the results of number of previous studies like the 'long-wave analysis' of Kheshgi and Scriven (1988) to include the influence of a substrate which removes a component of the fluid. The proposed model is general for the leveling of a suspension on a porous surface. The surface can also take up the fluid via diffusion mechanism. The model is directed at the leveling of ink films on coating layers.

The composition and the structure of the coating as well as the ink properties influence the substrate capability to allow fluids such as ink mobile phase to transfer into the coating layer. However, no complete model has been proposed to investigate the relative importance of physical and chemical properties of the ink and the coating on the leveling rate.

1.13.1. Leveling Model on Rough but Nonporous Substrates

Glatter and Bousfield (1996) demonstrated a leveling model, Eq. 1.13, based on Kheshgi and Scriven (1988) for various rough substrates. Their assumptions included ink as Newtonian fluid, no drying or absorption of ink solvents, and ink acts as a continuous fluid.

$$\partial h/\partial t = (-\gamma/3\mu)\cdot\{[(\partial^4 h/\partial x^4)\cdot(h-h_p)^3]+[(3\partial^3 h/\partial x^3)\cdot(h-h_p)^2\cdot(\partial h/\partial x)]\} \quad (1.13)$$

where, viscosity, μ, surface tension of the ink, γ, surface profile of ink and paper, h and h_p, respectively, time, t, lateral distance, x.

This final working equation was solved with standard finite-difference techniques. A modeling result on roughness development as a function of time t is illustrated in Figure 1.18. This result should be consistent with experimental result for its validation. As seen, thicker ink film levels rapidly in a short time.

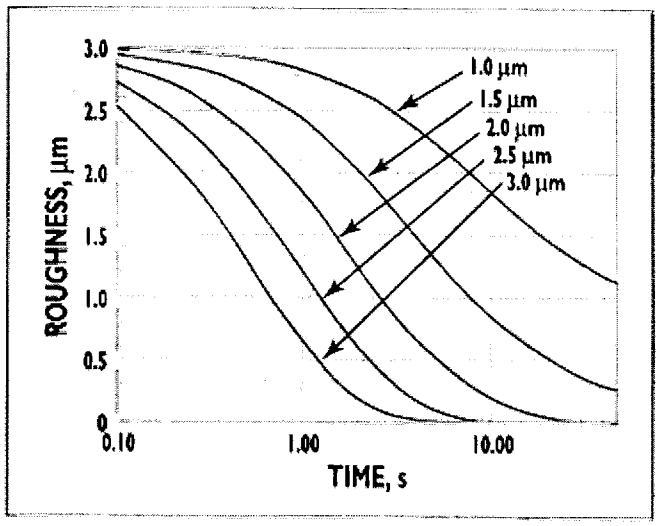

Figure 1.18: Model results showing predicted change in film roughness as a function of log time for thin films (1~3 µm) leveling on a rough substrate (Glatter and Bousfield, 1996).

1.13.2. Model Development on Porous Substrates

Desjumaux and Bousfield (1998) further developed a leveling model based on the work of Glatter *et al.* (1996). The problem of interest is an individual ink hill that is printed on a coated substrate, as shown in Figure 1.19, and levels as some ink mobile phase is removed by capillary pressure effect or by swelling of the latex in the coating. A very high viscous layer, called filtercake (or gel layer) is assumed to form next to the coating surface, considering that the diffusion of ink pigments and resins back into the bulk layer

is slow compared to the leveling event. The opposite of this assumption is that, as ink mobile phase leaves the ink layer, the concentration increases uniformly throughout the layer. However, it is reasonable to make the assumption that there is a layer of very high viscosity next to the coating surface.

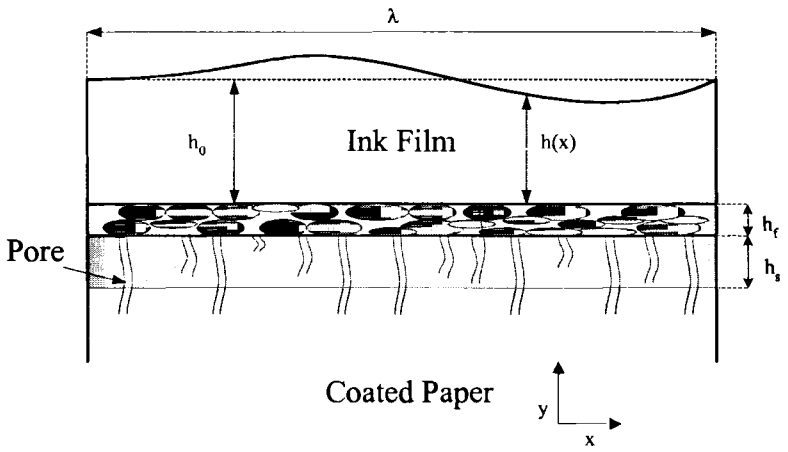

Figure 1.19: Schematic illustration of cross-sectional fluid layer on a porous surface. where, h_o is the thickness if level is complete, λ, the wavelength of disturbance, $h(x)$, the distance to free surface from substrate, h_f, the filtercake thickness and h_s, the depth of penetration.

The equations that describe the fluid motion due to surface-tension forces are developed. If the film thickness, h_0, is very small compared to the wavelength of disturbance, λ, lubrication type arguments are valid to reduce the two-dimensional transient problem to a one-dimensional transient problem. Considering a thin ink film with relatively large wave length, this assumption is considered valid. Evolution of surface profile is finally obtained as,

$$\frac{\partial h}{\partial t} = -V_p - \frac{\gamma}{3 \cdot \mu} \cdot \frac{\partial}{\partial x} \cdot \left(\frac{\partial^3 h}{\partial x^3} \cdot (h - h_f)^3 \right) \tag{1.14}$$

where V_p is velocity of penetration, t is time. In addition of this working equation, two other mass balances link the penetration depth with the growth of the filtercake as,

$$\frac{\partial h_s}{\partial t} = V_p \cdot \frac{1}{\varepsilon} \tag{1.15}$$

$$\frac{\partial h_f}{\partial t} = V_p \cdot \frac{\phi_s}{\phi_f \cdot (1 - \phi_s)} \tag{1.16}$$

where ε is the void fraction of the substrate, ϕ_s, the volume fraction of solids in the ink and ϕ_f, the volume fraction of solids in the filtercake. Note that Equation 1.16 is revised from the original equation to account correctly for ink volume.

The velocity of penetration is a function of two different terms, V_c and V_d, representing respectively the velocity of penetration by capillary pressure effects and by diffusive effects. The total velocity of penetration is given as,

$$V = V_c \cdot \varepsilon + V_d \cdot (1 - \varepsilon) \cdot (1 - PVC) \tag{1.17}$$

where capillary absorption, V_c, is given by,

$$V_c = \frac{2 \cdot \gamma \cdot \cos(\theta)/r}{\mu \cdot \left[\frac{h_f}{K_f} + \frac{h_s}{K_s}\right]} \tag{1.18}$$

The dynamic contact angle is assumed not to be a function of the rate of capillary rise. To describe the diffusive mechanism, the equation for the diffusion of a component A through a semi-infinite slab of component B (Bird *et al.*, 1960) is simplified to obtain the penetration velocity by diffusive effects as,

$$V_d = \sqrt{\frac{D_{AB}}{\pi \cdot t}} \tag{1.19}$$

where D_{AB} is the diffusion coefficient. The model describes the film profile '*h*' as a function of time by Equations (1.14), (1.16), (1.17), (1.18), and (1.19). Finite difference techniques are used to calculate the derivative in Eq. (1.14). Euler time integration can be used to calculate the change in the profile, the filtercake thickness and depth of penetration.

1.13.3. Leveling Model Parameters

The Darcy's law coefficient can be estimated from the Carman-Kozeny relation that applies to laminar flow in a packed bed of particles (Geankoplis, 1983) as,

$$K_{s(f)} = \frac{\varepsilon^3}{(1-\varepsilon)^2 . S_0^2 . k_1} \quad \text{and} \quad S_0 = \frac{3}{r_p} \tag{1.20}$$

where r_p is the radius of the pigment in the case of a filtercake or the radius of the coating pigment in the case of a coated substrate. Note that this is for spherical particle. Desjumaux (1999) used the experimental results obtained in Ström *et al.* (1999) to calculate the Darcy' law constant of the filtercake. An expression of the filtercake thickness is obtained as a function of the time.

$$h_f = \sqrt{\frac{4.K_f.\gamma.\cos(\theta)}{\mu.r}.\frac{\phi_s}{\phi_f \cdot (1-\phi_s)}.t} \tag{1.21}$$

A simple relation gives the percentage of ink remaining in the ink after printing, as the ink filtercake is building.

$$\%\ oil\ in\ ink = \frac{(1-\phi_s).h_0 - \frac{\phi_f}{\phi_s}.(1-\phi_s).h_f}{(1-\phi_s).h_0} \tag{1.22}$$

Equation 1.22 can be solved for h_f, assuming a certain percentage of oil remaining in the ink, e.g. 40%, after a certain time, t, e.g. 2 minutes, given in the work Ström *et al.* (1999). However, if one need to assume each value of remaining oil in the ink for each case, that may not give realistic prediction since that value may vary.

The thickness of the filtercake, about 1 ms right after the printing nip, may be estimated with a certain level of given pressure in the (e.g. Zang and Aspler, 1994).

Basically, the leveling model above can be applied on any surface. For instance, if the surface has a certain roughness, then the boundary condition may be changed accordingly. Also, surface profile can be applied as a function of amplitudes and wavelengths. For instance, Matsuda *et al* (2000) assumed that surface profile of a coated paper could be regarded as a cluster of waves of various frequencies and amplitudes.

$$F(x) = \sum_{n=1}^{n} \left[a_n \cdot \sin\left(\frac{x + c_n}{\lambda_{p_n}} 2 \cdot \pi \right) \right] \tag{1.23}$$

where, a is amplitude, $a_n = \frac{\pi \cdot (Ra)_n}{2}$, c_n is phase difference, λ_p is wavelength.

Darcy's law constant for the filtercake, K_f, could be calculated by AA-GWR filtration device using the equation as below,

$$K_f = \frac{1}{2} \frac{V_p^{\,2} \cdot \mu}{\Delta P \cdot t} \cdot \left(\frac{\phi_s}{\phi_f}\right)\left(\frac{1}{1-\phi_s}\right) \tag{1.24}$$

The velocity V_p is calculated from given volume, time and area. If we perform well-known filtration experiment and get a filter cake resistance, α, then Darcy's law constant can be related to the cake resistance using simple relations between Darcy's law and Carman-Kozeny equation or mass balance as,

$$K_f = \frac{1}{\alpha \cdot c_s} \cdot \frac{\phi_s}{\phi_f \cdot (1-\phi_s)} \tag{1.25}$$

$$K_f = \frac{1}{\alpha} \cdot \frac{1}{\rho_s(1-\varepsilon_f)} \tag{1.26}$$

$$L = \frac{c_s}{\rho_s(1-\varepsilon_f)} \cdot \frac{V}{A} \tag{1.27}$$

where A is filter area, L is filtercake thickness, c_s is solid weight per volume of mobile phase, ε_f is void fraction of filtercake, ρ_s is density of solid. This expression may give better access to get Darcy's law constant since it may be easier to measure 'c_s' and 'ε_f' than 'ϕ_f' value.

For capillary absorption velocity, a recently modified absorption model, Eq. 1.28, by Xiang and Bousfield (1998) may be incorporated,

$$V_p = \sqrt{\frac{r \cdot \gamma \cdot \varepsilon^2 \cdot \cos\theta \cdot t}{2 \cdot \mu \cdot \left(1 + \frac{\varepsilon^2 \cdot r^2 \cdot \phi_s}{8K_f \cdot \phi_f (1-\phi_s)}\right)}} \tag{1.28}$$

Equation 1.18 is substituted with the above modified model, then considering tortuous capillary model as well as external pressure contribution (e.g. Zang and Aspler, 1995), the penetration of mobile phase may be described as,

$$V_c = \frac{\varepsilon}{\tau} \sqrt{\frac{P \cdot r^2}{4 \cdot \mu} t_1 + \frac{r\gamma \cos\theta \cdot t_2}{2\mu\left(1 + \frac{(\varepsilon/\tau)^2 r^2 \cdot c_s}{8K_f \cdot \rho_s(1-\varepsilon_f)}\right)}} \tag{1.29}$$

where, t_1 is the penetration time under pressure in the nip, and t_2 is the time after the release of the applied pressure.

Final film profile h may be now calculated by incorporations with Equation 1.14, 1.16, 1.17, 1.19 and 1.29. Then we may convert 'h' to final gloss values from the relationship between roughness and gloss. Other parameters in this model can be measured directly in the lab.

2. EXPERIMENTAL METHODOLOGIES

2.1. Gloss

In the paper industry, standards for measuring gloss define what method best suits the measurement of each paper grade. Gloss level is commonly measured either at 20° (Tappi Test Method T653 pm-90) for high gloss papers or at 75° (Tappi Test Method T 480 om-92) for relatively low or matte grades. Indeed, since the amount of reflected light increases with the incident angle, it is easier to differentiate low gloss samples at high incident angle and high gloss samples at small incident angle.

Slightly different setting may be used for the glossmeter and the scanned are ranges from 17.4 to 21.3 mm in length and 9 to 11 mm in width when using the 75° method. The acceptance angle is then is about 11°. Any combination of photodetector and indicating device proving a numerical indication of the light flux through the receptor window and accurate over the entire scale to within ● 0.2 % of the full scale may be used. The test method also recommends an incandescent light source operating at a color temperature of 2850 ● 100 K. It has to be combined with filters at the photoreceptors to duplicate the CIE luminous efficiency function which has an effective wavelength of 572 nm (Tappi Test Method T 480 om-92).

The gloss meter used to obtain gloss at 75° angle was a D48 Optical Hd manufactured by Hunter Assoc. Lab. Inc. It meets the TAPPI test method requirements. Besides this 75° gloss, another glossmeter with different angles was used to accommodate wide range of gloss and better differentiation between high gloss samples. Print gloss often become higher than paper gloss and the print gloss from high paper gloss sample become hardly

differentiated. Hansen (1973) claimed the best angle for gloss measurements was 60°. Oittinen (1980) commented that for the best differentiation between samples as far as roughness effects were concerned, the optimum angle of incidence in measuring specular gloss varied for prints in the range of 45° to 60°. A portable glossmeter, micro-Tri-gloss, BYK Gardner was used to measure gloss at 20°, 60°, and 85°. Mostly in this work, 60° gloss was measured. The recommended range for 60° gloss is from 30 to 70 gloss units, therefore when the reading at 60° geometry is below 30, Tappi 75° gloss could be better to differentiate the samples in question. This glossmeter meets the standard requirements of ISO 2813, which is for 'Paints and vanishes' and also applicable to ink. It should be noted that there is no one standard for 'printed paper' though ISO 2813 comes nearest to a form of standard. For both instruments, gloss was measured on the samples back grounded with black non-glossy paper, otherwise noted.

2.2. Surface Roughness

The characterization of surface roughness of paper is important in many applications, especially printing. Describing the surface topography in measurable, quantitative terms is often more difficult. There are several ways to evaluate the surface roughness as reviewed. One of the most common methods is stylus profilometer method.

The stylus profilometer is used to characterize the sheet surfaces. The instrument used for the tests is an Alpha-Step 200 manufactured by Tencor Instruments. The instrument is a computerized step profiler with programmable X-Y stage, and a 9" video monitor, which plays a magnified view of the sample and stylus during the scan, as well as provides scan profiles and a summary of scan data. The system allows setting, and storing if desired, of

a variety of scan parameters, such as scan direction, scan length/sampling rate and vertical units (KÅ vs. μm). Measurement cursors are used for base line correction, to obtain a variety of data, and/or to zoom in on a particular section of a scan profile (Tencor Profilometer, Alpha Step 200 Manual). The technique uses a fine, cone-shaped diamond stylus tip in various sizes which is applied onto the surface with an adjustable load. Measurement of the vertical movement of the stylus occurs as the material is moved in the horizontal direction.

The available scan lengths are 80, 400, 2000 and 10000 μm, with scan times of 8 and 40 seconds. The highest resolution possible was 0.5nm with the upper limit of measurement being 320 μm, in the vertical direction. The horizontal resolution was down to 40 nm, with up to 2000 data points sampled on every scan. The stylus can be modeled as a 60 degree cone rounded to a spherical tip of 5 μm, as can be seen in Figure 2.1. The limitation posed by the size and geometry of the stylus on the measurable size of a groove is also illustrated. The dotted line shows the actual path followed during a scan, which differs from the ideal path, for the above reason. Stylus force is also controllable, which is the vertically applied force on the sample during measurement. A maximum of 25 mg is available with the Alpha-Step 200.

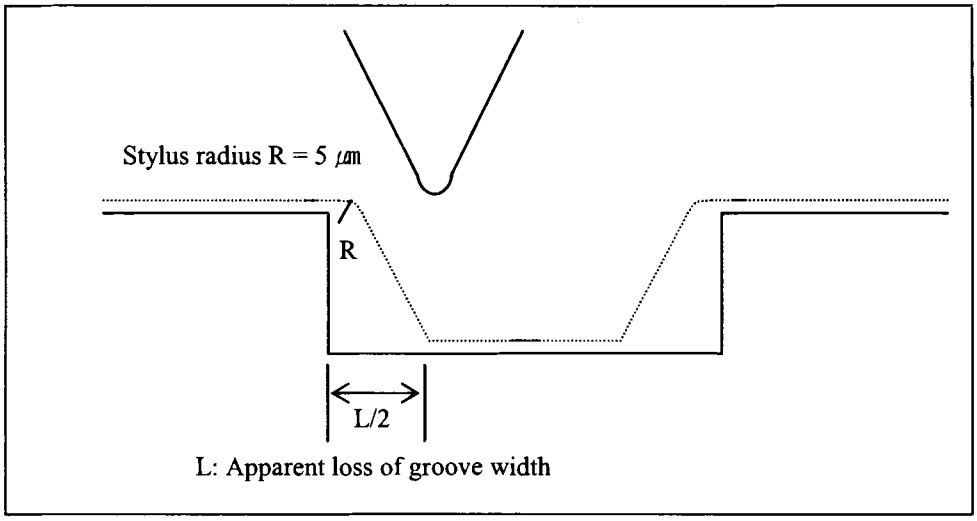

Figure 2.1: Stylus tip geometry and its effects on measurement.

The profilometer provides an analysis of four important surface characteristics, such as the average height, the difference between the highest and lowest points, the average roughness, and the cross-sectional area. The arithmetic average roughness (Ra) is determined using the graphical-centerline method. Figure 2.2 shows the principle of measurement;

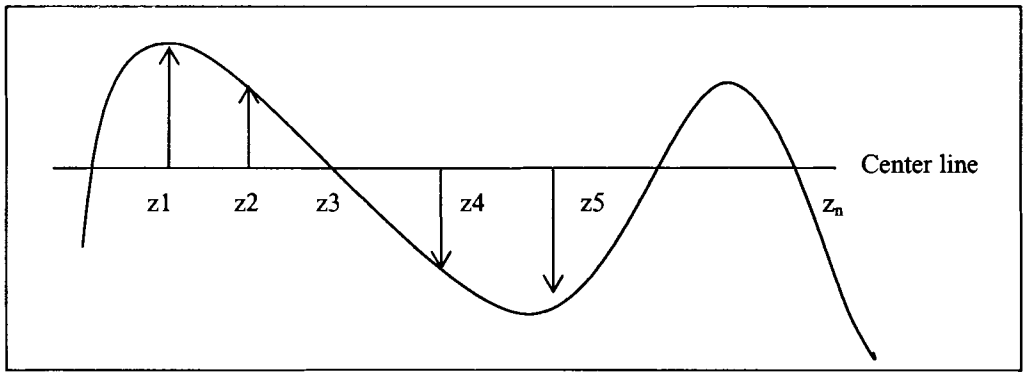

Figure 2.2: Measurement of roughness with the stylus profilometer (Tencor Profilometer, Alpha Step 200 Manual).

Ra is calculated as Equation 2.1.

$$Ra = \frac{\sum_{i=1}^{n} |z_i|}{n} \tag{2.1}$$

where n is the number of points between the measurement cursors and the distances are measured from the centerline as shown in Figure 2.2 (Tencor Profilometer, Alpha Step 200 Manual).

A surface topography, described by height z over an x-y plane, requires a huge amount of information to completely describe it. Therefore, the complex profile information is converted into a single number, which is easy to understand and compare using standard mathematical operations.

The more commonly used roughness parameters are most easily introduced in terms of a one-dimensional profile/surface z(x). The average, mean, or expected value of z(x) over distance L, is defined as follows,

$$\bar{z} = \lim_{L\to\infty} \frac{1}{L} \int_0^L z(x)dx \tag{2.2}$$

The surface z(x) = $\bar{z}$ would be considered perfectly smooth. Roughness is defined in terms of deviations from the mean value. The arithmetic average roughness σ_a or R_a is given by Equation 2.3.

$$\sigma_a = \lim_{L\to\infty} \frac{1}{L} \int_0^L \left| z(x) - \bar{z} \right| dx \tag{2.3}$$

Another surface-height average is the root-mean square (rms) roughness σ or R_q, which is also defined in terms of surface-height deviations from the mean surface.

$$\sigma = \{\lim_{L\to\infty} \frac{1}{L} \int_0^L [z(x) - \bar{z}]^2 dx\}^{1/2} \tag{2.4}$$

This definition depends upon the existence of the limit, as L approaches infinity. The two values, σ and σ_a, are usually close but larger σ for most surfaces, and the following Table 2.1 gives an idea of the differences for idealized surfaces.

Table 2.1: Differences between average and rms roughness for idealized surfaces.

Waveform z(x) (Peak to valley height: 2a)	σ_a	σ
Triangle	0.5a	0.58a
Sinusoid	0.64a	0.71a
Square wave	A	a
Circular cusp	0.51a	0.60a

An important point to be kept in mind is that the dependence of these calculations on height alone. Figure 2.3 shows two surfaces with different profile characteristics but the same roughness (σ or σ_a) (Stover, 1990).

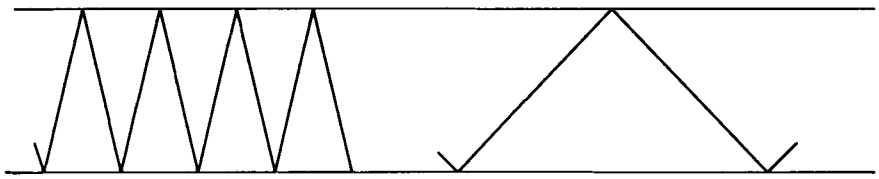

Figure 2.3: Two different surfaces with same roughness values.

Finally, two scan length of 80 μm and 400 μm, with sampling rate of 25 points/μm and 5 points/μm respectively, and a force of 7 mgf were used for the measurements. The stylus is easily capable of etching a path on coated paper as reviewed, and hence a low magnitude of force was used though a lower force entails the risk of the stylus losing contact with the sample during the scan. Practically, unless going down to the 5 pph of binder level at the given stylus configuration, the marking thought to be not large or severe based on Fesenti's work (1996) on the relation between the stylus marking force and latex binder levels. In the full-scale experiment stage, all the raw data was acquired and stored over the span length of 400 μm. Those data was further processed using Fourier domain filter by removing wavelengths above 100 μm. Since the minimum scan resolution was 0.2 μm, the maximum frequency (1/wavelength) became 2.5 μm^{-1} from the 3 data points connected over 0.4 μm. Then, the frequency removal from 0 ~ 0.01 μm^{-1} gave a desired filtered data. Data was zero mean leveled simultaneously and calculation of arithmetic and relative mean square roughness was followed using the Equation 2.3 and

2.4. An exemplary processing is described in Figure 2.4. In fact, the instrument does level raw data by forcing both end measuring points toward zero; the processed data has often much of variations and vulnerable to large artifacts.

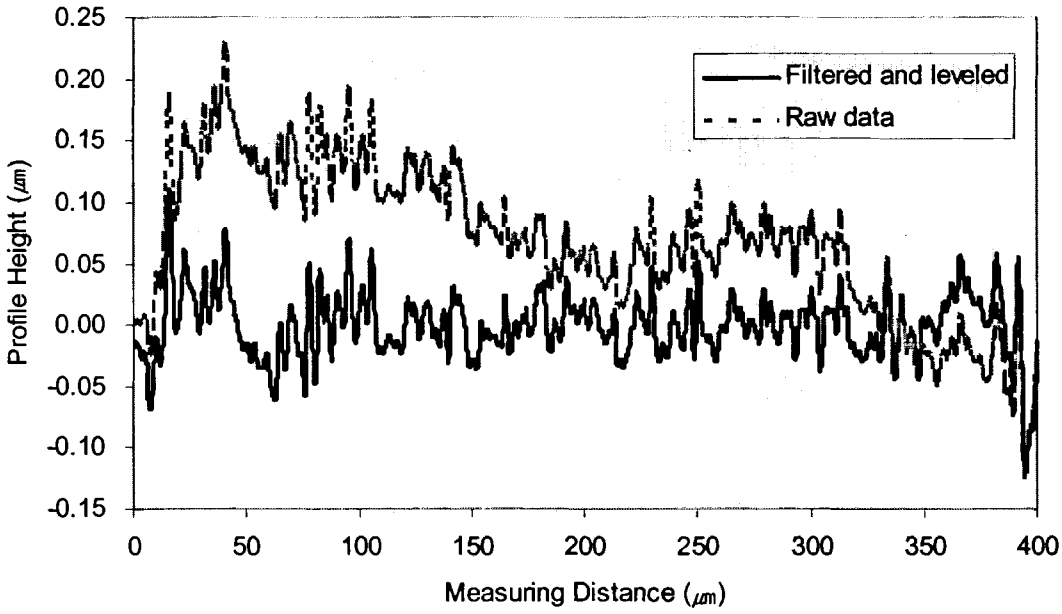

Figure 2.4: An example of roughness processing with Fourier domain filter.

2.3. Ink Filtercake Resistance

In the theoretical models for ink setting and leveling, the ink filtercake resistance is often used, there is no standard method to measure this quantity, but in other process, this is a common parameter to measure.

Ink was diluted and lowered in viscosity with a mineral oil, Magiesol-62 (Magie brothers Oil Co.) for measuring its filtercake resistance. The viscosity of ink, the diluted ink, and oil was measured by a CVO rheometer manufactured by Bohlin Instruments using a

concentric double-gap cylindrical geometry. The ink surface tension of oil was measured by the Sigma70 tensiometer using a standard De-Nuoy ring.

The theory of filtration was adapted to the pigmented ink absorption process to evaluate the ability of the pigment cake to hinder further absorption of the ink into the coating (MaCabe et al, 1985). The specific filtercake resistance, α, as defined in equation 2.6, is an easily determinable quantity to compare the filtercake-forming ability of pigmented inks. The experimental procedure consists of applying air pressure to force ink through a 0.1 micron polycarbonate filter, into a blotter paper, for a given amount of time. The instrument used was a gravimetric water retention meter manufactured by Kaltec Scientific. The experimental setup can be seen in the following Figure 2.5.

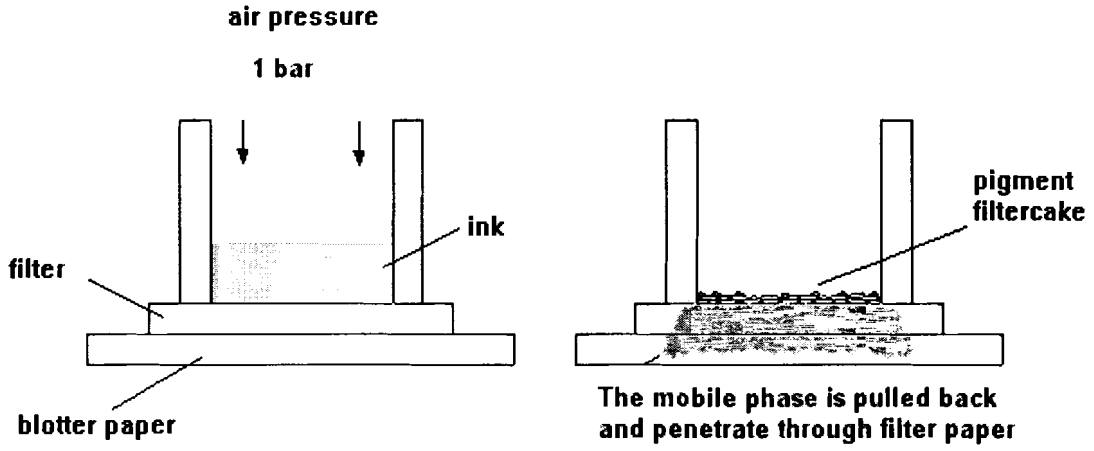

Figure 2.5: Pressurized filtration apparatus.

The basic filtration equation is written as,

$$\Delta P = \frac{k_1 S_o^{\,2}(1-\varepsilon_f)\cdot \upsilon \mu' c_s}{\rho_s \cdot \varepsilon_f^{\,3}} \cdot \left(\frac{V}{A_f}\right) \qquad (2.5)$$

where ΔP is the overall pressure drop over filtercake and filter medium, μ' is the viscosity of the filtrate, S_o is the specific surface area of particle per volume, A_f is the filter area measured perpendicular to the direction of the flow, V is the volume of filtrate collected from the start of the filtration to time t, ρ_s is the density of solid particle and ε_f is the void fraction of the cake. The term υ in Equation 2.5 is defined as,

$$\upsilon = \frac{dV/dt}{A_f} \tag{2.6}$$

The specific filtercake resistance α is defined as,

$$\alpha = \frac{k_1 S_o^{\,2}(1-\varepsilon_f)}{\rho_s \cdot \varepsilon_f^{\,3}} \tag{2.7}$$

Another way of estimating the value of α is a graphical method, which uses different values of t for filtration, as opposed to the above method, for which a single measurement can suffice. The graphical method involves the following calculations. For constant pressure filtration, the filtration equation can be written as,

$$\left(\frac{dt}{dV}\right) = K_c V + Q \tag{2.9}$$

where K_c and Q are defined as,

$$K_c = \frac{\mu \cdot c \cdot \alpha}{A^2 \cdot \Delta p} \tag{2.10}$$

$$Q = \left(\frac{dt}{dV}\right)_0 = \frac{\mu \cdot R_m}{A \cdot \Delta p} \tag{2.11}$$

where the subscript '0' refers to the value at time=0, and R_m is the filter medium resistance.

Integrating Equation 2.9 between the limits of (0,0) and (t,V) gives

$$\frac{t}{V} = \left(\frac{K_c}{2}\right) \cdot V + Q \tag{2.11}$$

A plot of t/V vs. V is linear with a slope equal to $K_c/2$ and an intercept of Q. A pressure of 1 bar, and *t* values ranged from 1 to 60 seconds were used for the measurements.

2.4. Mercury Porosimetry

The pore size distribution is measured using mercury porosimetry. Mercury porosimetry uses the principle of pressurized capillary penetration by mercury to measure the pore size distribution of a substrate or powders. The instrument used is a Poresizer 9320 manufactured by Micromeritics. The pores shape is assumed to be cylindrical. The poresizer has two built-in low pressure ports and one high pressure chamber. Data collection, data reduction, and data display are processed by the optional control module (Poresizer 9320 Manual).

The method involves submerging a porous sheet in mercury and then applying pressure to the mercury. The instrument covers the pressure range from 0 to 30,000 psia with an accuracy of ±0.1% psia of full scale. This pressure range covers 0.006 to 360 μm in pore size. When a sufficient pressure is reached, the mercury will enter the pores of the sheet. The size of the intruded pores is related to the pressure causing the intrusion and the volume of the intruded pores is the volume of mercury forced into them. If this process is continued over a range of pressures, the result is a distribution of the pore volume of the sheet with respect to its pores sizes, i.e., a pore size distribution (Winslow, 1969).

After finishing the data collection, the poresizer gives different types of data and curves. The data are cumulative intrusion, incremental intrusion, and differential intrusion, log differential intrusion, cumulative pore area, and incremental pore area (Poresizer Manual). From the pressure versus intrusion data, the volume and pore size distribution are generated using the Young-Laplace equation, assuming 'cylindrical' pores.

$$P = \frac{-2\gamma\cos\theta}{r} \tag{2.12}$$

where P is the pressure causing the intrusion, r is the radius of the cylindrical pore being intruded, γ is the surface tension of mercury, and θ is the contact angle between the mercury and the pore wall. Here, surface tension of 485 dyne/cm and contact angle of 130^0 are used.

Compressibility effect was corrected based on the method of Gane et al (1996). However, their samples were homogeneous lumps of dried coating material and accordingly the description on the correction method was given. Since the samples in this work are not

just 'lumps', but coated one on the polyester films. Therefore, some additional steps and consideration on correction was necessary.

The pressure table was optimized for the differentiation over the normal coating pore size range. The correction steps started from a blank run all over the working pressure range without sample inside penetrometer. Secondly, pure base substrates were measured at the same condition. As shown in Figure 2.6, the measured porosity of base substrate was significant. Finally, the coated specimen was loaded and measured. During the measurements, all of the raw data were stored and recalled for analysis.

Unfortunately, the data from blank, base, and coated sample can not be just simply compared and subtracted or corrected. That is because the raw data is based on per unit weight of sample and each coated sample has inevitably different weight or portion of base substrate. Another important reason is that coated sample has two sides; one is coated, the other is just as base substrate. Consequently, step-by-step correction needed. Blank run, free of any sample, was subtracted from the base substrate run as shown in Figure 2.7. Then, the results are converted per unit weight base. By considering one side coating, porosity potions down to 0.1 μm was reduced by half. Below this region, the consideration on one side coating may not be valid because it was thought that the porosity in that region mainly came from compressibility. The measured bulk volume of polyester film was around 1.35g/cm^3, which was larger than 1.39g/cm^3 of pure one due to surface roughness or porosity. Then the calculated porosity became 3.14% with a given sample weight. However, the measured porosity rose above 5%, which reflected there was compression. When the pore volume down to around 0.04 μm pore size was used as intrusion volume of polyester, the calculated density became close to pure film. In other

words, the porosity below 0.04 ㎛ pore size were considered to be compressed volume. It should be noted that the small figure of base porosity is very significant quantity compared to that of coating layer. Once the portion of base correction was established, the corresponding correction amount of base by knowing the coat weight and basis weight was determined and subtracted from the sample run. At this time, this subtraction will remove base portion of measured volume and compressibility of base as well. Now, based on the method of Gane et al (1996), the compressibility of coated layer only can be corrected by determining compressibility modulus M_{ss} in Equation 1.6. A exemplary result is presented in Figure 2.8.

Further, the corrected sample data can be converted to cumulative, incremental, and log differential data as wished. Bulk porosity ε_{bulk}, corrected intrusion porosity ε_{int}, and porosity below 1 ㎛ of pore diameter are calculated as,

$$\varepsilon_{bulk} = \left(V^{1}_{bulk} - V_{base} - V_{solids}\right) \Big/ \left(V^{1}_{bulk} - V_{base}\right) \tag{2.13}$$

$$\varepsilon_{\text{int}} = V_{\text{int}} \Big/ \left(V_{solids} + V_{\text{int}}\right) \tag{2.14}$$

where V_{base} is volume of base substrate, V_{solids} is volume of coating solid defined as,

$$V_{solids} = M_{sample} \cdot \left(\frac{w_{pigments}}{w_{pigments} + w_{binders}} \cdot \frac{1}{\rho_{pigments}} + \frac{w_{binders}}{w_{pigments} + w_{binders}} \cdot \frac{1}{\rho_{binders}} \right) \tag{2.15}$$

where M_{sample} is the mass of the sample, w the weights of pigment and binder, and ρ the densities.

Blank runs were repeated almost every 5 tests and base runs were repeated 3 times with 30 seconds equilibrium time (ET). The reproducibility may be seen in Figure 2.6. Because of abnormality from blank run when it is operated at 30 seconds ET, many of trial & error was done to find optimum ET, at which the porosity should not increase in an extrusion region, i.e. reduction in pressure. The temperature in operating room was 23 ± 2 °C, and mercury density as a parameter was accordingly adjusted.

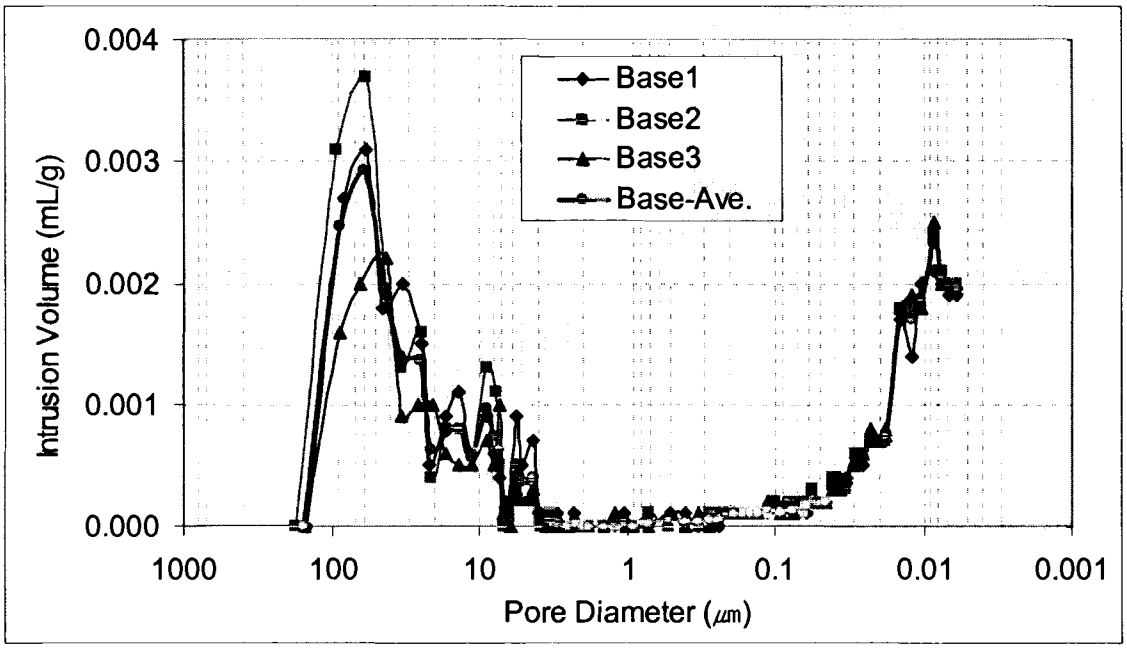

Figure 2.6: Pore distribution of coating base substrates from mercury porosimetry.

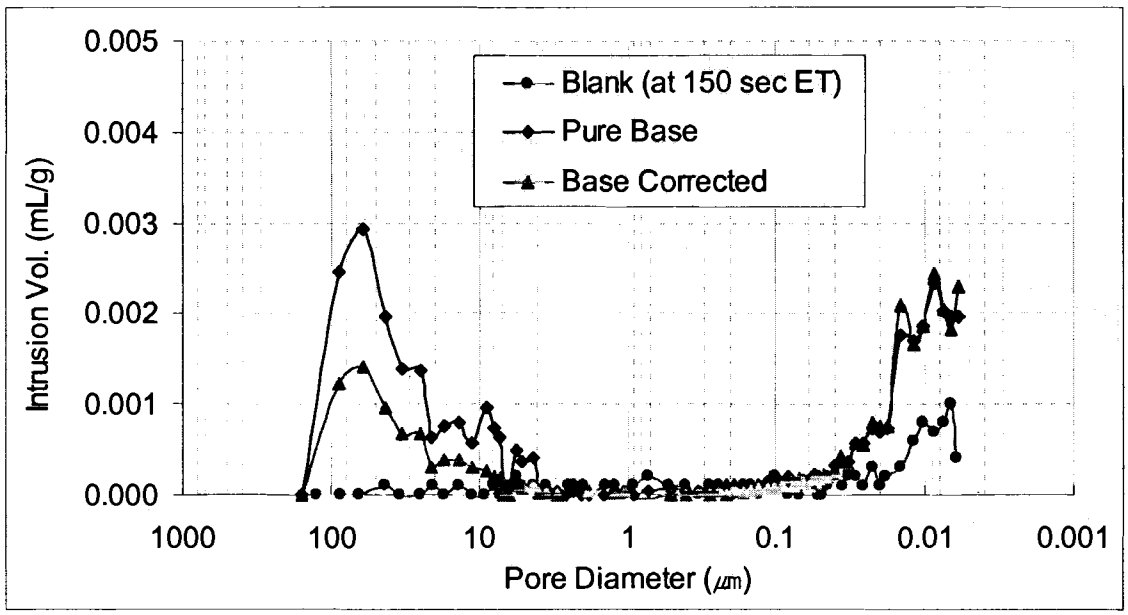

Figure 2.7: The pore distribution from blank run and base substrate. Blank data shows its significant increase in pore volume below 0.02 μm region. Solid triangle is a corrected result for coated case by reducing pore volume by half down to 0.1 μm point.

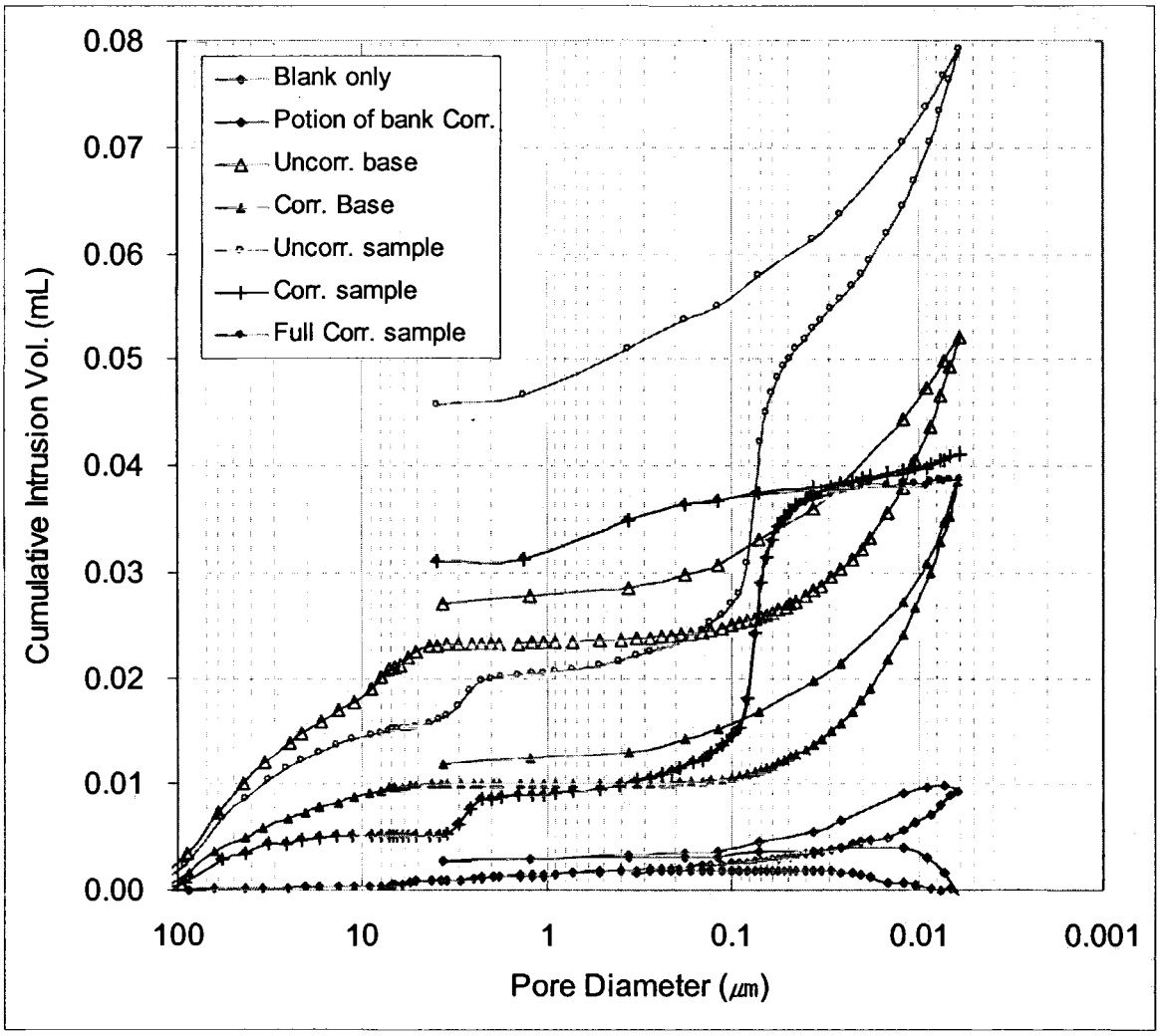

Figure 2.8: Compressibility correction of mercury porosimetry. Blank run is lowest curve while original data for a coated sample is the highest. The void triangle is pure base substrate and the solid is the corrected portion for coated sample. Crosshair is corrected coated sample after subtracting blank and base portions, and finally solid circle is fully corrected coated layer.

2.5. Dynamic Print Gloss

The gloss of the ink film printed on the coated samples was measured immediately after the printing nip, as described in Glatter and Bousfield (1996). A specially designed glossmeter, directly mounted on a laboratory printing press, recorded the ink gloss evolution every tenth of a second. Figure 2.9 is a schematic of the device.

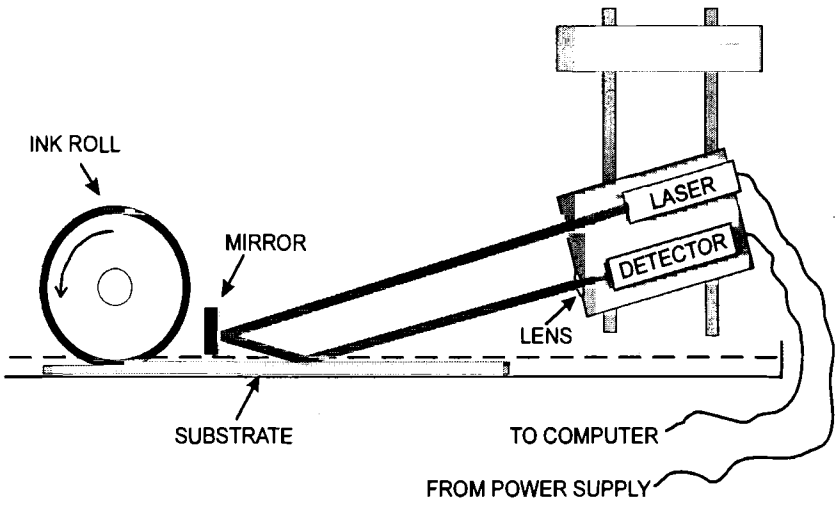

Figure 2.9: Schematic of the experimental glossmeter.

A laser light source (675 nm, 1.0 mW, M38, 920, Edmund Scientific) was mounted at 75 degree angle from the vertical. However, this angle can be changed to get a certain desired signal range. In this work, the angle was adjusted and kept at 66°, at which the glossmeter produced 9.98 Volts reading closed to its maximum of 10 Volts from the surface of 98 % Tappi gloss while generating enough signal from very low gloss samples away from its minimum 0 Volts. Therefore, this angle was confirmed to be the best configuration to get a wide enough signal from matt to high glossy surfaces. The laser sent a beam of light that was reflected off the mirror to the sample that has just moved

through the print nip and stopped 10 cm from the nip. The reflected light from the sample was collected by the detector through a lens. The size of the light spot on the sample was adjustable. However, a too small spot was found to give different results every time because of the variation of gloss along the sample, even when printing on plastic films. Therefore, a spot size of 13 mm (light direction) × 7 mm (cross light direction) was chosen. This diameter was large enough to give reproducible results. The light was reflected off the ink film onto a $5.2.10e^{-6}$ m^2 light detector (OPT201, BurrBrown). The voltage signals from the light detector were collected with a computer. Another critical variables was sample mounting because of its high sensitivity on flatness of samples. Even slight inclination could generate much of difference. Consequently, double sided adhesive tapes are used to stick samples to the printing plate thoroughly (Partial attachment was still not satisfactory). However, it is cautioned not to use this way for the thin samples because adhesive tape itself has non-uniformity. The sample thickness of around 150 μm from this work was found to be thick enough. Also any curvature of printing plate could generate variation due to different stop position in measuring area. The flatness of plates was checked every 10 printing tests and measuring area on the plate was adjusted to a certain same spot. Another step to enhance reproducibility was to check the gloss reading on the base itself without anything on it every time before printing. For instance, the base gloss value was 1.68 Volts at a given configuration and if there is any change over ±0.02 Volts, then the configuration and mirror angle are checked and adjusted. This slight but probably significant change was routinely happened mainly because of the impact when the printing plate hit the stoppage end of printing pathway. This impact may generate a strong disturbance on printing surface though it wasn't

investigated at all. So, additionally, a cushion was attached on the end of the printing path. The voltage values collected from the detector ranged between 0 and 10 Volts and these readings are known to be linear with Tappi 75° gloss. The calibration procedure between dynamic glossmeter and standard Tappi gloss is necessary to convert an arbitrary Voltages signals to 'sensible' gloss value. Even though Glatter et al (1996) reported a calibration chart in his paper, however, one calibration can not be valid to another case when there is even a slight change in configuration. Gloss at 60 and 75 degrees using conventional Tappi glossmeter and 'micro-Tri-glossmeter' was measured before and right after finishing recording dynamic gloss. The dynamic glossmeter was set at 66 degrees. The generated data were used for drawing relationship chart between them. The calibration results will be presented in later. More details of the experiment and data collection have been given in Glatter (1996).

A print test was conducted on the KRK laboratory printability tester described later. Once a sample was mounted on the moving member or plate, the test was actuated, and the operator also called the computer to collect data. The sample stopped, within 0.1 second after the printing nip and the gloss was recorded in time. The gloss value was sampled every 0.1 seconds. According to Glatter et al (1996), individual runs could vary as much as 30 percent, but the optimum configuration gave reasonable results. The coefficient of variation was down to around 15%.

2.6. Printing

The printing test was performed using KRK laboratory printability tester. The printing conditions are summarized in Table 2.2.

Table 2.2: Experimental printing conditions.

Parameters	Experiment I	Experiment II
Pressure, kgf/cm	25	30
Speed, m/s	4	2
Printing roll type (Width, cm)	Rubber (4)	Aluminum (2)
Inking on roll (cc)	0.3, 0.5	0.1 ~ 2

The amount of ink on the rolls was adjusted to achieve various levels of wet ink film thickness so that results could be sorted out at certain constant levels of 'ink on samples'. Printing procedures are followed by KRK's manual: inking on distribution rollers for 30 seconds, then apply inking roll for another 30 seconds. Weights of roll before and after printing were routinely measured to obtain a transferred ink amount on paper and ink transfer ratio. The balance used had 5/10,000 grams resolution and tolerance was also ±5/10000 grams, which may be little bit high to get small difference in transfer parameters for case of 2 cm inking roll (± 1/10000 gram resolution is recommended).

The ink was a typical commercial cyan quick-set ink (Capiplus III Process Cyan, Flint Ink Co.). The samples were allowed to condition in the test room for several days at 23°C and 50 % relative humidity prior to printing.

2.7. Tack

In this work, custom made laboratory tack-meter was used to evaluate the setting behavior of coated samples. Below are adopted descriptions from the original documents (Xiang et al, 1999).

Figure 2.10 illustrates the simplified schematic of the measuring device, called the Micro-Tackmeter. To apply a certain amount of ink onto the probe tip of Micro Tackmeter, an inked plastic film, such as Mylar, using laboratory printer is normally used as an 'ink supplier'. Once the probe is inked, then the probe contacts a substrate and starts to measures the force to pull the probe away from the surface. The splitting force between inked probe and inked paper is proportional to the deflection of the leaf spring which is measured by the Linear Variable Differential Transformer (LVDT). A computer controls the motor and records the LVDT output. When running the Micro-Tackmeter, the LVDT reads zero before the assembly is moved downward because there is no deflection of the springs. Next, the computer controls the motor and moves the probe, the springs, and the LVDT simultaneously downward until the probe deflects upward and the LVDT outputs the desired voltage or force, which is -0.5 Volts or around -100 mN. This procedure results in the probe contacting the substrate with a known force. Once this contact force is established, the computer reverses the motor and runs it upward until the probe breaks away. The maximum deflection of the probe downward is recorded by the computer and is taken as the tack value. The motor speed is 15mm/min but this can be adjusted to some degree.

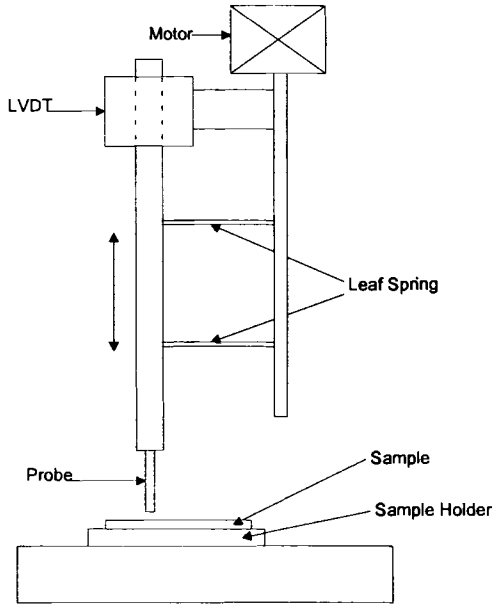

Figure 2.10: Schematic of the laboratory tack measuring device. The LVDT and motor are connected to a computer for motor control and data acquisition. The LVDT records the relative position of the probe to the motor assembly.

A series of analytical balance weights from 0.5 to 25g were used to convert this raw voltage signal to the absolute force. Figure 2.11 shows the relationship of force with the voltage reading.

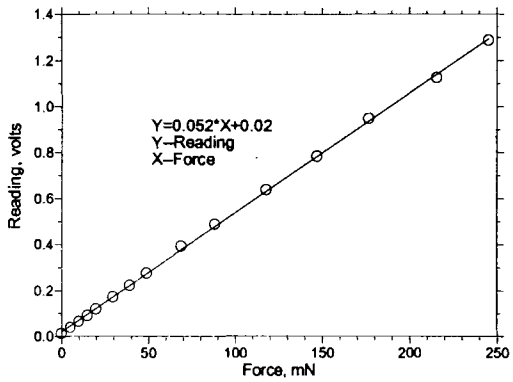

Figure 2.11: Calibration curve for the Micro-Tackmeter.

In this paper, the probe with diameter of 1.1 mm is used. Xiang et al (1999) described their experienced procedures such as way to inking on the probe, however, another type of 'ink supply' was used in this work as shown in Figure 2.12. Small thin grooved cell has about 8 μm ($\pm$ 2 μm) depth. A little amount of ink was deposited just up front of the cell and squeezed down by a razor blade twice slowly. Then the device was activated to let the probe touches the inked cell and the supplier was moved while operating to let the probe contact a desired position on the samples. Assuming a 50-50 split of ink film, around 4~5 μm of ink film are thought to be transferred to the probe. The inked probe touches the test paper many times continuously at a single point to measure the change of ink tack with time. An even split again would result in around 2~3 μm thick ink film on the sample. However, this amount is hard to actually measure and may change during setting. This new inking accessory helped to minimize the time interval between the inking and the first measuring point as well as the loss of ink solvent before doing tack measurement as well. At this time, only one cell was used to avoid any variation from different depth of cells, in a reverse way, this means various inking levels could be applied using this one. In a practical sense, it was convenient and fast.

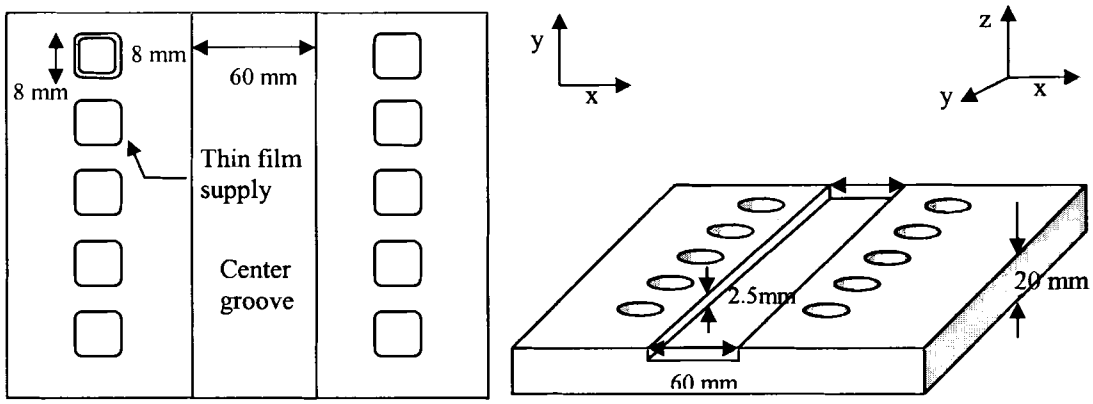

Figure 2.12: Ink supply tool for tack measurement.

A graph of the tack forces versus elapsed time is generated and is used to interpret the ink/paper interaction. In this way, the time interval between inking and the first measuring point was virtually dependent on the motor speed and about 3 seconds maximum, though this time scale is still long compared to the time interval between printing units. Both printing and tack measurement were carried out in a 23°C and 50% relative humidity standard room. The ink used was the same with the one for the print test; a typical quick-set offset ink. This test results had relatively large amount of small scale noise. Therefore, the raw data was filtered and smoothed using Loess filter (Table Curve 2D, Systat Software). The procedure is a locally weighted regression smoothing algorithm that performs a full least-squares fit for each data point. Final results also had a large variation due to local variation and some potential artifacts of this instrument reaching up around 30% of coefficient of variation. Five tests on different spots are collected and averaged in this report.

2.8. Sample Preparation: General

2.8.1. Coating Color Preparation

Throughout this work, all the coatings are formulated with calcium carbonate pigments. Though there were many of trials mixed with clay pigments to get better industrial situation, they are sorted out in the initial stage to avoid structural compromise in dual pigments system and maintain simplicity. This will be described later. Most of calcium carbonate pigments are obtained in a slurry form from manufacturers, which can be readily in use. However, the pigments in dry type were dispersed with a certain amount of distilled water while adding small amount of polyacrylate type dispersant (Dispex N-40, Applied Colloids Inc.) toward an optimum dosage where low viscosity of the slurry becomes minimum. The Cowles type disperser was used. Besides this slurry preparation process, each of slurries was agitated well before mixing.

Low carboxylated Styrene-Butadiene latex (cp Dow 620 na, Dow Chemical Co.) was used as binder. The size and Tg was known as 0.17 ㎛ and 15 °C from manufacturer. The addition level varies from 6 parts per hundreds (pph) to 40 pph based on 100 parts of the dried weight of pigments. Additionally, 5 pph of plastic pigment (PP 788, Dow Chemical Co.) was used to control porosity and roughness easily in the calendering stage. The size of the plastic pigment (PP) was 0.13 ㎛. Also 0.5 pph of calcium stearate type lubricant (Suncote 655, Omnova) was applied both for preventing the coated surface from dusting and picking in the calendering stage. This also served for better calendering performance. Once ingredients are prepared, addition water, pigments slurry, plastic pigments, binder, and lubricant are mixed respectively whiling keeping agitation. Mixing was slowed down

at the binder addition stage to avoid a bubble formation. pH was checked and targeted toward 8.5~9 using 5 % solution of sodium hydroxide (NaOH). Besides, each addition was followed in 2 minute gap. After completion of addition, the suspension was fully agitated at a relatively high speed for at least 10 minute to ensure well dispersed mixing. Solid contents were checked by drying method and set toward 63%. This was relatively low solids level compared to industrial situation but this work does not require exact level because final properties are directly handled and of this work's concern. In fact, relatively low solid level was favored to reduce wound-rod marking on the coating surface due to fast consolidation in the coating stage.

2.8.2. Coating

Coatings were performed using a laboratory draw-down coater throughout this work to prepare coated samples. Coating speed was maintained as constant as possible while adjusting the other two parameters, the gap between rods and coating plate and number of rods to control the desired coat weight.

As base materials influence gloss of coated surface due to double reflection from coating surface and base substrate, non-glossy polyester film was used as base substrates. The Tappi 75° gloss of the film was 4.5 %. The coating on this matt type film should be also much easier than normal Mylar film. However, high amount of coat weight was desired to avoid the roughness influence from that of base film and also to accommodate the following roughness modification process, which will be described later. Eventually, 40 g/m^2 of coat weight was chosen on one side only. A small amount of ethanol was applied on the base film to promote better coating on non-porous materials. The base film Sheet

dimension was 210 mm (grain) × 200 mm (cross grain). This size may cause non-uniformity in coat weight due to the artifacts of coater, which should be carefully calibrated and controlled.

2.9. Structure Differentiation

2.9.1. General Approaches

Pore size was designed to be controlled mainly by pigments sizes, while porosity was mainly changed by controlling binder contents of coating. The more binder formulated, the rougher surface obtained mainly due to binder shrinkage. The pore size also change with binder contents, generally becomes smaller at higher amount of binder formulation. There might be an exception if one use non-film forming binders at operating conditions (Lepoutre et al, 1981, Alince et al, 1981). Another expectation with non-film forming binders was that it might not change pore size at various addition levels. It was also necessary to acquire a way to control roughness as designed level to investigate its effects on print gloss, while maintaining a leash to pore size and porosity. In Figure 2.13, a schematic experimental design is illustrated.

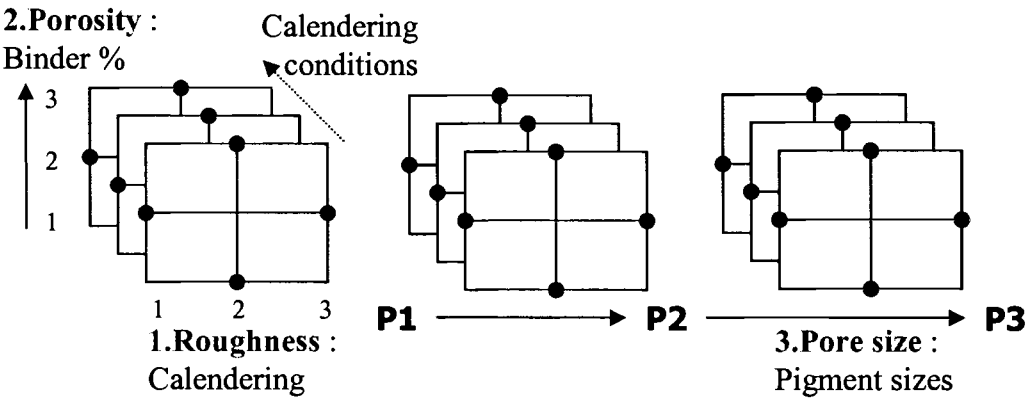

Figure 2.13: Conceptual factor control and experimental design.

2.9.2. Roughness and Pore Structure Control

A number of trial & error was done. Here are overall descriptions on the strategies tried in this project.

General requirements;

- As broad as possible coverage in terms of roughness, porosity, and pore size.
- Use pigments with narrow particle size distributions such as Precipitated Calcium Carbonate (PCC) to prevent or minimize pore size transform when changing porosity by binder contents of its coating formulation.
- Use calcium carbonate and clay mixture systems to get closer to the industrial situations.

Strategies;

- Base substrates with different levels in surface roughness to make samples to have various roughness at similar pore structure,

- Pigments with similarity in size but difference in shapes to get similar roughness but different pore structure,
- Non-film forming binders to restrain roughness and pore size change when varying porosity by its addition levels,
- Calendering sample with various rough materials to make samples with various levels in roughness at similar pore structure. During this process, pore size should be controlled to a certain constant level.

Trials and Results;

Figure 2.14 demonstrates pore structures of some commercial samples obtained from different countries. The data was for glossy wood-free coated papers, but the data range was similar regardless of grade from matt to glossy type. As observed in Figure 2.14, a desired pore size ranged from 0.04~0.2 μm.

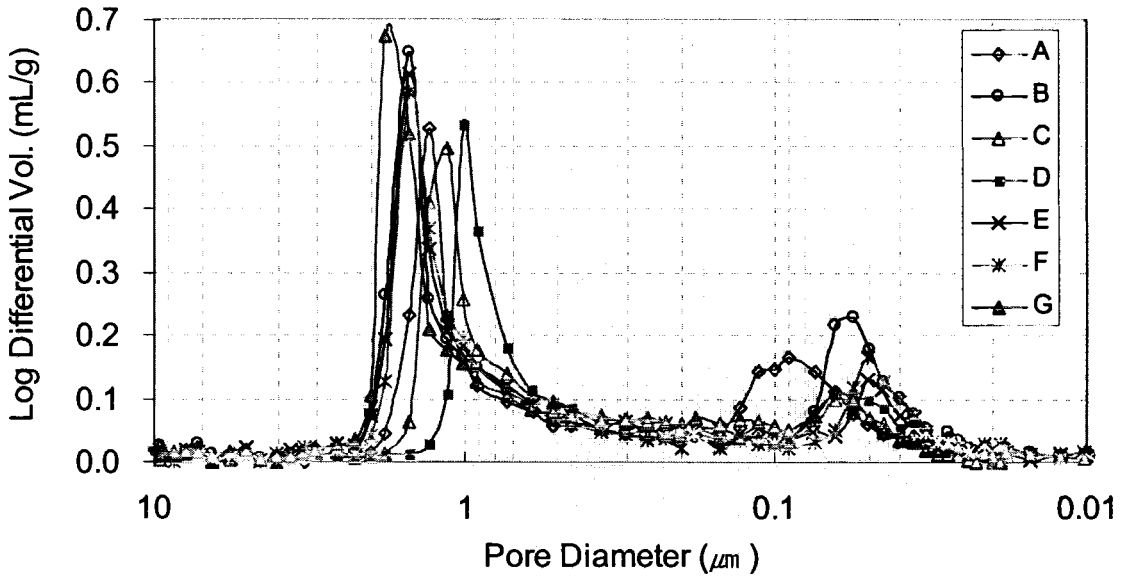

Figure 2.14: Pore size distribution of commercial glossy wood-free coated papers from various manufacturers in different countries.

Enough numbers of various PCCs were not available at the time of experiments and, as a consequence, some Ground Calcium Carbonate (GCC) was adopted. PCC with narrow particle size distribution looked like maintaining the same pore sizes when the pigment was formulated with various binder contents as observed by Donigian et al (1997), but, unfortunately, it was noticed at high resolution steps in mercury porosimetry that even this type of pigments shifted the mean pore size. The exemplary results are described in Figure 2.15 and 2.16.

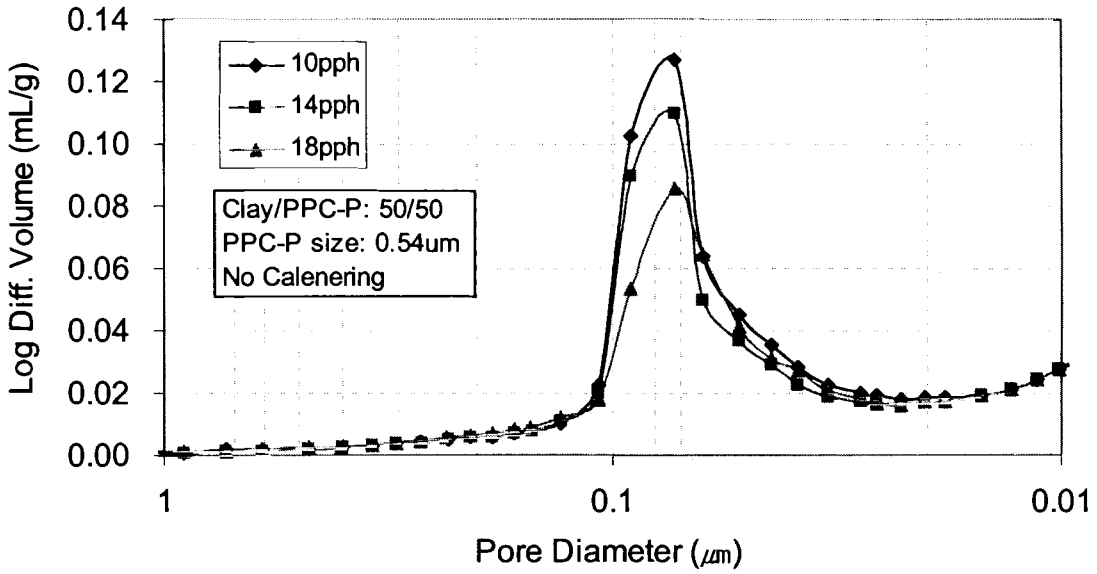

Figure 2.15: Porosity and pore size change with different binder contents for prismatic PPC and glossy clay mixture systems. It looks like there is no change in pore size.

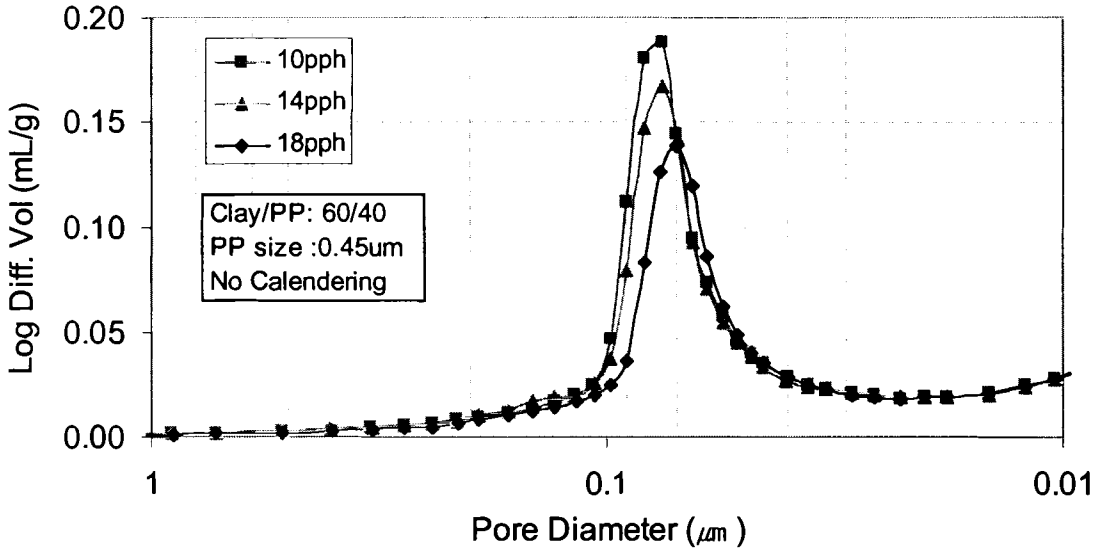

Figure 2.16: Porosity and pore size change with binder contents for PP and glossy clay mixture systems. Note that even the discrete PP systems show change in pore size with various binder levels.

For the first trial to use various rough base substrates, a smooth polyester film was grinded by conventional sanding tool with different grades of sand papers from 300 to 1500 grits. 'Grit' is a reference to the number of abrasive particles per inch of sandpaper. Coating was performed as described earlier. The resulted coating surface showed quite different roughness but the pigments particles are so much aggregated on the coating layer. The rougher surface was, the severer aggregation generated. Eventually, this method was dismissed. The second trial with pigments in similar particles sizes didn't give results as expected probably due to another potential reasons including rheological difference. However, the results are included in some another way, which will be presented later in preliminary experimental result. The third trial to utilize non-film forming binder also didn't produce consistent results. The binder, modified carboxylated

SB-latex, had Tg of 25°C and size of 0.13 μm. When this was formulated with GCCs and PCCs, the change of pore volume and pore size as well as roughness was almost unpredictable though mostly it depended on the size ratios. (If one can obtain various particle sizes but same spherical type of PCCs, then it may be worthy to try).

Laboratory supercalender was used to 'transfer' roughness to the sample surface. The roughness modification using calendering technique was very easy to perform, as shown in Figure 2.17., however it was a time-consuming job to match a certain pore size for a given pigment series, which has various binder contents. Each of calendered representative samples are analyzed to find its mean pore location using mercury porosimeter such that eventually a single pigment series with different porosity should have a certain same pore size. Pressure, temperature, speed, and number of nip pass were used as major control parameters.

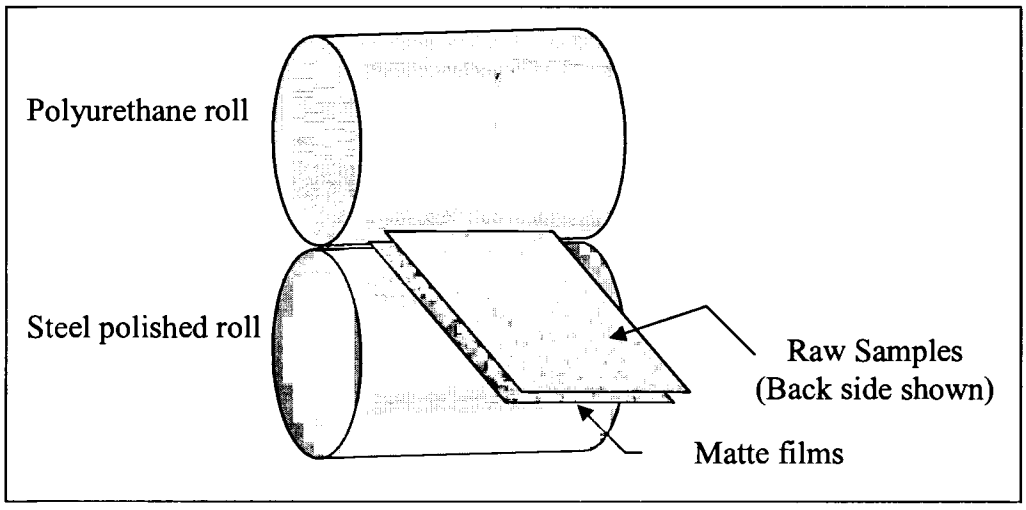

Figure 2.17: An illustration of sample calendering facing with matt surface materials.

Experimental procedures overview;

In summary, overall experimental procedure is described in Figure 2.18. The most critical stage was how to differentiate the factors.

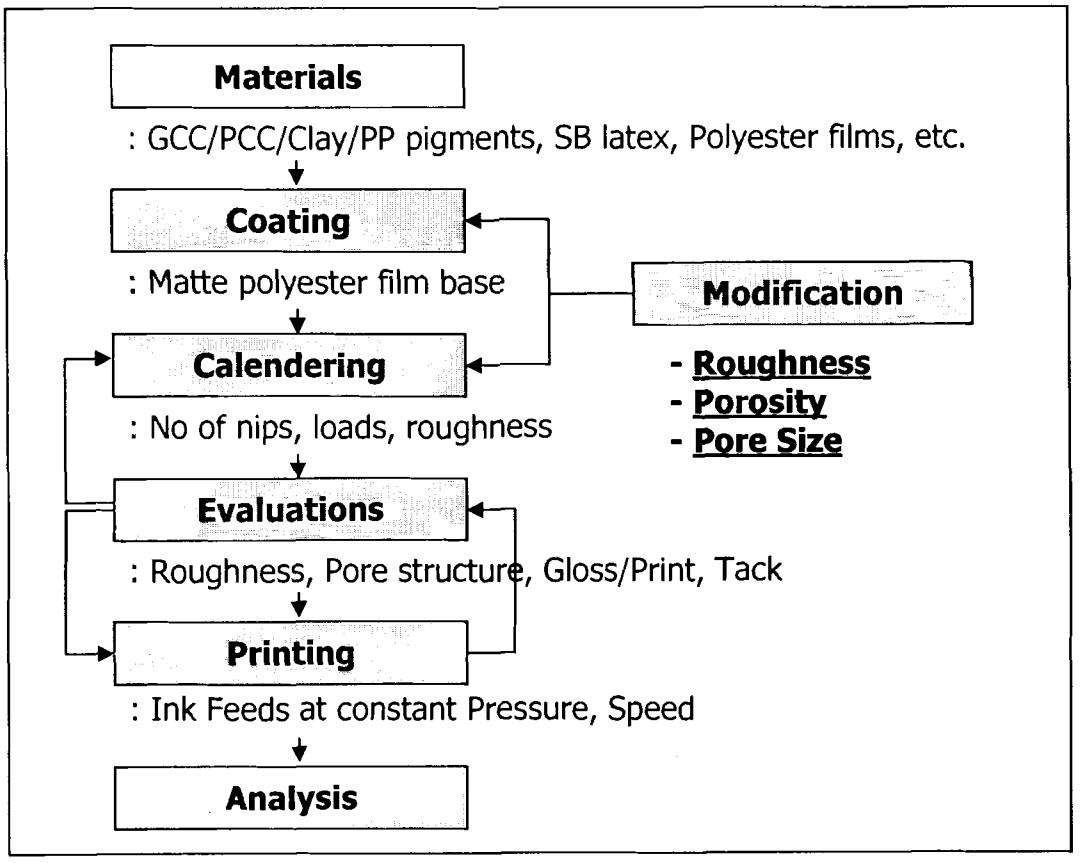

Figure 2.18: Schematic experimental procedures.

3. PRELIMINARY EXPERIMENTS

A preliminary work was necessary not only to find out adequate methodologies, but also find out a 'pathway' toward full-scale experiments and potential results otherwise enormous work in full-scale stage could be in vain. In this preliminary work, various methodologies were tried, previous findings are confirmed, and new aspects are emphasized.

3.1. Coating and Structure Modification

Sample coatings are performed on polyester film using laboratory draw-down coater following the general steps as described in Chapter 2. The grammage and roughness of base film was 112.5 g/m^2 and 2.3 μm, respectively. Pigments are summarized in Table 3.1 and the roughness of rough substrates for sample surface modification is given in Table 3.2.

Table 3.1: A summary of pigments used. Particle sizes are from manufacturers.

Pigment Code	Type	Particle size (μm)
G1-0.3	GCC	0.30 (96% < 2 μm)
G2-0.4	GCC	0.44 (95% < 2 μm)
G3-1.5	GCC	1.50 (60% < 2 μm)
P1-0.4	PCC- Aragonite	0.40
P2-0.6	PCC- Rhombohedral	0.60
P3-0.57	PCC- Prismatic	0.57

Table 3.2: The PPS roughness of substrates used for roughness control during calendering.

Type	Polyester Film							Sand Paper		
Code	PEN	PE1	PE2	PE3	PE4	PE5	PE6	SP1	SP2	SP3
Roughness (μm)	n/a	1.45	1.60	2.12	2.30	4.68	4.80	8.07	9.02	9.47

The pigments are formulated with different SB latex binder contents from 10 to 18 pph, for the sample No. 1 to No. 3, so that the porosities are accordingly changed. The other samples are fixed in binder addition level to 14 pph. Then various combinations between coated samples and rough materials are calendered. Calendering temperature was 65°C and the speed was maintained at minimum for maximum dwell time of samples under the nip. Calendering pressure was changed from 123 to 215 kN/m. At least two nip passes was found to give better roughness transfer. The prepared samples and their properties are summarized in Table 3.3. More details will be presented in the results. The roughness values are arithmetic average roughness based on leveled center line without long wave filtering. The area of 15 mm x 15 mm was scanned at least 10 times each, however, it was noted that roughness values was accompanying large deviation, which require more representative measurements and proper processing in the future work.

Table 3.3: Summary of prepared samples and their surface properties.

SAMPLE		Cal. Pressure	Roughness (um)		Paper Gloss 60°		Paper Gloss 75°	
No.	Code	(kN/m)	Ave.	Std. Err.	Ave.	SD	Ave.	SD
1	10G2-0.44-SP2+PE6	215	0.337	0.036	13.7	0.5	42.4	0.9
2	14G2-0.44-SP2+PE6		0.314	0.029	14.2	0.5	43.4	1.0
3	18G2-0.44-SP2+PE6		0.315	0.032	14.8	0.6	44.6	1.3
4	G2-0.44-SP1+PEN		0.258	0.026	23.0	1.2	51.7	2.1
5	G2-0.44-SP2+PE3		0.320	0.036	14.0	0.6	43.6	1.2
6	G2-0.44-SP3+PE6		0.284	0.050	17.0	0.2	48.1	1.1
7	G3-1.50-SP1+PEN		0.358	0.033	11.2	0.2	40.7	1.0
8	G3-1.50-SP2+PE3		0.337	0.028	7.7	0.2	36.7	0.9
9	G3-1.50-SP3+PE6		0.418	0.027	8.9	0.4	33.6	1.4
10	G3-1.50-PEN		0.154	0.030	21.6	0.4	61.2	0.6
11	G3-1.50-PE3		0.181	0.009	12.5	0.2	50.9	0.7
12	G3-1.50-PE6		0.294	0.014	12.3	0.8	49.2	1.4
13	G3-1.50-SP2		0.850	0.022	2.1	0.1	5.9	0.4
14	G1-0.30-SP2	137	0.841	0.103	4.0	0.2	14.1	0.4
15	G1-0.30-PE6		0.201	0.025	23.8	0.2	60.7	0.3
16	G1-0.30-PE1		0.107	0.017	36.7	1.0	71.4	0.5
17	G2-0.44-SP2		0.922	0.171	3.1	0.2	11.7	0.6
18	G2-0.44-PE6		0.209	0.048	21.0	0.6	58.6	0.4
19	G2-0.44-PE1		0.101	0.013	31.4	0.6	67.7	0.6
20	P1-0.40-SP2		1.045	0.145	2.4	0.1	5.8	0.1
21	P1-0.40-PE6		0.190	0.025	19.9	0.4	57.6	0.2
22	P1-0.40-PE1		0.158	0.015	29.0	0.2	66.7	0.6
23	P2-0.60-SP2		1.147	0.200	2.5	0.1	7.1	0.5
24	P2-0.60-PE6		0.239	0.027	18.9	0.2	56.4	0.4
25	P2-0.60-PE1		0.158	0.031	26.4	0.8	64.2	0.7
26	P3-0.57-SP2		0.899	0.195	3.0	0.1	9.7	0.4
27	P3-0.57-PE6		0.217	0.050	17.4	0.4	54.4	0.5
28	P3-0.57-PE1		0.092	0.012	24.9	0.8	62.4	0.3
29	G1-0.30-PE1-L	123	0.105	0.017	34.0	0.6	68.5	0.3
30	G2-0.44-PE1-L		0.101	0.009	30.4	1.0	66.4	0.6
31	P1-0.40-PE1-L		0.154	0.015	26.6	0.4	65.1	0.5
32	P2-0.60-PE1-L		0.131	0.017	24.4	0.2	62.4	0.6
33	P3-0.57-PE1-L		0.131	0.023	22.6	0.6	60.6	0.4
34	G1-0.30-PE1-H	184	0.086	0.009	34.3	0.2	69.3	0.3
35	G2-0.44-PE1-H		0.114	0.028	32.5	1.0	66.9	0.7
36	P1-0.40-PE1-H		0.112	0.013	28.4	0.2	66.1	0.9
37	P2-0.60-PE1-H		0.120	0.016	26.6	0.2	63.8	0.8
38	P3-0.57-PE1-H		0.135	0.024	25.2	0.2	62.1	0.6

3.2. Results and Discussions

3.2.1. Modified Structure

The samples are calendered with various rough materials and their combinations following by structural analysis using mercury porosimeter. Extremely rough or low gloss surfaces were obtained with sand papers, while matte to high gloss region was controlled with polyester films. Figure 3.1 shows the pore structure of the samples calendered sand paper and polyester film one after another. The mean or peak pore sizes are positioning almost at the same location though there is little bit of change in pore volume with the sample No.6. The observed values are given in Table 3.4. The compressibility was not corrected throughout the preliminary work.

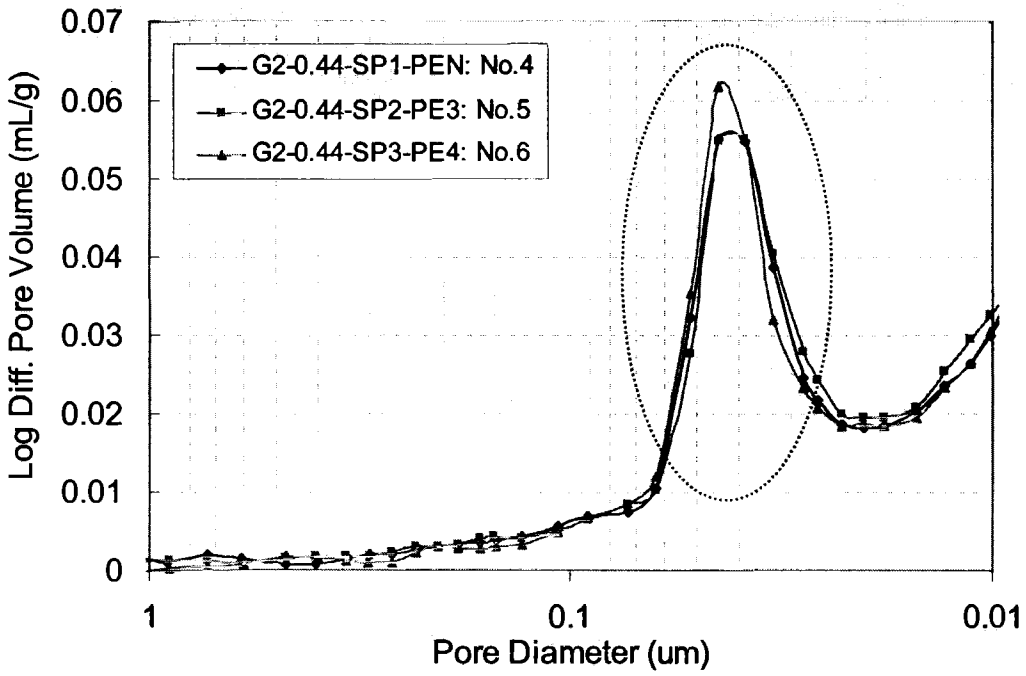

Figure 3.1: Pore size distribution of samples calendered with different combination of rough materials (sand paper + polyester film). Pore volume on Y is for the sample itself.

Table 3.4: Pore structure characteristics of the samples calendered with different combination of rough materials (sand paper + polyester film).

Samples		Roughness	75° Gloss	Pore diameter	Pore Volume
No.	Code	Ra (μm)		at peak (μm)	below 1 um (mL/g)
4	G2-0.44-SP1+PEN	0.258	51.7	0.040	0.136
5	G2-0.44-SP2+PE3	0.320	43.6	0.040	0.141
6	G2-0.44-SP3+PE6	0.284	48.1	0.042	0.136

It was thought that the sand papers may destruct the surface and reconstruct the surface with their large scale roughness features. Then polyester films with relatively small scale roughness than the sand papers may not maintain the same pore structures. As a result, it does little bit, however the change was within 0.005 um in peak pore size between the smoothest one and roughest one, as shown in Figure 3.2. Sand paper produced little collapsed structure shifting the peak region toward larger side. However, when the incremental pore distribution was checked, its peak was not much different with others. The collected data are given in Table 3.5. Therefore, it was concluded that the roughness modification with this calendering technique can be applied to produce various roughness with no or less change of pore structure.

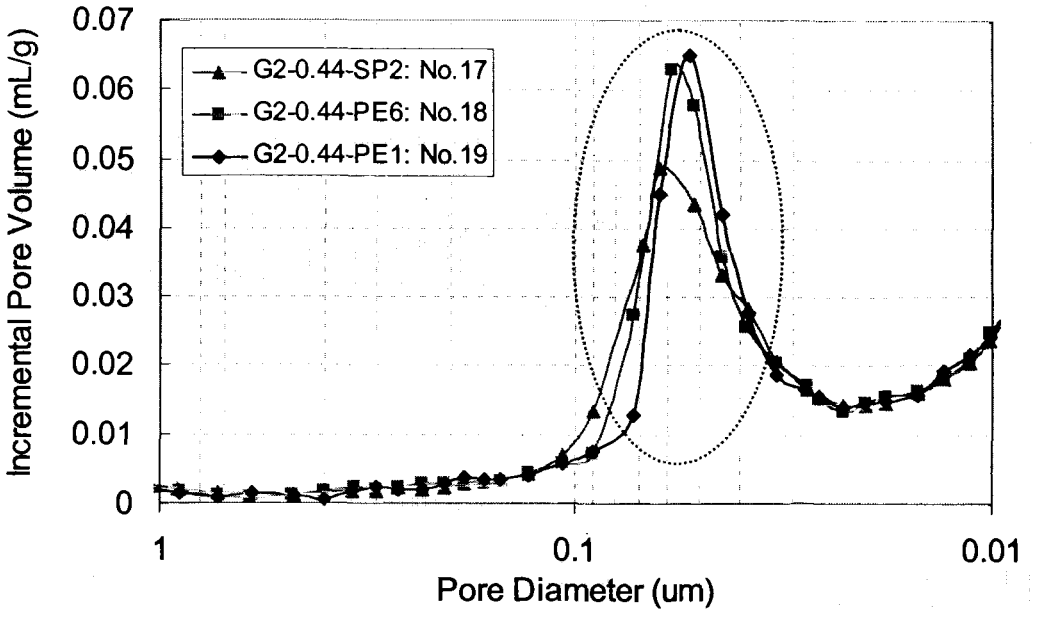

Figure 3.2: Pore size distribution of samples calendered with sand paper and polyester films separately. Pore volume on Y is for the sample itself.

Table 3.5: Pore structure characteristics of the samples calendered with sand paper and polyester films separately.

Samples		Roughness	75° Gloss	Pore diameter	Pore Volume
No.	Code	Ra (μm)		at peak (μm)	below 1 um (mL/g)
17	G2-0.44-SP2	0.922	11.7	0.058	0.173
18	G2-0.44-PE6	0.209	58.6	0.058	0.176
19	G2-0.44-PE1	0.101	67.7	0.052	0.169

3.2.2. General Results

The relationship between measured stylus roughness and paper gloss is presented in Figure 3.3. Even though there was relatively large variation in roughness values, the relationship was found good enough to be used except some extreme region. Thereby,

gloss may be used as roughness indicator or vice versa. However, gloss is a very steep function of roughness which may have large deviation; therefore conversion from measured roughness to gloss should be careful, if needed. Another thing worthy to note from this result was that the experimental relationship was far from theoretical one, shown in Figure 1.4 in Chapter 1. That may because of different roughness scale depending on measurement configurations. Many other reasons could exist, which will be discussed later.

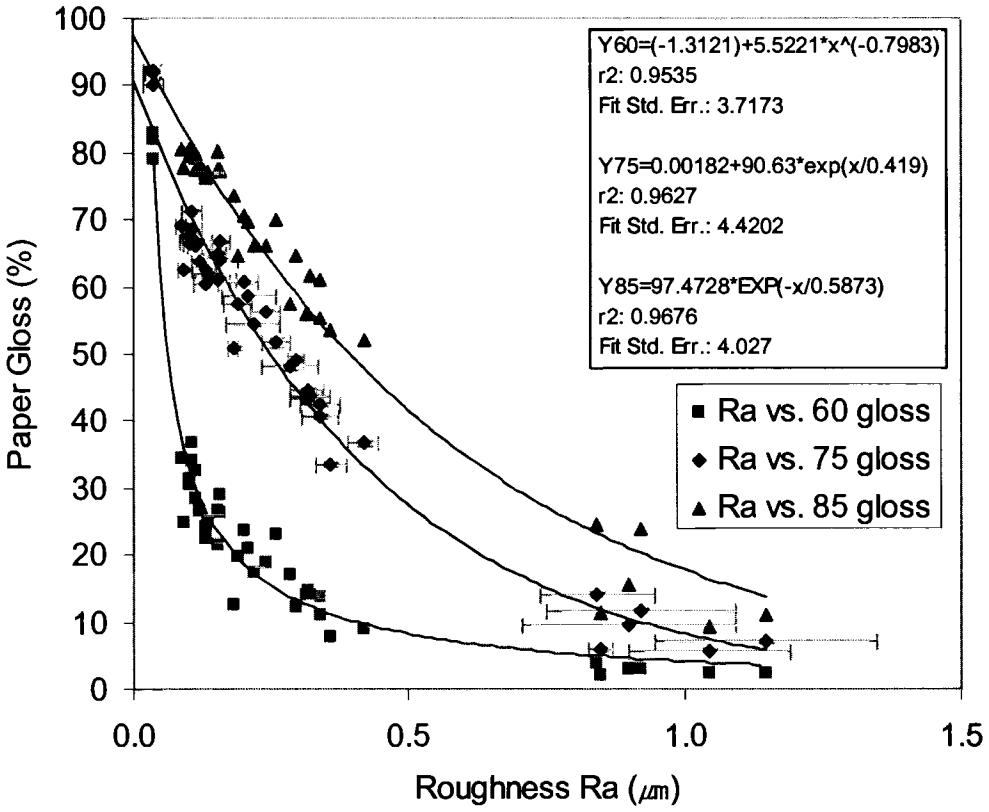

Figure 3.3: The relationship between measured roughness and paper gloss.

Print gloss was monitored with total 3 glossmeters at 3 different angles as described in Chapter 2. Consequently, calibration between them should be useful to convert one to another, especially for the case of laboratory dynamic glossmeter. Figure 3.4 is relationship between the voltage from the dynamic glossmeter and conventional 60° and 75° glosses. As expected, the relation between dynamic gloss and conventional 60° gloss was linear due to their geometrical similarity. This relation may be used to get a conventional print gloss value right after printing with dynamic glossmeter.

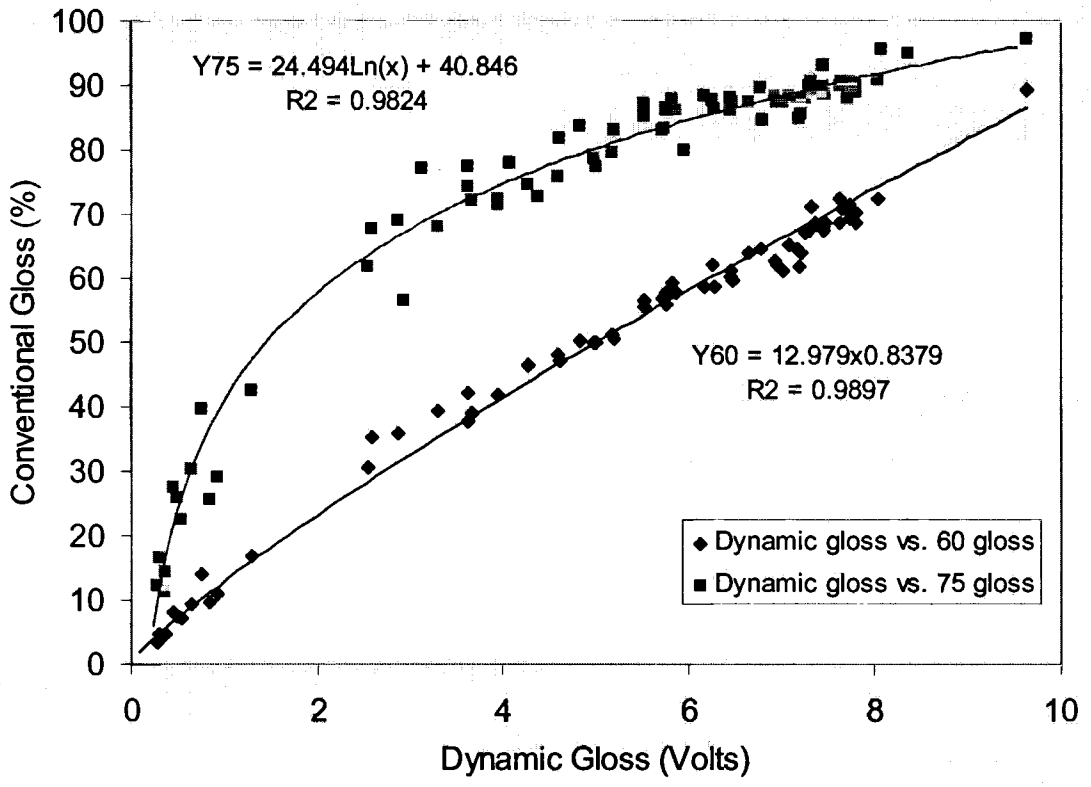

Figure 3.4: The relationship between laboratory dynamic gloss meter and conventional 60° and 75° gloss.

According to the Desjumaux (1999), dynamic print gloss after 10 seconds showed a good correlation with final print gloss. However, more time is needed to have higher relation with final print gloss as shown in Figure 3.5. These two different observation may be explained by considering different type of sample configuration; the samples in this work had wide variety in roughness and high roughness reduced the initial gloss rise drastically. Eventually, the dynamic gloss here was monitored for minimum 300 seconds.

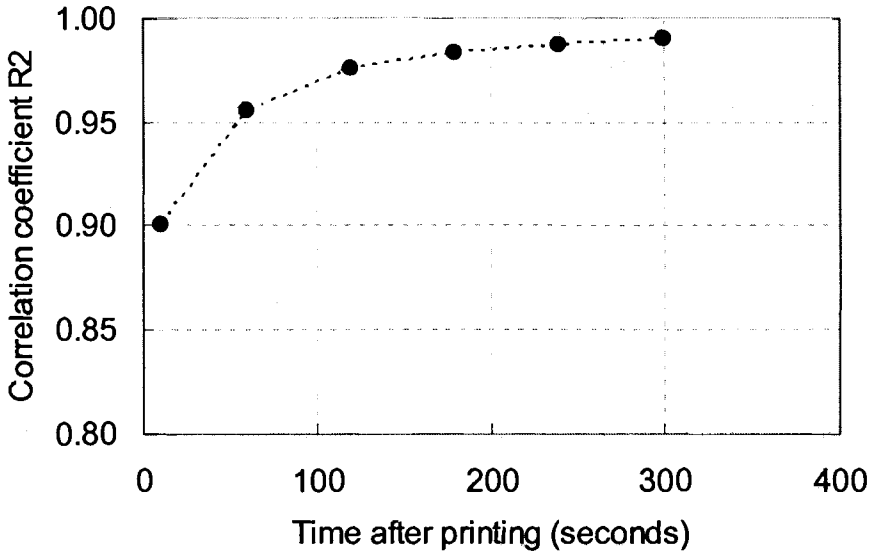

Figure 3.5: Correlation coefficient R^2 between dynamic print gloss and print 60° gloss as a function of measuring time.

Observed coating structures and the print gloss are summarized in Table 3.6. The presented roughness is arithmetic mean average value Ra over a 400 ㎛ tracking length from stylus profilometer. Void characteristics are the converted values for a coated layer without compressibility correction. The representative values for one sample will be used

for the samples with the same coating formulation but different roughness. Print gloss was obtained at 1.5~2.5 g/m^2 and reported at 2.0 g/m^2 ink level on the samples.

Table 3.6: Summary of coating structure and print gloss results.

SAMPLE		Roughness (um)	Paper Gloss		Pore Dia. at Peak	Pore Vol. (<1 um)	Total Int. Vol.	Print Gloss (%) after	
No.	Code	Ave.	60° Ave.	75° Ave.	(μm)	(mL/g)	(mL/g)	300s	days
1	10G2-0.44-SP2+PE6	0.337	13.7	42.4	0.050	0.159	0.212	34.0	28.5
2	14G2-0.44-SP2+PE6	0.314	14.2	43.4	0.042	0.133	0.195	48.0	30.5
3	18G2-0.44-SP2+PE6	0.315	14.8	44.6	0.032	0.107	0.179	64.0	36.0
4	G2-0.44-SP1+PEN	0.258	23.0	51.7	0.040	0.136	0.185	58.0	42.1
5	G2-0.44-SP2+PE3	0.320	14.0	43.6	0.040	0.141	0.187	55.4	34.6
6	G2-0.44-SP3+PE6	0.284	17.0	48.1	0.042	0.136	0.192	50.6	33.6
7	G3-1.50-SP1+PEN	0.358	11.2	40.7	-	-	-	57.7	-
8	G3-1.50-SP2+PE3	0.337	7.7	36.7	-	-	-	53.9	-
9	G3-1.50-SP3+PE6	0.418	8.9	33.6	-	-	-	48.8	-
10	G3-1.50-PEN	0.154	21.6	61.2	-	-	-	-	-
11	G3-1.50-PE3	0.181	12.5	50.9	-	-	-	62.7	-
12	G3-1.50-PE6	0.294	12.3	49.2	-	-	-	51.6	-
13	G3-1.50-SP2	0.850	2.1	5.9	-	-	-	10.1	-
14	G1-0.30-SP2	0.841	4.0	14.1				11.2	9.5
15	G1-0.30-PE6	0.201	23.8	60.7	0.044	0.174	0.214	47.7	47.5
16	G1-0.30-PE1	0.107	36.7	71.4				65.7	61.5
17	G2-0.44-SP2	0.922	3.1	11.7	0.058	0.173	0.233	12.3	9.8
18	G2-0.44-PE6	0.209	21.0	58.6	0.058	0.176	0.213	55.5	52.5
19	G2-0.44-PE1	0.101	31.4	67.7	0.052	0.169	0.210	68.9	65.5
20	P1-0.40-SP2	1.045	2.4	5.8				4.6	3.4
21	P1-0.40-PE6	0.190	19.9	57.6				51.1	44.5
22	P1-0.40-PE1	0.158	29.0	66.7	0.083	0.227	0.267	59.4	55.6
23	P2-0.60-SP2	1.147	2.5	7.1				5.0	4.1
24	P2-0.60-PE6	0.239	18.9	56.4				57.1	52.6
25	P2-0.60-PE1	0.158	26.4	64.2	0.106	0.232	0.274	67.8	64.1
26	P3-0.57-SP2	0.899	3.0	9.7				7.5	6.1
27	P3-0.57-PE6	0.217	17.4	54.4				55.7	52.9
28	P3-0.57-PE1	0.092	24.9	62.4				70.8	66.1
29	G1-0.30-PE1-L	0.105	34.0	68.5				56.3	57.4
30	G2-0.44-PE1-L	0.101	30.4	66.4				72.0	65.9
31	P1-0.40-PE1-L	0.154	26.6	65.1				65.9	59.5
32	P2-0.60-PE1-L	0.131	24.4	62.4				69.3	65.7
33	P3-0.57-PE1-L	0.131	22.6	60.6	0.110	0.229	0.274	70.1	64.4
34	G1-0.30-PE1-H	0.086	34.3	69.3				61.7	60.7
35	G2-0.44-PE1-H	0.114	32.5	66.9	0.049	0.160	0.191	69.7	64.8
36	P1-0.40-PE1-H	0.112	28.4	66.1				62.3	58.6
37	P2-0.60-PE1-H	0.120	26.6	63.8				69.0	64.7
38	P3-0.57-PE1-H	0.135	25.2	62.1				67.8	63.8

3.2.3. Effect of Coating Roughness at Constant Pore Structure

After printing with various amount of ink, the print gloss data were extracted based on a certain amount of transferred ink on samples using interpolation. In most cases, the ink transfer ratio ranged from 20 to 49 % was decreasing with increasing the amount of ink feed on roller, thereby the printed surface assumed to be 100% ink covered solid image. Roughness effect was sought by plotting the print gloss of the samples with the same coating but different paper roughness. The print gloss 300 seconds after printing is given in Figure 3.6 while final print gloss in Figure 3.7. Note that the abscissa is in log scale, pore size is given in 'nm', and pore volume of coating layer is for the region below pore size of 1 μm in 'mL/kg'. The roughness of paper influenced the print gloss for the whole range of parameters, even when the ink thickness was larger than the roughness. Also the significant difference in print gloss level at the same roughness can be explained by analyzing other factors, i.e. their pore structure. At this point, it will be interesting to see the effect of roughness in terms of paper gloss. The results are given in Figure 3.8 and 3.9. As shown, the relationship became clearer than that of roughness. Highest roughness was belong to 'matt' category of paper while lower one to 'dull to gloss' category. G1 series with smallest pore size produced lowest print gloss, while G2 series with larger pore size but similar pore volume with G1 had higher print gloss. The difference may be explained by considering their expected setting and leveling behavior such that the larger pore size of G2 has slow setting due to its low capillary force to pull down the mobile phase of ink, in turn gives more time to level down, and finally reach higher print gloss. This interpretation also expands to the case of P1, P2, and P3 series though it was hard to distinguish P2 from P3 in terms of their structure.

However, there was an uncertainty between G2 and P1. G2 has smaller pore size but small pore volume compared to P1, which finally reached low print gloss close to that of G1. At this point, this competitive result can not be determined or explained in a quantitative way. Another noticeable result was the behavior of G2-1 series with smallest porosity. This series showed relatively high print gloss at 300 seconds after printing but drastically reduced value after several days. The distinct features of this series were its low porosity and the only one treated with the combination of 'sand paper and polyester film' in this comparison group. Therefore, slow setting toward to rougher paper surface might result in relatively high initial print gloss but eventually lowered end. This may be one of clear reflections of the roles of roughness and leveling on print gloss development. Then, conversely, it was questioned whether a rough surface with relatively fast setting could produce higher print gloss if it stops leveling earlier before the drastic reduction in print gloss. This query is certainly interesting and under pursuit. More results are reported in the full-scale stage.

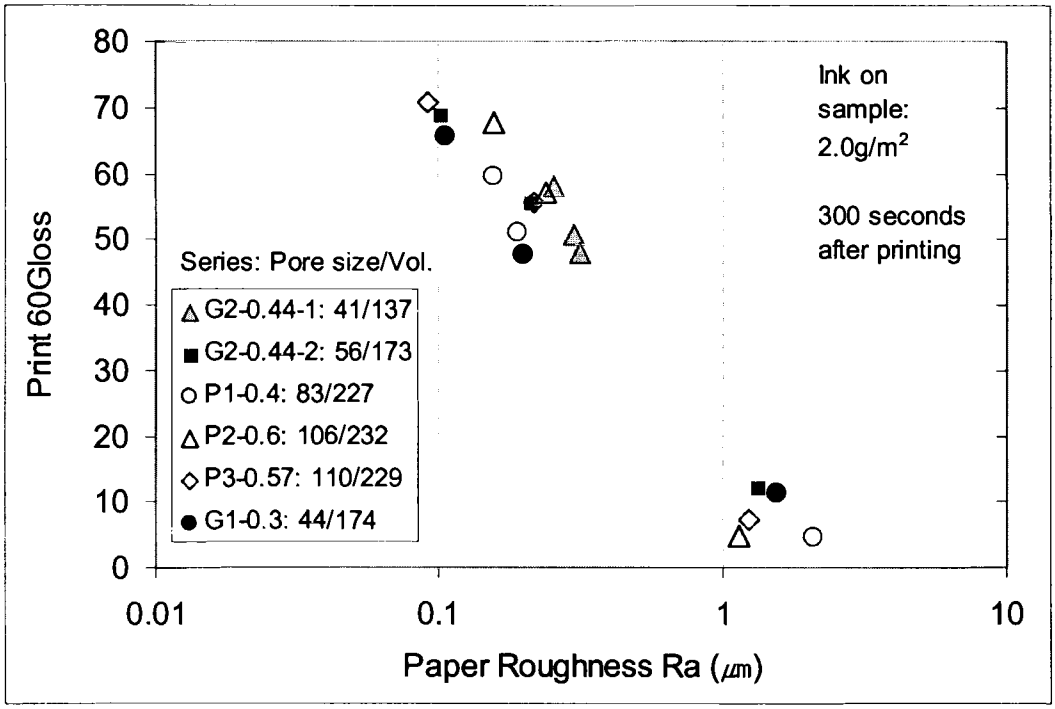

Figure 3.6: Influence of roughness on print gloss 300 seconds after printing.

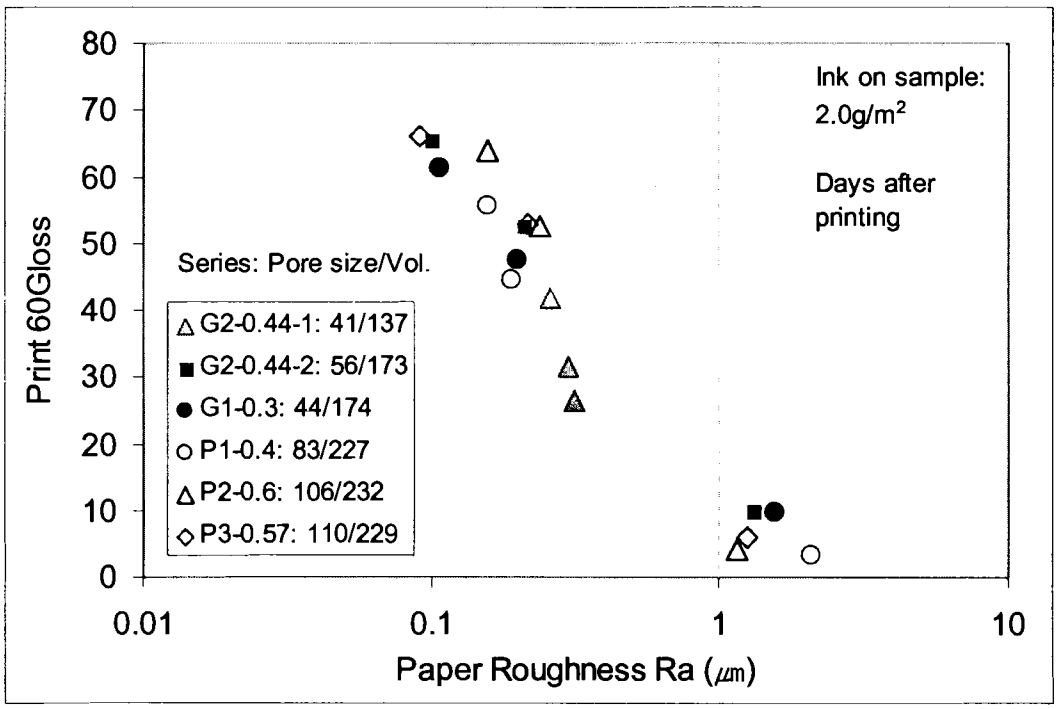

Figure 3.7: Influence of roughness on 'final' print gloss.

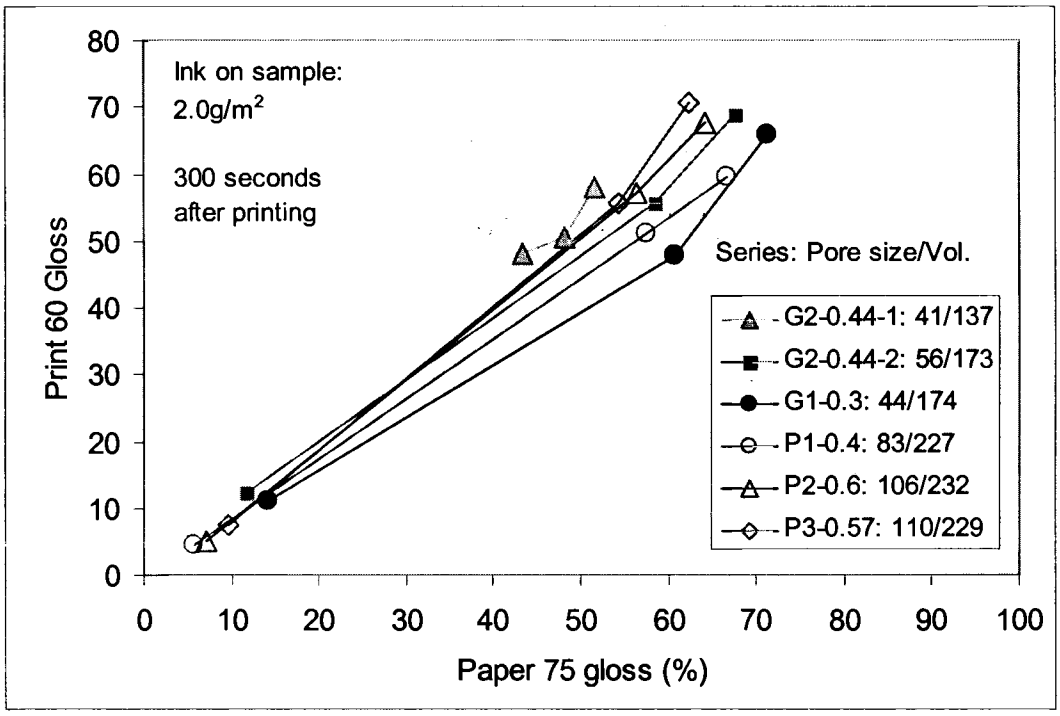

Figure 3.8: Print gloss 300 seconds after printing as a function of unprinted paper gloss.

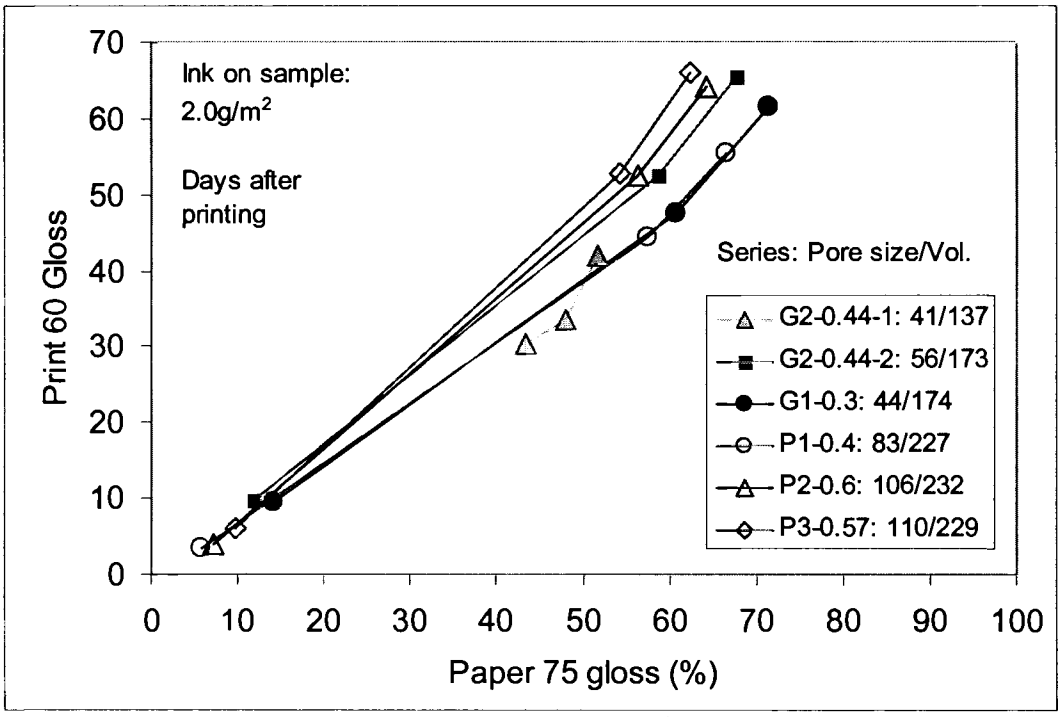

Figure 3.9: Print gloss several days after printing as a function of unprinted paper gloss.

3.2.4. Effect of Porosity at Constant Roughness

Samples with different porosities with a certain same pore size were desired to find the effect of porosity only on the print gloss. However, the prepared samples with various binder contents did not match the mean pore size as Figure 3.10 shows. Indeed, the set of samples were overlapping one after another depending on the addition levels, respectively. This obstacle should be overcome in the full-scale stage. However, the samples may still show some effect of porosity since the lower porous samples did not have more small pores than higher one. This means that higher porous samples have additional porosity ahead of different pore size.

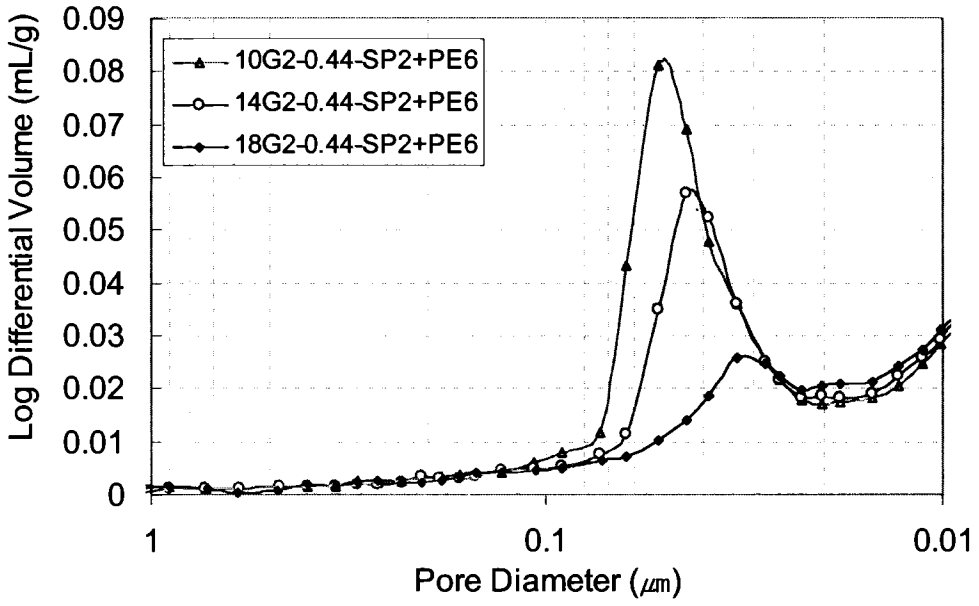

Figure 3.10: Pore structures of the samples with various binder contents. Pore volume on Y-axis is for the sample itself.

The printed results are given in Figure 3.11. Relation was rather linear within the sample range and showed that porosity was certainly one of major factors on print gloss. Again, more porous coating has more potential to uptake mobile phase of ink reducing setting and leveling time, in turn producing a lower print gloss. Large gloss drop was also observed with the given samples, which were calendered with a combination of sand paper and polyester film.

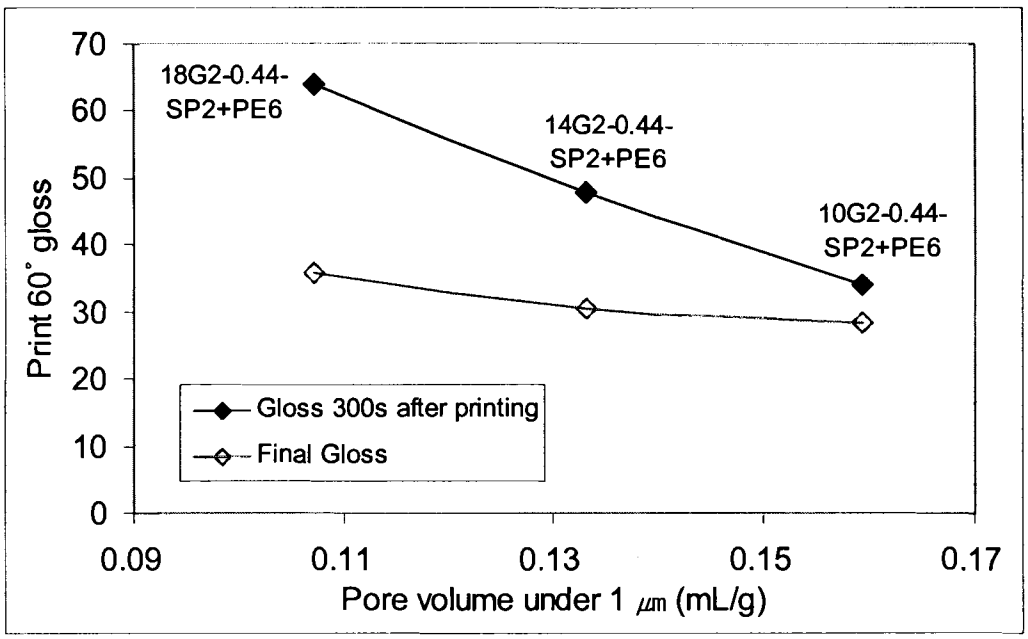

Figure 3.11: Effect of porosity on print gloss at a constant roughness. Roughness ranges from 315 to 337 nm (gloss from 42.4 ~ 44.6%). Ink on sample; 2.0g/m^2.

3.2.5. Effect of Pore Size at Constant Porosity and Roughness

Since roughness and porosity are handled as above, finally, this part concerns on the effect of pore size on print gloss. It must be necessary to maintain the roughness and porosity at the same condition for undisrupted observation of pore size effect. Samples

with similar roughness and porosity are sorted out and plotted in Figure 3.12 and their structures in Figure 3.13.

The similarity between sample No.15 and 18 as well as No.22 and No.25 made it possible to find the effect of pore size. The range of factors were roughness from 110 to 210 nm (75 paper gloss from 58 ~ 67%), pore size from 44 ~ 110 nm, pore volume (< pore size of 1 ㎛) from 0.034 ~ 0.46 mL/g. As expected, the increase in print gloss was observed with larger pore size by the way explained earlier. Sample No.35 deviates from No.15 and No.18 for lower roughness and porosity. The different level between (No.15 and 18) and (No.22 and No.25) can be explained by their porosity difference despite of larger roughness of the first group. One thing to note was that the sample No.33 and No.35 had almost the same print gloss despite of their much different structure; The high print gloss of No.35 was thought to come from low roughness and porosity, while that of No.33 mainly from large pore size. However, this result may not be enough to explain this competitive result.

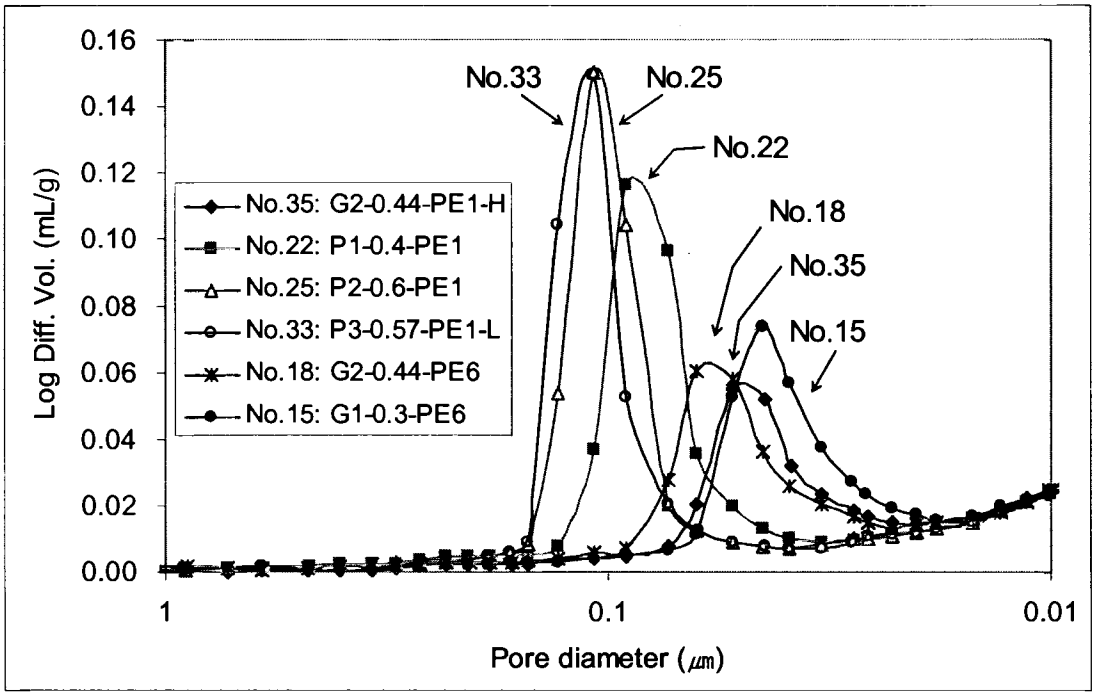

Figure 3.12: Pore structure of the sorted samples for pore size effect. Pore volume on Y is for the sample itself.

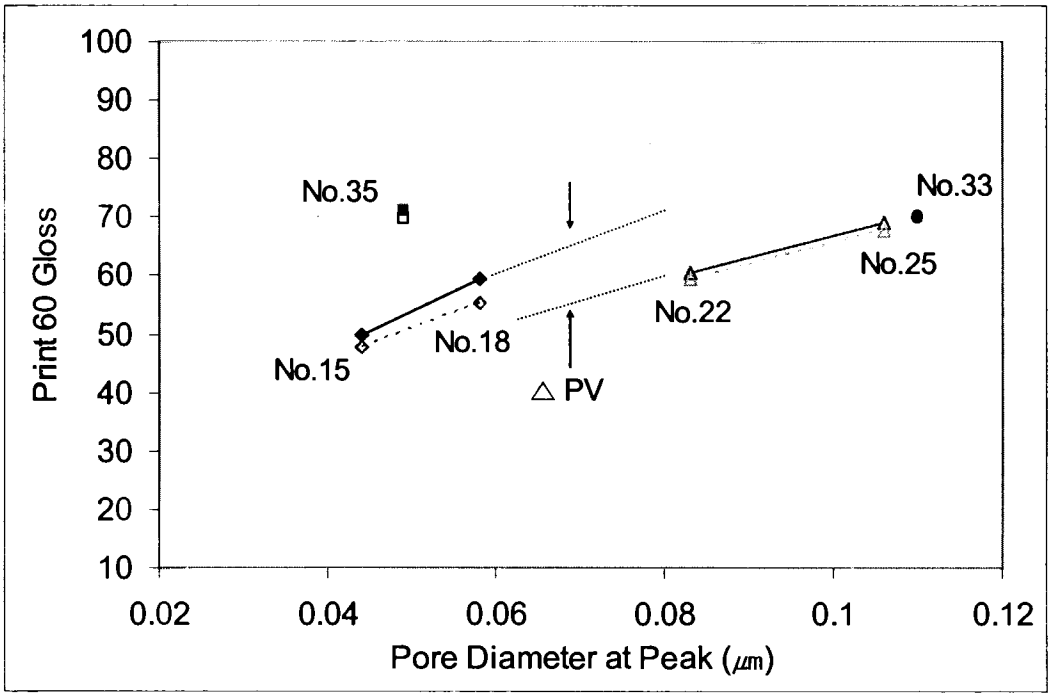

Figure 3.13: Effect of pore size on print gloss at similar roughness and porosity levels.

3.2.6. Structural Effect on Print Gloss Dynamics

Further investigation on print gloss development can be expanded by monitoring gloss development as a function of time with dynamic glossmeter. A conceptual gloss evolution in time is given in Figure 3.14. Amplitude represent a roughness of ink film and the graphs in second column show leveled off portion of the surface roughness components based on wavelengths. As time goes by, also included was potential roughness emergence due to ink film shrinkage and particle protrusion. Corresponding roughness values and gloss response to the change of surface profile is shown in right side. Another probable source of contoured flow along with sample roughness will be discussed later. The rapid initial increase in gloss dynamic curves is best explained by considering a rapid leveling of small scale roughness of the ink film, continuously and simultaneously following by that of longer scale ones. The selected samples reported earlier in this chapter are analyzed and the focus was on the initial growth behavior of the print gloss with various structures.

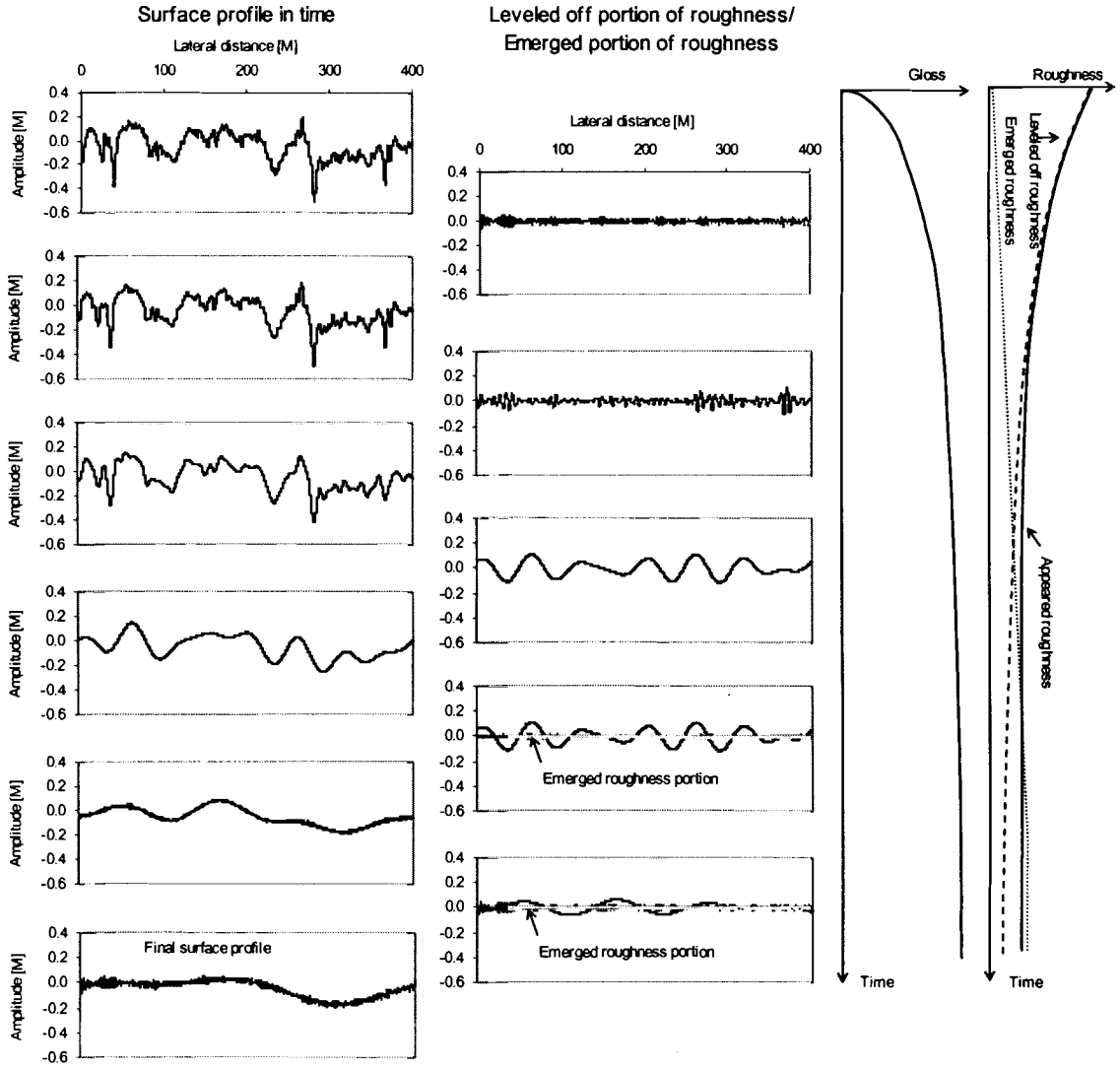

Figure 3.14: Schematic illustration on surface feature change and gloss development. Left side graphs are the evolution profiles of a surface in time. The profiles in the middle graphs describe changed portions of surface profile in time. A conceptual roughness emersion is depicted. Right graphs are schematic development curves of print gloss and roughness, from left to right, respectively.

The print gloss development on various rough coatings is presented in Figure 3.15. The values are interpolated at the same ink amount on samples. The effect of roughness was again consistent with the results of the final gloss. The 'critical gloss rise' time to maximum or 90% of maximum at an initial stage was also in the same order as coating gloss, as observed, however the dynamic gloss level itself was restricted by their roughness level. When the result was plotted in a log scale of time for clearer observation on the very initial behavior of print gloss (Figure 3.16, 3.17), it was found that the print gloss were initially different from the starting point depending on the roughness of coating surface at a given ink amount on coating. This may reflects the roughness effects on ink transfer or ink splitting. However, it is hard to differentiate at this time whether this initial difference is exactly caused from different ink feed amount, i.e. the rougher surface is, the more ink is usually fed to get a same ink amount on sample, or influence of the roughness on splitting phenomenon, i.e. the rougher surface is, the more splitting may occur. The decay or deflection in print gloss will be discussed in the following sections.

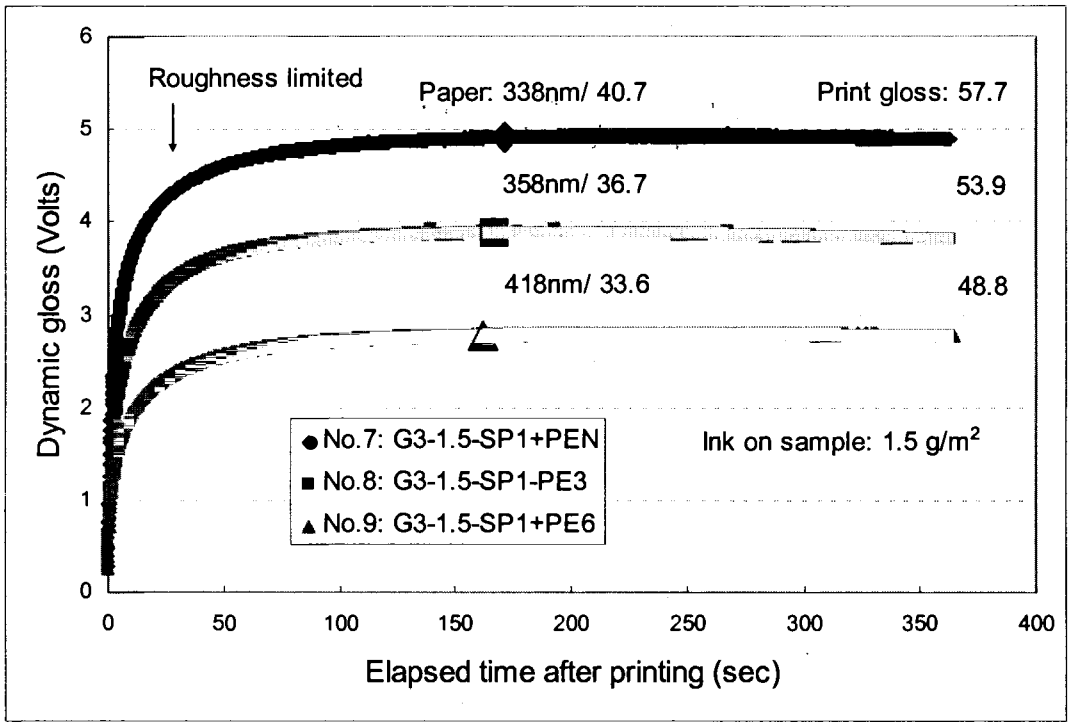

Figure 3.15: Dynamic print gloss as a function of time and roughness of coating surface.

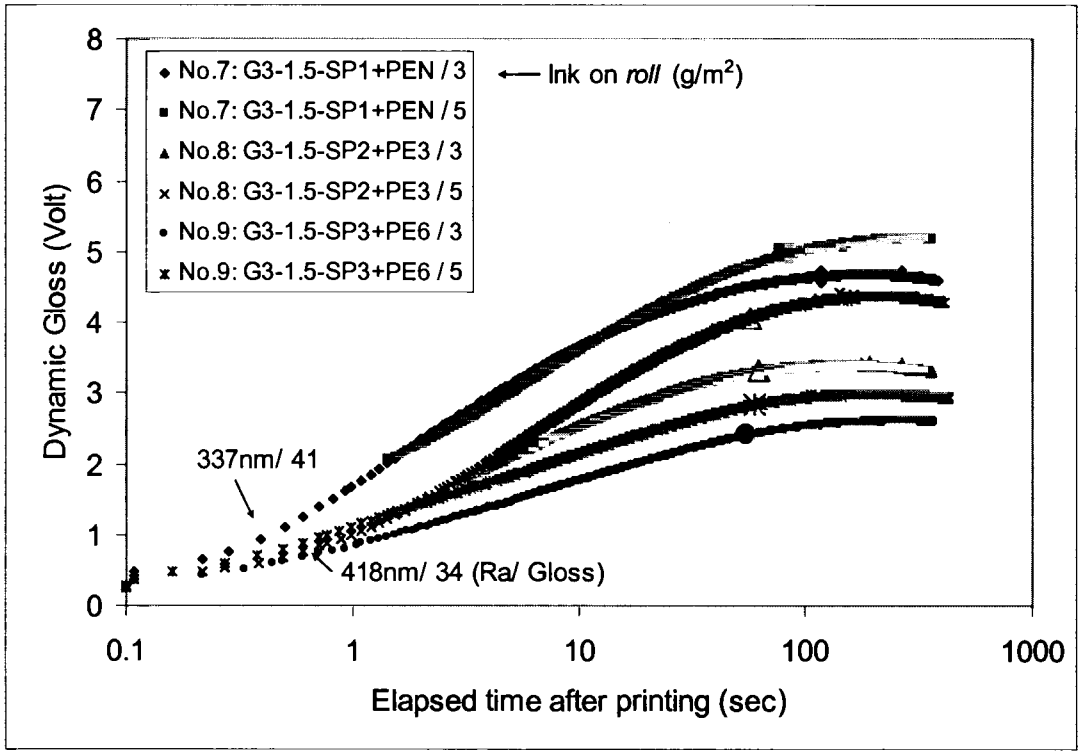

Figure 3.16: Initial dynamic print gloss as a function of time in log scale and roughness of coating surface. No.7~9 of G3 series. Note that inking amounts are based on the roll.

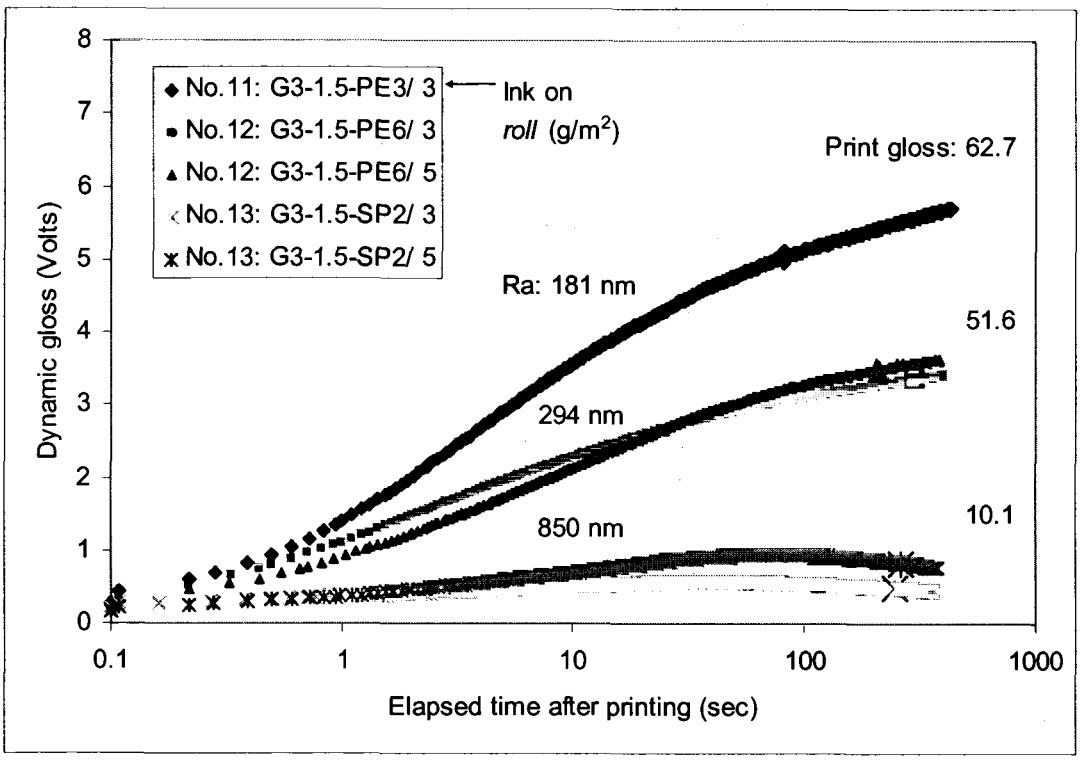

Figure 3.17: Initial dynamic print gloss as a function of time in log scale and roughness of coating surface. No.11~13 of G3 series. Note that inking amounts are based on the roll.

The behavior of print gloss development for different porosities, as shown in Figure 3.18, is different from that of roughness and pore size. Unlike the roughness effect, which determined the gloss level from the starting point, the porosity effect at short times was reversed order compared to long time such that low porosity has low dynamic print gloss, as seen in Figure 3.19. The low initial gloss for less porous surface could be explained partly because of larger splitting pattern formation (Glatter et al, 1996). Again, the initial difference may also come from different amount of ink supply, i.e. the more binder, the less transfer, in turn the more ink supply for a certain amount of transferred ink on sample (e.g. Zang and Aspler, 1998). Within 10 seconds here, the dynamic gloss of each sample followed in a consistent order with their final print gloss. While the dynamic print

gloss of less porous one has been relatively 'accelerated', that of higher porous one was restricted and even deflected toward lower side from its maximum. Accordingly, their critical gloss rise time were observed to be much different from each other. Therefore, the influence of porosity was thought not to be level-determining type but to be leveling potential with time. Small porosities seem to produce longer filaments that level slowly, but longer times for leveling.

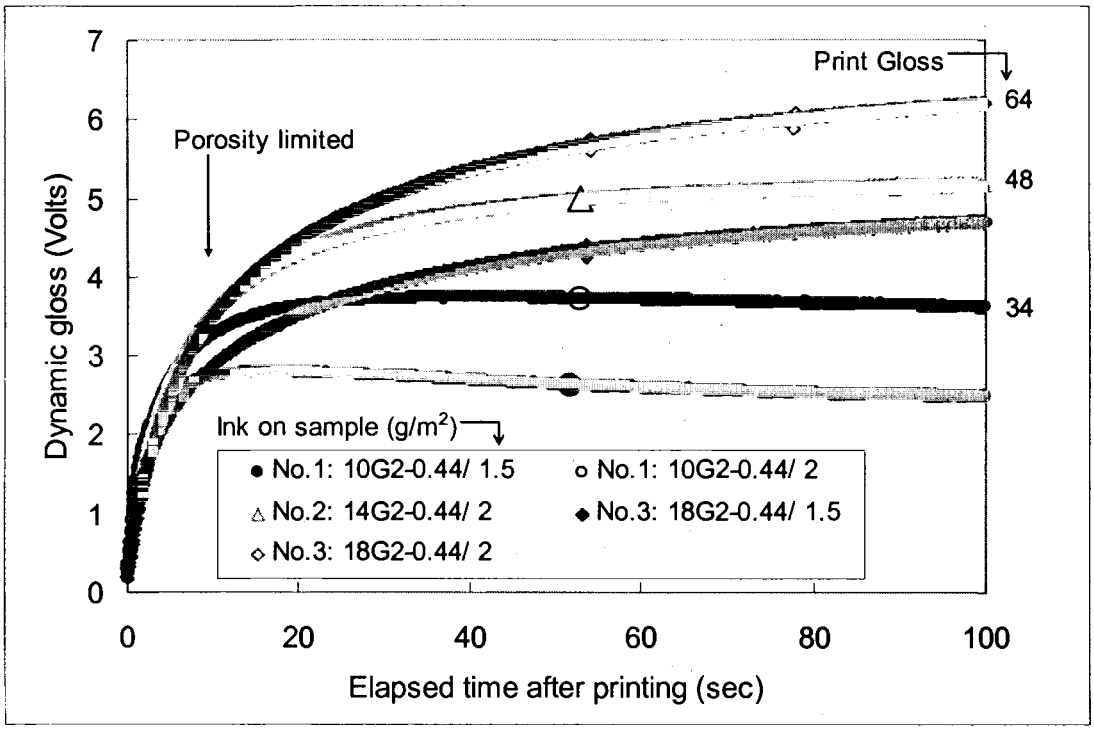

Figure 3.18: Print gloss development as a function of time and porosity

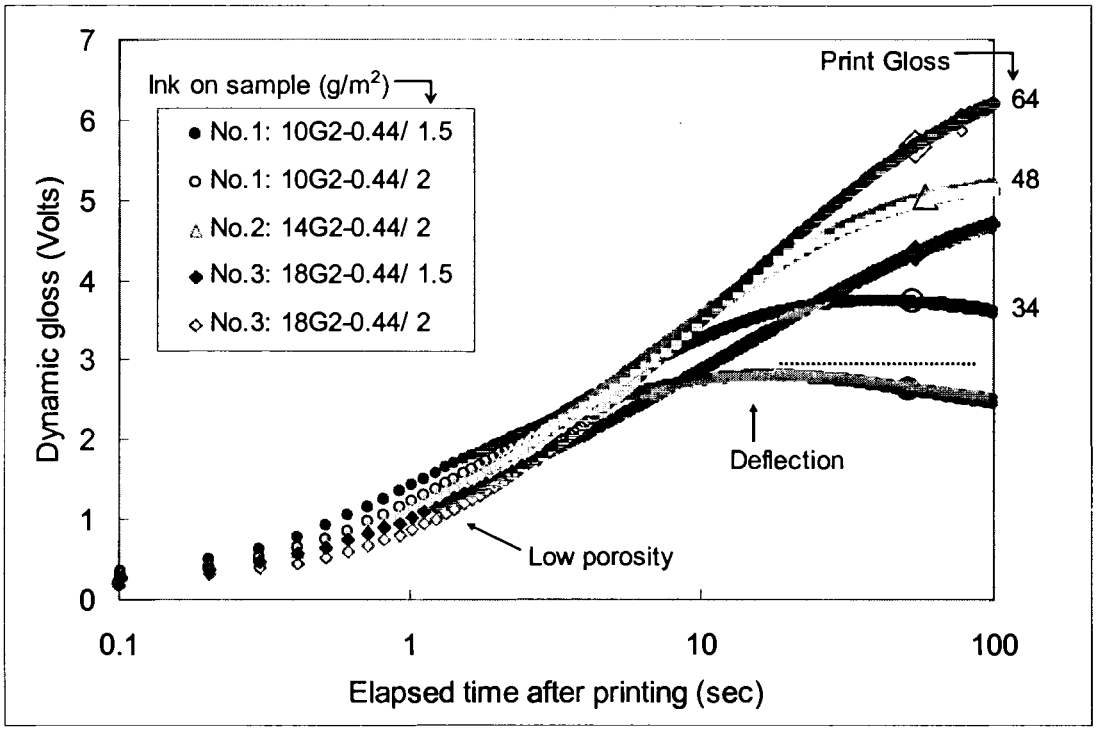

Figure 3.19: Print gloss development as a function of log time and porosity.

The decrease from the maximum gloss was another features observed. Several reasons could exist for this declination; film shrinkage, protrusion of ink components, extended movement along with coating surface. During ink setting process, relatively high amount loss of solvent into the porous coating layer may cause earlier oxidation accelerating the shrinkage of ink film, leading lower print gloss. Layering or packing of ink film is another aspect; a certain amount of ink solvent is removed into coating at a rate depending on the absorption potential of coating layer associated with ink rheological properties. Pigment volume concentration (PVC) will of course increase. Surface tension forces the ink film to level and maintains a level surface whereas ink particles are pushed down and gradually lose their mobility due to increased viscosity and developed viscoelasticity. At a certain point in time and over further shrinkage with mobile phase loss, the surface tension may no longer maintain a level surface if the capillary force is strong enough. Consequently, the surface of ink film may form around the particles protruding out of wet glossy surface profile and result in a rugged surface. Imbibition amount and rate may determine the protrusion or menisci formation. This kind of roughness development may occur only after a certain amount of solvent loss (e.g. Field, 1995). Resin component may also depart from surface to inner side along with solvent on a highly absorptive surface, resulting more rugged surface with ink pigments than on a slow surface, producing less print gloss (e.g., Preston et al, 2002). These two potential reasons, however, may not successfully explain the gloss reduction only on rough surfaces. As illustrated in Figure 3.14, leveling is simultaneous but successive happening because of difference in leveling time of each feature. In practical sense, the surface of leveling base, i.e. coating surface, is neither smooth nor identically arrayed with the

surface profile (or roughness) of ink film. Even though the ink film may split along with the surface profile of coating surface as postulated by DeGrace et al (1984), split pattern may recoil and transform into various amplitude and wavelength. Therefore, once the small features of ink film are quickly leveled down increasing gloss, relatively larger features will continue to level on eclipsed array of coating roughness, which may give a maximum at a certain point and decrease as the ink film continue to flow down contouring that of coating roughness. A conceptual illustration is given in Figure 3.20. Only large enough roughness may cause this contouring and significant gloss reduction. The deflection time will also vary depending on the other factors such as pore structure.

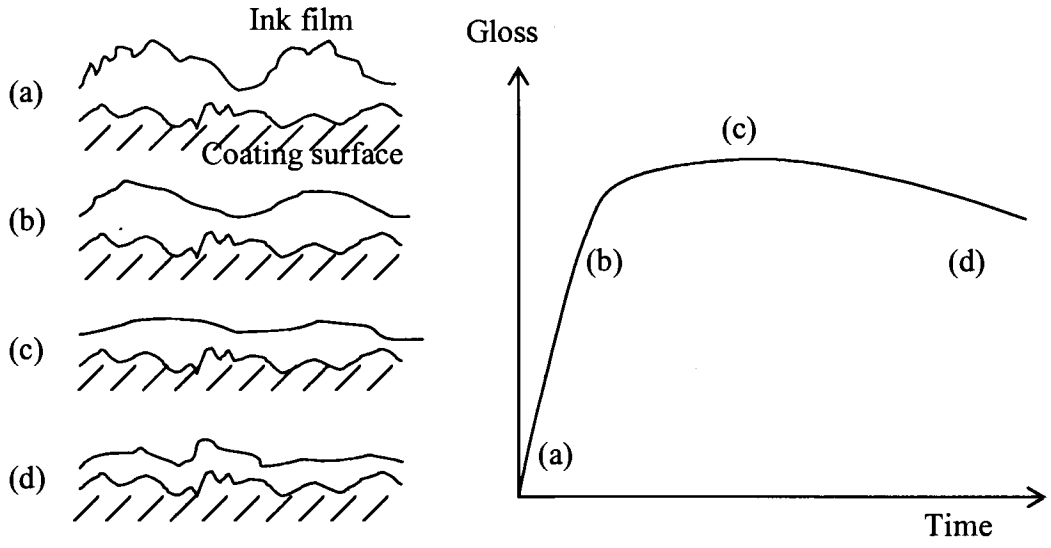

Figure 3.20: A conceptual illustration on gloss decrease in time. (a) on initial surface, (b) rapid gloss growth region, (c) maximum point, (d) reduction in gloss.

The effect of pore size was so clear that the larger pore size, the higher print gloss produced (Figure 3.21). However, pore size did not show their significant influence on the initial gloss though the levels of print gloss in time distinguished each other (Figure

3.22). Therefore, pore size was thought to be one of level determining type factors on print gloss.

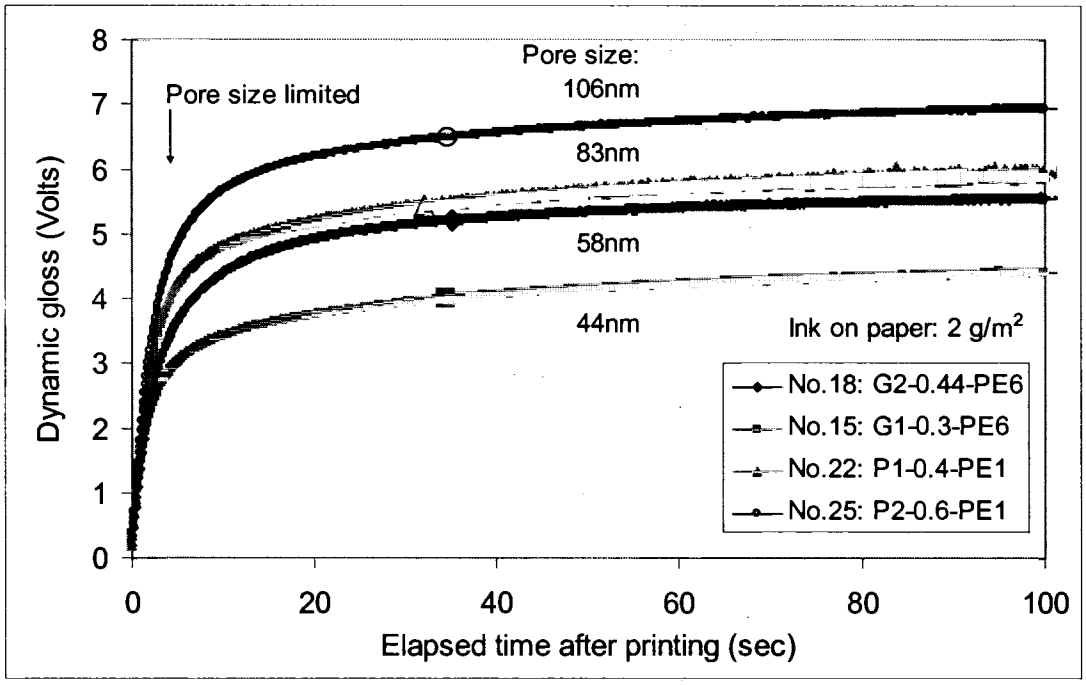

Figure 3.21: Print gloss development as a function of time and pore size.

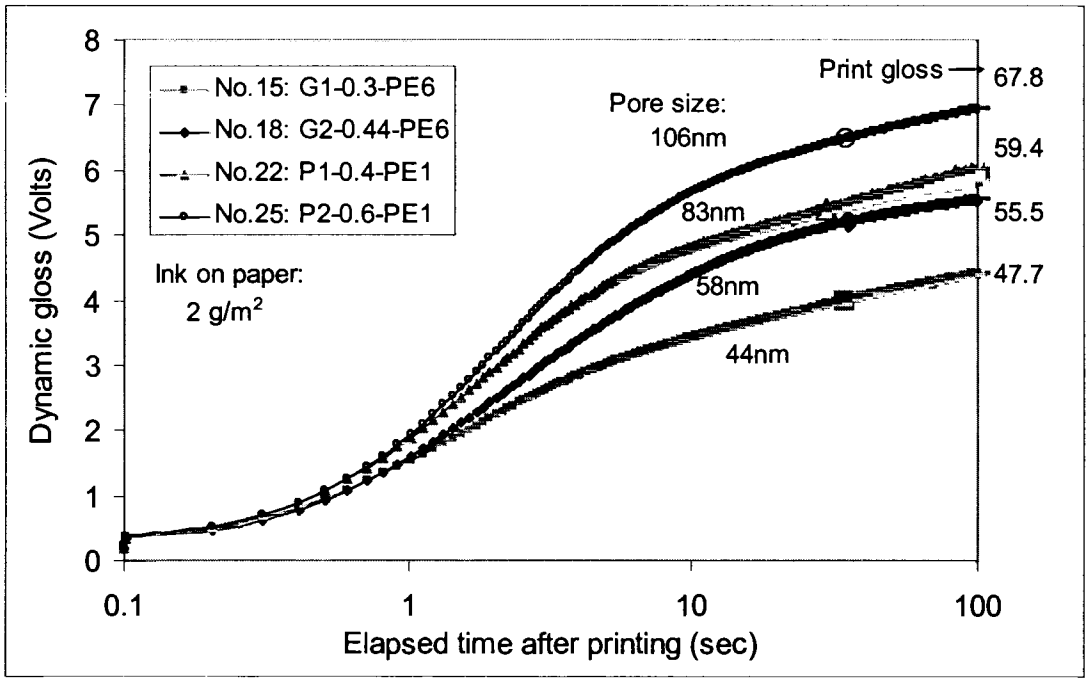

Figure 3.22: Print gloss development as a function of log time and pore size.

3.3. Conclusions

Throughout this preliminary work, we summarize our conclusions in two sections; one is for experimental methodologies in full-scale experiments, the other is for significant findings in this work.

The experimental methodologies are:

- Roughness modification was possible with a simple calendering technique with less or no compromise with pore structure.
- Pore structure differentiation should be refined for reliable information.

The initial findings are:

- The behavior of print gloss development was first monitored related to the structural factors of coating.
- Roughness influenced print gloss from initial film splitting stage and had consistent effect even down to the small (100 nm) microroughness region over high inking levels.
- Rough and low porosity coatings give high initial roughness or lower print gloss. Pore size does not seem to have much influence on filamentation. There was no clear differentiation whether this difference comes from different amount of ink supply or the influence of structure on ink splitting at the exit of nip.
- It was confirmed that larger pore size and less porosity produces higher print gloss. However, these factors seem to give results in yet unknown competitive way.

4. Full-Scale Experiments

In this part of work, extensive samples based on full factorial experimental design to access wide levels of the factors are prepared and characterized. The approaches are based on the findings from earlier work in Chapter 3. Roughness, porosity, and pore size effects were obtained in a systematic and quantitative way such that their significance on print gloss will be addressed.

4.1. Experimental Methodologies

Sample coatings are performed on matt polyester film using laboratory draw-down coater following the general steps as described in Chapter 2. The grammage and Tappi 75° gloss of base film was 173.7 g/m^2 and 4.3, respectively. Pigments are summarized in Table 4.1. The roughness of rough substrates for sample surface modification is given in Table 4.2. PCC and GCC pigments were obtained from Specialty Minerals Inc. and Imerys, respectively. Most of polyester films were given from Dupont.

Table 4.1: A summary of pigments used in full-scale experiments. Particle sizes are from manufacturers.

Pigment Code	Type	Particle size (μm)
G1-0.32	GCC	0.32 (96% < 2 μm)
G2-1.50	GCC	1.50 (60% < 2 μm)
P1-0.30	PCC- Rhombohedral	0.30
P2-0.60	PCC- Prismatic	0.60
P3-2.20	PCC- Prismatic	2.20
PP	Plastic Pigment	0.13

Table 4.2: The stylus roughness and gloss of the substrates used for roughness control during calendering. The gloss of PE1 was beyond reading range over 100 gloss units.

Materials	PE1	PE2	PE3	PE4	PE5	PE6	PE7	PE8
Thickness (μm)	125	50	125	50	125	23	125	50
75° gloss	-	97.9	92.4	83.6	62.6	37.9	4.3	4.7
Roughness Ra (nm)	10.5	99.6	118.7	159.2	236.0	445.3	825.1	853.5

The pigments are formulated with various SB latex binder contents from 6 to 40 pph to change the porosities. Each set of coated samples are calendered with five different kinds of polyester films from normal clear smooth PE1 to roughest PE8. One thing to be cautious related to the gloss of polyester was that the reflective index of polyester film was known to be 1.64~1.67 (from manufacturer). The range of pore size from different pigment series was expected from 0.04 to 0.15 μm. Coating formulations are summarized including calculated PVC levels in Table 4.3. Since each pigment series combined with various binder additions have 5 different roughness levels, total sorted samples counted up to 105 samples. Samples are represented here as 'Pigment-Binder-Roughness', e.g. 'G1B06R1' means pigment G1, binder of 6 pph and roughness level '1'. The roughness

level varies from one to five; however, the number is just arbitrary grade of roughness though they are usually in order with actual measured roughness.

Table 4.3: Coating formulation for full-scale sample preparation.

Components		Particle Size*	SAMPLE CODE				
Generic	Class or type	(μm)	G1 Series***	G2 Series	P1 Series	P2 Series	P3 Series
GCC	G1 (96%<2um)	0.32	100				
	G2 (60%<2um)	1.50		100			
PCC	P1 (Rhombo)	0.30			100		
	P2 (Prismatic)	0.60				100	
	P3 (Prismatic)	2.20					100
PP	Polystyrene	0.13	5**	5	5	5	5
Binder	SB Latex	0.17	6,10,15,20**	6,10,15,20	10,15,20,30,40	10,20,30,40	10,20,30,40
Lubricant	Calcium stearate	-	0.5**	0.5	0.5	0.5	0.5
pH control	NaOH	-	targetted to pH 8.5				
PVC level (%)			88,81,74,68	88,81,74,68	81,74,68,59,52	81,68,59,52	81,68,59,52

* From manufacturers, **Parts per hundred to pigment, ***Each series has 5 levels in roughness.

Calendering conditions were carefully controlled to match the pore sizes of a certain pigment series with different binder contents as described in Chapter 2. Since the binder was a normal shrinking type, the more binder, the smaller pore size was generated. Unlike the systematic change of binder contents in coating color and consequent pore size variation, the calendering response of the coated samples were not systematic, rather arbitrary. Therefore, the pore-size matching by calendering for each pigment series was associated with mercury porosimetry throughout a number of trials.

Once the desired sets of samples were prepared, their surface roughness and gloss were evaluated. The roughness values are arithmetic average roughness (Ra) after filtering out wavelength of above 100 μm using Fourier domain processing. Relative Mean Square roughness (rms or Rq) was also evaluated but Ra was found to give better results during

analysis. Therefore Rq is omitted for simplicity in the report. The measuring area of 15 mm x 15 mm was scanned at least 10 times each.

High sensitivity of dynamic glossmeter required new calibration, so revised calibration with conventional gloss was done on unprinted and printed samples during the printing tests. Four different levels of inking were targeted. The inking on roll was controlled for each sample. Duplicates were made and averaged. Dynamic print gloss was recorded around up to 300 seconds after printing followed by conventional gloss measurements. The printed samples are kept in standard room at 23℃, relative humidity (RH) 50% until print gloss measurements were repeated again on presumably dried printed surface as final values. Tack tests with the same ink used in printing test were followed as described in Chapter 2. Non-porous polyester films with various roughness levels were included for all kinds of test, especially for accessing extreme situation.

General analysis procedures are outlined in Figure 4.1. The analysis started with extracting print gloss at given transferred ink levels by interpolation. Then roughness, porosity, and pore size effects were sorted out in a systematic way. Finally, statistical analyses to figure out the significance of the factors were tried.

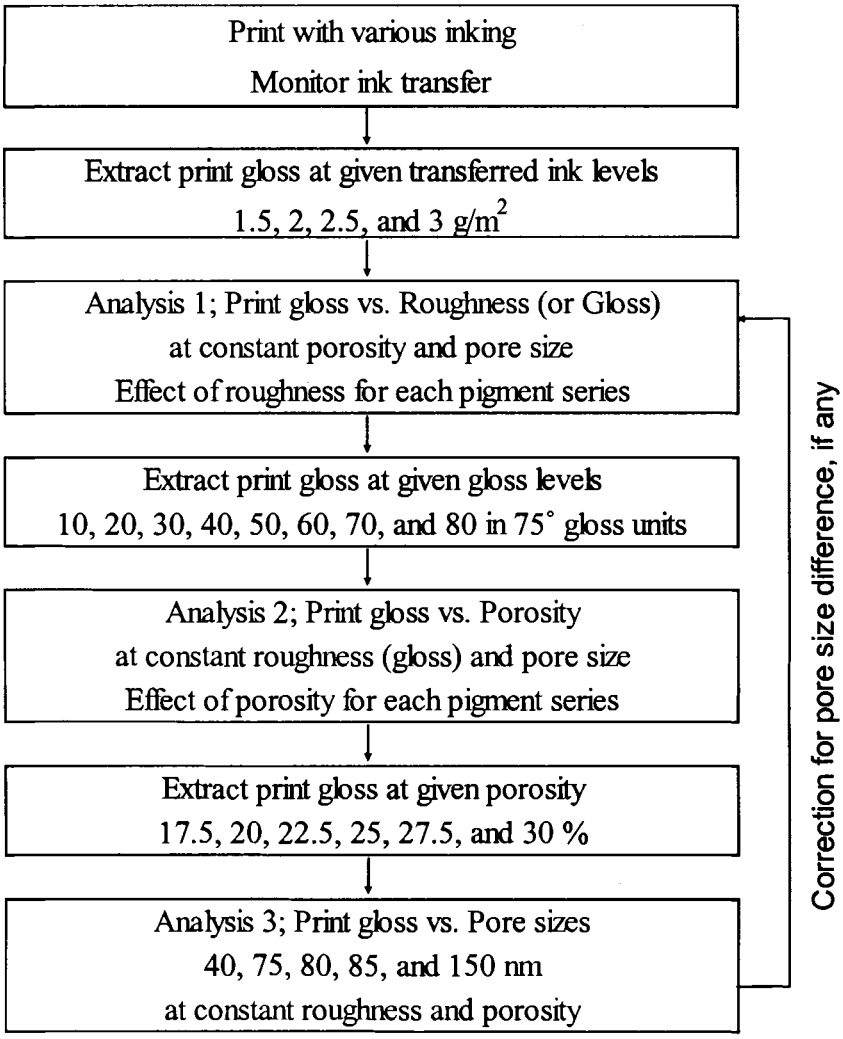

Figure 4.1: Diagram of analysis procedures in full-scale stage.

4.2. Results and Discussions

4.2.1. Modified Structures

The surface properties and printing results from prepared samples are given in Appendix A. The relationship between surface roughness Ra and gloss at various angles is presented in Figure 4.2. Experimental data was close to theoretical relation (Lee, 1974) proving the effectiveness of roughness filtering. However, deviation from theoretical one was noticed in the range before and after 200 nm of roughness. The refractive index of coating used in the theoretical calculation was assumed to be 1.54, but the effective refractive index may be lower than the ideal value; another component of 'air' with refractive index of unity and surface conditions may reduce the apparent refractive index (e.g., Gate and Parsons, 1993). About 13% lowered refractive index gave an experimental maximum here. The lack of predictability in relatively large roughness region is rather intrinsic character of the model which, back to its origin, is based on the small scale microroughness respect to the wavelength of the light. On the large scale of roughness, Gaussian distribution of surface reflection may be disrupted by light becoming diffused as a result of multiple geometrical reflections in deep grooves of the surface (Oittinen, 1991). Gate et al (1974) pointed out that the average inclination of facets of the surface is an important parameter in the case of comparable or greater roughness respect to the wavelength of the light. The resolution of this matter was out of our focus and any need of conversion from roughness to gloss, or vice versa, was made with the experimental regressions, given in Appendix B.

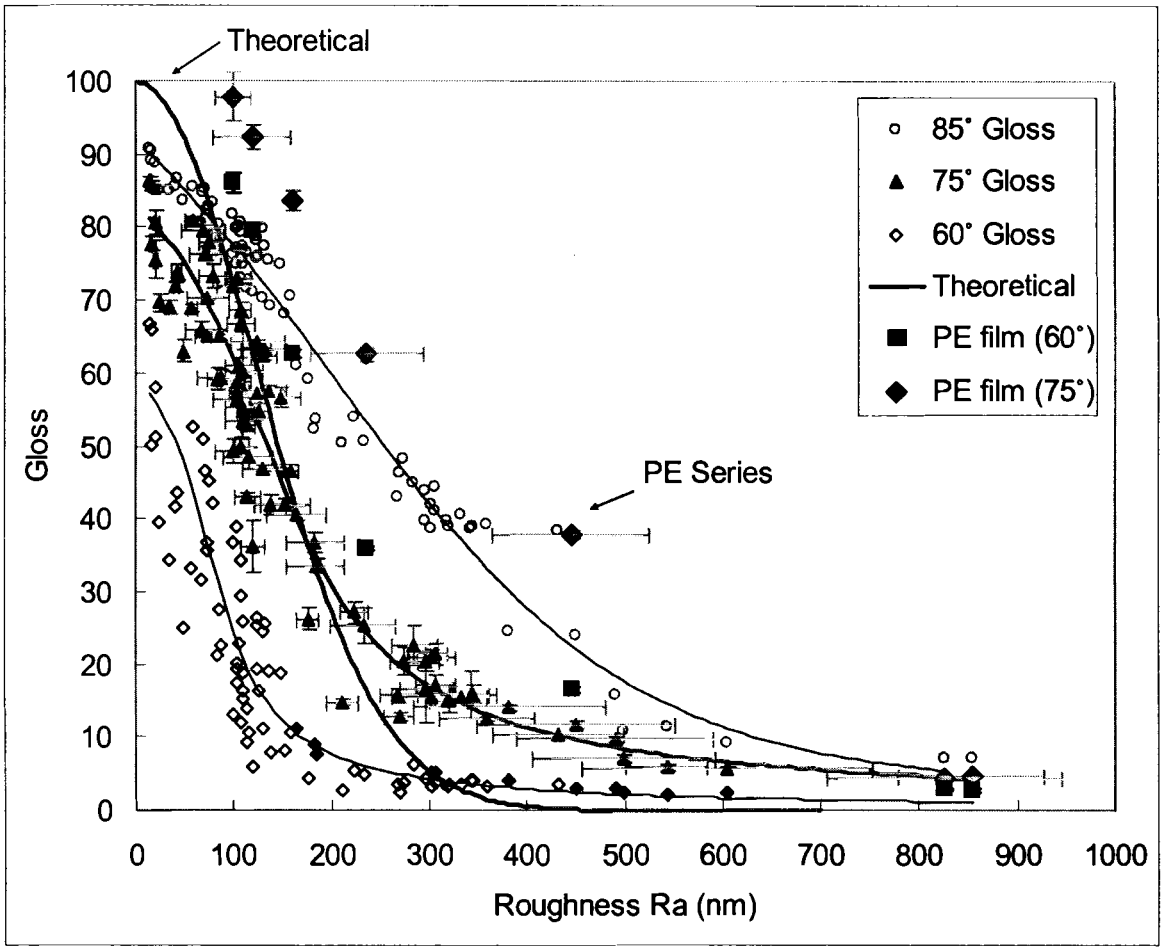

Figure 4.2: The relationship between roughness Ra and gloss at various angles.

The final pore structures of controlled samples are presented in Figure 4.3 and 4.4 and their structural features are summarized in Table 4.4. Additionally, their SEM surface images are given in Appendix C. Each pigment series had almost matching same pore size while their porosities varied. Therefore, this made possible to process the first approach, roughness effect on print gloss with various porosity at the same pore size assumption.

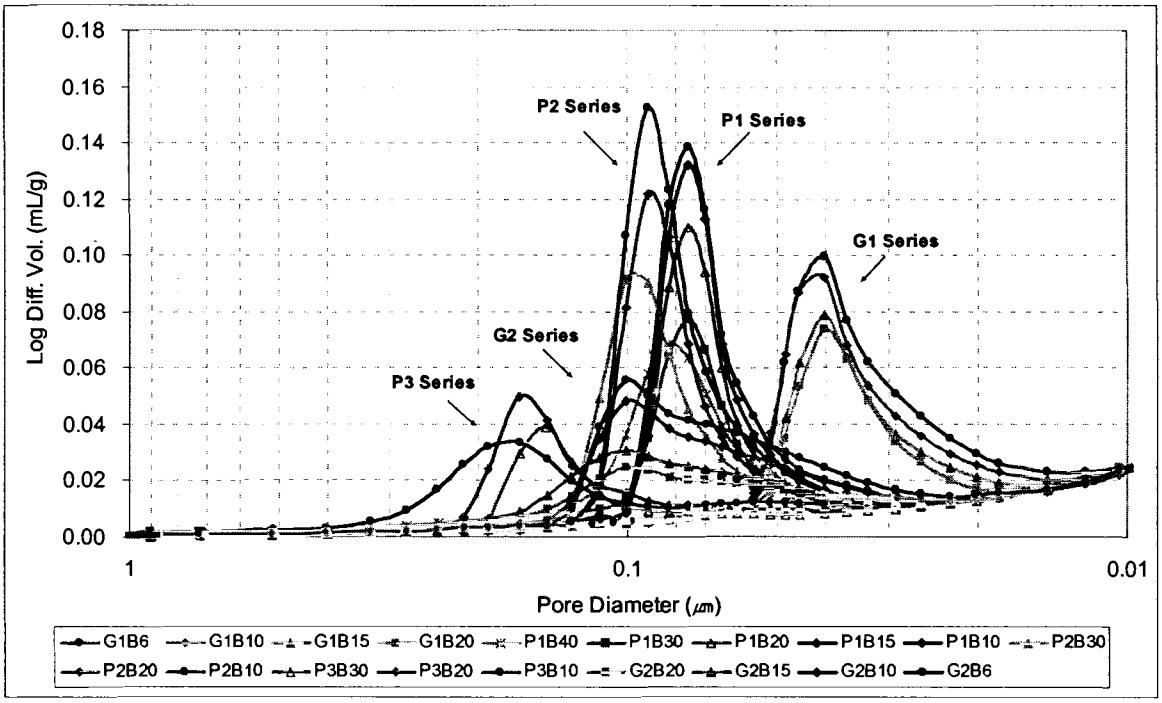

Figure 4.3: Controlled pore size distribution of the prepared samples in full scale. Note that porosity scale is pore volume per total sample weight (coating and base substrate).

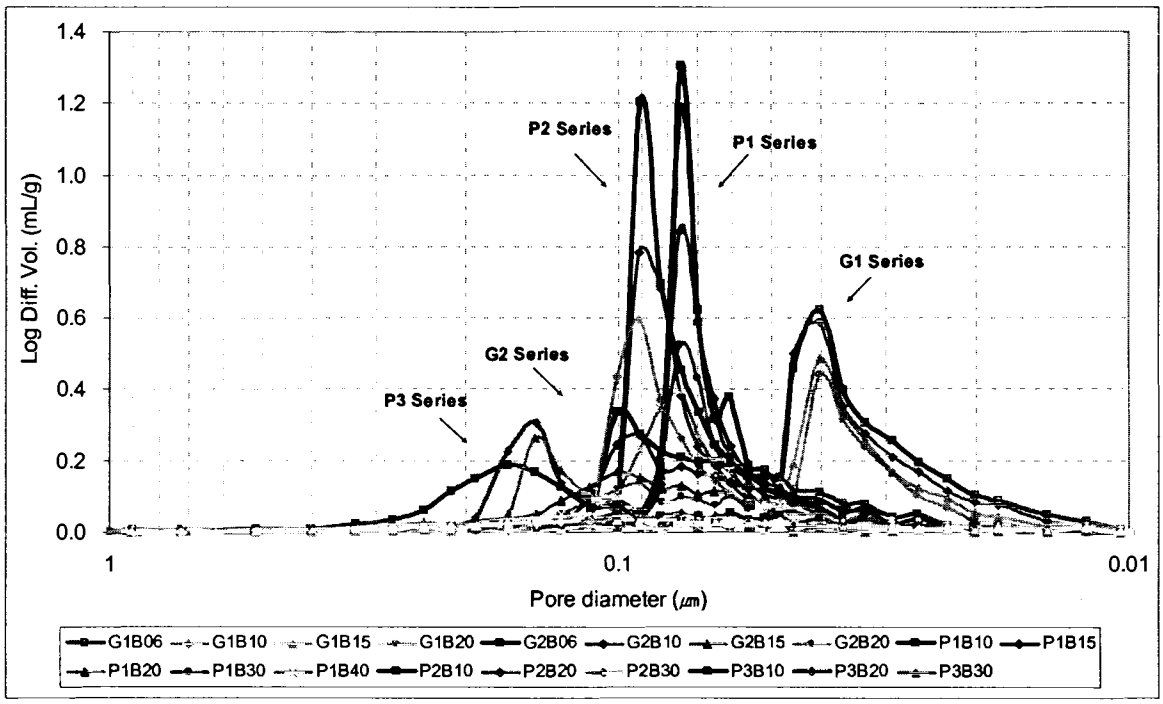

Figure 4.4: Compressibility corrected pore size distribution of the full-scale samples. Given porosity is converted into pore volume per coating weight only.

Table 4.4: Summary of pore-structural features of prepared sample series.

Sample Code	Pore size (μm)					Porosity (%)			
	at Peak	Uncorr.* Pore Vol.	Corr.** Pore Vol.	below 1 μm+ Corr. Pore Vol.	Targetted	Bulk	Uncorr.	Corr.	Corr. below 1um
G1B06	0.040	0.040	0.0414	0.0379	0.0390	31.5%	29.6%	29.4%	23.6%
G1B10	0.040	0.040	0.0436	0.0395	0.0390	28.7%	28.6%	28.3%	20.7%
G1B15	0.040	0.040	0.0430	0.0390	0.0390	24.0%	23.1%	22.9%	16.7%
G1B20	0.040	0.040	0.0409	0.0394	0.0390	20.2%	19.6%	18.9%	14.5%
G2B06	0.100	0.069	0.0869	0.0761	0.0804	24.2%	25.3%	24.7%	20.4%
G2B10	0.098	0.074	0.0953	0.0804	0.0804	21.9%	23.0%	22.4%	17.2%
G2B15	0.100	0.078	0.1113	0.0878	0.0862	20.3%	20.5%	20.1%	14.7%
G2B20	0.100	0.072	0.1158	0.0823	0.0804	16.2%	17.9%	17.1%	11.4%
P1B10	0.076	0.074	0.0777	0.0745	0.0750	29.0%	29.5%	29.3%	23.2%
P1B15	0.076	0.073	0.0774	0.0749	0.0750	25.7%	25.8%	25.6%	20.9%
P1B20	0.076	0.072	0.0774	0.0746	0.0750	21.8%	21.6%	21.1%	17.5%
P1B30	0.076	0.073	0.0812	0.0759	0.0750	18.4%	20.0%	19.1%	14.6%
P1B40	0.079	0.075	0.0868	0.0817	0.0750	16.3%	18.8%	17.7%	13.1%
P2B10	0.091	0.085	0.0910	0.0862	0.0862	31.6%	31.1%	30.8%	25.5%
P2B20	0.091	0.085	0.0916	0.0862	0.0862	26.8%	25.9%	25.6%	19.9%
P2B30	0.091	0.086	0.0955	0.0913	0.0862	22.8%	22.1%	21.7%	18.3%
P3B10	0.165	0.132	0.1852	0.1532	0.1500	20.8%	20.4%	20.0%	14.7%
P3B20	0.155	0.137	0.1705	0.1432	0.1500	18.0%	20.1%	19.7%	12.8%
P3B30	0.145	0.131	0.1910	0.1356	0.1500	13.0%	16.6%	15.8%	8.4%

*Corr.: Corrected, **Uncorr.: Uncorrected, +below 1 μm: calculated for the range below 1μm pore size

4.2.2. Ink Transfer and Print Gloss

Ink transfer should be monitored to ensure that the values are reasonable enough to compare with each other around and beyond maximum ink transfer region, which produces solid-printed image and closes in practical printing conditions. Also important is the ink supply condition for each sample since the inking conditions influence on the ink splitting. Figure 4.5 shows ink transfer characteristic curves for the employed polyester films with various roughness levels. The rougher surface is less receptive to ink. The difference before their maximum is known to be due to 'contact area', while extremely lowered transfer in high inking region is attributed to roughness providing numerous nucleation sites for cavitations and filament formation (De Grace and Mangin, 1984). Sample PE6 was so thin that the ink transfer was lowered due to increased macroroughness originated from that of adhesive tape backside. However, this roughness effect on ink transfer was not found consistently with all of the samples, e.g. Figure 4.6. The declination of the ink transfer ratio confirmed the inking condition was around and beyond the maximum ink transfer region, in which the inking amount might be high enough to reduce the difference. The coatings with high binder contents were also expected to have less ink transferred (Zang and Aspler, 1994), but the general effects of porosity on ink transfer did not always reach discernible levels within the experimental conditions. That may also be partly due to their narrow sensitivity compared to the relatively large scale of the balance used to measure ink transfer. Nevertheless, this may provide a condition to investigate the influence of roughness and porosity on initial print gloss development regardless of the ink feed.

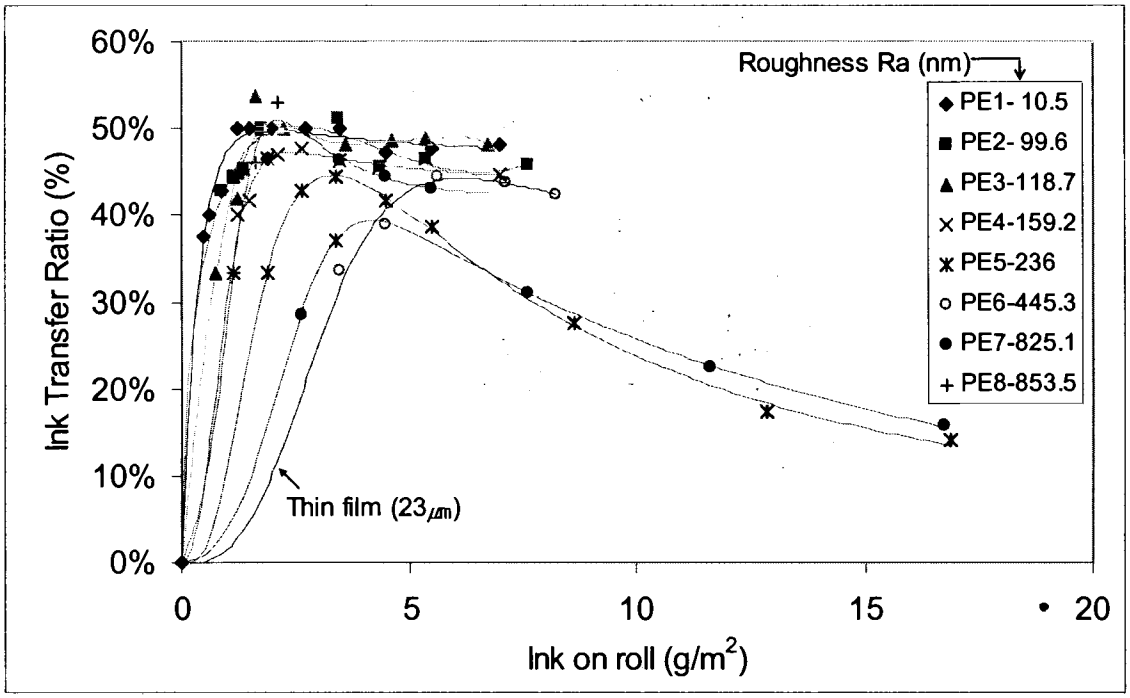

Figure 4.5: Ink transfer curves of polyester films with various roughness levels.

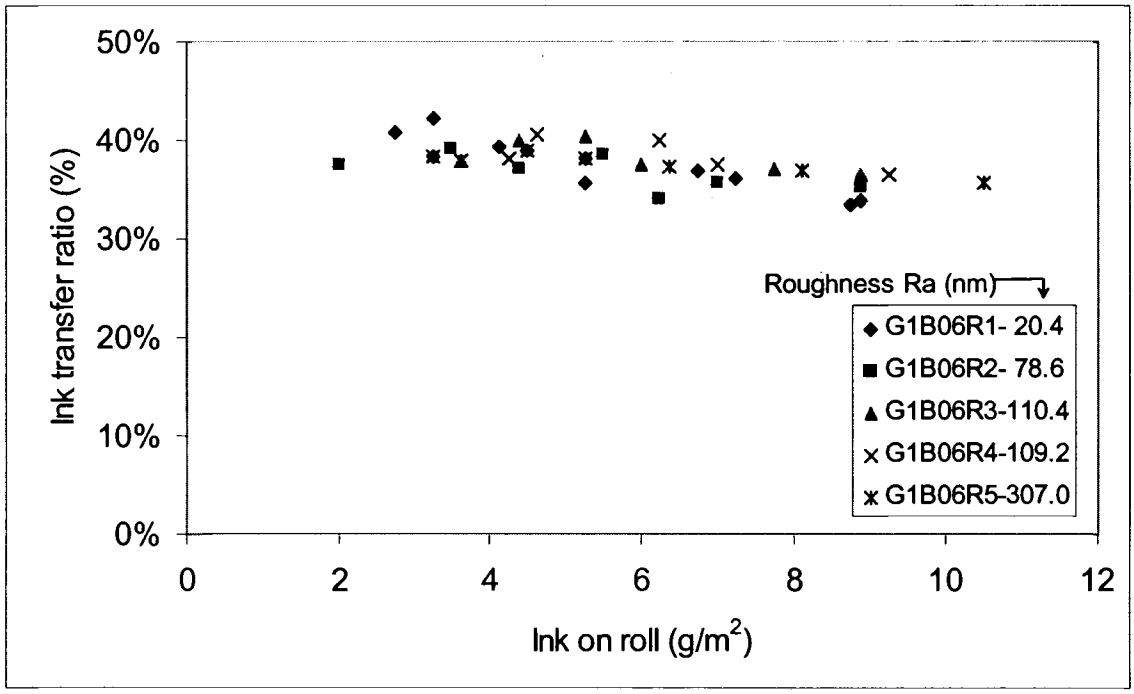

Figure 4.6: Ink transfer ratio of G1B06 series with various roughness levels.

The print gloss values at various levels of transferred ink on samples are plotted as shown in Figure 4.7 through 4.10. The smoothest polyester PE1 showed a decrease over small inking region due to increased roughness with transferred ink until it reached maximum ink transfer, and then the print gloss rose up toward the characteristic gloss of ink (e.g., Oittinen, 1980), as shown in Figure 4.7. Coated sample G1B06 also showed similar behavior as in Figure 4.9. As expected, 60° gloss gave better differentiation between samples over the high gloss range. Regressions were made for each sample and the values at given ink amounts of 1.5, 2, 2.5, and 3 g/m^2 are interpolated and extracted for comparisons as indicated in Figure 4.9.

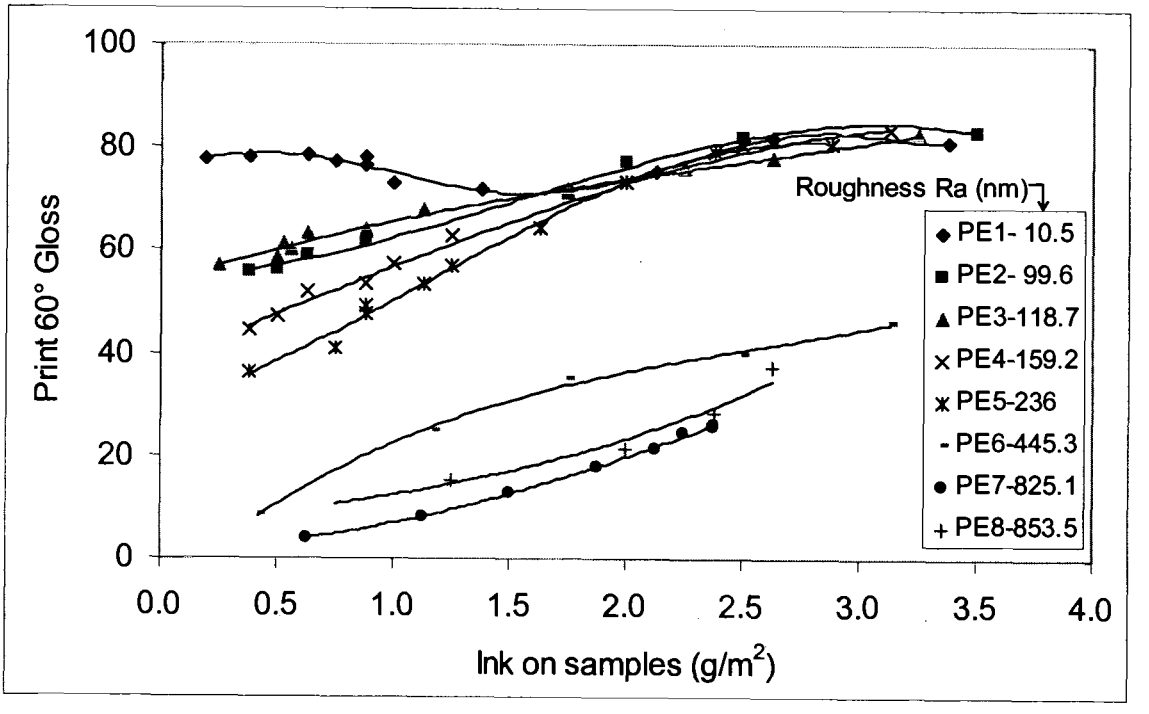

Figure 4.7: Print 60° gloss of polyester films as a function of ink-feed.

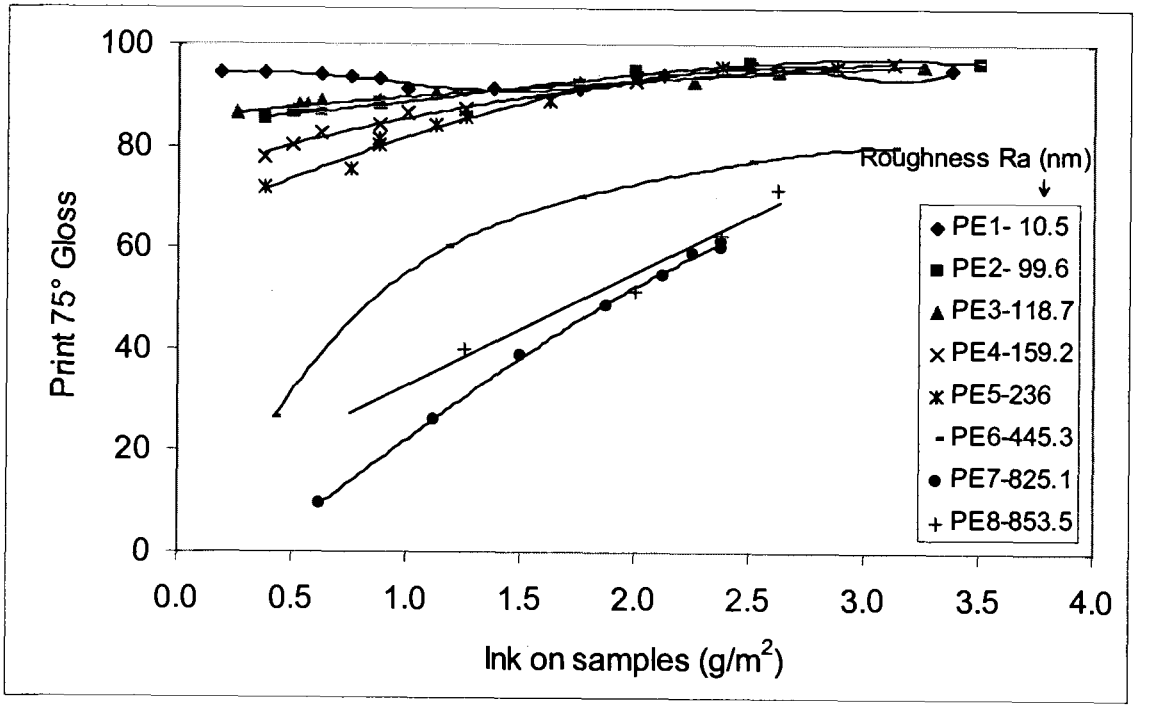

Figure 4.8: Print 75° gloss of polyester films as a function of ink-feed.

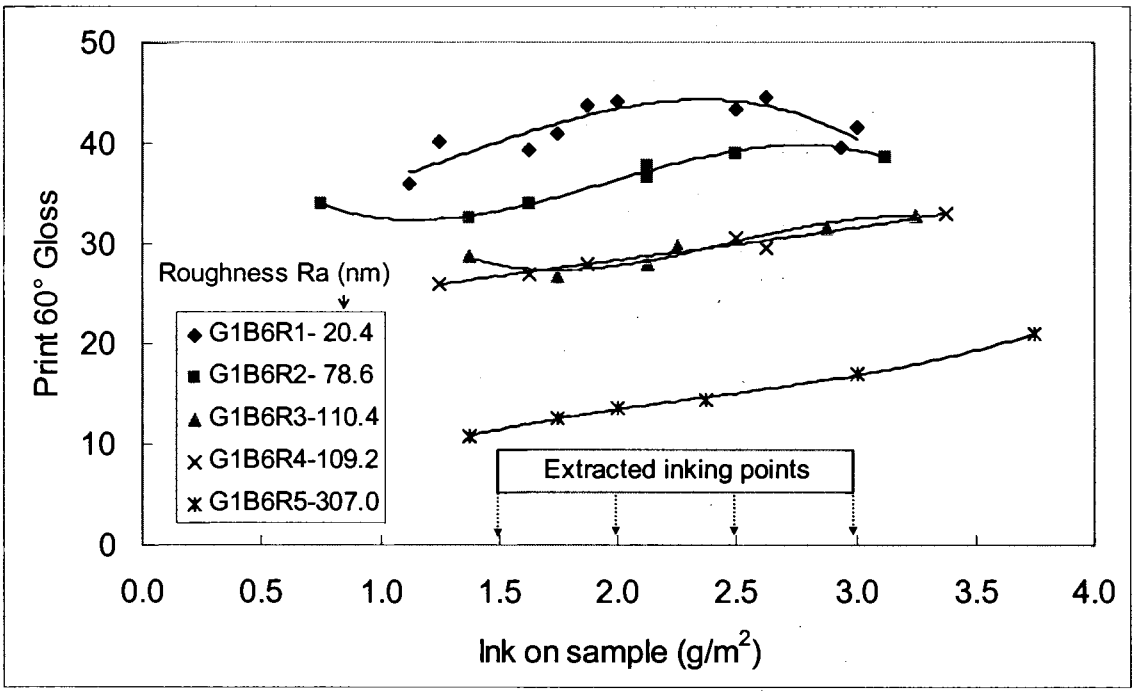

Figure 4.9: Print 60° gloss of G1B06 series as a function of ink-feed.

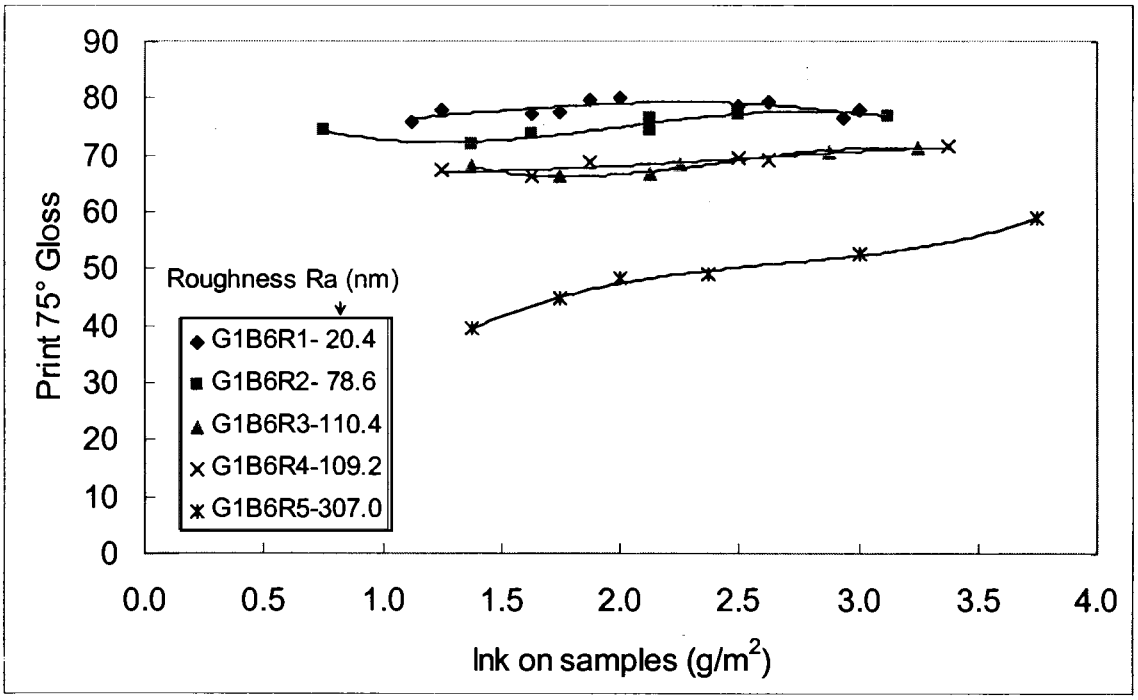

Figure 4.10: Print 75° gloss of G1B06 series as a function of ink-feed.

4.2.3. Effect of Roughness on Print Gloss

Initially, an attempt was made to plot print gloss as a function of measured roughness, however the results were so confused and entangled with each other that the differentiation can be hardly made between samples. That may be caused by the relatively large deviation in roughness measurement and lack of representation to distinguish a delicate difference thereby. The plotting of the print gloss as a function of paper gloss made the result clear. From a practical point of view, the presentation in gloss may give better sensibility and communications of the results. Gloss will be used interchangeably with roughness in the following analytical descriptions otherwise stated. Figure 4.11 describes the obtained print gloss for each sample series at 1.5g/m^2 ink level. Note that the ordinate is exaggerated. The unprinted gloss of polyester films was higher than that of coating at the same roughness level due to their higher refractive index. To facilitate a same comparison base in terms of roughness, the gloss of polyester films are converted to equivalent coating 75° gloss using the experimental gloss-roughness relation. There is also a dotted 45° plotting line between paper gloss and print gloss, which tells whether a certain sample has positive or negative print-snap (or delta-gloss).

The effect of coating gloss (or roughness) was consistent all over the given range. The gaps between series are due to their different pore size and porosity. Though it may be hard to see clearly the rank of the series in print gloss, it could be observed that the results are generally positioned depending on their pore size and porosity; a series with larger pore size and/or small porosity produces higher print gloss. As evidenced in Figure 4.11, G1 series with the smallest pore size of 39 nm lied in lowest region, in which G1B06 with high porosity of 31.5 % placed in lowest, while P3 series with the largest

pore size of 153 nm here produced the highest print gloss at given roughness levels. Other pigment series, G2, P1, and P2, were close and crossed each other due to their small difference in pore size and porosity, but mostly their difference can be differentiated, which will be analyzed in the following sections.

The print gloss of polyester series was generally higher than any of coated samples due to its non porous characteristics, which give virtually maximum time for ink film leveling. Because of that non porosity, the roughness does not make an appreciable effect on print gloss before it reaches certain amplitude, at which roughness may strongly interfere in leveling process with large amount of splitting pattern as well. As a reminder, both roughness and inking on the roll may influence the formation of ink splitting pattern. The fitted line of those print gloss looked like an enveloping curve over the whole results, outlining an attainable high 'print gloss region'. However, this does not necessarily mean that they are presenting a maximum achievable 'print gloss' itself. That is partly because a non porous substrate can have larger amount of ink splitting pattern than that on porous surface after the printing nip (Glatter and Bousfield, 1996, Ercan, 2001).

It was noticed that there was a surprisingly steep drop in print gloss below 25 gloss units of polyester film. Most of coated samples also showed a similar drastic change in print gloss over low paper gloss region (large roughness) as well as rather linear relation over higher paper gloss range. Since the ink-transfer ratios of coated samples were not significantly different for various roughness levels unlike the case of polyester film, these consistent results indirectly confirm the speculation that roughness is involving leveling process and thereby surface formation of final ink film apart from the influence of inking conditions.

Another interesting aspect may be that the result directly points out a sort of product strategy; the result may indicate that even small improvement in gloss over low gloss region can result in a significant increase in print gloss or print-snap. However, it should be reminded that the gloss become less sensitive to the change in roughness over high roughness region. Therefore, the small increase in gloss may not be achieved by mild decrease in roughness. Matt or dull grade papers, gloss of which generally range up to 20, 40 gloss units respectively (Romano, 1998), may have the benefits from the reduction in roughness, preferably macroroughness to maintain low paper gloss with microroughness.

At this point, the response of print gloss to the change of roughness is worthy to interpret. The coating gloss was converted to roughness (Ra) value using the experimental relationship, and then plotted with the print gloss in Figure 4.12. As seen, the result looked like a reversed shape of Figure 4.11, but the steep change observed in low gloss region seemed to relax, especially up to larger roughness level for the case of polyester film series as shown in small window. A crossover was expected to happen between G1 series and P1 or P2 series in low gloss region in Figure 4.11, but the trends in Figure 4.12 showed it could hardly occur. This kind of combined analysis may avoid imbalanced interpretation.

Next point in question was how this relation would change in higher inking conditions. Print 75° gloss of all the samples at various given ink levels are presented in Figure 4.13 through 4.15. In general, higher inking levels on samples increased the print gloss and seemed to reduce little bit of the roughness effect. Though the P3 series was almost flat at

the ink level of 3.0 g/m^2, the overall dependency of print gloss on roughness was still evident.

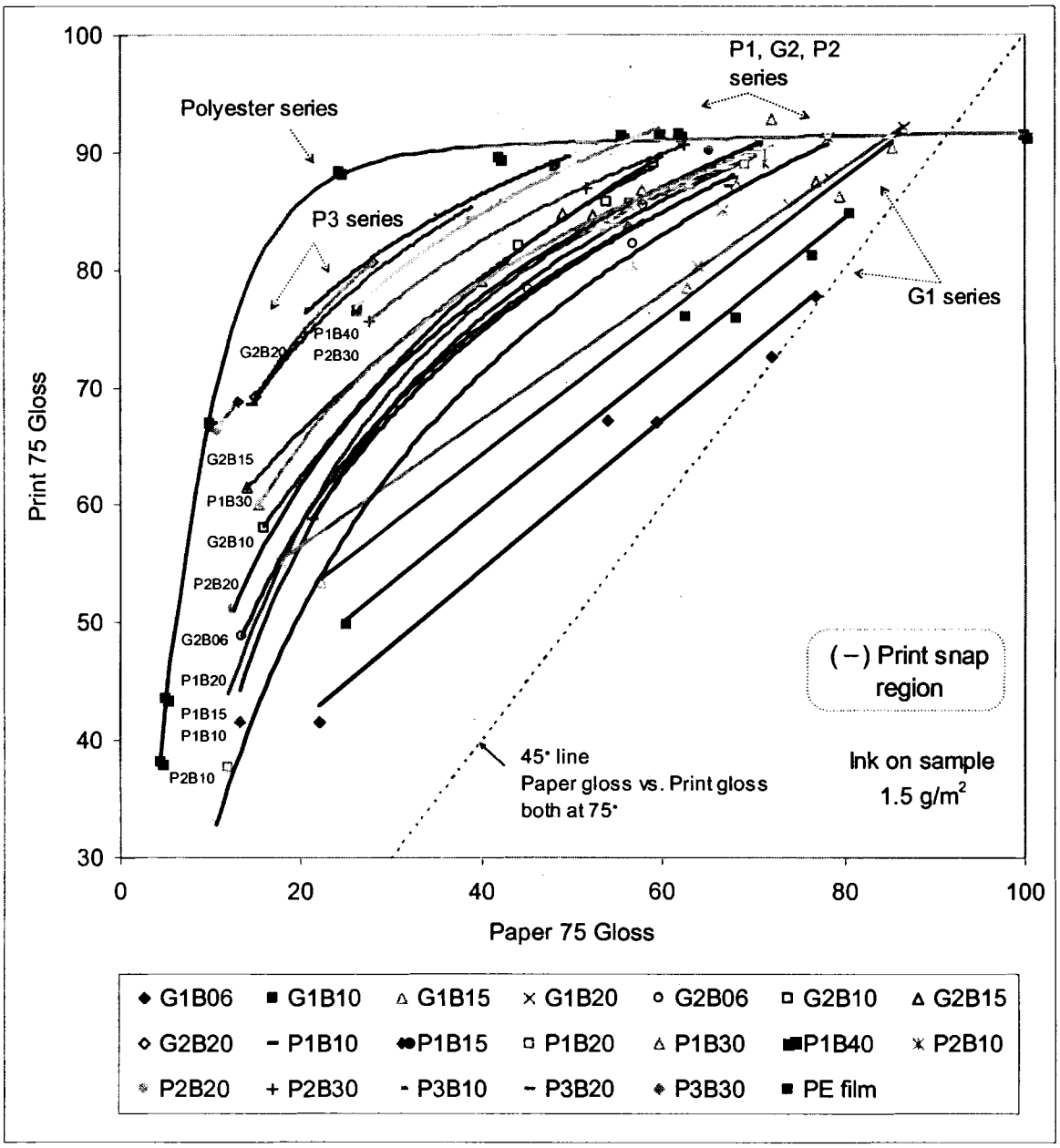

Figure 4.11: Print 75° gloss of coatings as a function of paper gloss at 1.5 g/m^2 ink on samples.

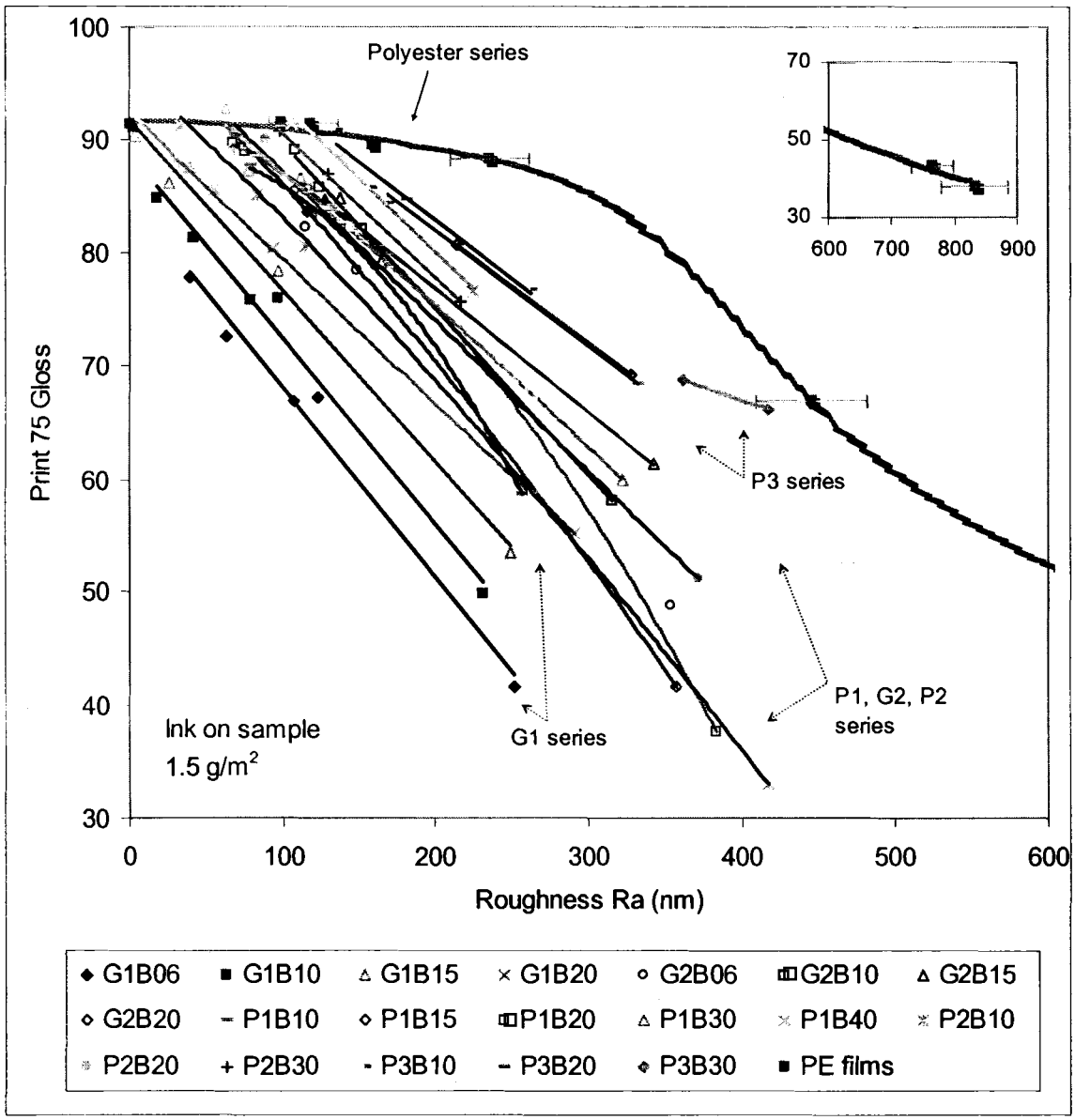

Figure 4.12: Print 75° gloss of coatings as a function of roughness at 1.5g/m^2 ink on samples. The print gloss of polyester film series over extended range is shown in small window.

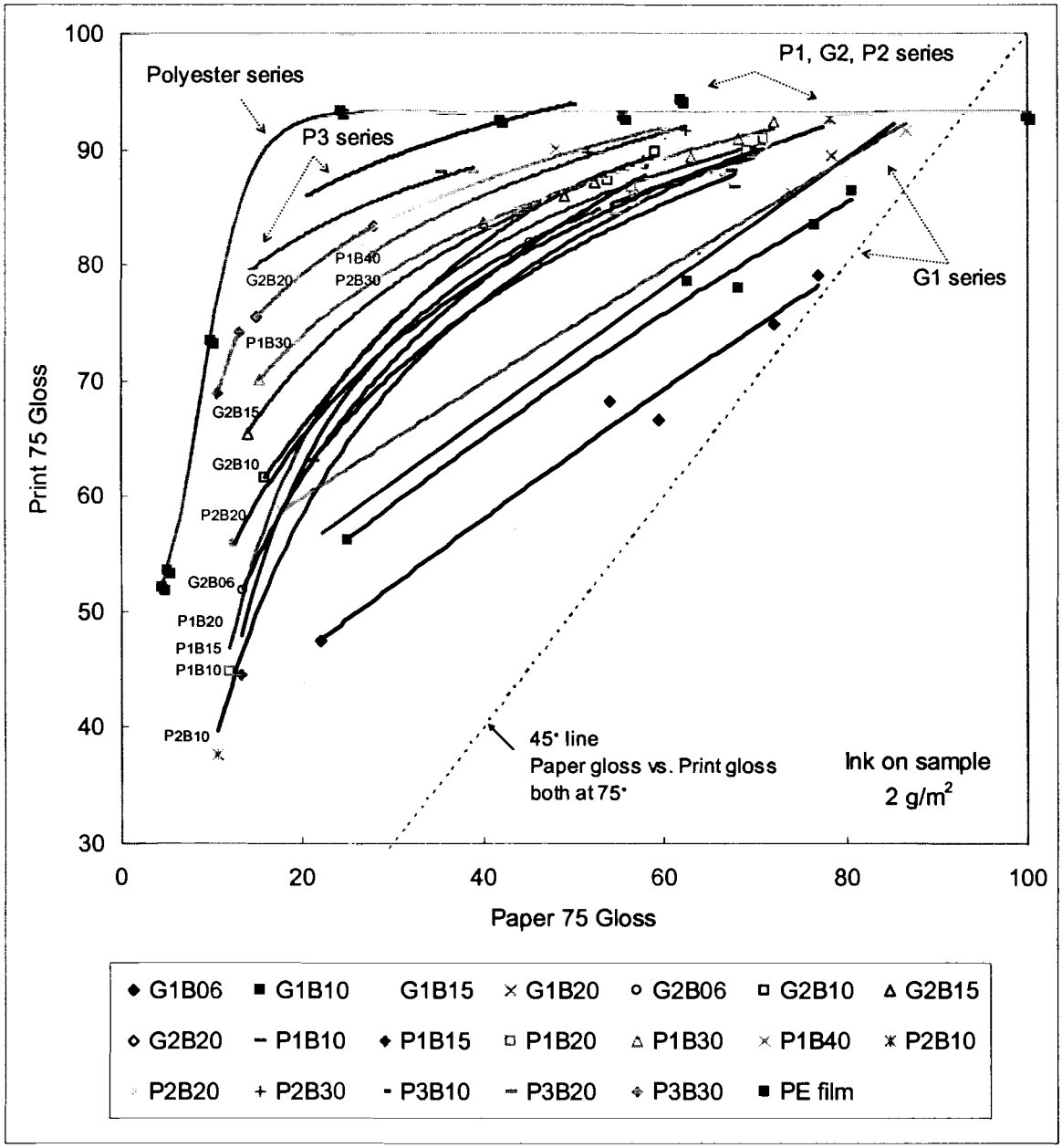

Figure 4.13: Print 75° gloss as a function of paper gloss at 2.0 g/m^2 ink on samples.

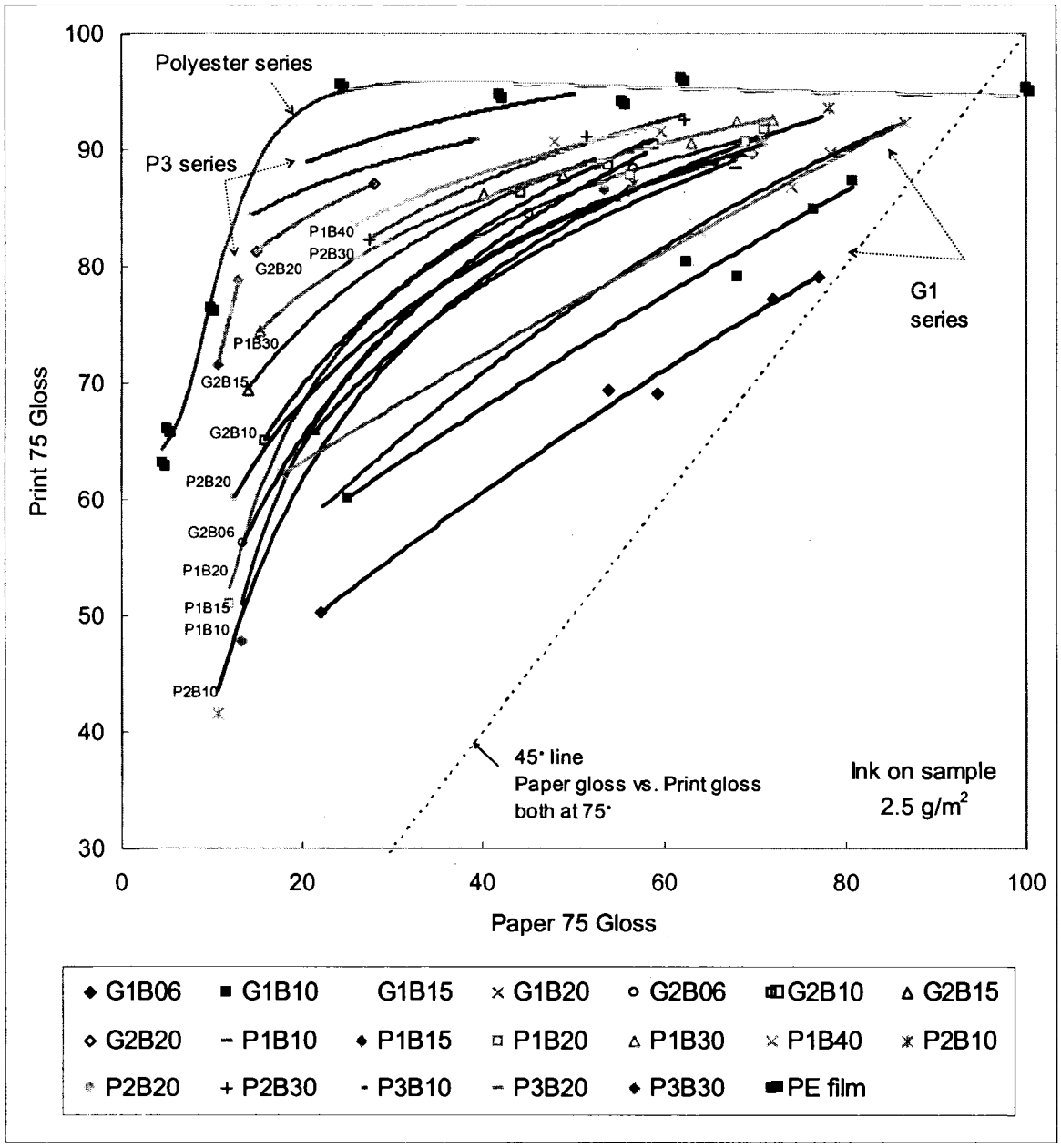

Figure 4.14: Print 75° gloss as a function of paper gloss at 2.5 g/m^2 ink on samples.

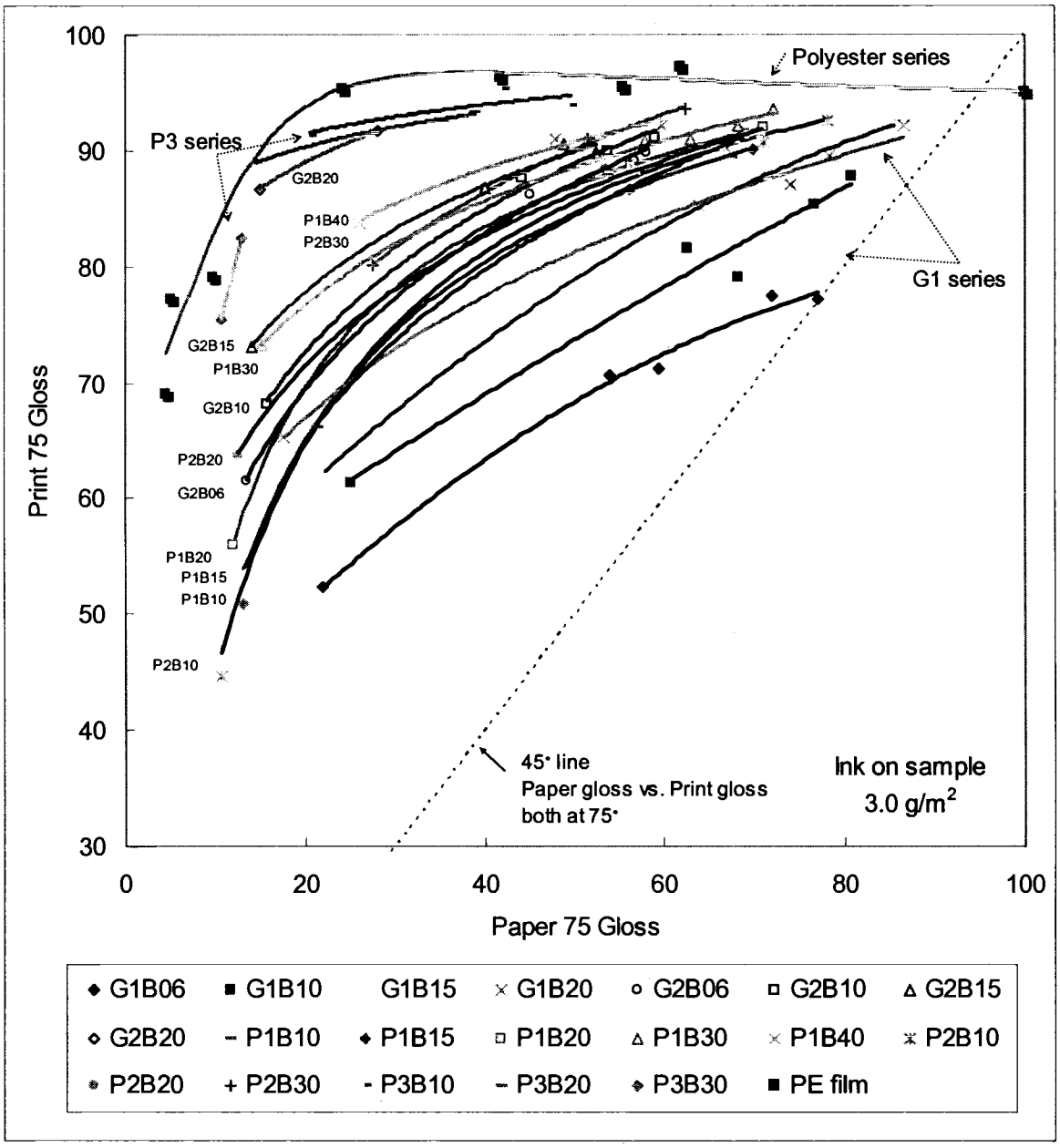

Figure 4.15: Print 75° gloss as a function of paper gloss at 3.0 g/m^2 ink on samples.

The change of print gloss of P3 series and G2B20 series was remarkable such that their gloss ran almost parallel with that of polyester series especially at high inking levels. Those series were common in that they had low porosity and relatively large pore size. Therefore, the ink film on those coatings may have a longer time than other coated series to level down and develop its print gloss with their slow absorptivity and, additionally, large amount of inking. With these conditions working together, the influence of roughness is small and the results become analogous to that of non-porous films. These results are observed under the general dependency of print gloss on the roughness; note the steep change in print gloss of those series around 20 gloss units. Another hidden point related to this leveling off could be that 75° gloss becomes less sensitive over high gloss range so that a change in print gloss values get smaller and smaller. The presented results should also be in terms of 60° gloss in Figure 4.16.

The question relates to convergence of print gloss in the small roughness region. The difference between pigment series converged toward a maximum in an uncertain extended small roughness region, e.g. Figure 4.15. If it does, that means the effect of pore structure is compromised with that of roughness. There must be a leveling off or maximum point as seen in polyester series and some coated samples. In Figure 4.16, the same result but with print 60° gloss is presented at the ink level of 2.5 g/m^2. Other plots at different inking conditions are given in Appendix D. The leveling off and/or converging tendency was too weak to be noticed; the result rather showed clearer straight dependency on roughness, far from reaching a certain maximum. At low inking level, print 75° gloss of coated samples was narrowly reaching that of polyester films. But in the print 60° gloss graph, it was observed that the print gloss of coated samples was way

beyond that of polyester films (e.g. Figure D.4, Appendix D). The print gloss of P3 series, which was almost parallel to that of polyester films, has also been deflected presenting a significant effect of roughness. Because of this clarity in differentiation between samples, the following analysis was done in terms of print 60° gloss otherwise noted. The plots of 60° vs. 75° gloss are also given in the graph so that the values can be readily interpreted at the same geometrical condition. The relation between 60° and 75° gloss was different for printed and unprinted surfaces. The characteristics of the unprinted and printed surfaces may be different because of varying refractive indices and major roughness features, which may result in different response from one measuring angle to another. Matsuda (2000) reported that higher relationship between roughness and gloss on printed surface was found in the larger frequency region than the case of unprinted surface. The reason may come from various other sources, but this is rather out of the scope of this work. The important practical point, however, was that a positive print-snap is seen for the 75° geometry, but the same gloss or even negative print-snap in terms of 60° gloss. This discordance could contribute even to the disagreement between a perceived gloss and instrumental gloss since the 60° gloss is known to give better resolution or differentiation than 75° gloss especially in the high gloss range.

In overall, the effect of roughness on print gloss extended over a wide range unless coating was non-porous. Higher inking never covered up the difference in roughness. Since the prepared samples covered almost all the practical gloss range of commercial coated papers except cast coated or photographic gloss, the print gloss free from roughness effect may be hardly seen in actual conditions.

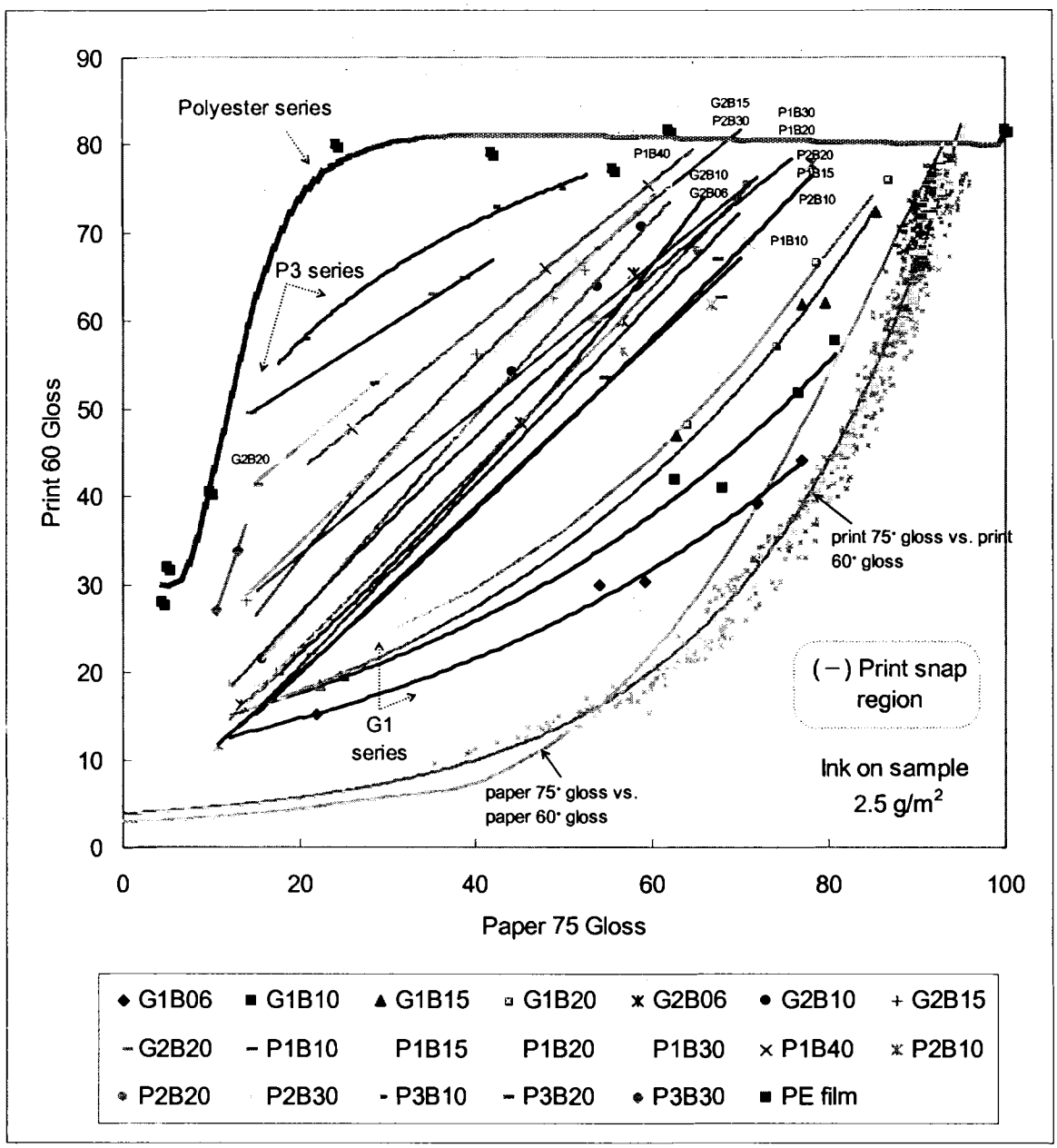

Figure 4.16: Print 60° gloss as a function of paper gloss at 2.5 g/m^2 ink on samples.

There was an unforeseen result from P3 series which deserve to note. For most samples, the decrease of porosity resulted in a higher print gloss because of an extended leveling time and fluidity of ink film. Unlike other series, P3 series showed an opposite trend. P3 series was formulated with large PCC pigment (2.2 ㎛), therefore it was likely to produce a coating with large pore sizes, but its coating structure in depth direction might have quite different packing due to the large pigments. As well known, pigments in large size require small amount of binder because of small surface area. In other words, the same amount of binder additions could cause a significant decrease in porosity. P3B30 series was little bit out of the same roughness range, but P3B10 and P3B20 were in comparable range, in which less porous P3B20 series showed lower print gloss than P3B10 series. The reason, however, was readily found by observing the printed surfaces as shown in Figure 4.17. When the porosity decreases (P3B10 > P3B20 > P3B30), a splitting pattern was formed on the surfaces resulting in lower print gloss. As observed in the SEM surface images given in Appendix C, the surface of P3B30 was almost closed and covered by latex films. Bitla (2002) found that this same large pigment can settle during drying, depleting the pigment concentration of the surface but increases latex concentration. This result thought to come from many of sources combined together; e.g., surface latex contents, roughness, porosity, ink affinity, ink film thickness, and ink transfer.

Ink transfer ratios of P3B20 and P3B30 series were significantly lowered down to below 10% when it was tried to achieve a desired high ink amount on samples. Low ink transfer ratio means that there was 'larger quantity of ink supply' on roll, which is known to increase the splitting pattern formation as reported in many literatures (Glatter et al 1996,

Ercan 2001). De Grace and Mangin (1984, 1988) also reported that splitting asymmetry on non porous substrates increased as the ink film thickness increase. 'Surface sealing by latex films' was a strong factor to reduce the ink transfer. Zang and Aspler, (1995, 1998) explained it not by reduced ink immobilization, but by more asymmetric splitting of the nonimmobilized free ink with a postulation of ink filtercake formation during the nip transfer. It was, however, unlikely that low or non porosity nature alone caused to lower ink transfer otherwise that of all polyester films should have suffered from that. When the 'roughness' was combined in effect, the ink transfer onto the surface became severely hindered as also seen in the case of polyester films with large roughness. De Grace et al (1984) attributed it to closer splitting of ink film to the substrate surface due to microroughness which provided numerous sites of cavitations and filament formation. Since P3B10 and P3B20 were in comparable roughness range, the effect of roughness was thought to be a supplementary condition. Another aspect was that the surface latex contents, as well known, makes the coated surface more hydrophilic and may decrease the affinity or receptivity to ink films. Even though the effect of surface free energy on the ink transfer was reported as negligible (De Grace et al, 1984), it does not necessarily mean that the surface affinity does not influence on the formation of splitting pattern. The ink filaments may gather together at the exit of nips creating larger patterns. This may be one of differences between non-porous polyester and latex-rich less porous surface.

In summary, the result of P3 series indicated that extremely low porosity may not necessarily produce a higher print gloss. High print gloss from low porosity was attributed to extended leveling time for ink film, but the P3 series was controlled by the

ink transfer and splitting pattern formation. The large filament patterns would not level down.

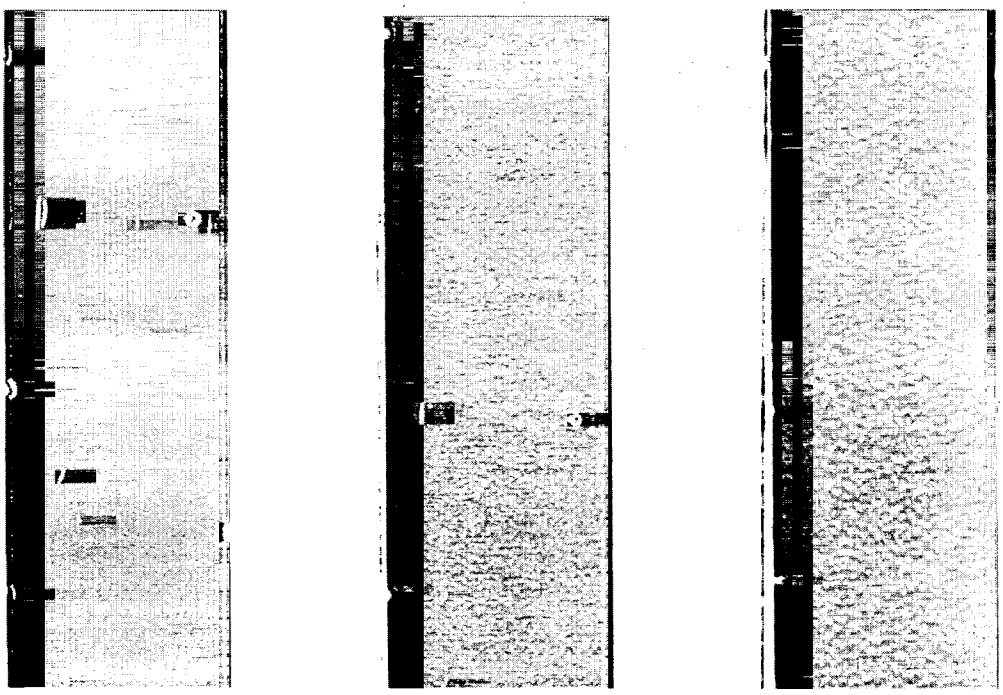

P3B10R5 (20.6, 2.13g/m^2) P3B20R4 (39, 2.13g/m^2) P3B30R2 (13, 1.90 g/m^2)

Figure 4.17: Scanned images of printed samples of P3 series (75° gloss, ink amount on sample).

4.2.4. Overall Dependency of Print Gloss on Pore Structure

The print gloss at given roughness levels was extracted using interpolation from the fitted curves. The print gloss in the edge range in a series was obtained partly using limited extrapolation within less than 10 gloss units of 75° gloss. The results are plotted as a function of porosity and coating gloss in Figure 4.18. Each series represents the print gloss at a certain base gloss level. Various porosities had been plotted and compared to get a best result, but there was not much of difference even between corrected and uncorrected porosities for mercury compressibility. It was thought that a significant portion of error or compressibility was removed during the subtraction of base polyester potion in the mercury correction process. The given porosity is bulk porosity. Though the data in each series had scatter due to the difference in pore size, the trend lines should show the overall dependency of print gloss on porosity. A series with missing data, '80', was not given a trend line. The gaps between the series indicated the roughness effect, which was again consistent producing a systematic change in print gloss.

The effect of porosity had a significant influence on print gloss. Low porosity generally results in high print gloss or vice versa. Base mechanism of this result mostly attributed to the extended leveling process due to slow absorption on less porous surface. The print gloss of coated samples was even higher than that of polyester films at low porosity in the high paper gloss series. The relatively low print gloss of polyester may be attributed to the combination of a relatively lower ink amount and larger splitting pattern on smooth surface than coating layers. The porosity influence looks like get strong in the high paper gloss region, but from the relationship between 60° and 75° gloss, one can readily interpret that the results will be a convex shape in terms of 75° gloss. Therefore the slope

distribution should be interpreted with caution; relatively mild slope in low paper gloss series may have a significantly large change in 75° gloss. Keeping this issue in mind, the results at various inking levels were compared. The print gloss at 2.5 g/m^2 ink level is presented in Figure 4.19. The increase in print gloss of low paper gloss series was noticeable to the similar parallel tracks of other series. Therefore, the effect of porosity seems to be strong as the ink film thickness increases.

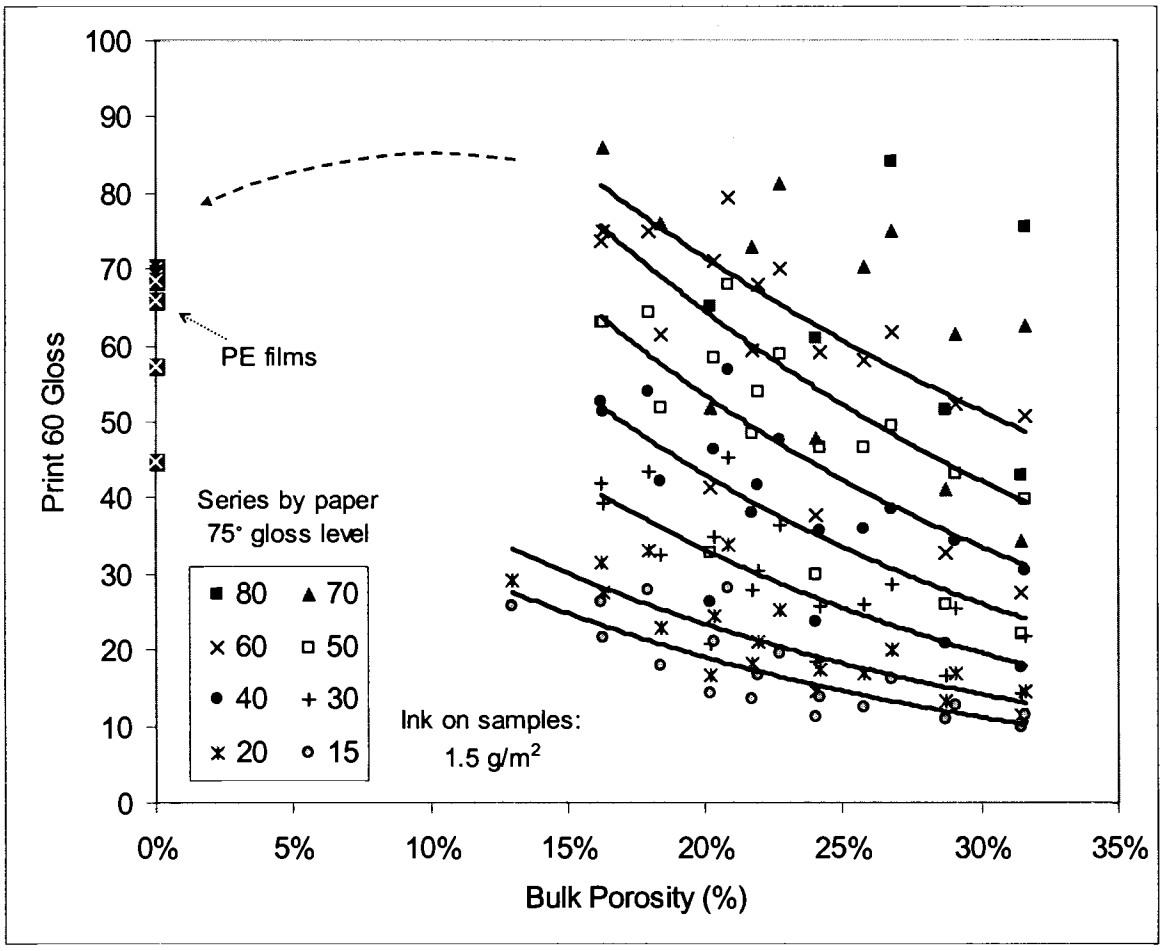

Figure 4.18: Overall trend of the relationship between print 60° gloss and porosity at 1.5 g/m^2 ink on samples. Note that there is no trend line given for '80' series due to missing data set.

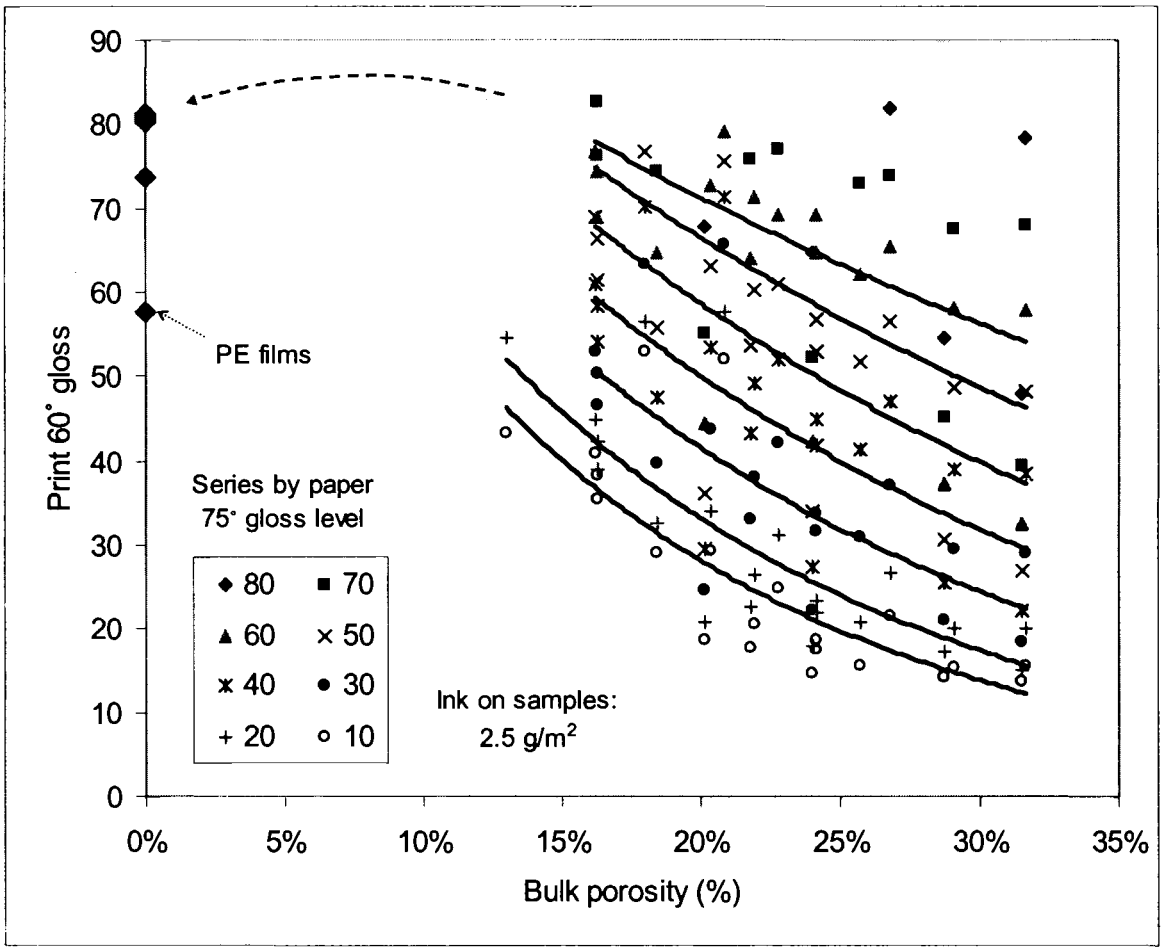

Figure 4.19: Overall trend of the relationship between print 60° gloss and porosity at 2.5 g/m^2 ink on samples. Note that there is no trend line given for '80' series due to missing data set.

Overall effect of pore size was also sought in a similar way with porosity effect analysis, and the results are presented in Figure 4.20 and 4.21, at the ink levels of 1.5 and 2.5 g/m^2 respectively. The relation was rather convex shape and the change in print gloss was even larger than the case of pore volume within a given range of parameters. As expected, it was clear that a coating with larger pore size generally produced a higher print gloss regardless of paper roughness. Here, the base mechanism of this result mostly attributed to the extended leveling process due to low absorption potential of a coating with large pore size. As observed in porosity effect, influence of pore size also became stronger especially over the low print gloss series in the higher ink film thickness.

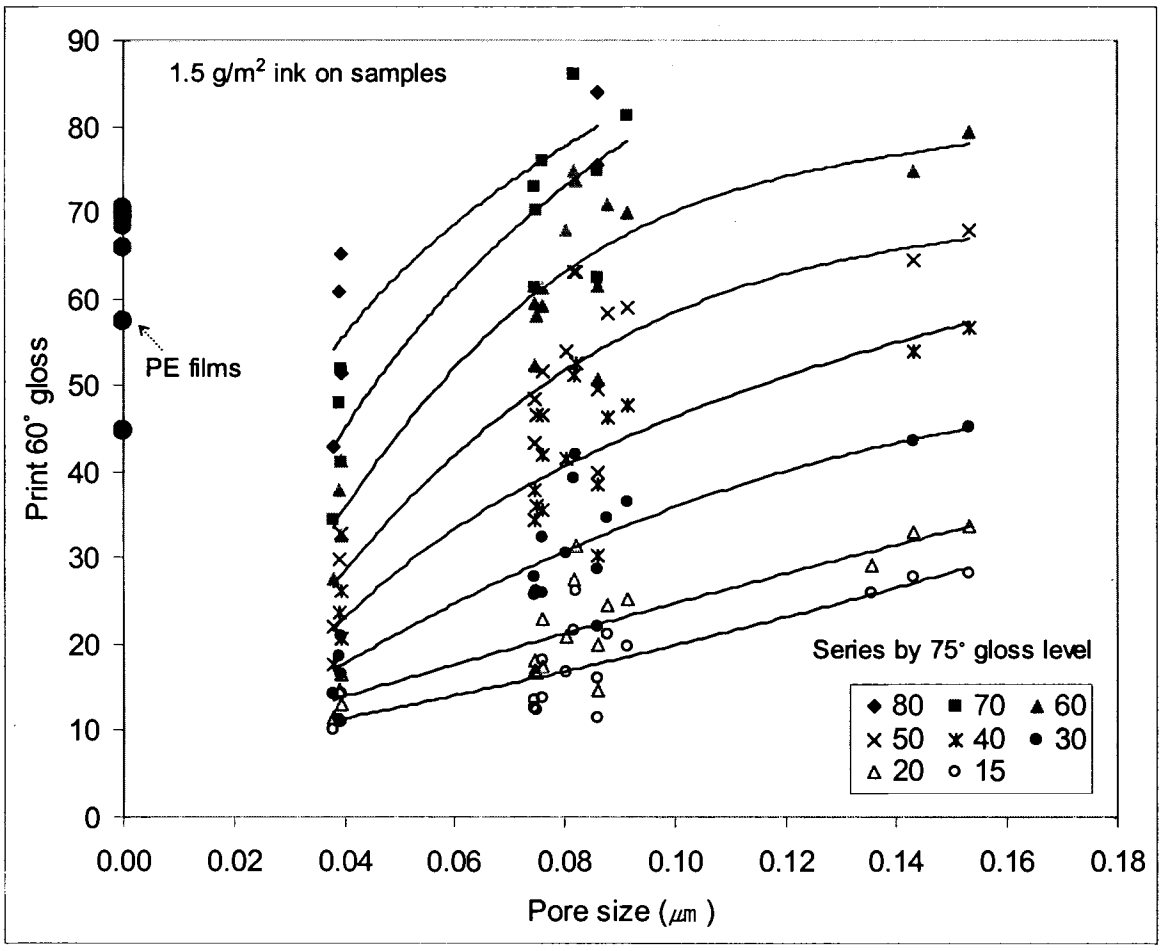

Figure 4.20: Overall trend of the relationship between print 60° gloss and pore size at 1.5 g/m^2 ink on samples.

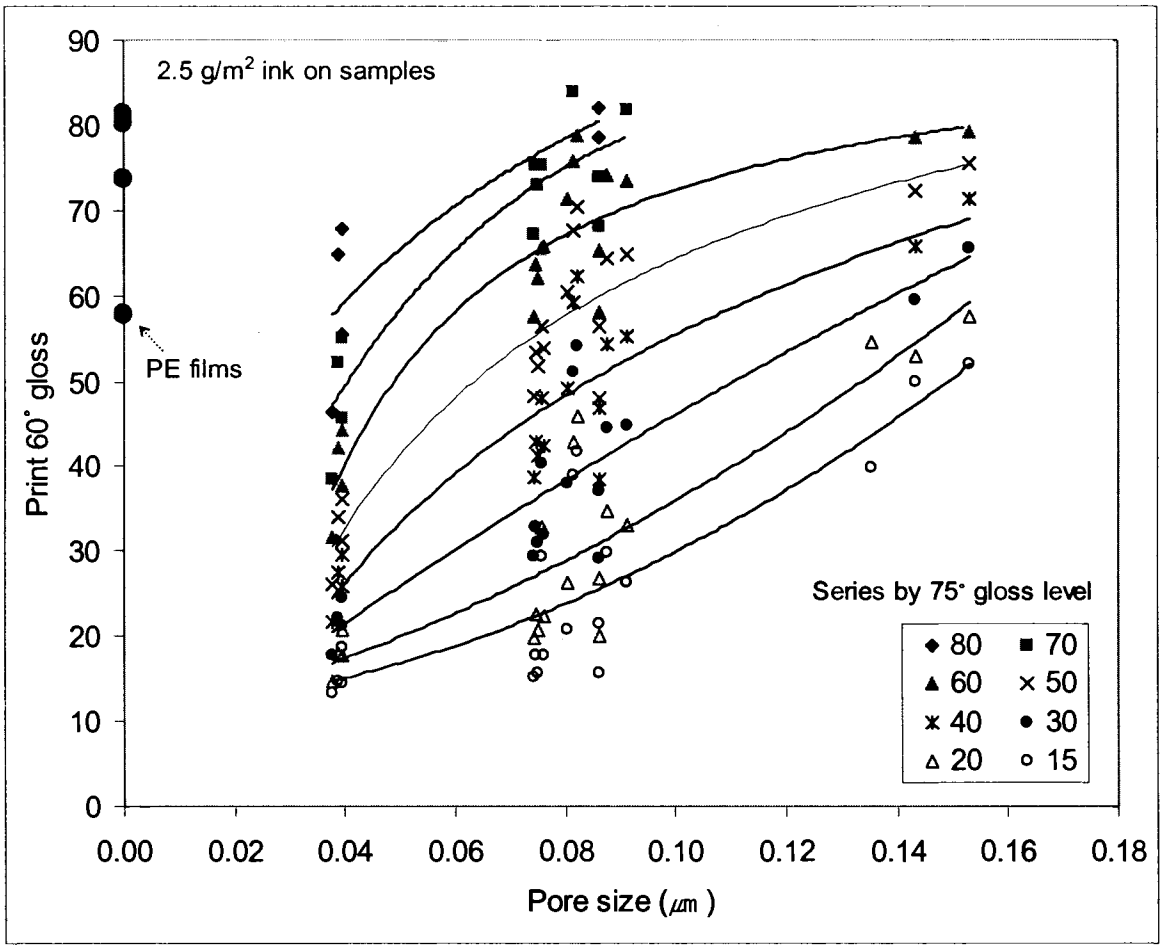

Figure 4.21: Overall trend of the relationship between print 60° gloss and pore size at 2.5 g/m^2 ink on samples.

4.2.5. Significance of Structural Factors on Print Gloss

Once the general relation was interpreted, the next step was to disintegrate each series into an individual pigment series to analyze localized results in detail. Figure 4.22a through 4.22h show print gloss development as a function of porosity and pore size at 2.5 g/m^2 ink level. Since this series of graphs were given stepwise over various range of paper gloss, roughness effect could be seen together. The decreasing print gloss of P3 series noted as '153 nm' can be observed. As a reminder, even though the measured porosity was partly in a comparable range with other series, the number of pores available might be much less than other series due to large pore size. Around 20 gloss units at 60° geometry, the results over low paper gloss region looked like leveling off; however, this will become rather linear in terms of 75° gloss. Sixty degree gloss becomes reliable beyond 30 gloss units to 70, which is a recommended measuring range. Besides the results at low paper gloss, print gloss of the '75 nm' and '80 nm' series showed a steep increase over less porous region below 22 % porosity. The samples in this range of porosity were formulated at the PVC levels of 68 % for G2 '80 nm' and 51.5 % for P1 '75 nm'. Therefore, it was likely that those samples were around or below CPVC level, to which the print gloss increase rapidly (Desjumaux, 1999). In an overall view, it can be seen that the slopes of fitted curves change just slightly while the gaps between each pigment series get larger. This may indicate the influence of pore size becomes strong over the small roughness region; however it should be reminded that this kind of observation is based on the measuring geometry. The trend would turn in a reverse way at 75° geometry. Overall, the pore size influence was clear in that the larger pore size, the higher print gloss.

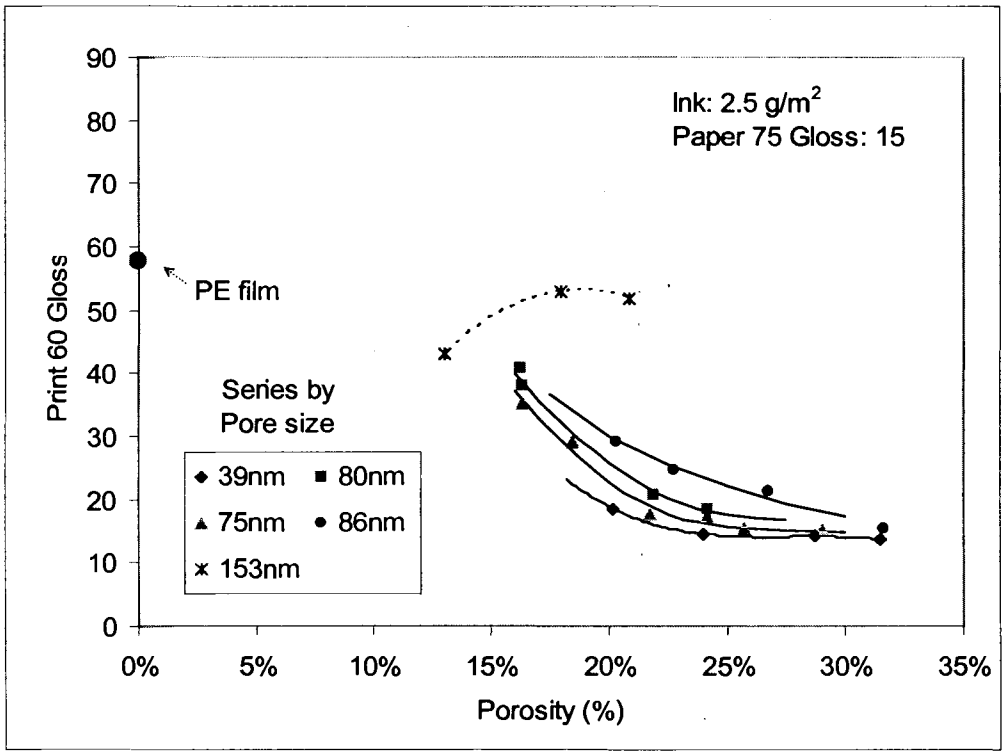

Figure 4.22a: Print gloss change as a function of porosity and pore size at 15 in 75° gloss.

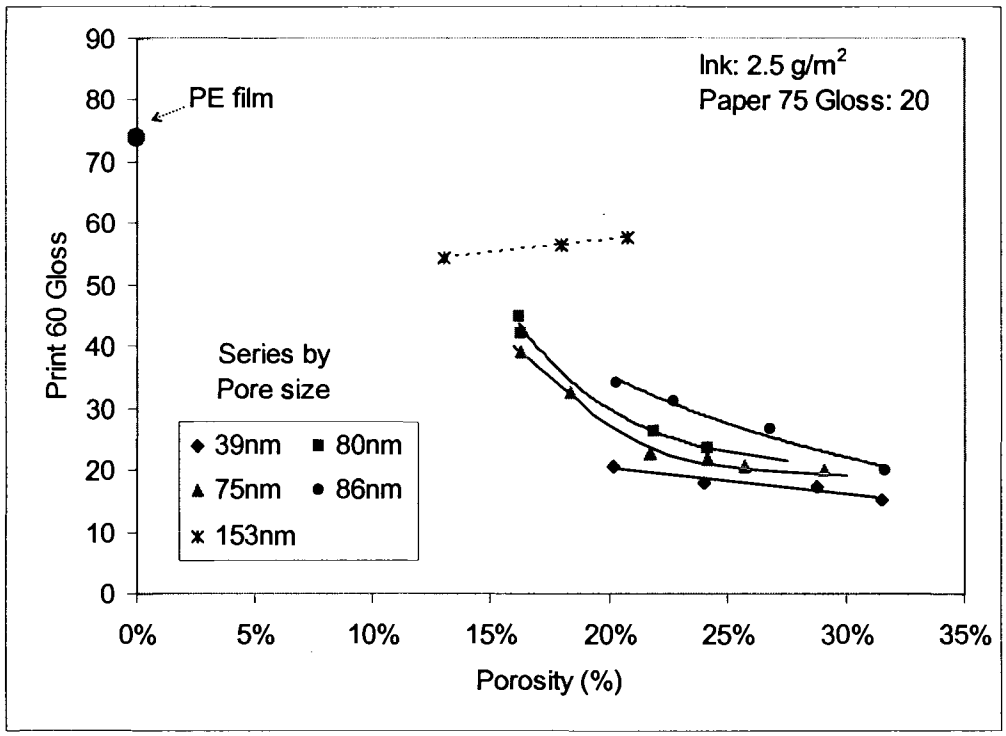

Figure 4.22b: Print gloss change as a function of porosity and pore size at 20 in 75° gloss.

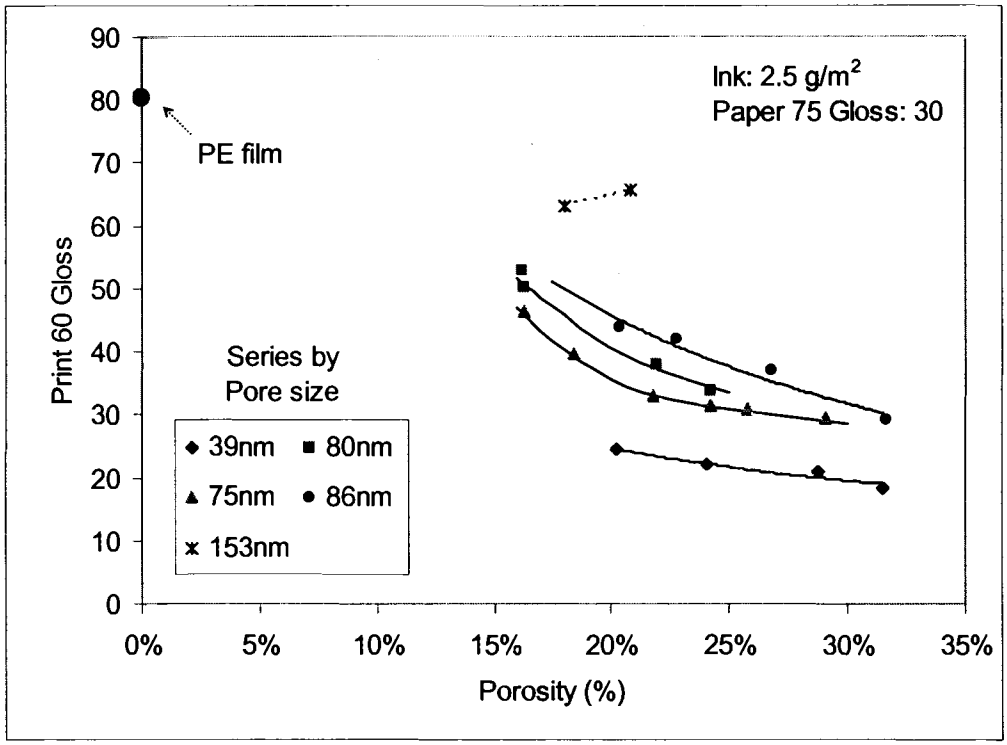

Figure 4.22c: Print gloss change as a function of porosity and pore size at 30 in 75° gloss.

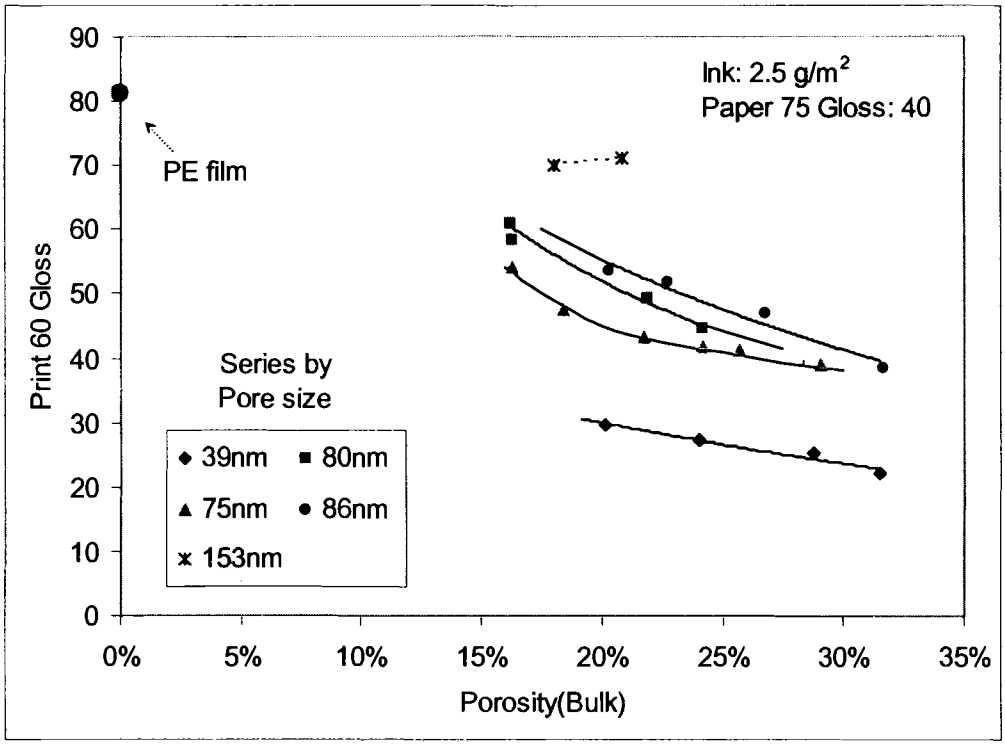

Figure 4.22d: Print gloss change as a function of porosity and pore size at 40 in 75° gloss.

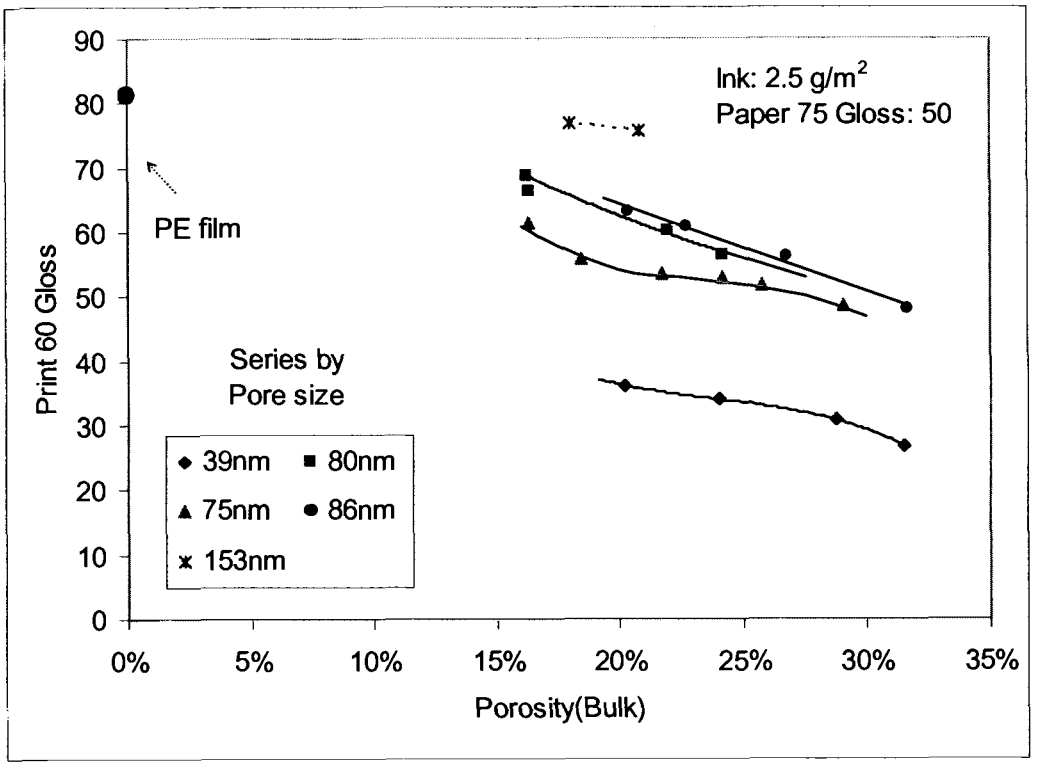

Figure 4.22e: Print gloss change as a function of porosity and pore size at 50 in 75° gloss.

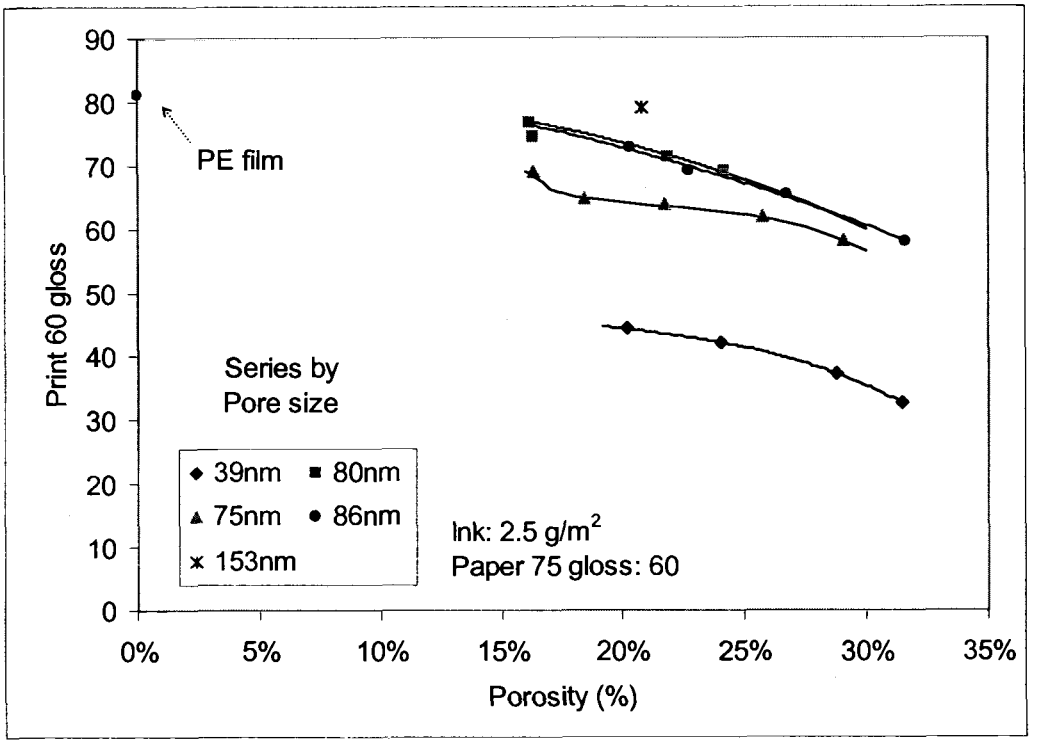

Figure 4.22f: Print gloss change as a function of porosity and pore size at 60 in 75° gloss.

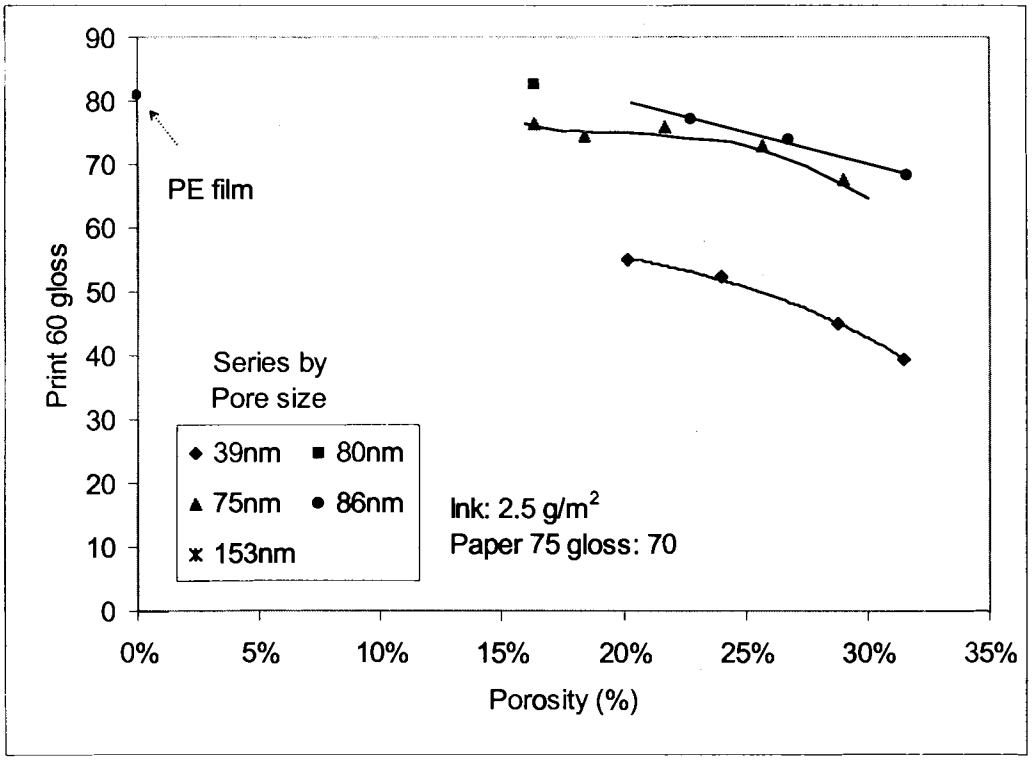

Figure 4.22g: Print gloss change as a function of porosity and pore size at 70 in 75° gloss.

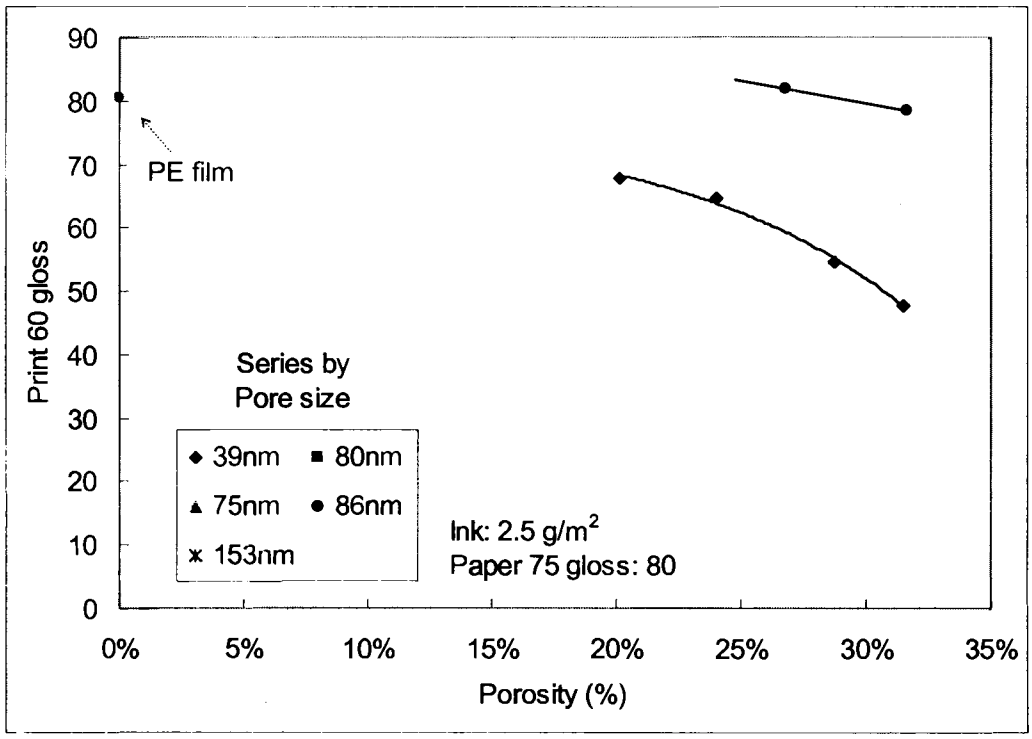

Figure 4.22h: Print gloss change as a function of porosity and pore size at 80 in 75° gloss.

The next step was to extract the print gloss at given porosity levels to get a set of designed experimental data with 3 independent factors and analyzed the significance of the involved factors. Commercial statistic software, Statistica Ver. 5.1, was used for practical processing. Due to the missing data set, 'central composite (response surface) analysis' module was used. First, a main effect was analyzed for overall parameter ranges and the result is given in Figure 4.23; paper gloss ranged from 15~80 gloss units at 75° gloss, pore size from 39 to 86 nm, and porosity from 16 to 32%. P3 series with 153 nm pore size was excluded in the effects calculation due to lack of data points, which may lead to imbalanced results. Rather than linear-only effect, linear and quadratic combined effect was chosen to consider non-linearity of the factors. The statistical analysis table is also given in Appendix E. The effect of roughness was bigger than that of the other parameters. As observed, its effect was linear and, consequently, the quadratic effect was negligible overall. The pore size effect was after the roughness. Pore size and porosity have significant quadratic effects. The quadratic effect of pore size was thought to come from the P3 series and its missing data. The interactivity between paper gloss and pore size might come from the fact that the small pore samples had higher paper gloss in the prepared sample set. The pooling of the small effect to error terms didn't alter the result. Visualized results of fitted response surface, as shown in Figure 4.24a through 4.24c, are presenting the response of the print gloss for the given factors. A value range over '90 gloss units' has less significance due to over prediction. The small dependency on porosity was remarkable though it was expected from the preliminary work. Therefore, in overall, this result may indicate that once the gloss level of paper is determined, the pore size control is considered to be more important than porosity.

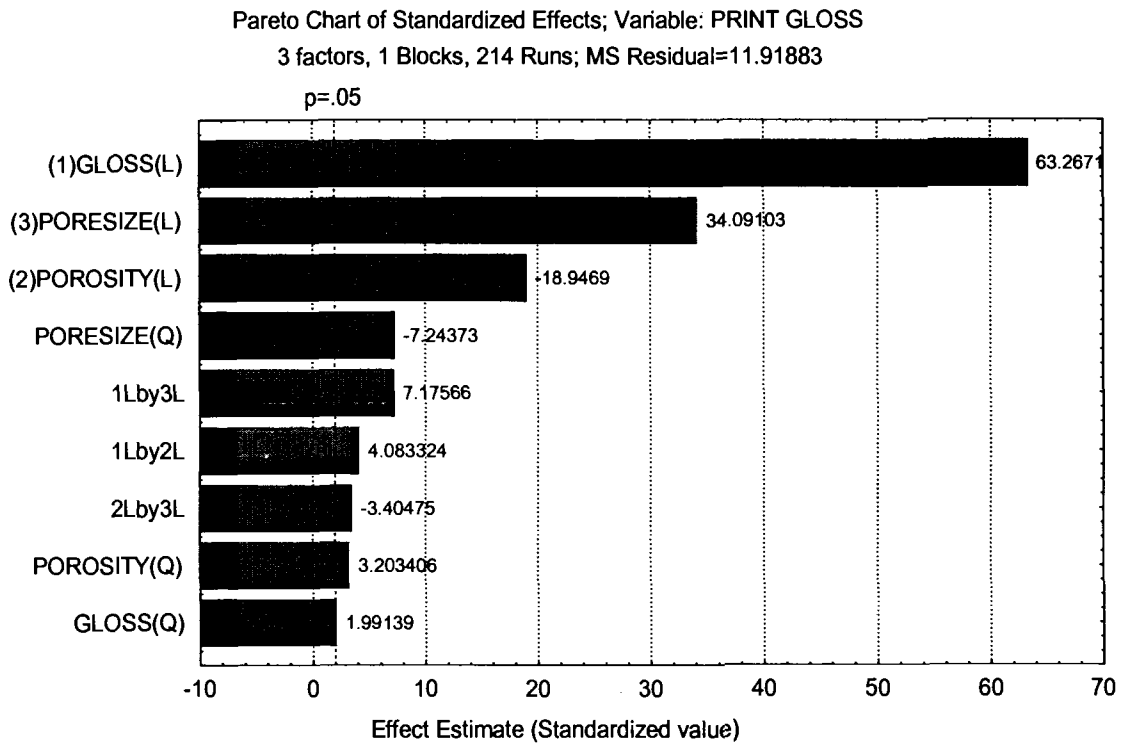

Figure 4.23: The result of main effect analysis for print gloss over all parameter ranges. The effects were from ANOVA estimates. The effects above p=0.05 were accepted as statistically significant. Here, 'p' is referred to reliability.

Paper Gloss: **15** gloss units at 75° geometry.

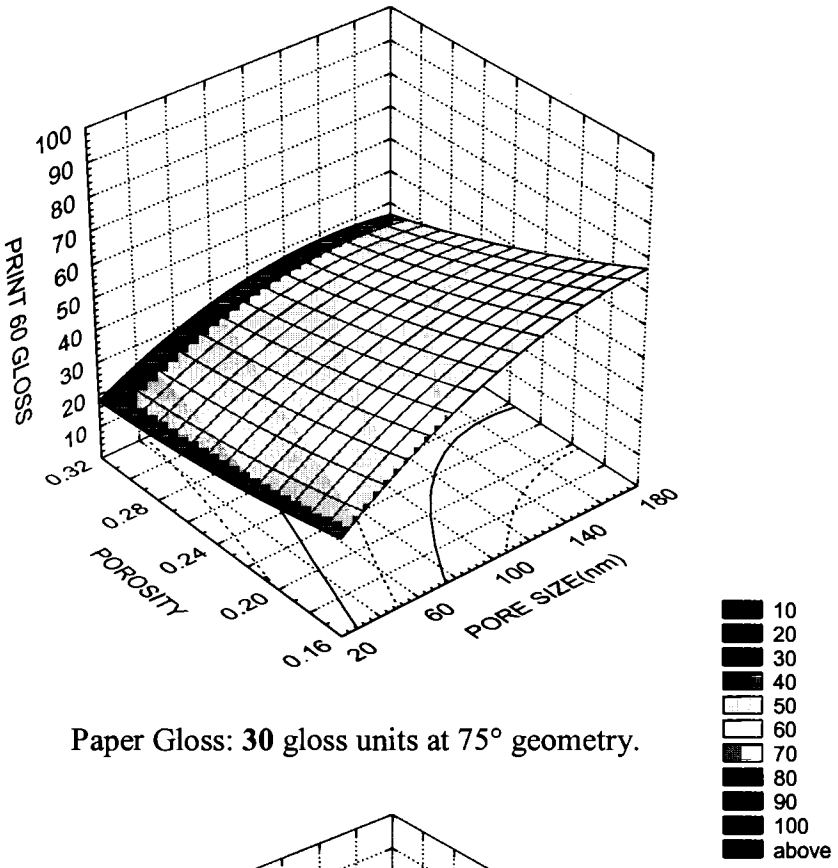

Paper Gloss: **30** gloss units at 75° geometry.

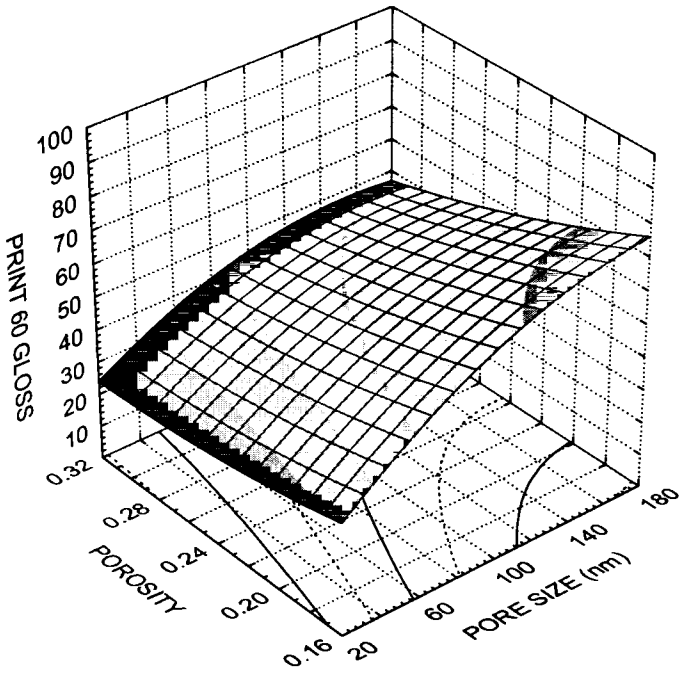

Figure 4.24a: 3-Dimensional fitted surface of print gloss as a function of coating structure.

Paper Gloss: **40** gloss units at 75° geometry.

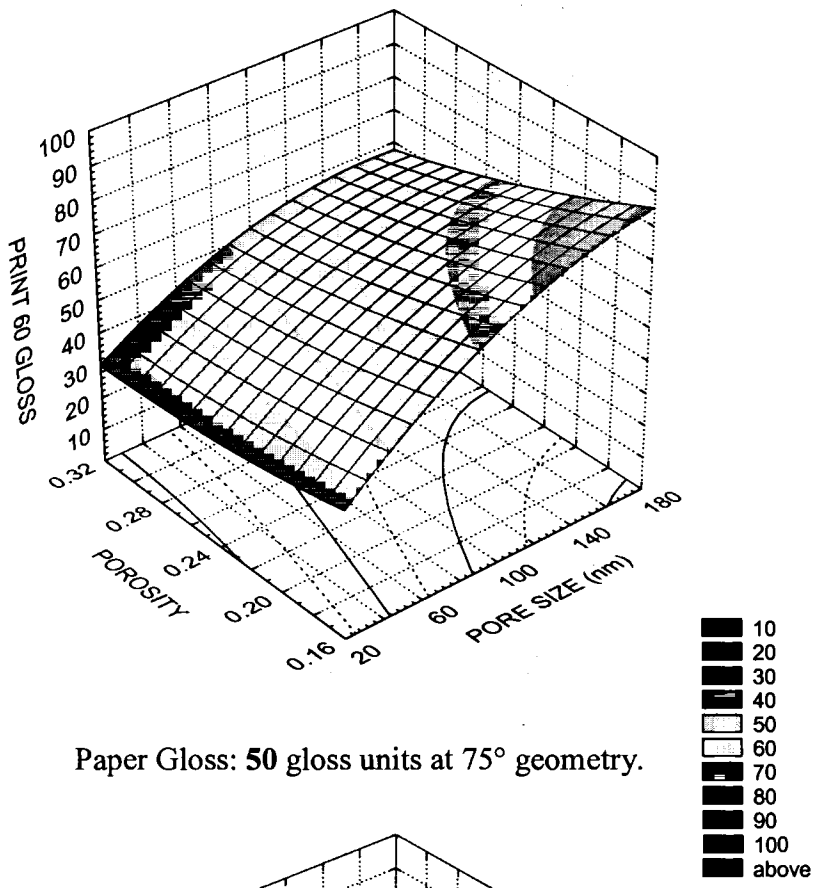

Paper Gloss: **50** gloss units at 75° geometry.

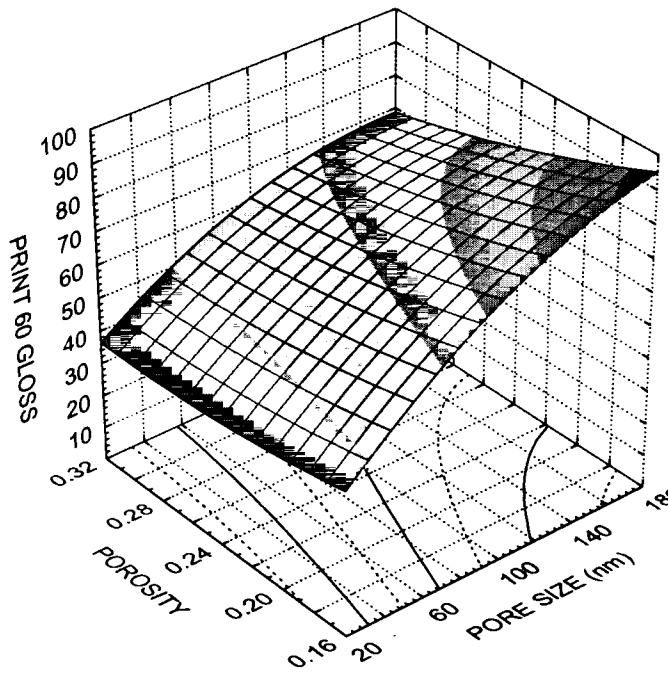

Figure 4.24b: 3-Dimensional fitted surface of print gloss as a function of coating structure.

Paper Gloss: **60** gloss units at 75° geometry.

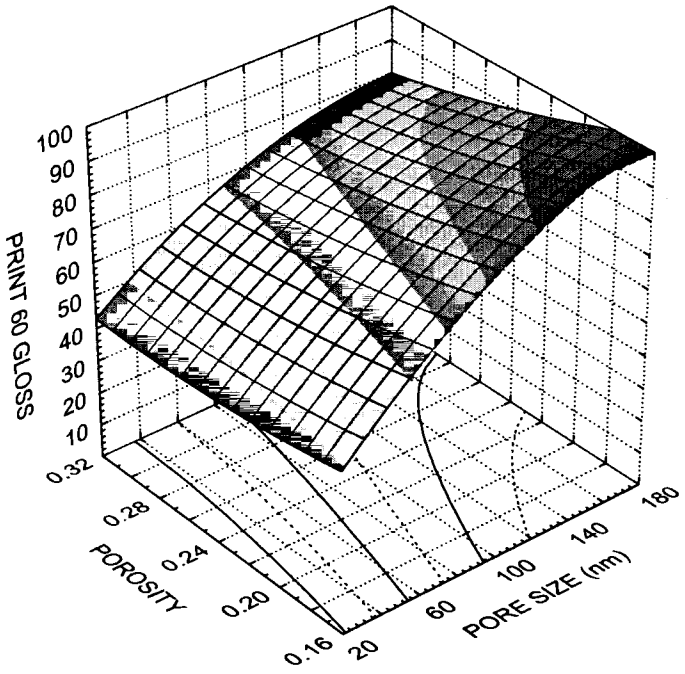

Paper Gloss: **70** gloss units at 75° geometry.

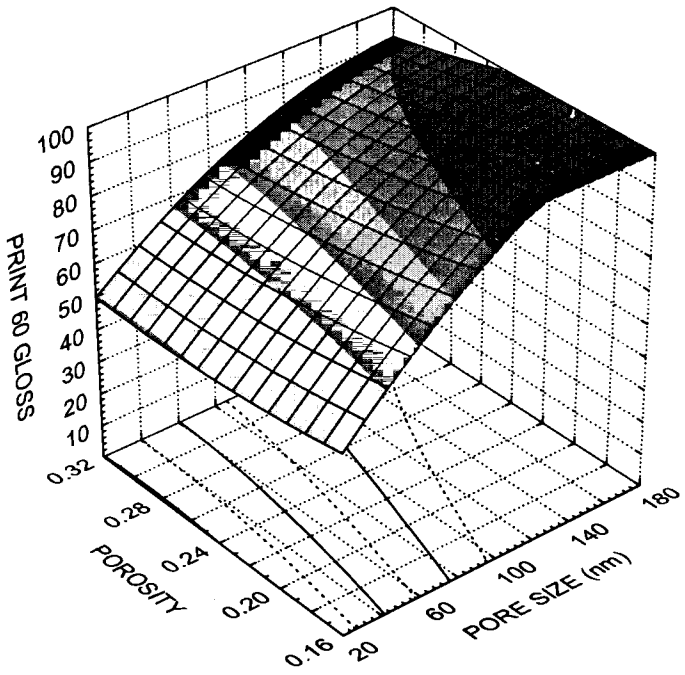

Figure 4.24c: 3-Dimensional fitted surface of print gloss as a function of coating structure.

In a practical sense, no single paper grade has the gloss range in this work. Therefore, the data are sectioned into two blocks based on the gloss level such that the gloss up to 40 gloss units may represent for matt and/or dull grade surface while the above for gloss and glossy grade.

Figure 4.32 describes the obtained result from the low paper gloss range data. The effects between roughness and pore structure remain in the same order as the overall results, but the gap became smaller. In summary for the low paper gloss range, the roughness effect was in the strongest position, but the competitiveness was high with pore size following by porosity. Therefore, even in the high roughness (low gloss) range, refined control of pore structure is important. Figure 4.33 presents the effect of pore size and roughness at given porosity over the low paper gloss region.

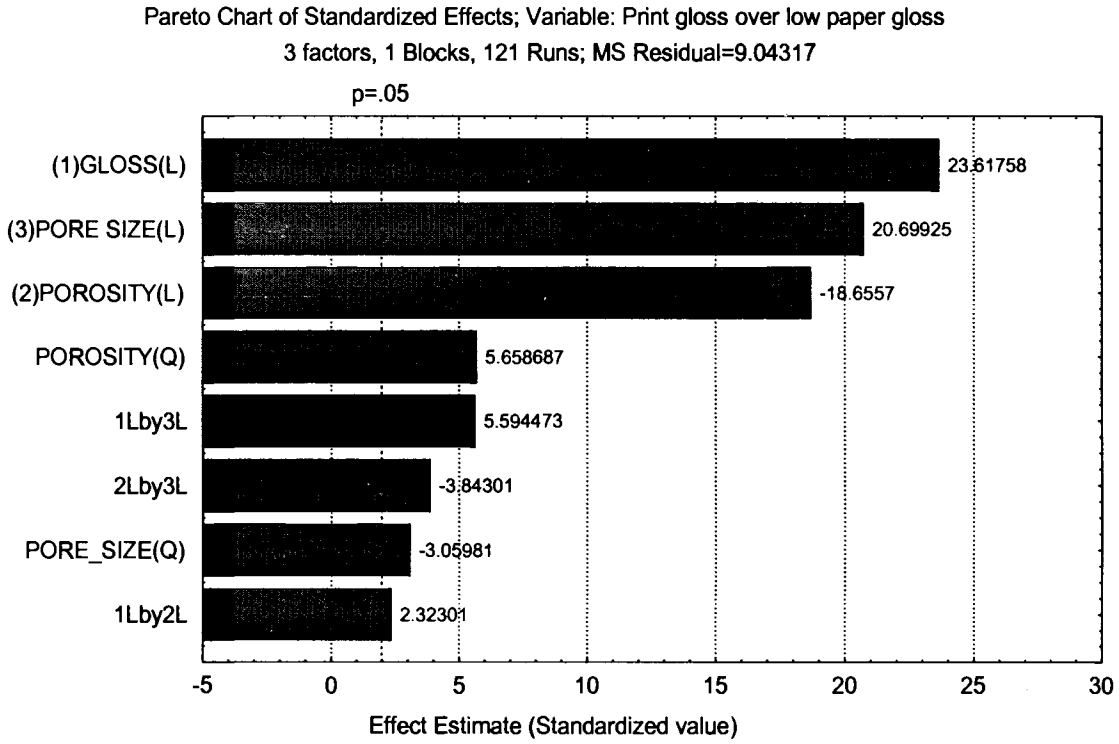

Figure 4.25: The result of main effect analysis for print gloss over low paper gloss ranges; (up to 40 gloss units at 75° geometry).

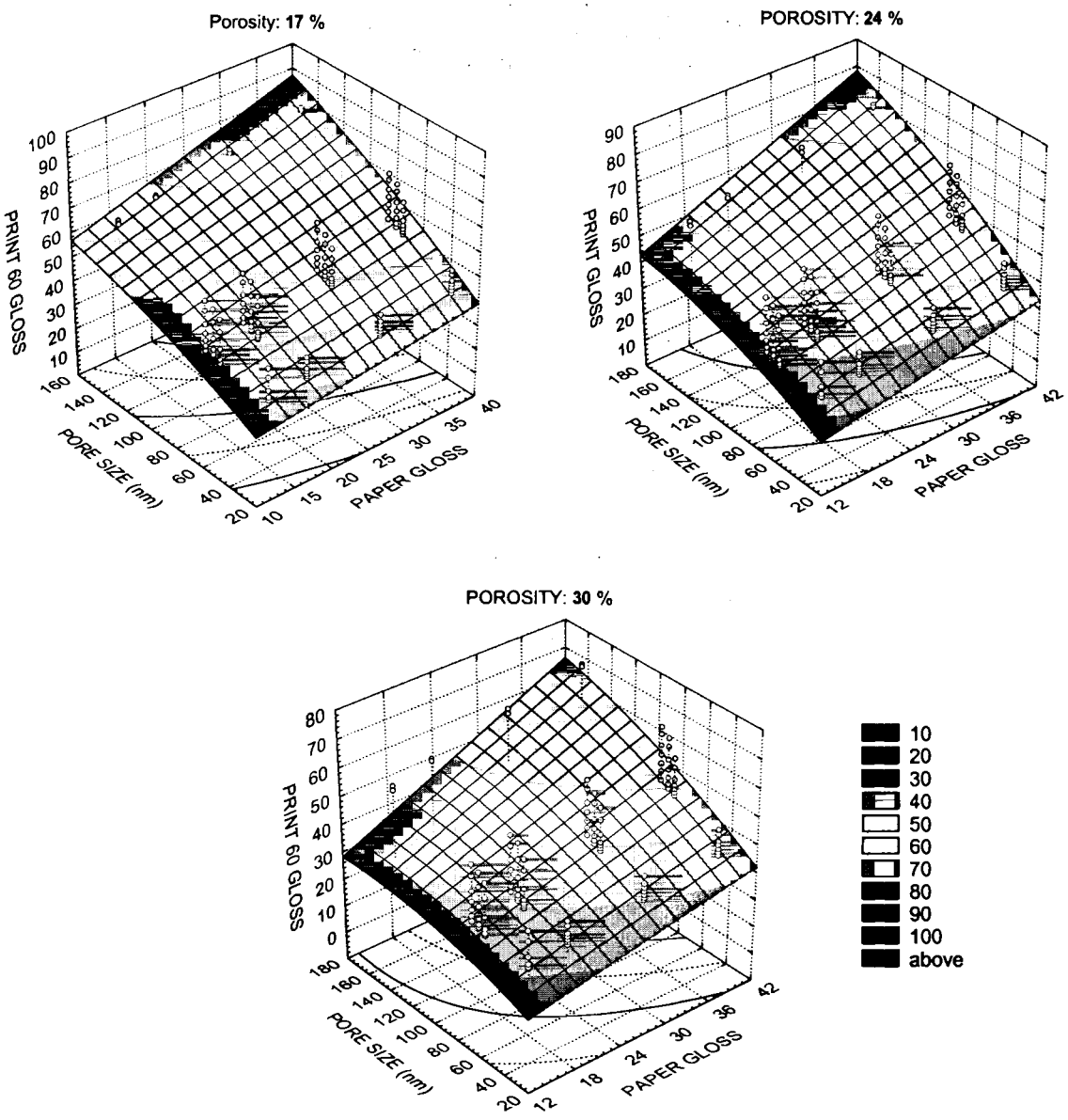

Figure 4.26: 3-Dimensional fitted surface of print gloss as a function of pore size and paper gloss over the given porosity levels.

The second section of analysis was done for the above 40 gloss units up to 70 gloss units. The rest of data as well as P3 series was excluded due to missing components. The result of main effects is given in Figure 4.34. Rather surprisingly, pore size effect was equivalent or even slightly larger than the paper gloss influence. Since porosity effect was relatively small and far below from these two factors, the significance is much on the pore size in terms of structures over high paper gloss region. In a practical sense, the structural difference from various products may lie in the pore size rather than paper gloss since it is controlled for a specific grade. This may mean that discriminated performance or end-use quality could follow from that. The order with relatively small effect difference between gloss and roughness could be altered in an analysis with print 75° gloss. The response surface of print gloss in this range is given in Figure 4.35.

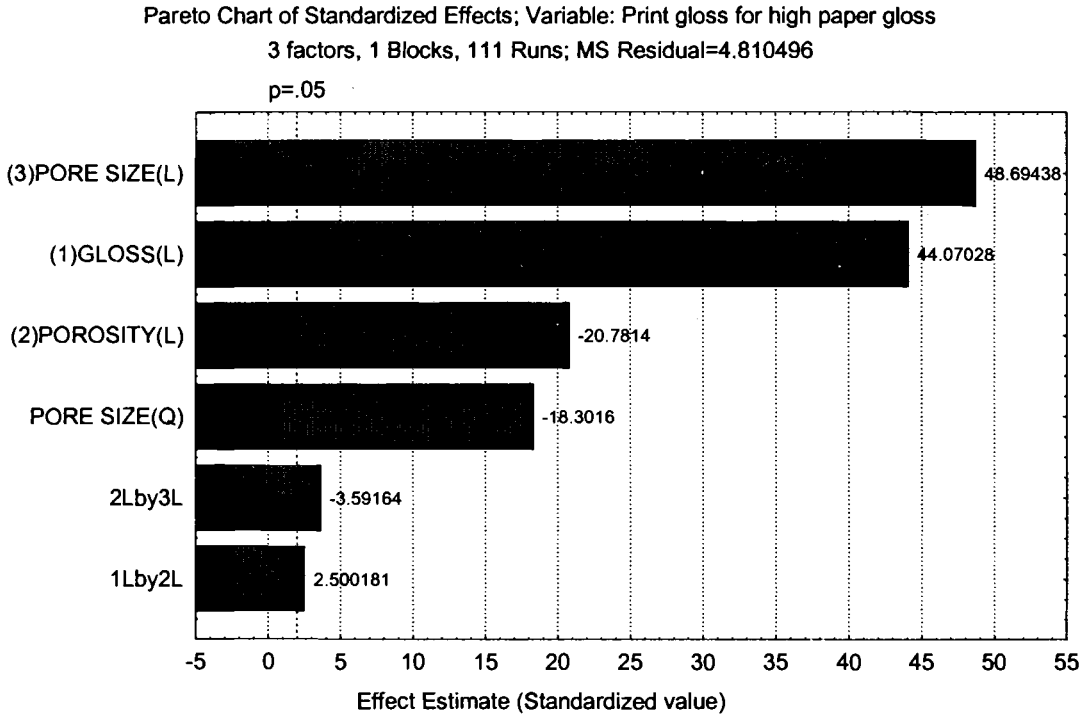

Figure 4.27: The result of main effect analysis for print gloss over high paper gloss ranges; (40 ~ 70 gloss units at 75° geometry).

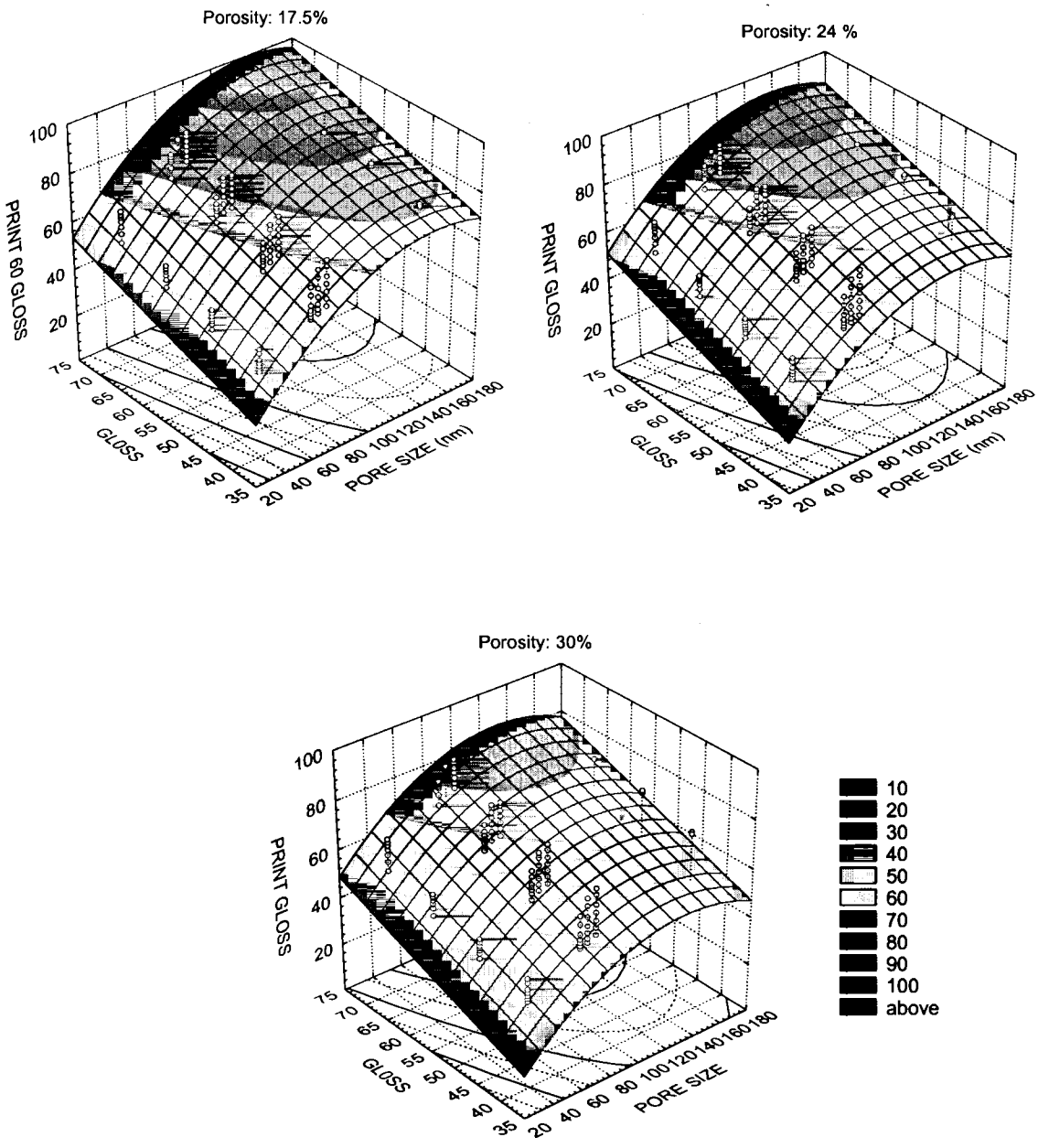

Figure 4.28: 3-Dimensional fitted surface of print gloss as a function of pore size and paper gloss at the given porosity levels over high paper gloss region.

5. CONCLUSIONS AND RECOMMENDATIONS

A well defined set of coatings with systematic change in roughness, pore size, and porosity was generated for the first time and analyzed with respect to the print gloss development.

As confirmatory results;

- ✓ The relationship between gloss and roughness (Ra) agreed well with the theory when the filtered roughness was used.
- ✓ Roughness affected the ink transfer overall inking regions from the result of polyester films. The difference before a maximum transfer region was thought due to available contact area while the deviation after the maximum was attributed to numerous cavitations from surface voids.
- ✓ The gloss at 60° geometry was better to differentiate gloss over the high print gloss beyond 20~30 gloss units (equivalent to 60~70 gloss units at 75° geometry), which conformed to the recommended use from the standard. On the other hand, 75° gloss was good for the low print gloss range. Therefore, it should be noted what geometry was used for analysis, otherwise the behavior or response trends may become incompatible each other.

Our findings throughout this research are summarized;

- The initial behavior of print gloss development was analyzed with respect to the structural factors for the first time. The structural factors seemed like involve in the print gloss development in different ways each other. Roughness and porosity showed their effects from the start of print gloss evolution indicating their influence on ink transfer and ink-film splitting, while pore size set forth in the immobilization and setting stage.
- Once the ink film start to level, roughness and pore size restricted and determined the print gloss level in short time after passing the printing nip. However, porosity effect was in a reversed order initially, and then rather than determining the final print gloss level, it looked like involving in acceleration or deceleration of print gloss development.
- For the first time, presented was a systematic response of print gloss development with primary structural factors, i.e. roughness, porosity, and pore size, based on exclusive relations. The presented result provides quantitative effect analysis with given parameters.
- Higher amount of inking on a surface increased the print gloss within the given inking range overall. Increased inking fills up the roughness and reaches a plateau and/or maximum in print gloss on a certain surface. However, higher ink film thickness on the rough surfaces did not cover up the effect of various roughness within a given range of the parameter (10~85 gloss units). This was also supported

by the sudden drop in print gloss of high roughness non-porous film, which was relatively free of roughness effect to certain extent.

- Even though there seemed like an estimated trend of convergence in print gloss at 75° geometry over low roughness range, it did not happen at 60° gloss. This result confirmed the overall consistency of roughness effect as well as pore structure.
- Under the overall trend, print gloss of the coatings with low porosity and large pore size may have small dependency on roughness.
- Porosity effect seemed to increase exponentially as coating reaches around CPVC region.
- Even though low porosity with large pore size generally produced higher print gloss, surface sealing by latex films may strongly impede ink transfer and/or generate large splitting patterns, consequently resulting in low print gloss. This surface effect may not be accessed by simple bulk porosity values.
- The effects of porosity and pore structure proved to be significant regardless of roughness levels while the importance became larger at higher inking levels.
- Roughness was in the most important factor, followed by pore size and porosity, respectively. This order of main effects was consistent in the low paper gloss region (below 40 gloss units at 75° geometry), but the gap became narrow meaning a high competitiveness between each other. However, pore size effect became strongest factor slightly overcoming the roughness effect in the high paper gloss region (above 40 gloss units at 75° geometry). Porosity effect was still significant but less than that of roughness and pore size. Therefore, at a given level of paper

gloss or roughness, this may indicate that pore size control is more important than others.

- In an extended point of view, the results of main effects on print gloss may imply that the print gloss mottle could also be affected by those structural factors in a similar competitive way.
- The relationship between 60° and 75° gloss was different for printed and unprinted surfaces probably due to slightly altered surface conditions such as refractive indices and major roughness features. This difference may lead inconsistent or imbalanced result in print gloss or print-snap appraisal depending on the geometries used.

Recommendations;

Throughout the projects, need of further investigation is summarized;

- During the print gloss development, it was often observed there was a gloss drop. The magnitude of the decrease in print gloss was various depending on the amount of ink, surface roughness, and pore structure. Therefore, it may merit further research to access knowledge on this phenomenon, which may also lead to an important product strategy in a practical point.
- Related to gloss development, the effect of ink drying process with respect to print gloss may need to be further investigated so that the significance and role of ink may be more elucidated.

- Print gloss is important for product quality, while ink tack affect on the runnability and quality as well related to print mottle etc. These qualities are bounded strongly together but the desirability is often in an opposite side each other. Therefore, an investigation on their relationship and an optimized compromise merits further research.
- Suggested models related to leveling and print gloss development may be proven with experimental data generated in this work.

REFERENCES

Abrams, L., Maynard, R., and Favorite, C. (1996). Correction for compressibility in mercury intrusion measurements. The Micro Report, 7 (4), 1.

Abrams, L., Capano, P. J., Favorite, C. W., and Johnson, R. W. (1996). Using mercury porosimetry to characterize coating pore structure and its relation to coating optical performance. Tappi Coating Conference Proceeding, 185.

Alince, B., and Lepoutre, P. (1979). Porosity and optical properties of clay coatings. J. of Colloid and Interface Science, 76 (2), 439-444.

Alince, B., and Lepoutre, P. (1980). Plastic pigment in paper coating. Tappi J., 63 (5), J49-53.

Alince, B., and Lepoutre, P. (1981). Sintering of latex particles in pigmented coatings: II Influence of the latex particle size. J. of Applied Polymer Sci., 26, 799-808.

Apps, E. A. (1964). Gloss inks and matte inks. Ink technology for printers and students, Chemical Publishing, New York.

Arai, Y., and Nojima, K. (1997). Coating structure for obtaining high print gloss. Tappi Coating Conference Proceeding, 133.

Aschan, P. J., Makkonen, T., and Pakko, J. (1986). Board surface structure and gravure printability, Paperi Ja Puu-Papper och Tra, 1 (30), 30-31, 33-34.

Askew, F. A. (1969). The printing ink manual. W. Heffer and Sons, Cambridge, UK.

Aspler, J.S., and Lepoutre P. (1991). The transfer and setting of ink on coated paper. Progress in Organic Coatings, 10, 333.

Aspler, J. S., Maine, C., De Grâce, J. H., Zang, Y. H., and Taylor, S. (1994). Printing tack, Part I: Influence of paper structure on ink "Tack" measured in a printing nip. Adv. Printing Sci. Tech., 22, 139.

Banks, W. H., and Mills, C. C. (1954). Some observations on the behavior of liquids between rotating rollers. Proc. Roy. Soc. London, A223, 414.

Barber, E. J. (1953). Defining the surface smoothness of paper with the Brush surface analyzer. Tappi J., 36 (11), 158A.

Bassemir, R. W. (1976). The gloss of ultraviolet cured press applied films. Radiation Curing, 3, 10.

Bassemir, R. W., and Krishnan, R. (1991). Paper Coating Fundamentals Symposium Proceeding, CPPA, 69.

Bassemir, R. W., Costello, G., and Parris, J. (1994). International Printing and Graphic Arts Conference Proceedings, CPPA, 159.

Bekk, J. (1932). Paper Trade J., 94 (26), 41.

Béland, M. C., Nguyen, N., De Silveira, G., and Lepoutre, P. (1992). A new image analysis method for fiber-rising measurement. International Printing and Graphic Arts Conference Proceeding, 179.

Béland, M. C., and Mangin, P. J. (1995). Three-dimensional evaluation of paper surfaces using confocal microscopy. Surface Analysis of Paper. Conners, T. E. and Bannerjee, S. Eds., CRC Press, Boca Raton, Fla.

Béland, M. C., and Mattson, L. (1996). Optical print quality of coated papers. International Printing and Graphic Arts Conference Proceeding, 123.

Béland, M. C. (1997). CLSM and AFM applied in pulp and paper research-A literature review. Proc. European Conference on Pulp and Paper Research-The Present and the Future. European Commission Publication, Italy, 200-221.

Béland, M. C., Johansson, P.-A., and Lindberg, S. (1998). Optical measurements and perception of gloss quality of printed matte-coated paper. International Printing and Graphic Arts Conference Proceeding, 187.

Béland, M. C. (2001). Ph.D. Thesis. Royal Institute of Technology, Sweden.

Bennett, H. E., and Porteus, J. O. (1961). Relation between surface roughness and specular reflectance at normal incidence. J. Opt. Soc. Am., 51, 123.

Bery, Y. (1978). An ink transfer equation. Proc. of Tech. Association of Graphic Arts, 172-191.

Bery, Y.A., and Loel, P. A. (1992). Nature of ink film splitting. International Printing and Graphic Arts Conference Proceeding, 53.

Bird, R. B., Stewart, W. E., and Lightfoot, E. N. (1960). Transport Phenomena. John Wiley & Sons, NY.

Bitla, S. (2002). M.S. Thesis. University of Maine.

Bousfield, D. W. (1987). Analysis of surface tension driven leveling in viscoelastic films. J. of Non-Newtonian Fluid Mech., 22, 219.

Bousfield, D. W. (1991). A model for the leveling of coating defects. Tappi J., 74, 163.

Bousfield, D. W. (1991). Long-wave analysis of viscoelastic film leveling. J. of Non-Newtonian Fluid Mech., 40, 47.

Bristow, J. A., and Bergenblad, H. (1992). Paper structure and ink setting: factors influencing the set-off test. Adv. Printing Sci. Techn., 21, 412.

Bryntse, G. (1981). A method for the analysis of ink mottle using polarized light reflection. Ph.D. Thesis. The Royal Institute of Tehcnology, Stockholm, Sweden.

Bureau, W. (1983). The interaction of light, ink, and paper. Part 2: color and gloss. Graphic Arts Monthly, 55, 153-154.

Casey, J. P. (1981). Pulp and Paper, A Wiley-Interscience Publication, 3, 1756.

Chapman, S. M. (1955). Tappi J., 38 (2), 90.

Chinmayanandam, T. K. (1919). On the specular reflection from rough surface. Phys. Rev., 13 (2), 96-101.

Climpson, N. A., and Taylor, J. H. (1976). Pore size distribution and optical scattering coefficients of clay structure. Tappi J., 59, 89.

Coupe, R. R., and Hsu, B. (1960). Penetration of varnishes and inks into paper under pressure. J. of Oil Colour Chem. Assoc., 43, 720.

Crawshaw, D. B., Kahn-Schneider, C. H., and Clark, P. C. (1982). The influence of pigment particle shape on the performance of a paper coating. Proc. 1982 Coat. Conf., Tappi Press, 143-164.

Davis, P. J., and Smith, D. M. (1989). Using NMR spectroscopy to analyze the pore structure of coatings. Tappi J., 72 (5), 85-89.

De Grâce, J.H., and Mangin, P.J. (1984). A mechanistic approach to ink transfer. (1). Effect of substrate properties and press conditions. Adv. Printing Sci. Tech., 17, Chap. 20, 312-332.

De Grâce, J. H., and Mangin, P.J. (1988). A mechanistic approach to ink transfer. (2). Splitting behavior of inks in printing nips. Adv. Printing Sci. Tech., 19, Chap. 10, 146-161.

De Grâce, J. H., and Dalphond, J. E. (1989). Development of print density and print-through in newsprint. TAGA Proc., 582-609.

De Jidas, L. M., and Destree, T. M. (1988). Sheetfed offset press operating. Graphic Arts Technical Foundation, Pittsburgh, PA.

Desjumaux, D. M. (1999). Ph.D. Thesis, University of Maine.

Desjumaux, D. M., and Bousfield, D. W. (1998). Modeling of ink film leveling with mobile phase removal, International Printing and Graphic Arts Conference, 103-109.

Donigian, D. W., Ishley, J. N., and Wise, K. J. (1997). Coating pore structure and offset printed gloss, Tappi J., 80(5), 163-172.

Durchon, P. (1991). Papiers et impressions offset. Editions du Moniteur, Paris.

Eklund, D. (1975). Pigment particle size-Its significance in paper coating. Cell. Chem. Technol., 9 (3), J299-J312.

Enomae, T., Onabe, F., and Usuda, M. (1993). Application of new profilometry using topographic scanning electron microscope to paper surface topography. Tappi J., 76 (1), 85-90.

Enomae, T., and Onabe, F. (1994). IS&T's 47th Annual Conference Proceedings, Vol. 2, The Society for Imaging Science and Technology, Springfield, VA, 841-844.

Enomae, T., and Lepoutre, P. (1995). Stylus Profilometry on Paper: Marking by the Stylus. Tappi J., 78 (10), 173-176.

Ercan, S. N. (2001). Ph.D. Thesis, University of Maine.

Fairfield, R. (1960). Influence of modified phenolic resins on gloss inks. AIM, 10, 30.

Fetsko, J. M., and Zettlemoyer, A. C. (1962). Factors affecting print gloss and uniformity. Tappi J., 8, 667.

Fetsko, J. M., Witherell, F. W., and Poehlein, G. W. (1974). Relationship between gloss and surface roughness of paperboard samples and prints. Proc. 12th Int. Conf. of Printing Res. Int., Guildford, IPC Press, 67.

Field, R.J. (1995). Matt paint films: real-time observation of film shrinkage and associated roughening of the surface during drying. Proc. of the Third Nürnberg Congress.

Fujiwara, H., and Kaga, C. (1990). Measurement of gloss profile. Tappi Coating Conference Pro., Tappi Press, 1092-1098.

Gane, P. A. C., and Seyler, E. N. (1994). Tack development: an analysis of ink / paper interaction in offset printing. Tappi Coating Conference Pro., Tappi Press, 244.

Gane, P. A. C., Grunwald A., and Hooper, J. (1995). Coating pigment orientation: A comparative analysis of the application mechanisms and properties of blade and roll coating. Tappi Coating Conference Pro., Tappi Press, 383-390.

Gane, P. A. C., Kettle, J. P., Matthews, P., and Ridgway, C. J. (1996). Void space structure of compressible polymer spheres and consolidated calcium carbonate paper-coating formulations. Ind. Eng. Chem. Res., 35, 1753-1764.

Garey, C. L. (1982). Surface porosity of coated paper. Tappi Coating Conference Proceeding, Tappi Press, 117.

Gate, L.F., Windle, W., and Hine, L. (1973). The relationship between gloss and surface microtexture of coatings. Tappi J., 56 (3), 61.

Gate, L.F., and Parsons, D.J. (1993). The specular reflection of polarized light from coated paper. Trans. 10th Fundamental Research Symposium, Oxford, 263-284.

Geankoplis, C. J. (1983). Transport processes and unit operations. Englewood Cliffs, Prentice-Hall, New Jersey.

Ginman, R., Makkonen, T., and Nordman, L. (1974). Profile measurement on printing paper. Proc. 12th Int. Conf. of Printing Res. Inst., W. H. Banks (Ed.), Guildford, IPC Press, 46-52.

Glass, J. E. (1978). Dynamics of roll spatter and tracking. Part III: Importance of extensional viscosities. J. Coatings Technology, 50, 53.

Glatter, T. P., and Bousfield, D. W. (1996). Print gloss development on model substrates. International Printing and Graphic Arts Conference Proceeding, 139.

Glatter T., and Bousfield D.W. (1997). Print gloss development on a model substrate. Tappi J., 80 (7), 125.

Glatter, T. P. (1996). M.S. Thesis, University of Maine.

Gunning, J. R., and Farrel, W. R. (1976). A device for measuring mottle in coated paper. Tappi J., 59 (8), 92.

Hachey, S. W., Niles, C. D., and Robie, S. P. (1994). The impact of web oven parameters on 20° print gloss. International Printing and Graphic Arts Conference Pro., 119.

Hansen, A. and Hansen, W. (1973). Gloss of prints. Scand. Paint Printing Ink Res. Inst., Rept. no. T 11-73, 47.

Harrison, V.G.W. (1945). Definition and measurement of gloss: a survey of published literature, Heffer and Sons Ltd, Cambridge, England.

Hattula, T., and Oittinen, P. (1982). Analysis of ink penetration into pigment coatings. Paperi Puu, 64 (6-7), 407-408, 410-412.

Hayashi, T., and Amari, T. (1992). Dynamics of transfer and splitting of emulsified ink. International Printing and Graphic Arts Conference Pro., 75.

Hayashi, T., Morita, K., and Amari, T. (1993). Rheological properties and printabilities of polybutadiene / carbon black ink. J. Jpn. Soc. Colour Mater. (SHIKIZAI), 66, 655.

Hayes, P. C. (1994). Styrene butadiene latex polymers in coated papers. Technical Research Report., No.503.01, Gencorp.

Hecklau, F. L., and Pavol, M. (1967). Gloss and ink hold-out properties of coated paper and paperboard as influenced by clay pigmentation. Tappi J., 50, 61.

Hemstock, G. A., and Bergmann, R. J. (1968). Studies of relationships between suspension and paper coating film properties. (1). clay-water systems. Tappi J., 51 (11), 489-496.

Hruzewich, J. N. (1990). Annual Convention of the Gravure Association of America, New York.

Huang, T. and Lepoutre, P. (1996). Effect of Base-Stock Absorbency on Coating "Hold-Out" and Coated Paper Properties. 1996 Tappi Coating Conference Pro., Tappi Press, 167-176.

Hunter, R. S. (1936). Methods of determining gloss, Am. Soc. Test. Mater. Proc., 30 (Part II), 738-806.

Hunter, R. S. (1952). Bulletin No. 186. ASTM, Philadelphia.

Ishley, J. N., and Osterhuber, E. O. (1990). A new precipitated calcium carbonate pigment for high gloss coated papers. Tappi Coating Conference Proceeding, 237.

Iyer, R. R., and Bousfield, D. W. (1996). The leveling of coating defects with shear thinning rheology. J. Chem. Eng. Sci., 51, 4611.

Kappor, S. G., (1977). A stochastic approach to paper surface characterization and printability criteria. Ph. D. Thesis, University of Wisconsin, Madison.

Kartunnen, S., Kaotto, H., and Oittinen, P. (1971). New modification of ink transfer models. Adv. Printing Sci. and Technol., 11, 33.

Kelly, J. M., Russell, P. J., and Graham, F. H. (1971). Results of an investigation into ink setting behavior on coated papers. 14th Eucepa Conference in Budapest, 15.

Kent, H. J., Climpson, N. A., Coggon, L., Hooper, J. J., and Gane, P.A.C. (1986). Novel techniques for quantitative characterization of coating structure. Tappi J., 69 (5), J78-J83.

Keunings, R., and Bousfield, D. W. (1987). Analysis of surface tension driven leveling in viscoelastic films. J. Non-Newtonian Fluid Mech., 22, 219.

Kheshgi, H. S., and Scriven, L. E. (1988). The evolution of disturbances in horizontal films. J. Chem. Eng. Sci., 4, 793.

Larsson, L. O., and Busk, H. (1985). Must it be difficult to remove printing ink from waste newspapers? Wochenblatt für Papierfabrikation, 113, 573.

Lashof, T. W., and Mandel, J. (1960). Measurement of the smoothness of paper. Tappi J., 43 (5), 385.

Leach, R. H., Armstrong, C., Brown, J. F., Mac Kenzie, M. J., Randall, L., and Smith, H. G. (1988). The Printing Ink Manual. Blueprint Chapman and Hall, London.

Lee, D. I. (1974). A fundamental study on coating gloss. Tappi Coating Conference Proceeding, Tappi Press, 97-114.

Lee, D. I. (1982). Development of high-gloss paper coating latexes. Tappi Coating Conference Proceeding, Tappi Press, 125-135.

Lee, D. I., and Hendershot, R. E. (1986). Development of low glossing paper coating latexes: theories and concepts. Tappi Coating Conference Proceeding, 31.

Lee, S. J., and Hendershot, R. E. (1988). U.S. Patent 4,751,111.

Leekley, R. M., and Tyler, R. F. (1975). The measurement of optical unevenness. Tappi J. 58 (3), 124.

Lehtinen, E. (Ed.) (2000). Pigment coating and surface sizing of paper. Papermaking science and technology, Book 11, Finnish Paper Engineer's Association and TAPPI, Helsinki, Finland.

Lepoutre, P., and Rezanowich, A. (1977). Optical properties and structure of clay-latex coatings. Tappi J., 60 (11), 86-91.

Lepoutre, P. (1978). Liquid absorption and coating porosity. Paper Tech. Ind., 19 (9), 298-300.

Lepoutre, P., and De Grâce, J. H. (1978). Ink transfer characteristics and coating structure. Paper Tech. Ind., 19 (9), 301-304.

Lepoutre, P., De Grâce, J. H., and Mangin, P. J. (1979). Printability of coated papers. Tappi J., 62, 33.

Lepoutre, P., and Alince, B. (1981). Sintering of latex particles in pigmented coatings: I. Influence of the latex particle size. J. of Applied Polymer Sci., 26, 791-798.

Lepoutre, P., and Alince, B. (1982). A model for predicting the roughness of balde-coated papers. Svensk Papperstid., 85 (6), 51-56.

Lepoutre, P. (1989). The structure of paper coatings: an update. Progress in Organic Coatings, 17, 89.

Lindstrand, M. (1996). A conceptual approach to describe gloss variation in printing paper. M.S. Thesis, Linköping University, Sweden.

Lipshitz, H., Bridger, M., and Derman, G. (1990). On the relationship between topography and gloss. Proc. Polymers, Laminations & Coatings Conf., Tappi Press, Atlanta, GA, 12-22.

Lipshitz, H., Bridger, M., and Derman, G. (1990). Tappi 1990 Coating Conference Proceedings, Tappi Press, Atlanta, GA, 219.

Lohmander, S. (2000). Influence of shape and a shape factor of pigment particles on the packing ability in coating layers. Nordic Pulp & Paper Res. J. , 15 (4). 300-305.

MacGregor, M. A., and Johansson, P.-A. (1990). Submillimeter gloss variations in coated paper: Part I– The gloss imaging equipment and analytical techniques. Tappi J., 73 (12), 161-168.

MacGregor, M. A. and Johansson, P.-A. (1991). Submillimeter gloss variations in coated paper: Part II – Studying 'orange peel' gloss effects in a lightweight coated paper. Tappi J., 74 (1), 187-194.

Mangin, P.J., Lyne, M.B., Page, D.H., and De Grâce, J.H. (1981). Ink transfer equations: parameter estimation and interpretation. Adv. Printing Sci. and Technol., 16, 180.

Matsuda, N., Ichihashi, T., and Zama, Y. (2000). Influence of ultra fine surface profile to sheet and print gloss of coated paper. Tappi Coating Conf. & Trade Fair, 285-308.

McCabe, W.L., Smith, J. C., and Harriott, P. (1985). Unit Operations of Chemical Engineering, McGraw-Hill, New York, NY.

Miller, J. C., and Myers, R. R. (1958). A photographic study of liquid flow in a roll nip. Transactions of the Society of Rheology II, 77.

Moore, D. O., and Hunter, R. S. (1941). J. Am. Soc., 24, 167.

Murakami, K. (1973). Characteristics of the paper surface, particularly surface roughness (as measured) by the stylus method. Japan Tappi, 27 (2), 55-64.

Myers, R. R., Miller, J. C., and Zettlemoyer, A. C. (1959). The splitting of thin liquid films kinematics. J. Colloid Sci., 14, 287.

Nguyen, N., Jordan, B., and De Grâce, J. (1992). Measurements of ink splitting patterns by image analysis. International Printing Graphic Arts Conference Proceeding, 81.

Nieto-Vesperinas, M. (1991). Scattering and Diffraction in Physical Optics, Wiley, New York, NY.

Ogilvy, J. A. (1991). Theory of Wave Scattering from Random Rough Surfaces, IOP Publishing, Bristol, UK, 150.

Oittinen, P. (1980). Surface reflection of coated papers and prints. Adv. Print Sci., 15, 344-370.

Oittinen, P. (1983). The Limits of Gloss in Prints. Paperi Ja Puu, 11, 718-724.

Oittinen, P., Saarelma, H., and Tuovinen, P. (1990). Microscale gloss of papers and prints. Tappi Int'l Printing and Graphic Arts Conference Proc., Tappi Press, 147-151.

Oittinen, P. (1991). Relations between print gloss and print density. Graphic Arts in Finland, 20 (2), 3-7.

Oittinen, P., and Saarelma, H. (Eds.) (1998). Printing, Book 13, TAPPI Press, Helsinki, Finland.

Oldring, P.K.T. (Ed.) (1991). Chemistry and technology of UV and EB formulation for coatings, inks and paints, SITA Technology, London, UK.

Orchard, S. E. (1962). On surface leveling in viscous liquids and gels. Applied Science Research, 11, 451.

Parker, J. R. (1976). The fundamental properties of paper related to its uses, Cambridge Conference BPBIF, 2, 517.

Parker, J. R. (1981). Measurement of printing roughness. Tappi J., 38 (2), 90.

Parsons, C.L., and Abson, R. R. (1978). Predicting print gloss mottle. Tappi J., 61 (9), 81.

Paulsen, F., Pan, R., Bousfield, D. W., and Thompson, E. V. (1996). The dynamics of bubble / particle attachment and the application of two disjoining film rupture models to flotation. Part I: Non draining model. J. of Colloid and Interface Science, 178, 400.

Pesenti, F. (1996). M.S. Thesis, University of Maine.

Plowman, N. (1989). Printing systems. Ink Tack-Part I: How is it measured? Graphic Arts Monthly, 110.

Plowman, N. (1989). Printing systems. Ink Tack-Part II: Wet film thickness. Graphic Arts Monthly, 126.

Plowman, N. (1989). Printing systems. Ink Tack-Part III: Surface measurement. Graphic Arts Monthly, 114.

Plowman, N. (1989). Printing systems. Ink Tack-Part IV: Blanket release forces. Graphic Art Monthly, 133.

Plowman, N. (1992). Ink setting and ink drying. Graphic Arts Monthly, 162.

Porteus, J. O. (1963). Relation between the height distribution of a rough surface and the reflectance at normal incidence. J. Opt. Soc. Am., 53, 1394.

Poresizer 9320 Manual, Micomeritics, Norcross, GA.

Preston, J.S., Elton, N.J., Legrix, A., and Nutbeem, C. (2001). The role of pore density in the setting of offset printing ink on coated paper. Adv. Coating Fundamentals Symposium Proc., Tappi Press, 21-36.

Preston, J. S., Elton, N. J., Husband, J. C., Dalton, J., Heard, P.J., and Allen, G.C. (2002). Investigation into the distribution of ink components on printed coated paper. Part 1: optical and roughness considerations. Colloid and Surfaces A: Physicochem. Eng. Aspects, 3, 183-198.

Ranger, A. E. (1983). Coating pore structure analysis by fluid penetration and permeation. The Role of Fundamental Research Papermaking. BPBIF Symp., 2, 685.

Riley, R. R., Vincent, E. M., and Lee, D. M. (1993). Fundamental of styrene butadiene latices. Technical Research Report, 502.01, Gencorp.

Roehr, W. W. (1955). Effect of smoothness and compressibility on the printing quality of coated paper, Tappi J., 38 (11), 660-664.

Romano, R.M., and Romano, F. J. (1998). The GATF encyclopedia of graphic communications. GATF, Prentice Hall, NJ.

Sennett, P., Drexel, R. J. Jr., and Morris, H. H. (1967). The effect of pigment particle shape on the surface profile of light weight coated sheets. Proc. 1967 Coat. Conf., Tappi Press, 2-34.

Settlemeyer, L. A. (1992). Topography of gloss detailed with the scanning electron microscope. Proc. of the 44th annual TAGA conference, TAGA, 264-281.

Shiratori, N., Ishimura, H., Yoshidomi, N., Taniquchi, M., and Nakahara, Y. (1993). Study on quantitative evaluation of submillimeter gloss variations in coated papers. Proc. Advanced Coating Fundamentals, Tappi Press, 59-70.

Singh, S. P., Rao, N. J., and Bristow, J. A. (1991). Smoothness Characterization of Printing Papers, IPPTA Convention Issue, 1-13.

Sjodahl, L. H. (1951). Ink flow on rotating rollers. Am. Ink Maker, 3, 31.

Stefan, J. (1874). Sitzber, Akad Wiss. Wien. Math. Naturw. Kl. Abt. II 69, 713.

Stout, K. J. (1981). Surface roughness-measurement, interpretation and significance of data: Part I-Statistical parameters. Materials in Engg. Vol. 2, 260.

Stout, K. J. (1981). Surface roughness-measurement, interpretation and significance of data: Part II -Experimental consideration and significance of data. Materials in Engg. Vol. 2, 287.

Stover, J.C. (1990). Optical Scattering –Measurement and Analysis. Society of Photo-optical Instrumentation Engineers, McGraw-Hill, New York, NY.

Ström, G., Gustafsson, J., and Sjölin, K. (1999). Absorption of ink oils into coatings after Prüfbau printing. International Symposium on Paper Coating Coverage Proceeding. Session 3, 1-11.

Suzuki, H., Hirabayashi, T., and Fukui, T. (1996). Effect of surface property of coated paper on print gloss. Japan Tappi Pulp and Paper Research Conference Proceeding, 82-87.

Tappi Tests Method Specular gloss of paper and paperboard at 20 degrees (1990). T 653 pm-90, Tappi Test Methods, Tappi Press, Atlanta, GA.

Tappi Tests Method Specular gloss of paper and paperboard at 75 degrees (1985). Tappi Test Methods, Tappi Press, Atlanta, GA.

Thomson, I. G., and Young, F. R. (1975). High-speed photographic studies of ink filamentation. J. Oil Col. Chem. Assoc., 58, 389.

Toivakka, M., Salminen, P., Chonde, Y., and Bousfield, D. W. (1997). Consolidation of particulate suspension – Model study with plastic pigments. Tappi Coating Fundamentals Symposium Proceeding, 1.

User's Manual, Tencor Instruments, PO Box 3308, NH 03802, U.S.A.

Van Gilder, R. L., and Purfeest, R. D. (1994). Latex binder modification to reduce coating pick on six-color offset presses. Tappi J., 77, 230.

Van Gilder, R. L., and Purfeest, R. D. (1994). Commercial six-color press runnability and the rate of ink tack build as related to the latex polymer solubility parameter. Tappi Coating Conference Proceeding, 229.

Voet, A., and Geffken, C. F. (1951). The nature of tack. Ind. Eng. Chem., 7, 1614.

Wagberg, P., and Johansson, P-A. (1993). Surface profilometry - comparison between optical and mechanical sensing on printing papers. Tappi J., 76 (12), 115-121.

Wakebe, H., Hara, H., and Oye, R. (1986). Microtopography of paper surface. (1). stereoscopic observation of paper surface. Japan Tappi J., 40 (1), 79.

Walker, W. C., and Fetsko, J. M. (1955). A concept of ink transfer in printing. Am. Ink Maker, 33 (12), 38.

Washburn, E. W. (1921). The dynamics of capillary flow. Phys. Rev., 17, 273.

Watanabe, J., and Lepoutre, P. (1982). A mechanism for the consolidation of the structure of clay-latex coatings. J. Appl. Poly. Sci., 27, J4207-J4219.

Weber, R. W. (1960). The effect of pigment binders on paper gloss, printed gloss and oil absorption. Tappi J., 43, 833.

Williams, C. H. (1971). The problem of combining high finish and fast setting in lithographic inks. PARA/IARGAI International Conference on Applied Lithographic Technol., Res. Assoc. for the Paper and Board Printing and Packaging Ind.

Wygant, R. W., Pruett, R. J., and Chen, C. Y. (1995). A review of techniques for characterizing paper coating surfaces, structures and printability. Coating Fundamentals Symposium Proceedings, Tappi Press, Atlanta, GA, 1-14.

Xiang, Y., and Bousfield, D. W. (1998). The influence of coating structure on ink tack development, International Printing and Graphic Arts Conference, 93-101.

Xiang, Y., Bousfield, D.W., Hassler, J., Coleman, P., and Osgood, A. (1999). Measurement of local variation of ink tack dynamics. J. Pulp Paper Sci., 25 (9), 326-330.

Yamazaki, H. (1991). A modified method for the determination of the ink transfer parameters by non-linear optimization, Japan Tappi, 45 (7), 77.

Zang, Y. H., Aspler, M. Y., and De Grâce, J. H. (1991). Direct measurement of tensile stress in thin ink films. J. Rheol., 35, 345.

Zang, Y. H. (1992). Asymmetric splitting and ink transfer: a new ink transfer model. International Printing and Graphic Arts Conference Proceeding, 103.

Zang, Y. H. (1993). New approach for modeling ink transfer. Tappi J., 76 (7), 97.

Zang, Y. H. and Aspler, J. S. (1994). The influence of coating structure on the ink receptivity and print gloss development of model clay coatings. International Printing and Graphic Arts Conference Proceeding, 193.

Zang, Y. H., and Aspler, J. S. (1998). The effect of surface binder content on print density and ink receptivity of coated paper. J. Pulp and Paper Science, 24 (5), 141-145.

Zettlemoyer, A. C., and Myers, R. R. (1960). The Rheology of Printing inks in Rheology Theory and Applications. F.R. Eirich Ed., Academic Press, New York, NY.

APPENDIX A: SUMMARY OF PREPARED SAMPLES IN FULL-SCALE AND THEIR PRINT GLOSS.

SAMPLE CODE	Paper Gloss Measuring angles			Roughness Ra	Print 60° Gloss Ink on sample (g/m²)				Print 75° Gloss Ink on sample (g/m²)			
	60°	75°	85°	(nm)	1.5	2.0	2.5	3.0	1.5	2.0	2.5	3.0
G1B06R1	51.3	75.6	84.9	20.4	40.2	43.5	44.2	41.7	77.9	79.1	79.2	77.2
G1B06R2	42.3	73.3	83.5	78.6	33.3	36.4	39.3	39.4	72.7	75.0	77.3	77.5
G1B06R3	25.8	60.2	77.3	110.4	28.0	28.5	30.3	32.5	67.0	66.7	69.1	71.3
G1B06R4	18.9	55.3	76.9	109.2	26.8	28.0	30.0	31.6	67.2	68.2	69.4	70.7
G1B06R5	5.2	21.5	44.5	307.0	11.5	13.5	15.1	16.9	41.6	47.4	50.3	52.3
G1B10R1	58.0	80.7	88.8	21.3	54.8	56.6	57.8	58.4	84.8	86.4	87.4	87.8
G1B10R2	46.6	76.4	85.3	70.6	45.9	49.8	51.9	52.1	81.3	83.5	84.9	85.4
G1B10R3	34.3	68.7	80.8	106.9	37.2	39.2	41.0	42.0	75.9	78.0	79.1	79.1
G1B10R4	24.5	62.4	80.0	130.1	36.3	39.7	42.0	43.0	76.0	78.6	80.5	81.6
G1B10R5	6.2	22.6	44.8	284.7	14.8	17.6	19.4	20.2	49.8	56.3	60.1	61.4
G1B15R1	65.8	85.9	90.4	15.8	69.7	71.3	72.3	72.9	90.4	91.4	92.1	92.5
G1B15R2	52.5	80.8	85.5	59.2	57.9	60.3	62.0	62.5	86.3	88.1	89.4	89.4
G1B15R3	45.2	78.0	83.0	75.3	57.5	59.9	61.9	63.0	87.6	88.5	89.6	90.7
G1B15R4	25.7	63.2	77.3	131.3	41.8	44.5	46.9	49.0	78.5	80.9	83.0	84.7
G1B15R5	5.1	20.9	42.1	302.7	15.4	16.9	18.5	20.3	53.5	56.4	59.4	62.4
G1B20R1	66.6	86.3	90.7	14.4	75.4	76.9	76.1	75.3	92.1	91.7	92.3	92.2
G1B20R2	50.8	79.5	84.7	69.2	63.6	65.9	66.7	67.0	87.8	89.5	89.7	89.6
G1B20R3	38.9	73.1	79.9	104.3	57.5	57.3	57.3	58.0	85.6	86.3	86.8	87.0
G1B20R4	25.4	63.4	78.9	123.9	44.6	45.8	48.3	52.0	80.4	81.0	83.0	85.2
G1B20R5	4.1	15.9	39.0	345.1	15.8	18.0	20.2	22.3	55.2	58.8	62.2	65.4
G2B06R1	22.8	59.4	78.6	87.4	57.4	62.3	65.5	66.8	85.5	88.7	90.1	89.9
G2B06R2	19.3	57.2	75.6	124.0	51.5	56.4	60.1	60.9	82.2	86.2	88.5	89.1
G2B06R3	20.8	58.8	75.8									
G2B06R4	11.1	47.0	70.4	129.9	40.1	44.3	48.5	52.0	78.4	81.9	84.5	86.2
G2B06R5	3.5	15.1	39.0	321.3	12.0	13.9	16.2	19.1	48.8	51.9	56.2	61.5
G2B10R1	21.2	59.2	78.4	83.1	66.9	68.7	70.7	72.7	89.1	89.8	90.5	91.2
G2B10R2	17.5	56.5	75.0	103.2	58.1	61.2	64.0	66.5	85.8	87.3	88.7	90.0
G2B10R3	19.8	58.7	76.0									
G2B10R4	10.5	46.6	70.5	157.5	47.1	50.9	54.3	57.3	82.1	84.5	86.4	87.7
G2B10R5	3.9	17.2	41.3	306.4	17.3	19.4	21.5	23.9	58.1	61.6	65.0	68.3
G2B15R1	12.4	50.8	75.1									
G2B15R2	15.4	54.8	74.8	108.9	58.5	61.8	65.9	68.9	84.7	87.1	88.8	89.8
G2B15R3	10.7	48.4	72.7	114.6	58.8	61.0	62.8	65.7	84.8	85.9	87.8	90.6
G2B15R4	8.1	42.0	68.2	152.5	46.0	51.2	56.2	58.8	79.2	83.6	86.2	86.8
G2B15R5	3.4	15.1	39.7	318.8	20.0	22.9	28.3	35.5	61.5	65.5	69.4	73.2
G2B20R1	4.3	26.2	59.1	175.5	39.9	47.5	53.0	62.6	80.7	83.4	87.1	91.7
G2B20R2	3.9	27.2	57.1									
G2B20R3	4.2	26.4	58.5									
G2B20R4	3.8	25.0	55.5									
G2B20R5	3.4	15.6	38.8	302.3	26.2	33.2	41.3	50.4	69.2	75.5	81.3	86.7

(Continued)

SAMPLE CODE	Paper Gloss Measuring angles			Roughness Ra	Print 60° Gloss Ink on sample (g/m^2)				Print 75° Gloss Ink on sample (g/m^2)			
	60°	75°	85°	(nm)	1.5	2.0	2.5	3.0	1.5	2.0	2.5	3.0
P1B10R1	*36.7*	*65.1*	*82.4*	*72.5*	*59.7*	*66.5*	*67.0*	*66.9*	*87.1*	*88.2*	*88.9*	*89.4*
P1B10R2	*31.6*	*65.9*	*80.7*	*67.6*	*59.2*	*60.4*	*62.7*	*65.2*	*87.8*	*86.7*	*88.4*	*90.7*
P1B10R3	*31.8*	*66.5*	*80.6*									
P1B10R4	*16.4*	*53.3*	*75.7*	*108.7*	*47.5*	*50.2*	*53.5*	*57.6*	*83.9*	*84.3*	*85.7*	*87.8*
P1B10R5	*4.5*	*20.4*	*44.0*	*295.2*	*18.1*	*20.5*	*22.2*	*23.4*	*58.7*	*63.1*	*65.6*	*66.2*
P1B15R1	*39.5*	*69.7*	*85.0*	*25.0*	*70.4*	*71.8*	*73.1*	*74.3*	*90.1*	*89.8*	*89.8*	*90.1*
P1B15R2	*35.3*	*69.2*	*81.9*									
P1B15R3	*34.6*	*69.7*	*80.8*									
P1B15R4	*19.4*	*57.2*	*77.1*	*103.0*	*52.8*	*54.8*	*56.9*	*59.2*	*83.6*	*85.4*	*86.5*	*86.7*
P1B15R5	*4.0*	*15.8*	*38.7*	*342.4*	*11.6*	*12.8*	*13.9*	*15.2*	*41.6*	*44.6*	*47.8*	*50.9*
P1B20R1	*41.8*	*71.8*	*85.5*	*41.0*	*74.0*	*75.8*	*76.7*	*76.9*	*89.8*	*91.0*	*91.7*	*92.0*
P1B20R2	*35.6*	*70.2*	*82.3*	*73.8*	*67.7*	*70.1*	*71.6*	*72.2*	*89.0*	*89.9*	*90.8*	*91.5*
P1B20R3	*29.3*	*67.0*	*79.5*									
P1B20R4	*20.1*	*58.9*	*77.1*	*102.8*	*55.9*	*58.3*	*60.3*	*61.9*	*85.6*	*86.8*	*87.8*	*88.7*
P1B20R5	*4.4*	*16.7*	*39.8*	*296.4*	*10.7*	*12.5*	*14.6*	*17.2*	*37.7*	*44.9*	*51.0*	*56.1*
P1B30R1	*43.6*	*73.9*	*86.6*	*42.0*	*78.2*	*77.3*	*77.4*	*78.6*	*92.9*	*92.4*	*92.6*	*93.7*
P1B30R2	*33.2*	*69.0*	*80.7*	*57.8*	*67.0*	*71.4*	*73.8*	*73.4*	*87.3*	*90.9*	*92.5*	*92.1*
P1B30R3	*26.3*	*64.4*	*78.2*	*124.1*	*62.4*	*64.7*	*66.6*	*67.1*	*87.3*	*89.3*	*90.5*	*91.0*
P1B30R4	*19.1*	*57.6*	*75.4*	*135.9*	*57.1*	*61.7*	*64.7*	*66.1*	*86.8*	*89.1*	*90.5*	*90.9*
P1B30R5	*3.5*	*15.4*	*40.5*	*332.8*	*19.3*	*25.9*	*29.6*	*30.3*	*60.0*	*70.1*	*74.5*	*73.2*
P1B40R1	*23.0*	*61.0*	*80.0*	*106.0*	*73.9*	*74.7*	*75.3*	*75.9*	*91.5*	*91.4*	*91.6*	*92.2*
P1B40R2	*19.2*	*57.9*	*77.5*									
P1B40R3	*21.7*	*60.2*	*77.9*									
P1B40R4	*12.0*	*49.9*	*73.2*	*107.9*	*61.7*	*64.8*	*66.0*	*67.0*	*89.0*	*90.0*	*90.7*	*91.0*
P1B40R5	*4.8*	*25.3*	*50.7*	*232.6*	*34.3*	*44.0*	*47.8*	*48.2*	*76.6*	*82.2*	*83.5*	*83.8*
P2B10R1	*50.2*	*77.7*	*89.0*	*15.8*	*74.1*	*76.3*	*77.9*	*77.8*	*91.3*	*92.7*	*93.6*	*92.7*
P2B10R2	*36.7*	*72.0*	*81.8*	*99.3*	*64.7*	*66.5*	*68.8*	*71.7*	*89.1*	*90.2*	*90.7*	*90.7*
P2B10R3	*29.5*	*66.7*	*79.3*	*108.0*	*55.5*	*59.0*	*61.9*	*64.5*	*85.2*	*87.5*	*89.2*	*90.4*
P2B10R4	*18.8*	*56.7*	*74.9*	*148.3*	*48.8*	*53.1*	*56.7*	*59.6*	*80.5*	*85.9*	*87.1*	*88.3*
P2B10R5	*3.5*	*10.3*	*38.6*	*431.2*	*8.9*	*10.3*	*11.6*	*13.0*	*33.0*	*37.7*	*41.6*	*44.7*
P2B20R1	*34.2*	*69.1*	*85.1*	*34.0*	*75.3*	*74.8*	*75.4*	*77.1*	*90.7*	*90.2*	*90.4*	*91.2*
P2B20R2	*27.5*	*65.2*	*80.3*	*85.2*	*69.3*	*68.0*	*68.0*	*71.2*	*90.1*	*88.2*	*88.2*	*90.2*
P2B20R3	*29.4*	*67.8*	*80.2*									
P2B20R4	*16.3*	*54.8*	*76.0*	*126.4*	*53.2*	*56.7*	*60.2*	*63.8*	*83.5*	*84.9*	*86.6*	*88.4*
P2B20R5	*3.4*	*12.5*	*39.3*	*358.9*	*14.3*	*16.3*	*18.7*	*21.4*	*51.2*	*55.9*	*60.1*	*63.8*
P2B30R1	*25.0*	*63.1*	*83.6*	*48.0*	*72.9*	*73.6*	*75.0*	*77.3*	*90.8*	*91.7*	*92.6*	*93.6*
P2B30R2	*24.4*	*63.5*	*80.2*									
P2B30R3	*21.4*	*60.5*	*81.1*									
P2B30R4	*13.9*	*52.8*	*76.6*	*114.6*	*58.5*	*63.9*	*66.8*	*67.3*	*86.9*	*89.8*	*91.2*	*90.9*
P2B30R5	*5.5*	*27.1*	*54.0*	*223.0*	*33.7*	*39.6*	*41.7*	*40.2*	*75.6*	*80.8*	*82.3*	*80.1*

(Continued)

SAMPLE CODE	Paper Gloss Measuring angles			Roughness Ra	Print 60° Gloss Ink on sample (g/m^2)				Print 75° Gloss Ink on sample (g/m^2)			
	60°	75°	85°	(nm)	1.5	2.0	2.5	3.0	1.5	2.0	2.5	3.0
P3B10R1	*13.0*	*49.4*	*76.3*	*98.7*	*68.5*	*73.3*	*75.0*	*75.0*	*90.9*	*93.8*	*94.8*	*93.8*
P3B10R2	*14.2*	*49.1*	*76.2*									
P3B10R3	*13.0*	*48.0*	*74.7*									
P3B10R4	*9.4*	*43.0*	*71.6*	*113.7*	*58.0*	*69.3*	*72.9*	*73.7*	*85.8*	*92.6*	*93.7*	*95.3*
P3B10R5	*3.8*	*20.4*	*48.2*	*273.3*	*34.8*	*50.3*	*58.1*	*62.0*	*76.7*	*86.0*	*89.0*	*91.4*
P3B20R1	*6.1*	*36.3*	*71.1*	*119.6*	*50.6*	*58.1*	*63.0*	*68.4*	*84.8*	*88.0*	*90.1*	*92.6*
P3B20R2	*6.7*	*38.5*	*69.8*									
P3B20R3	*9.1*	*45.2*	*72.7*									
P3B20R4	*8.0*	*42.0*	*69.3*	*137.9*	*51.6*	*59.6*	*65.0*	*69.5*	*84.4*	*88.0*	*90.9*	*93.3*
P3B20R5	*3.4*	*15.7*	*43.1*	*268.4*	*27.2*	*41.0*	*49.5*	*55.0*	*68.5*	*79.7*	*84.5*	*89.0*
P3B30R1	*2.5*	*12.7*	*48.5*									
P3B30R2	*2.6*	*14.7*	*50.5*	*211.5*	*24.5*	*29.5*	*33.9*	*37.5*	*68.8*	*74.2*	*78.8*	*82.5*
P3B30R3	*2.5*	*13.3*	*47.2*									
P3B30R4	*2.5*	*12.9*	*46.3*	*268.8*	*23.0*	*26.1*	*27.2*	*31.0*	*66.3*	*69.0*	*71.7*	*75.5*
P3B30R5	*2.5*	*11.8*	*39.8*									
PE1				*10.5*	*72.0*	*73.3*	*81.7*	*81.7*	*91.4*	*92.9*	*95.3*	*95.0*
PE2	*86.2*	*97.9*	*79.9*	*99.6*	*69.3*	*76.2*	*81.8*	*84.7*	*91.6*	*94.3*	*96.3*	*97.2*
PE3	*79.5*	*92.4*	*0.0*	*118.7*	*70.1*	*73.9*	*77.3*	*80.8*	*91.4*	*92.9*	*94.3*	*95.5*
PE4	*62.7*	*83.6*	*69.5*	*159.2*	*65.4*	*73.1*	*79.2*	*83.3*	*89.6*	*92.6*	*94.7*	*96.3*
PE5	*36.0*	*62.6*	*51.9*	*236.0*	*62.7*	*73.3*	*80.0*	*80.4*	*88.4*	*93.2*	*95.7*	*95.4*
PE6	*16.5*	*37.9*	*13.5*	*445.3*	*30.8*	*36.4*	*40.7*	*44.7*	*67.0*	*73.5*	*76.5*	*79.2*
PE7	*2.9*	*4.3*	*7.0*	*825.1*	*12.6*	*19.8*	*28.1*	*36.0*	*38.2*	*52.2*	*63.2*	*69.0*
PE8	*2.7*	*4.7*	*7.0*	*853.5*	*17.1*	*23.4*	*32.0*	*43.0*	*43.6*	*53.6*	*66.1*	*77.2*

APPENDIX B: EXPERIMENTAL REGRESSIONS EQUATION BETWEEN ROUGHNESS Ra AND GLOSS.

For 75° gloss;

$Y_{75} = 104.69*(ATAN((x-127.82)/(-96.18))+1.5708)/\pi$

$r^2=0.9349$

Fit Std. Err. =6.42281

For 60° gloss;

$Y_{60} = (-0.2018)+71.8478*(ATAN((x-75.4257)/(-44.7777))+1.5708)/\pi$

$r^2=0.8684$

Fit Std. Err.=6.3386

APPENDIX C: SEM IMAGES OF PREPARED SAMPLES.

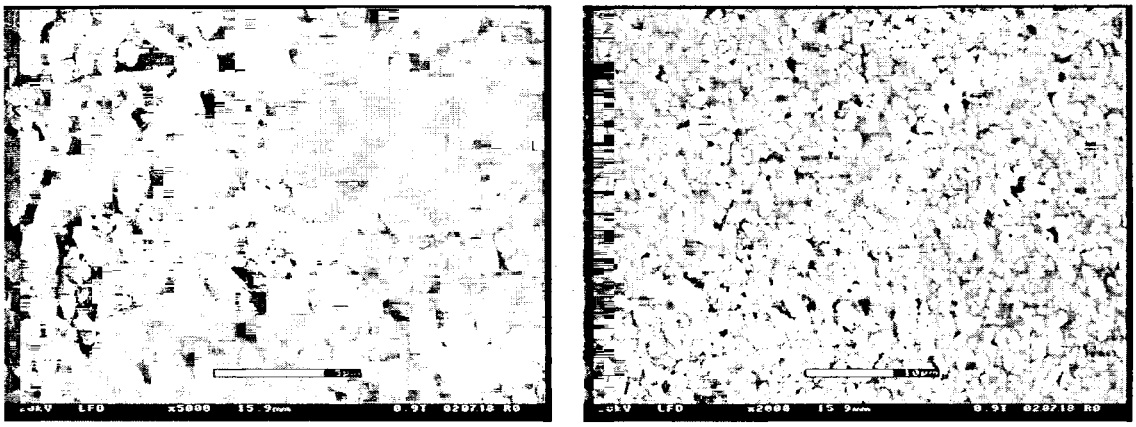

P3B10R1 (gloss: 50 at 75°, Pore size: 153 nm, Porosity: 20.8 %)

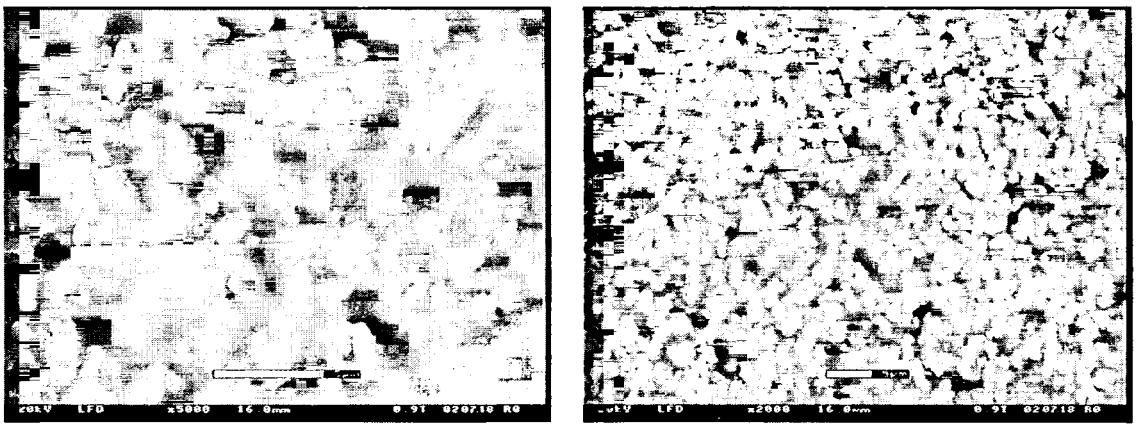

P3B20R1 (gloss: 35.4 at 75°, Pore size: 143 nm, Porosity: 18 %)

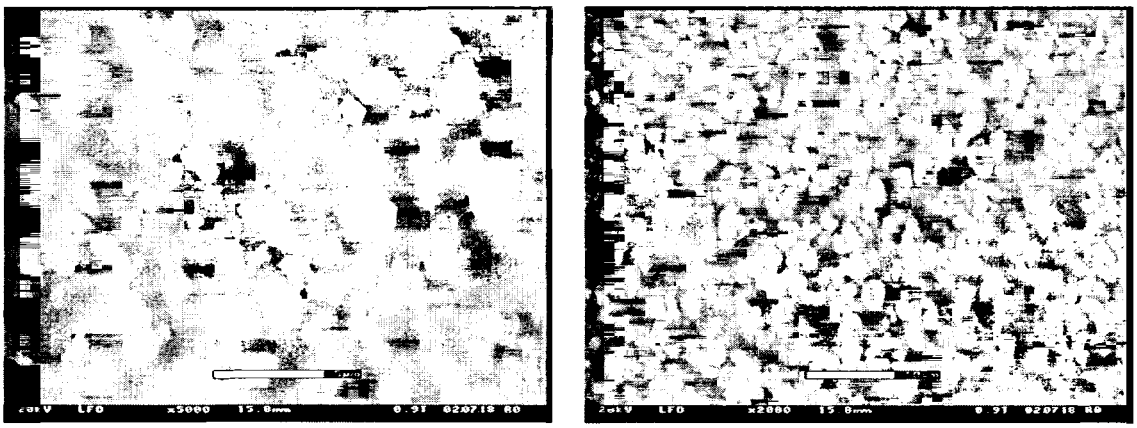

P3B30R2 (gloss: 13 at 75°, Pore size: 136 nm, Porosity: 13 %)

Figure C.1: SEM images of P3 series samples. Magnification: 5K for left, 2K for right.

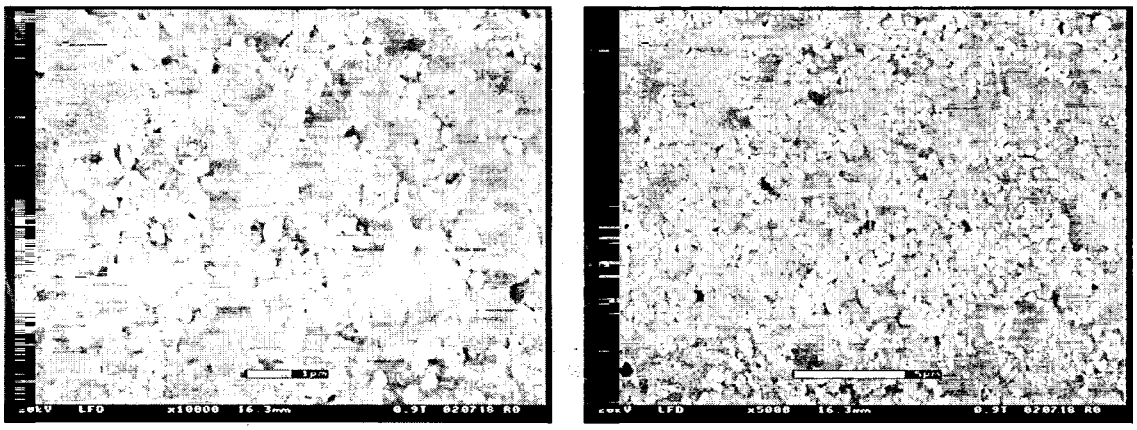

P2B10R1 (Roughness 78 at 75°, pore size: 86 nm, Porosity: 31.6 %)

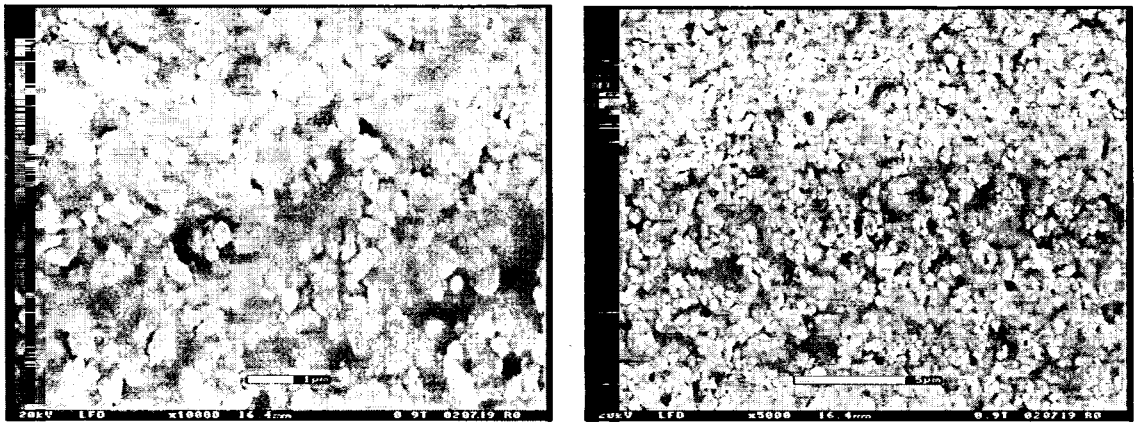

P2B20R1 (Roughness 70.8 at 75°, Pore size: 86 nm, Porosity: 26.8 %)

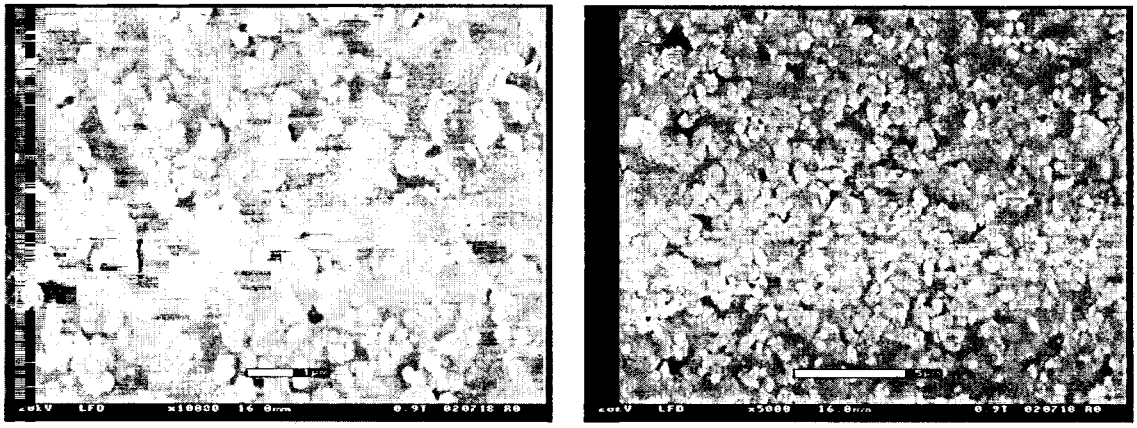

P2B30R1 (Roughness 62.4 at 75°, Pore size: 91 nm, Porosity: 22.8 %)

Figure C.2: SEM images of P2 series samples. Magnification: 10K (right) and 5K (left).

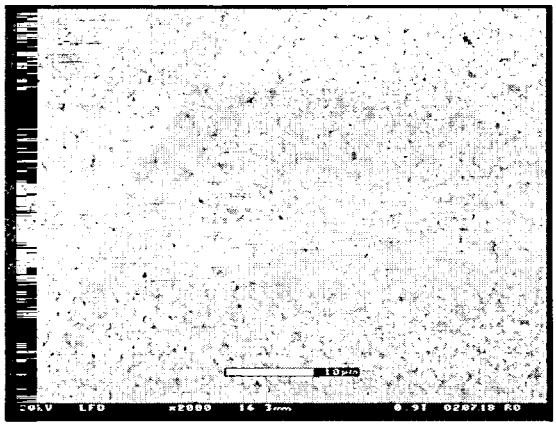

P2B10R1 (78)

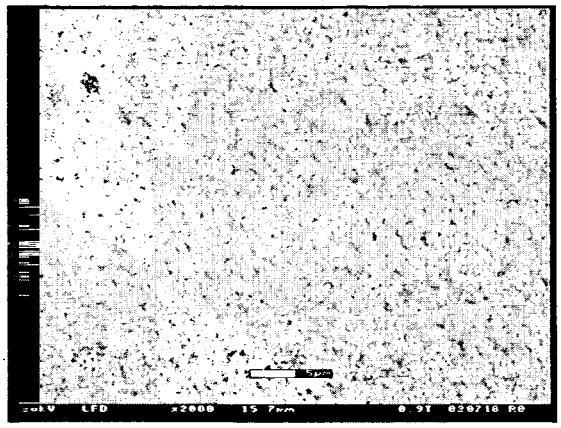

P2B10R2 (71)

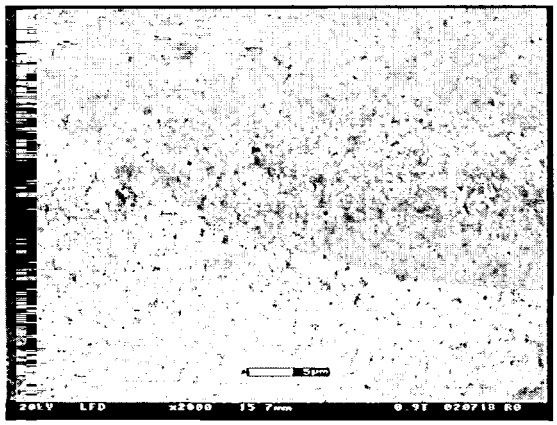

P2B10R3 (66.7)

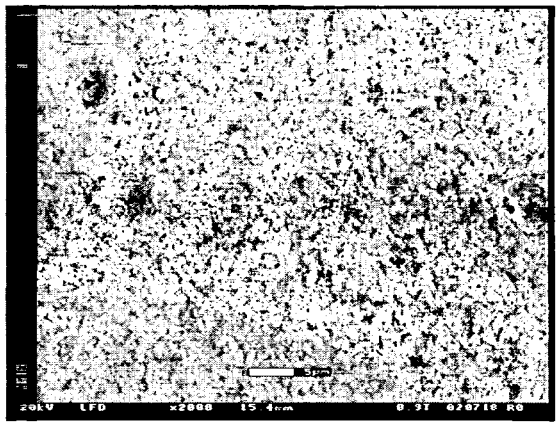

P2B10R4 (56.7)

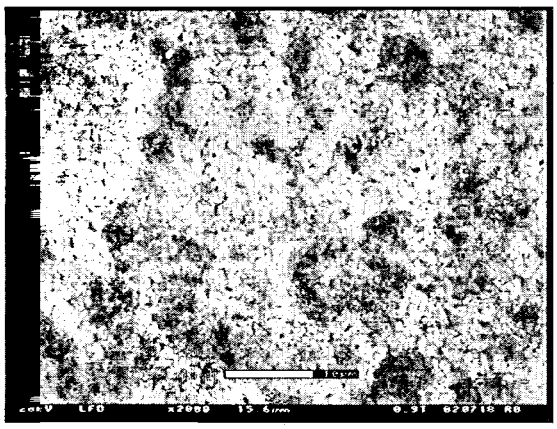

P2B10R5 (10.7)

Figure C.3: SEM images of P2B10 series (75° gloss). Magnification: 2K for all.

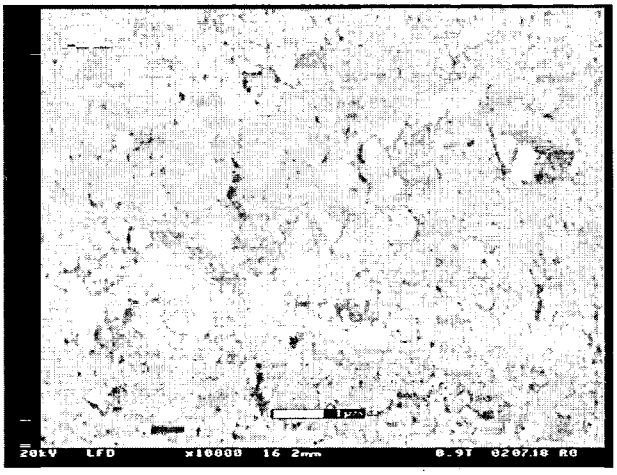

G1B06R1 (gloss: 77 at 75°, pore size: 38 nm, porosity: 31.5%)

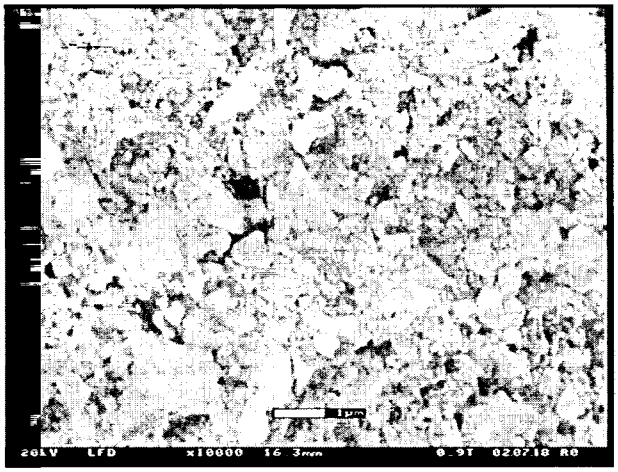

G2B06R1 (gloss: 58 at 75°, pore size: 76~80 nm, porosity: 24.2%)

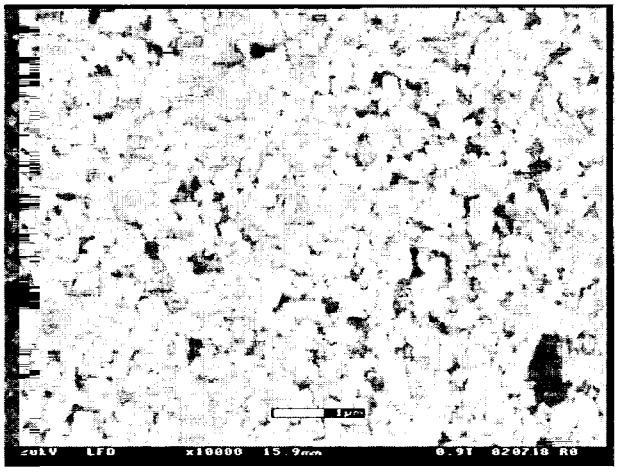

P1B10R1 (gloss: 67 at 75°, pore size: 75 nm, porosity: 29 %)

Figure C.4: SEM images of various pigment series. Magnification: 10K for all.

APPENDIX D: PRINT GLOSS AT 75° AND 60° AS A FUNCTION OF ROUGHNESS OR GLOSS AT VARIOUS INKING LEVELS.

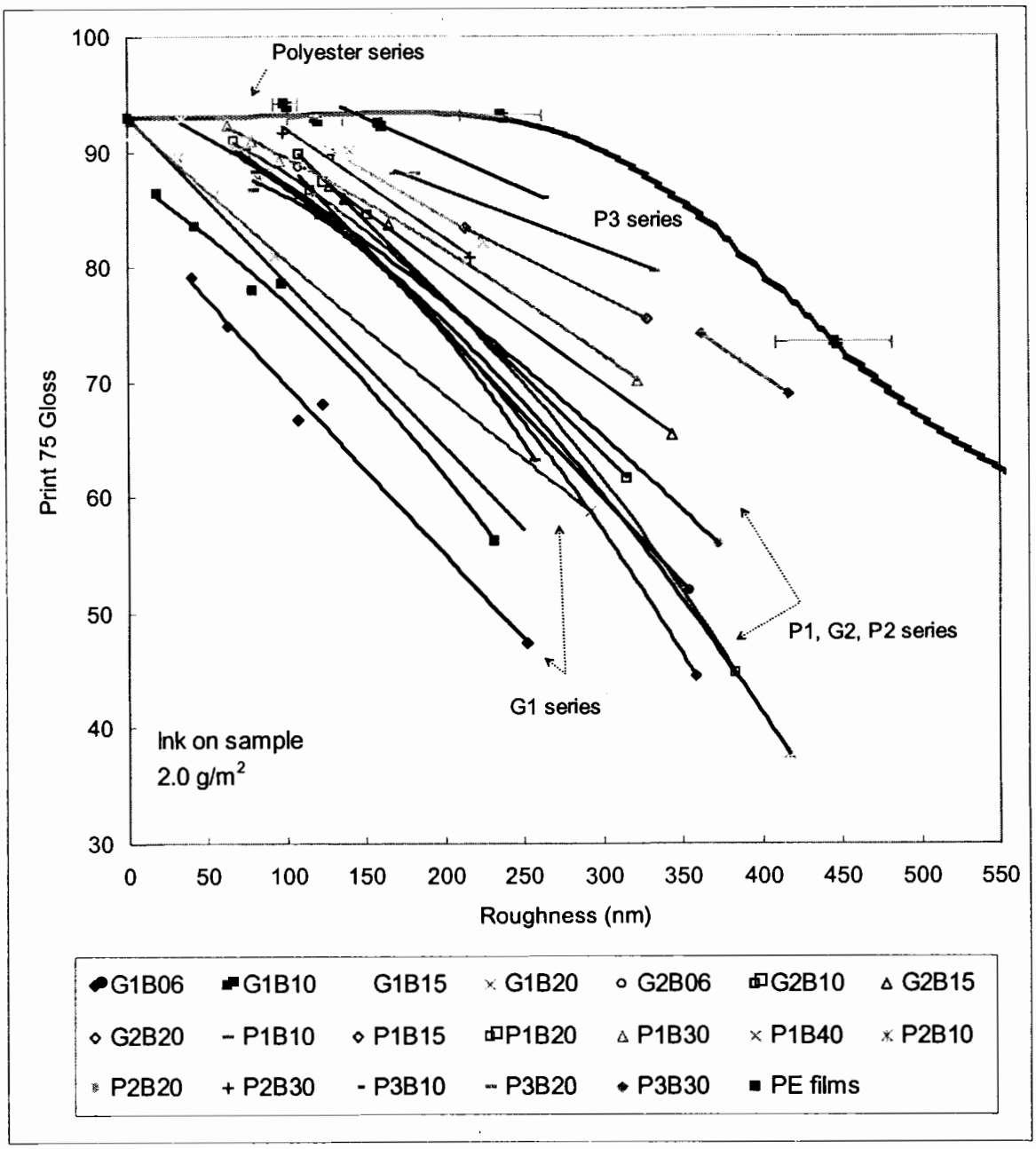

Figure D.1: Print 75° gloss as a function of converted roughness at 2.0g/m^2 ink.

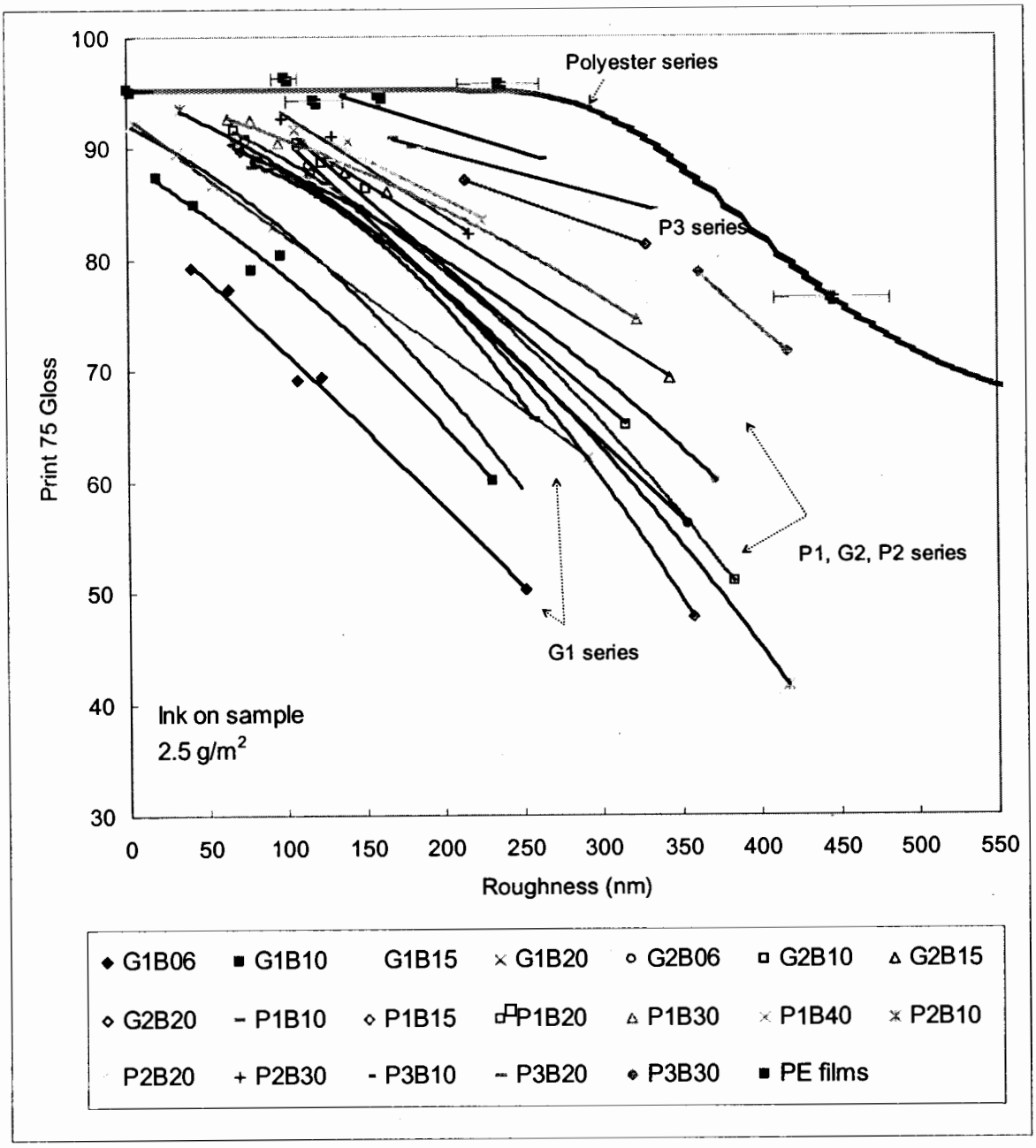

Figure D.2: Print 75° gloss as a function of converted roughness at 2.5g/m^2 ink.

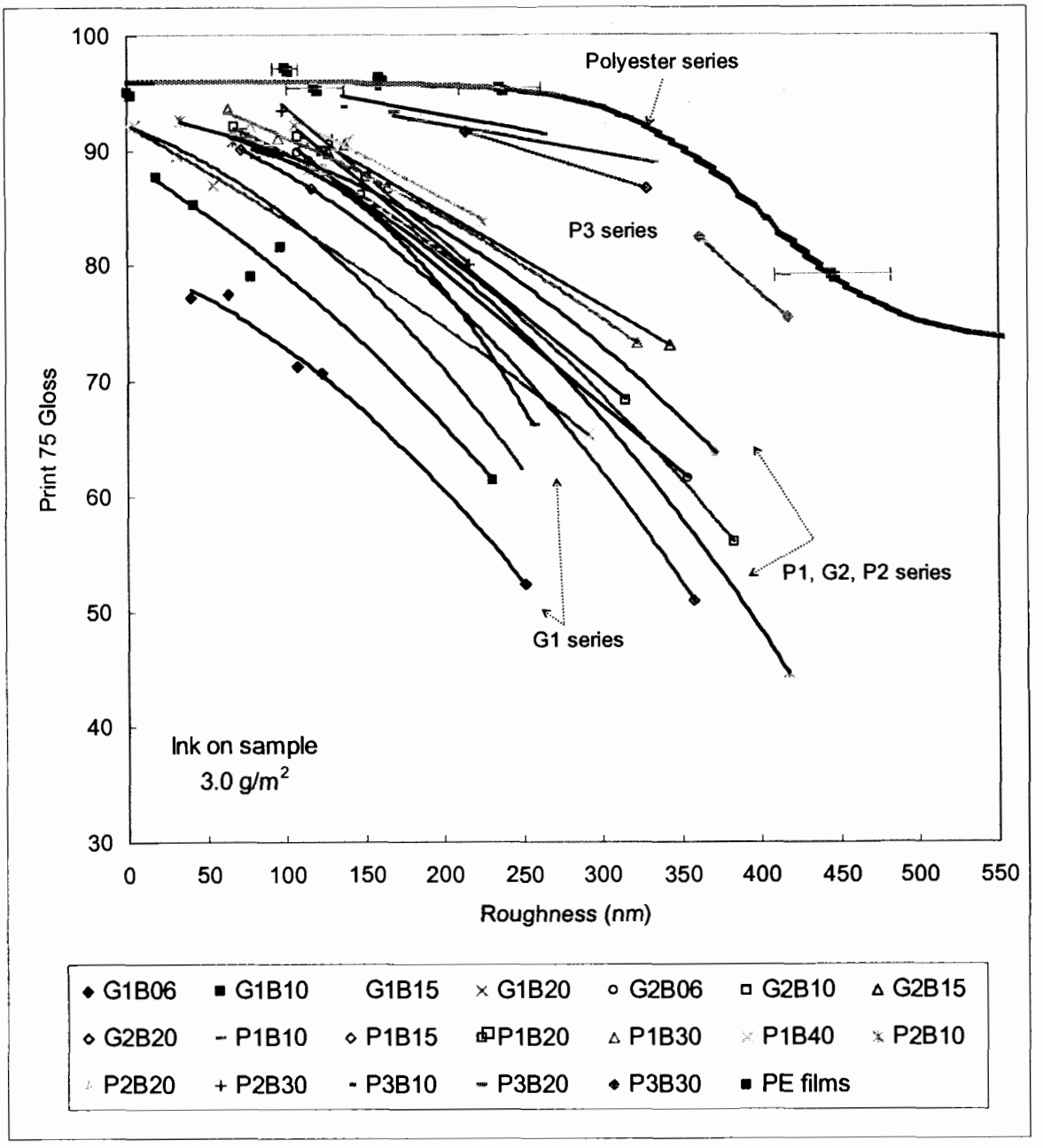

Figure D.3: Print 75° gloss as a function of converted roughness at 3.0g/m^2 ink.

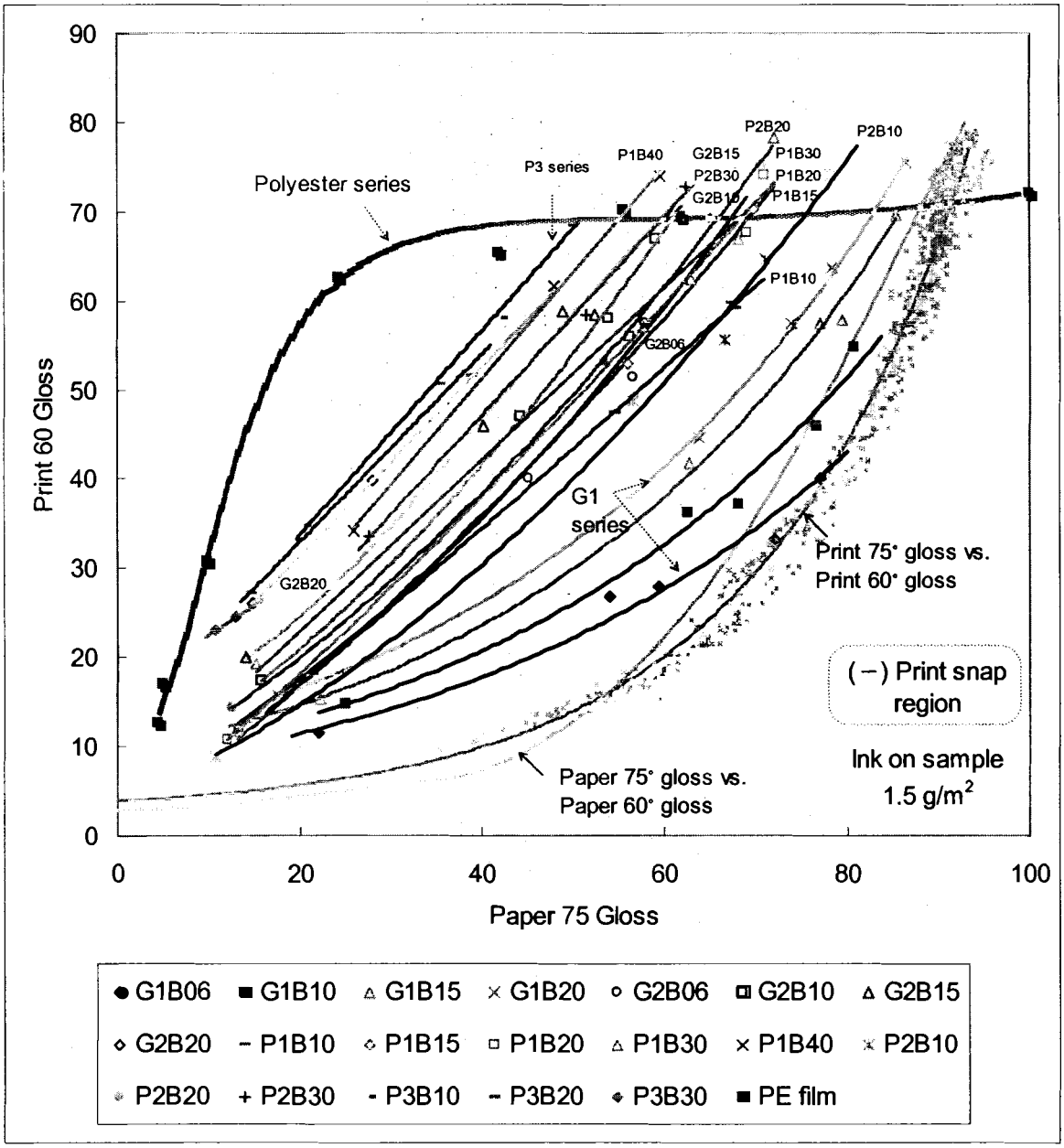

Figure D.4: Print 60° gloss as a function of converted roughness at 1.5g/m^2 ink.

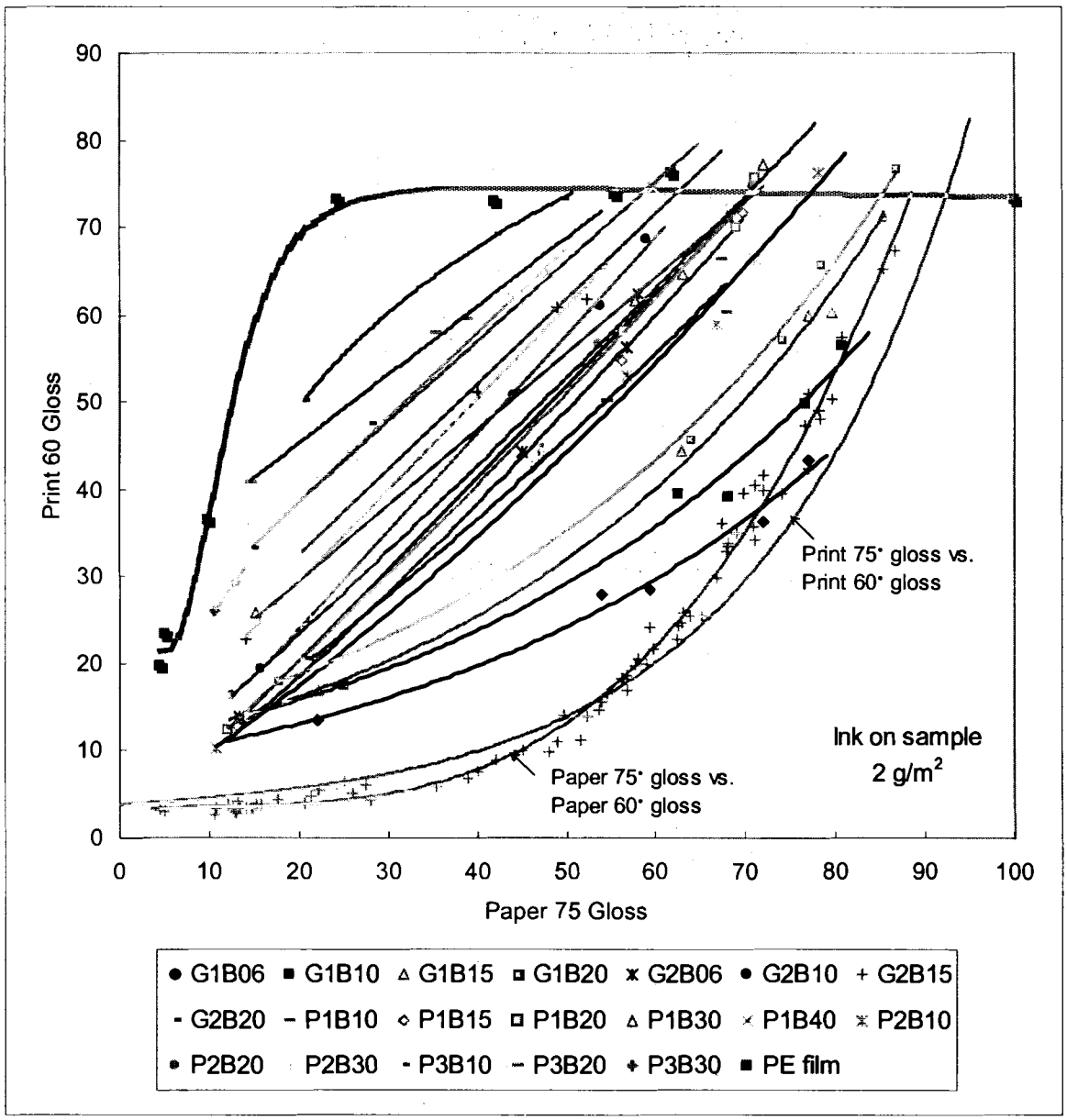

Figure D.5: Print 60° gloss as a function of converted roughness at 2.0g/m^2 ink.

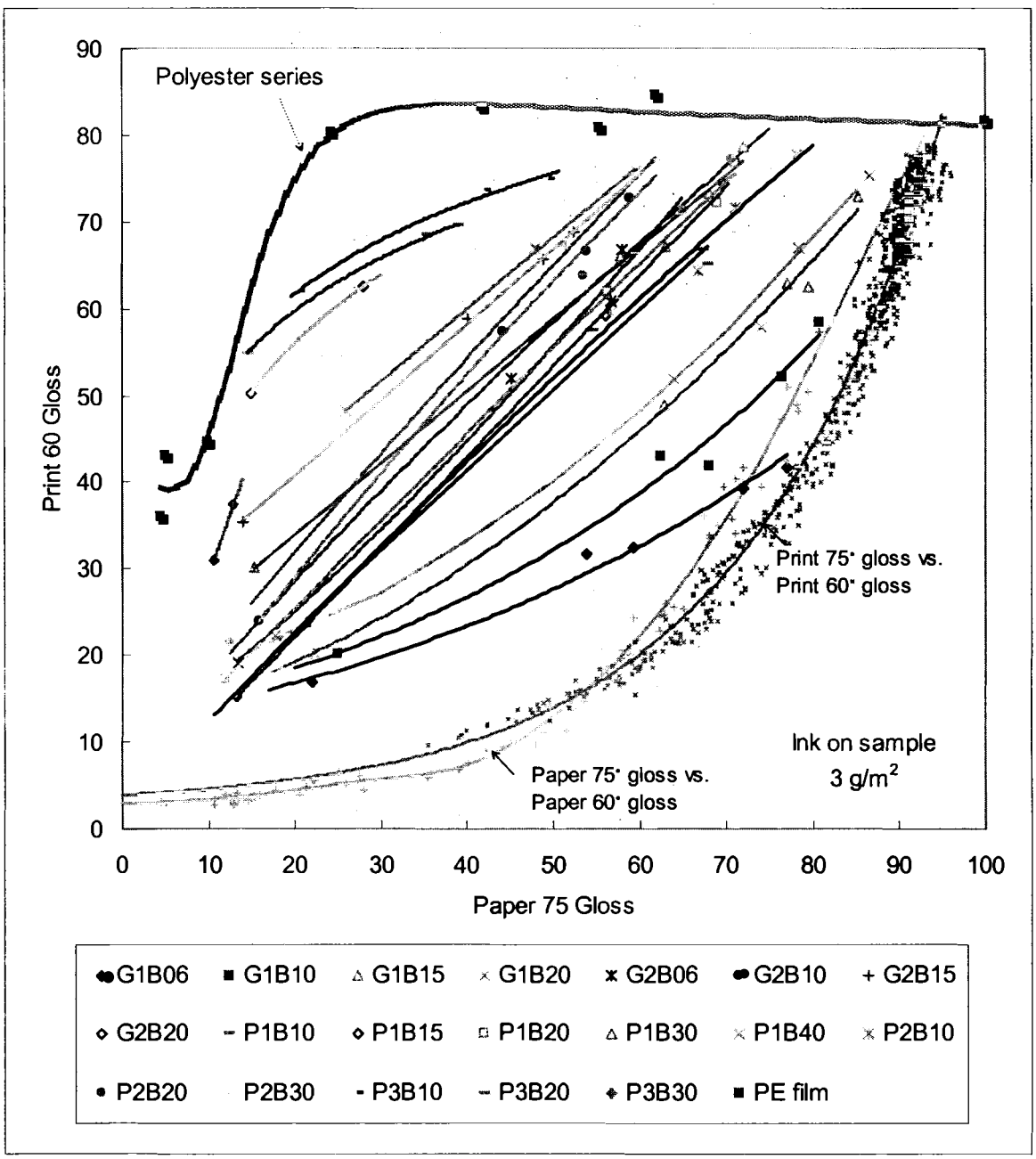

Figure D.6: Print 60° gloss as a function of converted roughness at 3.0g/m^2 ink.

APPENDIX E: STATISTICAL ANALYSIS RESULTS.

Table E.1: The result table of main effects analysis over the all factor ranges.

Effect Estimates; Var.: PRINT GLOSS; R-sqr=0.97079; Adj: 0.9695

3 factors, 1 Blocks, 214 Runs; MS Residual=11.91883

	Effect	Std.Err.	t(204)*	p	-95.% Cnf.Limt	+95.% Cnf.Limt	Coeff.	Std.Err. Coeff.
Mean/Interc.	45.7426	0.4931	92.7690	0.0000	44.7704	46.7148	45.7426	0.4931
(1)GLOSS (L)	**53.4256**	0.8444	**63.2671**	0.0000	51.7606	55.0906	26.7128	0.4222
GLOSS (Q)	2.7858	1.3989	1.9914	0.0478	0.0276	5.5440	1.3929	0.6995
(2)POROSITY(L)	**-14.7562**	0.7788	**-18.9469**	0.0000	-16.2918	-13.2206	-7.3781	0.3894
POROSITY(Q)	4.0171	1.2540	3.2034	0.0016	1.5446	6.4895	2.0085	0.6270
(3)PORESIZE(L)	**20.2551**	0.5941	**34.0910**	0.0000	19.0837	21.4266	10.1276	0.2971
PORESIZE(Q)	-1.7549	0.2423	-7.2437	0.0000	-2.2325	-1.2772	-0.8774	0.1211
1L by 2L	4.6695	1.1436	4.0833	0.0001	2.4148	6.9243	2.3348	0.5718
1L by 3L	5.3727	0.7487	7.1757	0.0000	3.8965	6.8490	2.6864	0.3744
2L by 3L	-2.8905	0.8490	-3.4048	0.0008	-4.5644	-1.2167	-1.4453	0.4245

* Standardized effects= Absolute effect / Std.Err.

Table E.2: The result table of main effects analysis over low paper gloss range; 40 gloss units in 75° gloss.

Effect Estimates; Var.:PRINT GLOSS_LOW; R-sqr=.9575; Adj:.95447

3 factors, 1 Blocks, 121 Runs; MS Residual=9.116395

	Effect	Std.Err.	t(111)*	p	-95.% Cnf.Limt	+95.% Cnf.Limt	Coeff.	Std.Err. Coeff.
Mean/Interc.	28.7907	0.4697	61.2926	0.0000	27.8600	29.7214	28.7907	0.4697
(1)GL_LOW (L)	**18.7276**	0.7930	**23.6176**	0.0000	17.1564	20.2987	9.3638	0.3965
(2)PORO_LO1(L)	**-16.8208**	0.9016	**-18.6557**	0.0000	-18.6073	-15.0343	-8.4104	0.4508
PORO_LO1(Q)	8.2385	1.4559	5.6587	0.0000	5.3538	11.1231	4.1192	0.7279
(3)PORE_LO (L)	**14.6645**	0.7085	**20.6992**	0.0000	13.2608	16.0682	7.3322	0.3542
PORE_LO (Q)	-0.8195	0.2678	-3.0598	0.0028	-1.3502	-0.2888	-0.4097	0.1339
1L by 2L	2.4718	1.0641	2.3230	0.0220	0.3635	4.5801	1.2359	0.5320
1L by 3L	3.3829	0.6047	5.5945	0.0000	2.1848	4.5810	1.6915	0.3023
2L by 3L	-3.8191	0.9938	-3.8430	0.0002	-5.7882	-1.8501	-1.9096	0.4969

* Standardized effects= Absolute effect / Std.Err.

Table I

gloss ur

Effect Est

3 factors,

Mean/Inte
(1)GL0SS
(2)PORO:
(3)PORE
PORE SIZ
1L by 2L
2L by 3L

* Standarc

Sung J.
raised i
Jeonju,
Enginee
Bachelo
Univers
the Divi